Theoretical and experimental techniques in the design of CRT deflection systems

Gillian Henery

Theoretical and Experimental Techniques in the Design of CRT Deflection Systems

Gillian Henery

SUBMISSION: MASTER OF SCIENCE

University of Durham
Philips Components Ltd.

1997 SUBMISSION

ABSTRACT

This investigation considers the design methodologies associated with the development and optimization of a magnetic deflection system for Cathode Ray Tube (CRT) Display Systems.

The development of a magnetic deflection system and the calculations necessary to determine the associated performance are both complex tasks. Their complexity arises from the detailed geometry involved in deflection unit designs, the wide range of product types and sizes, and variability in product performance specifications. The large variations of these issues compound the difficulty in realising an acceptable product design. Software simulation techniques which are able to accurately manipulate data and perform iterative calculations greatly aid this process.

This work introduces a simulation technique used within the Philips organisation, called DUCAD (Deflection Unit Computer Aided Design), which is used to analytically and numerically model the deflection system, with the objective of assessing and speedily realising a design. The simulation technique allows magnetic deflection product designs to be synthesized by simulating the magnetic field generated by the deflection system. Approximate solutions can be iteratively investigated leading to a greater understanding of the problem domain. To gain a degree of confidence with the simulation results the software design proposal is thereafter replicated in hardware allowing a full validation of the DUCAD. Extensive simulation studies and practical prototyping experiments are presented to support the theoretical development.

Comparing the calculated theoretical performance and the actual measured values, conclusions are drawn as to the quality of the simulation tool in deriving the intrinsic magnetic deflection characteristics of the generated product design. The level of agreement of theoretical prediction and experimental results are defined, and the design methodologies required to yield a slot based deflection system are assessed.

ACKNOWLEDGEMENTS

For their contributions and support during this work, I would like to thank both my supervisors;

Prof. E. A. Appleton, University of Durham,

and

Mr. Brian Howson, Product Development Manager, Philips Components Ltd., Washington.

I would also like to thank Mr. Gerrit Vink, of Philips Eindhoven, Raster and Convergence Group, for his valuable assistance in both the understanding of DUCAD and the design techniques involved in the optimization of a deflection unit.

TABLE OF CONTENTS:

6. CHAPTER SIX

LIST OF TABLES AND ILLUSTRATIONS:

PAGE NUMBER:

LIST OF APPENDICES

1. CHAPTER ONE

1.1 Introduction

This investigation considers the design methodologies associated with the development and optimization of a magnetic deflection system for Cathode Ray Tube (CRT) Display Systems.

The development of a magnetic deflection system and the calculations necessary to determine the associated performance are both complex tasks. Their complexity arises from the detailed geometry involved in deflection unit designs, the wide range of product types and sizes, and variability in product performance specifications. The large variations of these issues compound the difficulty in realising an acceptable product design. Software simulation techniques which are able to accurately manipulate data and perform iterative calculations greatly aid this process.

The Philips organisation currently use a simulation package and an associated technique, DUCAD (Deflection Unit Computer Aided Design) which allows the analytical and numerical modelling of a deflection system, with the objective of assessing and speedily realising a design. The simulation technique allows magnetic deflection product designs to be synthesized by simulating the magnetic field generated by the deflection system. Approximate solutions can be iteratively investigated leading to a greater understanding of the problem domain.

Market forces, together with the progression in winding technology, have resulted in the demand for higher performance designs at minimum cost. This has subsequently led to the necessity for a large number of additional correction components added to the design to realise the higher specifications required. The design outputs of DUCAD have not been thoroughly validated to date, particularly when discussing 'plated designs'. Minimization of overall system aberrations is currently reliant upon hardware prototyping. Iterative methods are used to create an final optimized design proposal. As full verification and validation has not been performed on the current

design methodology, the ability to perform initial design work employing DUCAD, was in question to some degree.

The aims of this investigation are therefore twofold; a full evaluation of the DUCAD simulation technique to verify its accuracy and value in determining a product design. To gain a degree of confidence between the simulation results and the experimentally gained data, practical testing was performed. Extensive simulation studies and practical experiments are presented to support the theoretical development and highlight any possible discrepancies with the DUCAD calculations. An optimized product design has therefore been created within the imposed practical constraints of the product type and the manufacturing processes. Both the computer aided design method plus theoretical electron-optical techniques have been employed to realise an acceptable product design

In parallel to the verification of DUCAD, the vehicle used to determine an acceptable product design was Slot Winding, an alternative technique for deflection unit manufacture to that currently employed by Philips. In the 1970's initial development work within Philips, Eindhoven created '*Yoke Winding*', now commonly termed *Slot Winding*. This technique allows the copper wire to be wound directly onto a plastic separator in a sewing machine style. The software simulation package, DUCAD-Y, was developed to aid the design process of Y(yoke) wound designs. With the development of more advanced winding techniques, 'pin-fired' winding was evolved, which create a deflection coil by winding the copper wire around a pressing jig. This coil is then formed, removed from the jig(mandrel) and then manually inserted into a plastic separator. It was found necessary to develop an extension to DUCAD-Y, called DUCAD-C, C- conventional winding, to more closely simulate the winding of coil halves in winding mandrels. Within DUCAD-C, it is possible to determine coil winding density and more detailed coil constructions to enable accurate characteristics to be simulated. As the wire(current) distributions are more detailed it is assumed the corresponding magnetic field calculations are more realistic and authentic.

Many critical design/manufacturing issues relevant to Slot Winding were unknown at the outset of this study due to Philips' lack of knowledge and experience of this current technique of coil manufacture. The inherent limitations upon the product design imposed by the slot winding technology therefore required full evaluation and consideration. An evaluation of both product design methodology and the winding process was therefore a requisite of the study.

This report aims to thoroughly investigate the ability of design methodologies such as DUCAD to accurately create an optimized product design within the imposed practical constraints of the product type design and the slot winding process criteria. Cross-correlation between the theoretical results predicted by the software and the prototype performance is the principal method in assessing and evaluating this method of coil design and manufacture. By comparing the calculated theoretical performance with the actual measured values of hardware prototypes, conclusions are drawn as to the quality of the simulation tool in deriving the intrinsic magnetic deflection characteristics of the generated product design. The level of agreement of theoretical extrapolation and experimental calculations are defined, and the design methodologies required to yield a slot based deflection system are assessed.

The remainder of this chapter shall briefly outline the main components within a CRT system together with some basic system terminology and product type variation.

1.2 Electromagnetic System Introduction

1.2.1 Basic Principles

Magnetic Deflection Systems are used extensively for deflecting electron beams in a variety of display instruments, typical examples being T.V. receivers, data display tubes, and scanning electron microscopes.

The use of electromagnetic applications is of greater prominence than electrostatics in the application of T.V. deflection systems for two main reasons. Firstly, the required

deflection voltage is unavoidably high for electrostatics, due to the necessity for high deflection angle and anode voltage. Secondly, in calling for deflection in two directions (horizontal and vertical), a second set of electrodes (rotated through 90 degrees) must be mounted behind the first set to prevent the two sets from interacting with each other. This has severe restrictions in tube design possibilities. Magnetic deflection systems are therefore the preferred arrangement for T.V. applications due to the ability to generate more cost effective solutions whilst maintaining low voltage requirements.

A CRT is a particular types of vacuum tube uses as display screens in televisions, computer terminals, radar screens and oscilloscopes.

The effect of heating metals to cause the release of electrons is known as thermionic emission and is employed in most vacuum tubes. The metal forms the cathode and can be heated by passing a current through it or by placing a filament near it. The emitted electrons form a 'cloud' near the cathode which gives rise to a force that repels the electrons subsequently emitted by the cathode. An anode, a positively charged electrode is placed near the cathode subjecting the electrons to a force of attraction. By increasing the positive voltage of the anode causes the flow of electrons to increase, at very high levels all the emitted electrons will be attracted by the anode.

The main parts of a T.V. assembly system, referred to as the tube/coil assembly, include the tube screen, cone neck, electron guns, shadow mask, diaphragm parts and deflection system. Electrons are produced by three guns located in the neck of the tube system. Each gun consists of an electrically heated cathode, a modulator and an anode. The modulator is held at a voltage negative with respect to the anode, and repels some of the electrons back towards the cathode. The effect of varying the modulator voltage allows adjustment of the screen brightness. The anode is held at a relatively high positive voltage (from + 1kV to +20kV) with respect to the cathode and attracts the negatively charged electrons and accelerates them down the tube. The anode recaptures a few electrons but most have enough momentum to travel through the anode and strike chemical materials called phosphors, coated onto the inside of the screen end, emitting light known as luminescence.

The predominant component generating magnetic deflection of the electron beams within the T.V. tube is referred to as the deflection unit. The magnetic deflection unit enables the electron beams to pass through the picture tube and thereafter scan the familiar raster to form two dimensional visible images on the screen. The magnetic deflection system employs current flowing through coils of circular cross section for deflection and focusing onto the screen of a CRT display. (Refer to Diagram 2).

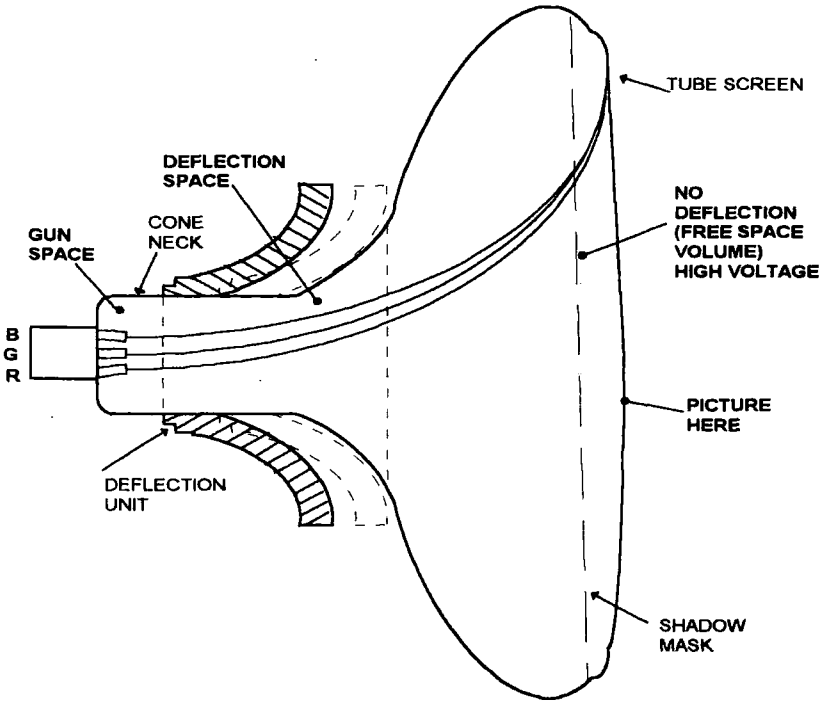

Diagram 1: Tube/Gun T.V. Assembly

The magnetic deflection unit determines the trajectory of each of the beams, and additionally ensures consistent scanning of the phosphor dots located on the inside of the glass. (The deflection space created by the deflection unit influences the trajectory of each of the electron beams firing them at the phosphors on the inside of the glass). The green gun is aimed along the main central axis while the remaining two (blue and red) lie at equal distances either side of the green in the vertical plane. The spatial relationship between the guns is such that in the undeflected state the electron beams land at the centre of the screen. This common landing point must also be maintained during beam deflection. Departures from this condition are termed misconvergence.

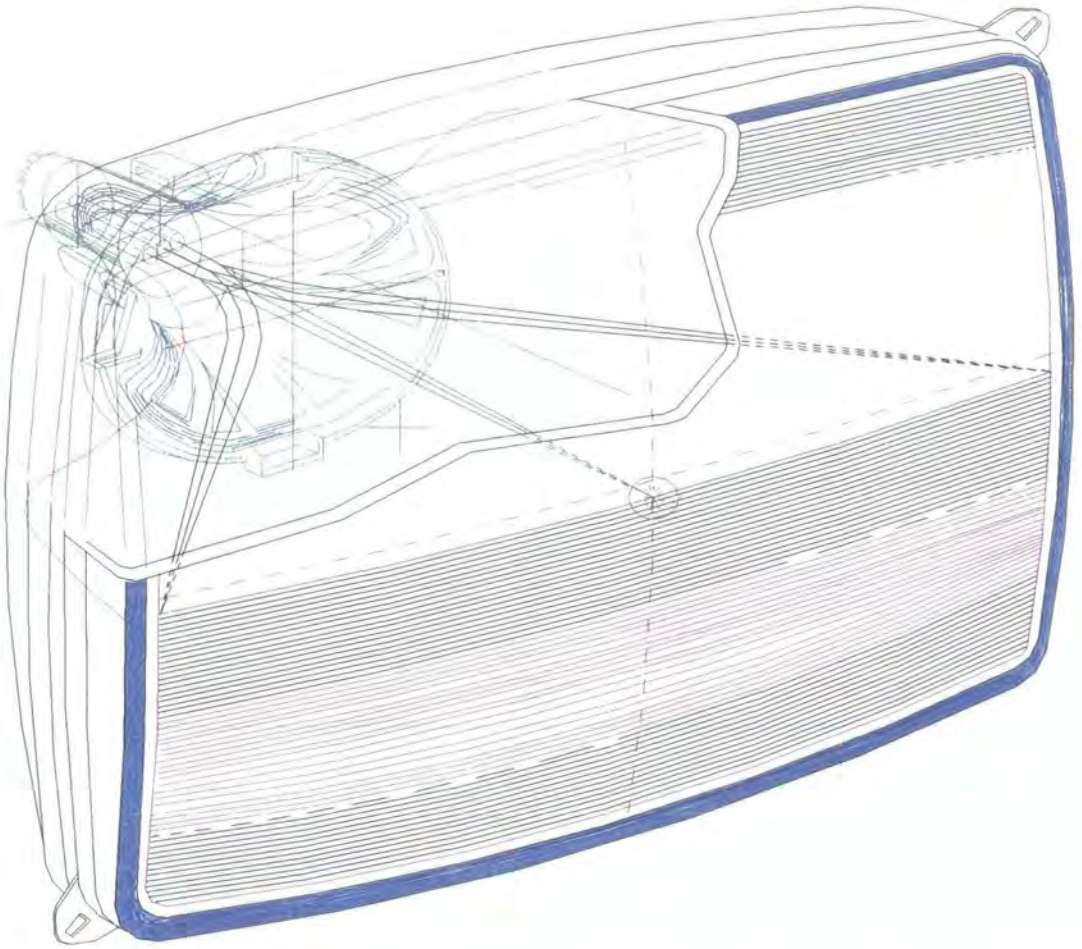

Diagram 2: Deflection Unit Positioned on a Television Tube

The shadow mask is a thin steel plate situated about 1 cm behind the inside surface of the screen of the CRT, perforated with many thousands of holes. Refer to Diagram 3. The phosphor layer consists of a group of dots, each group being made of red, green and blue phosphor areas. Ideally, the phosphor patterns and the perforations in the shadow mask are aligned such that the beam from one of the electron guns can only hit its associated phosphor. An important design consideration is the colour selection angle, dependent upon the screen position selected. Due to both the tube geometry and deflection coil construction this imposes a varying mask-to-screen distance across the screens surface.

In practice, large screen tubes (50 cm diagonally or greater) may have around 500 000 holes and phosphor groups. These are incorporated to ensure proper convergence and landing behaviour, as any beam landing beyond the edge of the correct phosphor will cause colour errors.

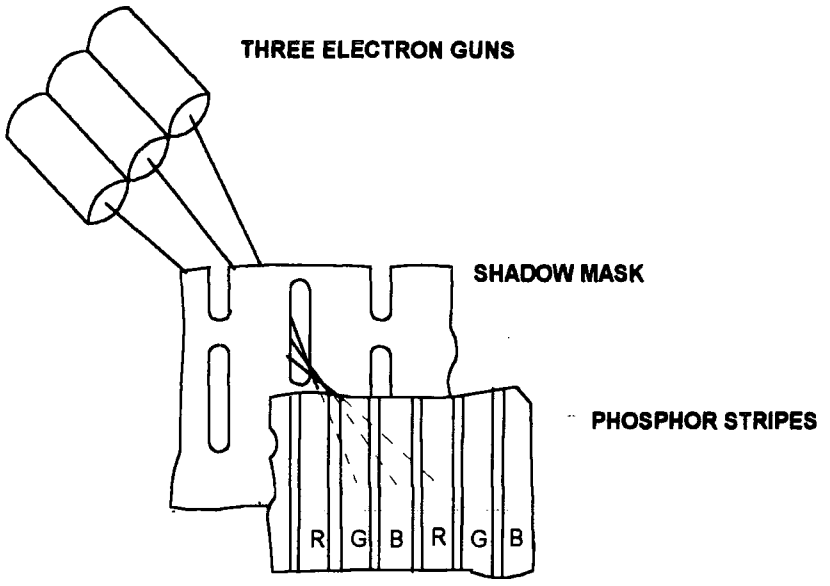

Diagram 3: The Principle of Operation of the Shadow Mask

A main drawback of this construction is poor energy efficiency. The shadow mask is required to intercept most of the electron beam current, converting the beams energy into heat. Only the electrons passing through the holes contribute to the light output, and this may be as little as 20% of the total beam generated by the three guns. This is further reduced by accommodating three guns in the neck of the tube, the diameter of the neck directly affecting the power required to produce the horizontal and vertical deflection fields.

1.2.2. Analysis Of Practical Deflection System And Component Parts

Colour T.V. pictures are generated by a technique of raster scan, causing the superposition of the three primary colour rasters. The electron beams are deflected horizontally and vertically to trace the outline of the picture, the electron beam

intensity being modulated in synchronism with the scan thus generating the image. Each individual primary colour electron gun placed in the neck of the tube produces an electrostatically focused beam, the intensity of which is modulated by the red, green and blue colour signals. The method of line scanning across the screen requires that the generated magnetic field must vary as a function of time and require a certain field strength dependent upon the point of scanning. Interlaced scanning is applied to prevent flicker of the picture. (Interlacing refers to the superimposition of the two fields making up the picture, one on top of the other, with the second field displaced (vertically or horizontally)).

A magnetic deflection system for a CRT consists principally of two pairs of deflection coils which if a current is passed through, both produce horizontal and vertical magnetic deflection of the electron beams. In an ideal system, the horizontal and vertical deflection currents are linear sawtooth waveforms with a peak amplitude sufficient to fully scan the tube and therefore the rate of change of both the horizontal and vertical deflection currents is constant while the active area of the picture is scanned (i.e. not during flyback scan). The relative position of the wire of the coils fundamentally determines the magnetic deflection fields generated and hence the overall deflection systems' performance.

To a close approximation, the angle of deflection is proportional to the magnetic field strength produced by the deflection coils, which in itself is proportional to the deflection current. In modern wide angle T.V. tubes the tube face is slightly curved and the radius of curvature is much greater than the trajectory of the electron beams from the deflection coils to the centre of the screen. In either direction therefore the deflection system is linear only near the centre of the screen as towards the edges of the screen an equal increase in the scan currents cause greater displacement of the scanning dot. (Refer to Diagram 4).

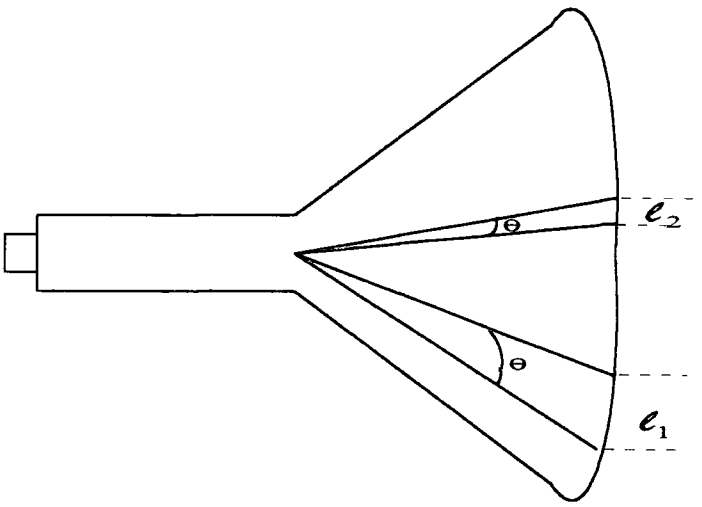

Diagram 4: Non Linearity of Deflection in Display Tubes

For the same change of deflection current and therefore deflection angle, the spot at the centre of screen moves a distance $\ell 2$, while nearer the edge it moves a distance $\ell 1$.

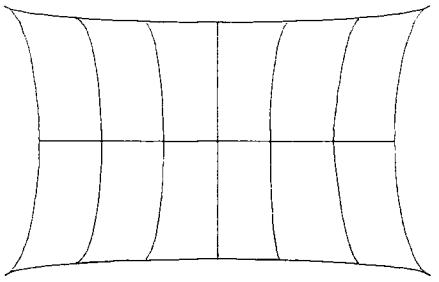

Diagram 5: Non-Linearity - Appearance of an Uncorrected Cross Hatch on T.V. Display

Interaction of the vertical and horizontal waveforms produce a characteristic pincushion shape towards the corners which is caused by the reduced curvature of the screen (FS screen , "flat" screen). In addition, the cross-hatches are spaced further apart.

Although the three beams are deflected by the same vertical and horizontal deflection fields they do not necessarily trace identical rasters on the screen. The three beams follow slightly different paths to the screen, and the rasters reproduced have slightly differing geometric distortion which results in convergence errors at various parts of the picture. (Refer to Diagram 5).

An additional component important in the deflection system is the ferrite magnetic core located outside the deflecting sections of both coils. This magnetic material with high permeability and low remanence controls the magnitude and shape of the magnetic fields to ensure maximum concentration within the interior of the yoke, increasing the field strength by as much as a factor of 2. The enhancement of the deflection field strength by the core increases the deflection sensitivity of the system, and reduces the drive circuitry requirements. Ferrites are the preferred material for cores due to their high magnetic permeability and low electrical conductivity (minimising eddy currents losses).

A further component in the deflection system is the plastic separator which provides electrical insulation between the horizontal and vertical coils and routing channels for wire termination. Connection of the deflection unit to the drive circuitry is from the terminal board mounted on the deflection unit. Additionally, a deflection unit can contain correction components, such as small plates and magnets, which help achieve the design performance objectives often unachievable with coils alone. A prime objective in deflection unit design is to exploit and optimize coil design and if necessary to at least minimise the additional correction components required if there is no further gain within the deflection coils.

1.2.3. Detailed Analysis of Deflection System

When designing a deflection system, the overall performance requirements for the picture tube and deflection unit combination are analysed. This study considers the design approach and methodology for the overall optimization of the performance of the deflection system only.

Three important electron-optical criteria to achieving an acceptable display with regard to the colour T.V. deflection systems are;

- **Purity** - a characteristic enabling independent control of the primary colours at any point on the screen.

- **Raster Shape** of the display screen - the image transmitted must be received and displayed on the screen with an insignificant level of distortion, i.e. the image must maintain the correct ratio between vertical and horizontal dimensions;
- **Convergence** - a crucial property of the display system relating to the superimposing of the three electron beams at every position on the screen, e.g. white line has no fringing.

In addition to the electron-optical behaviour of a deflection system, the electrical characteristics are of important consequence to the overall system performance. To scan the screen, a sawtooth current is passed through each deflection coil. The deflection system's "sensitivity" is specified by the currents generated in the deflection coils. Sensitivity is understood as the product of L and I squared for the line coil, and R and I squared for the frame coil. The smaller the product the more sensitive the unit. (L is the self-inductance of the line coils and R is the ohmic resistance of the frame coils). The current is transferred back and forth between the deflection unit and the circuit. This results in energy losses in the magnetic yoke ring (due to hysteresis), the deflection coils (due to the dynamic and static resistance of the coils) and the deflection circuitry itself (dissipation in electronic components).

For vertical deflection , where the vertical scanning frequencies are of the order of 50/60 Hz, power losses due to magnetic energy exchange between circuit and coils are small in relation to the resistance losses. The reverse is true for horizontal deflection where scanning frequencies are higher (16kHz/32kHz). Of marked consequence in the deflection performance characteristics therefore are the stored magnetic energy levels and inherent resistance losses.

1.3. Types and Associated Requirements (Size, Specification) Of Colour Deflection Systems

Deflection system designs may be split into distinct types, dependent upon the following parameters; deflection angle (90 degree and 100/110 degree - for a given tube/deflection unit assembly the deflection angle defines the angle between the

maximum (+) and minimum(-) deflection), beam parameters, diagonal screen size, internal contour of the picture tube. Differing methods of design and manufacture are utilised in order to produce the required deflection system, with regard to performance (convergence/raster/electrical), cost, size and flexibility.

Three distinct coil types exist characterised by various winding technologies referred to as toroidal, saddle and mussel coils. Toroidal coils essentially encircle the ferrite yoke ring with the copper wires are used for frame coil vertical deflection in 90 degree and some 110 degree systems. (Refer to Diagram 6). The coils are wound on relatively simple unsophisticated machines comprising of a rotating winding arm and clamping arrangement specific to the style/size of yoke ring. Toroidal coils generate the required deflection field by varying the wire compactness (current density) as a function of the subtended angle around the yoke ring core.

One advantage of toroidal winding is cost; due to the style of winding, no expensive winding jigs are required. In addition varying coil impedance is easily realised by varying wire diameter and the number of wire turns. The very nature of this less sophisticated winding technique causes electron-optical design limitations to exist. Approximately half the magnetic field generated by the vertical coil is emitted as stray, however it can provide a cost-effective design solution to the small to medium screen sizes.

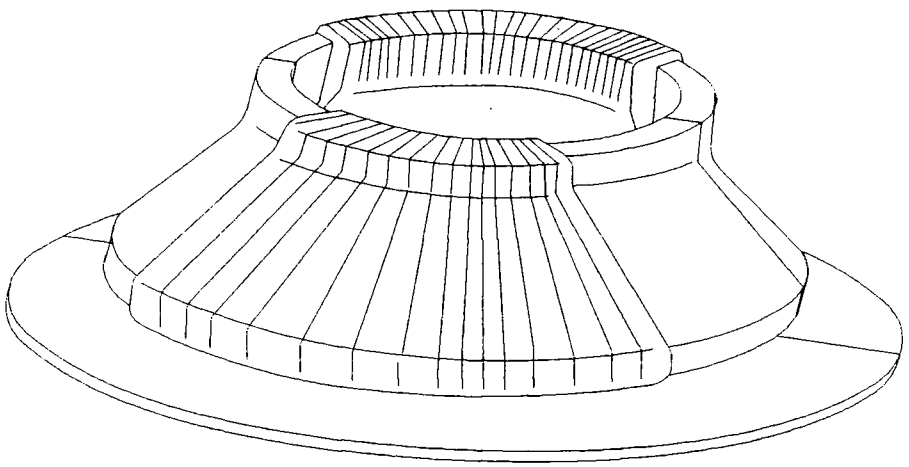

Diagram 6 : Diagram of a Toroidal Deflection Coil

Saddle coils are manufactured such that each half of the coil resembles a riding saddle, with a rounded lip at the top section and are used for line horizontal coil deflection in 90 degree and some 110 degree system. (Refer to Diagram 7).

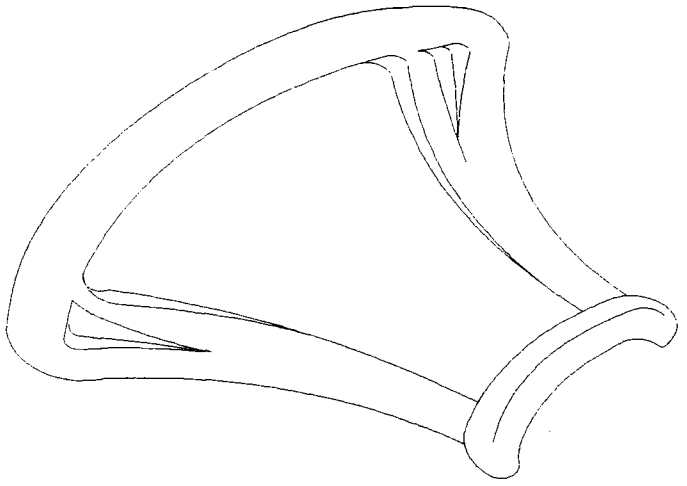

Diagram 7: Diagram of a Saddle Deflection Coil

Two methods of manufacture exist for this coil type, "Pin-Fired" Winding and Slot Winding, the former shall be utilised within this study. Pin-fired winding methods are employed throughout Philips are a standard design/manufacturing technique which principally consists of a rotating arm which circulates around a winding jig (called 'mandrel') feeding copper wire around the fixture. Use is made of sectional winding by firing pins at particular sections of the mandrel, hence creating a variety of coil designs. Varying the number of turns at specific coil sections enables preferred magnetic field configurations to be established. Thereafter, a high current is passed through the wound coil to 'bond' the copper wires together, a thermoplac layer surrounding the special wire fixates the coil rigidly. Slot Winding, a method of deflection coil manufacture extensively applied within non-Philips designs, allows the manufacture of saddle coils by positioning and winding the copper wire directly into grooves engineered into the plastic separator. Saddle coils are primarily employed for horizontal coil deflection and owing to their shape utilise a toroidal coil design for vertical deflection, and are therefore referred to as toroidal/saddle deflection coils.

Refer to Diagrams 8 and 9a/b. The ferrite yoke ring, being a split component is positioned around the coil halves and thereafter re-located by spring clips.
The saddle/toroidal coil design methodology offers flexibility in design opportunities and adequate levels of deflection sensitivity, approximately 1.5 times more sensitive than toroidal deflection coils. A major advantage of saddle coils is the many possibilities possible in changing the magnetic field shape, by small modifications to the winding pattern. In addition they are able to accommodate high frequency applications due to their relatively small number of copper turn windings and are therefore suitable for horizontal higher frequency deflection coils. However, this type of winding is an expensive design solution. Further, their ohmic losses are more than toroidal coils due to the relative number of wire windings. Because of the extension of their fields especially at the gun side, toroids produce more deflection than saddle coils for equal current levels, therefore the current of a toroidal coil must be reduced so decreasing the stored energy levels. Toroids have a lower resistance to inductance ratio (R/L) and hence their applicability to vertical deflection where the frequency of the waveform is less restrictive and limiting.

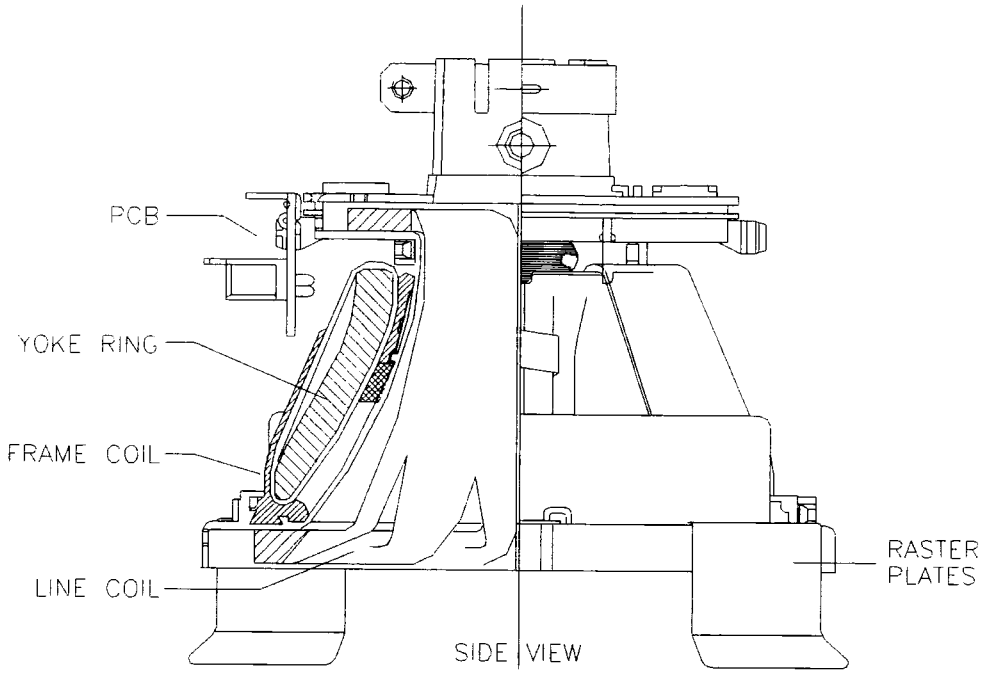

90° HYBRID TECHNOLOGY

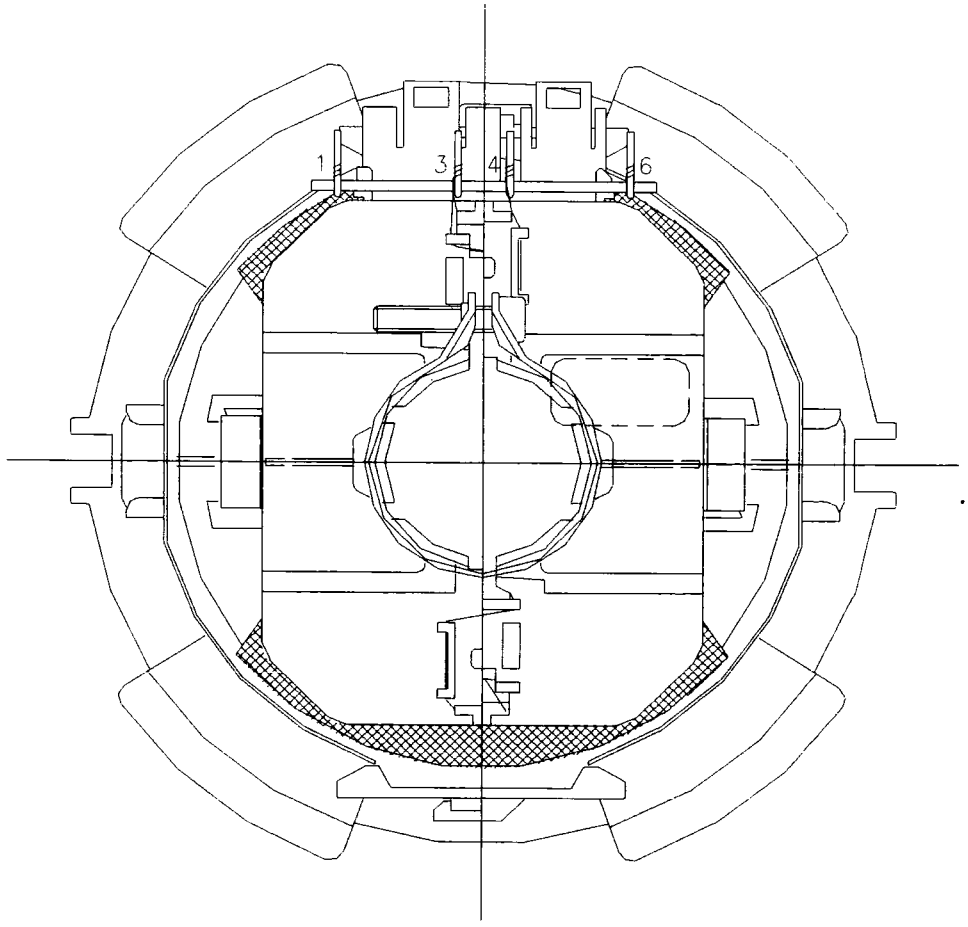

TOP VIEW

Diagram 8: Hybrid (Saddle/Toroidal) Deflection Coil Design

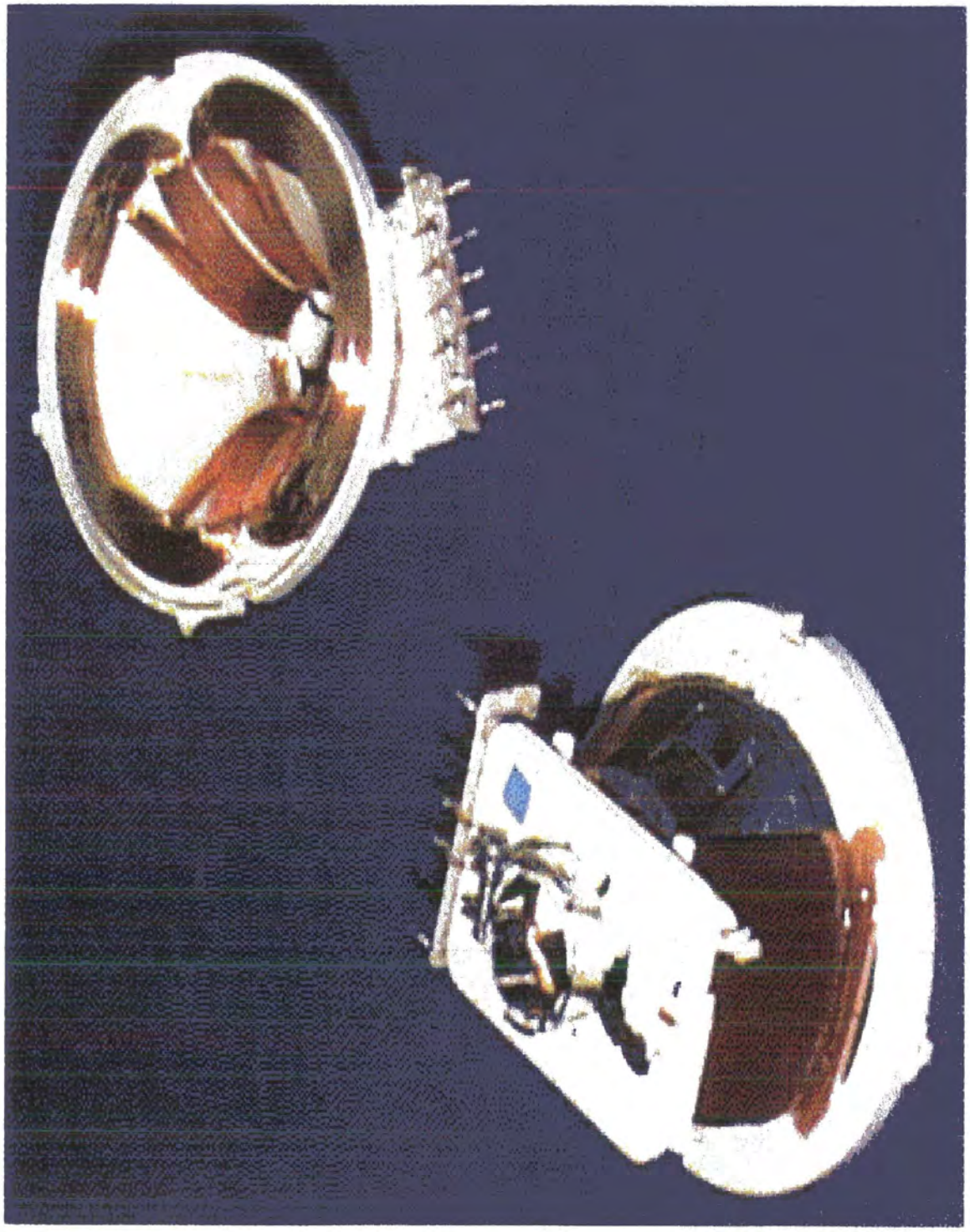

DIAGRAM 9a: SADDLE/TOROIDAL DEFLECTION COIL DESIGN

Diagram 9a: Saddle/Toroidal Deflection Coil Design

DIAGRAM 9b: SADDLE/TOROIDAL DEFLECTION COIL DESIGN

Diagram 9b: Saddle/Toroidal Deflection Coil Design

To overcome the design restrictions inherent in saddle coil winding, mussel coils are employed. The neck portion of a mussel coil is effectively folded back towards the picture tube accommodating greater possibilities in selection of wire position. A mussel coil, depicted in Diagram 10, is manufactured by conventional pin-fired techniques of automatic winding mandrels. If double mussel technology is employed there is no copper wire located outside the yoke ring and the frame coil copper wire follows the contour of the tube all the way back to the neck of the deflection system. This construction gives much more freedom in determining the line and frame field deflections starting points.

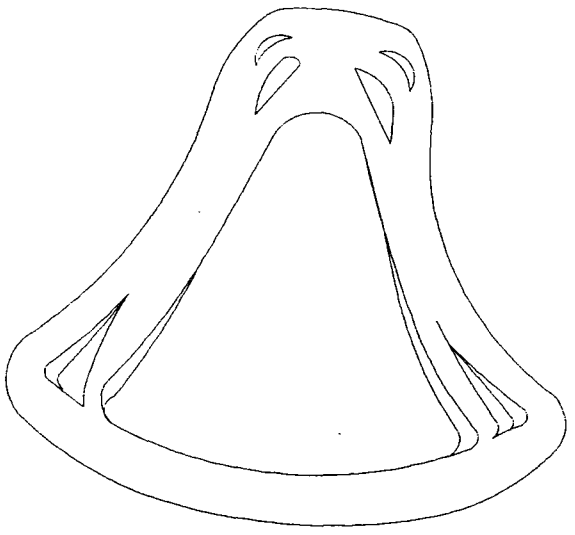

Diagram 10: Diagram of a Mussel Deflection Coil

This coil type provides immense flexibility in product design possibilities achieving a much higher gain in deflection sensitivity compared to saddle coils. Mussel coil winding is therefore employed in product designs requiring high performance capability, such as colour monitor tube units and the more 'elite' product sectors. Double mussel systems (where both the vertical and horizontal coils are manufactured in this way) are 20 % more sensitive than saddle/toroidal coil designs. Refer to Diagrams 11 and 12a/b.

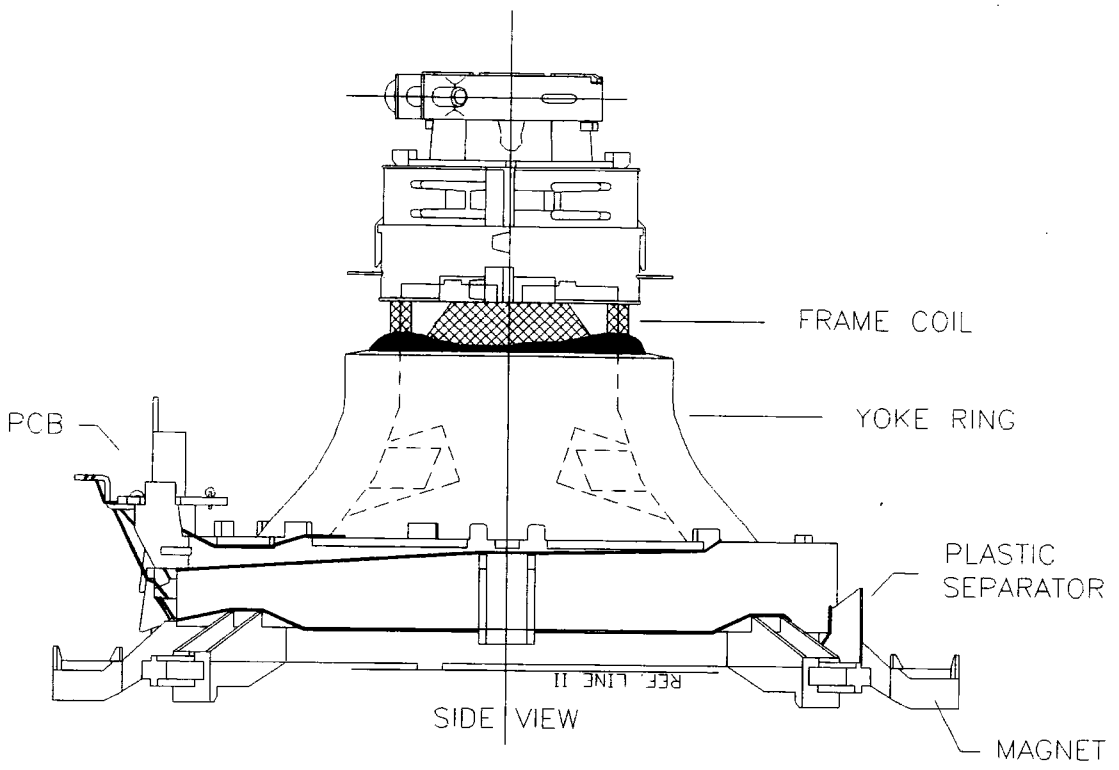

110° DOUBLE MUSSEL TECHNOLOGY

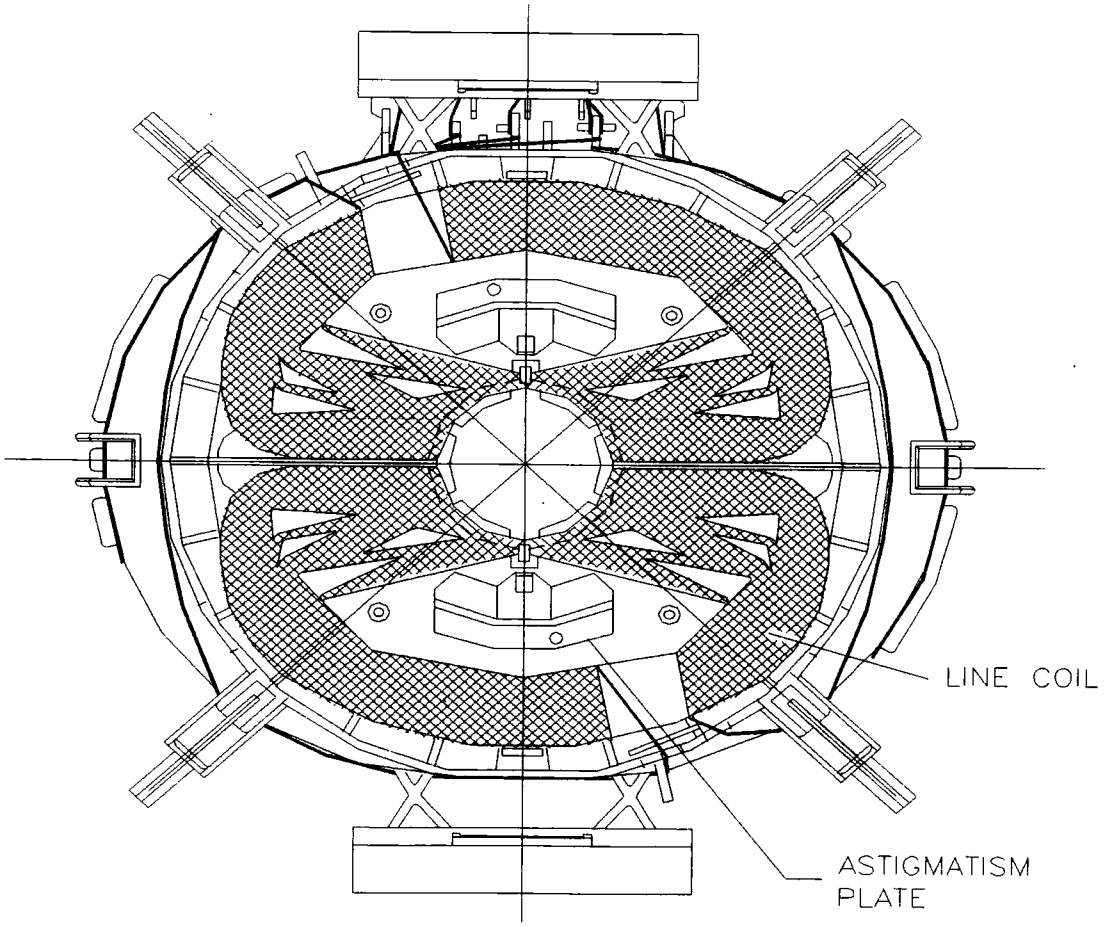

Diagram 11: Double Mussel Deflection Coil Design

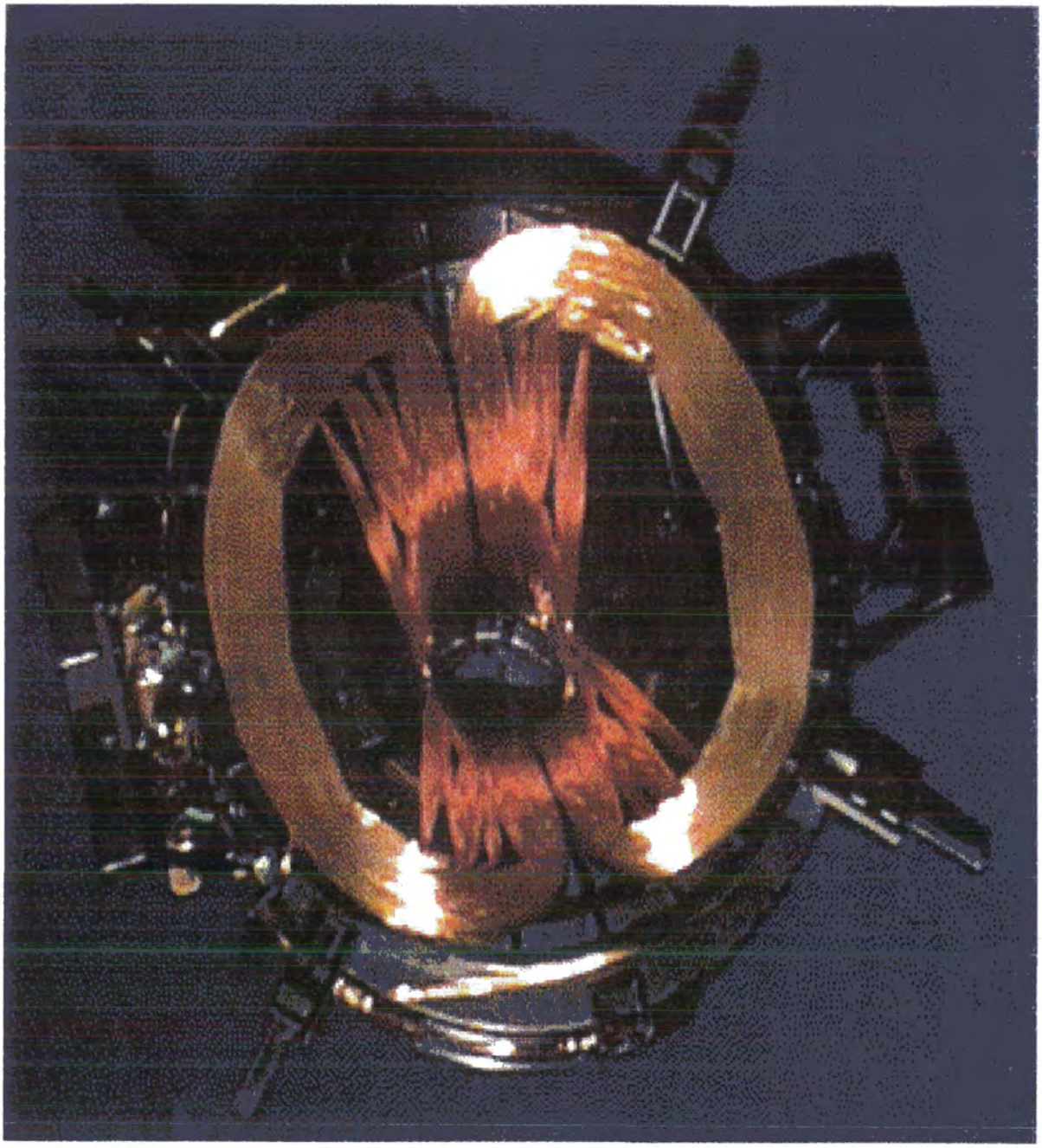

DIAGRAM 12a: 59FS DOUBLE MUSSEL DEFLECTION COIL DESIGN

Diagram 12a: 59FS Double Mussel Deflection Coil Design

DIAGRAM 12b: 59FS DOUBLE MUSSEL DEFLECTION COIL DESIGN

Diagram 12b: 59FS Double Mussel Deflection Coil Design

A slot based saddle/toroidal, refer to Diagram 13, is fully considered in this study to assess and verify the DUCAD predictions, and to identify any limitations in both the product and process methodologies.

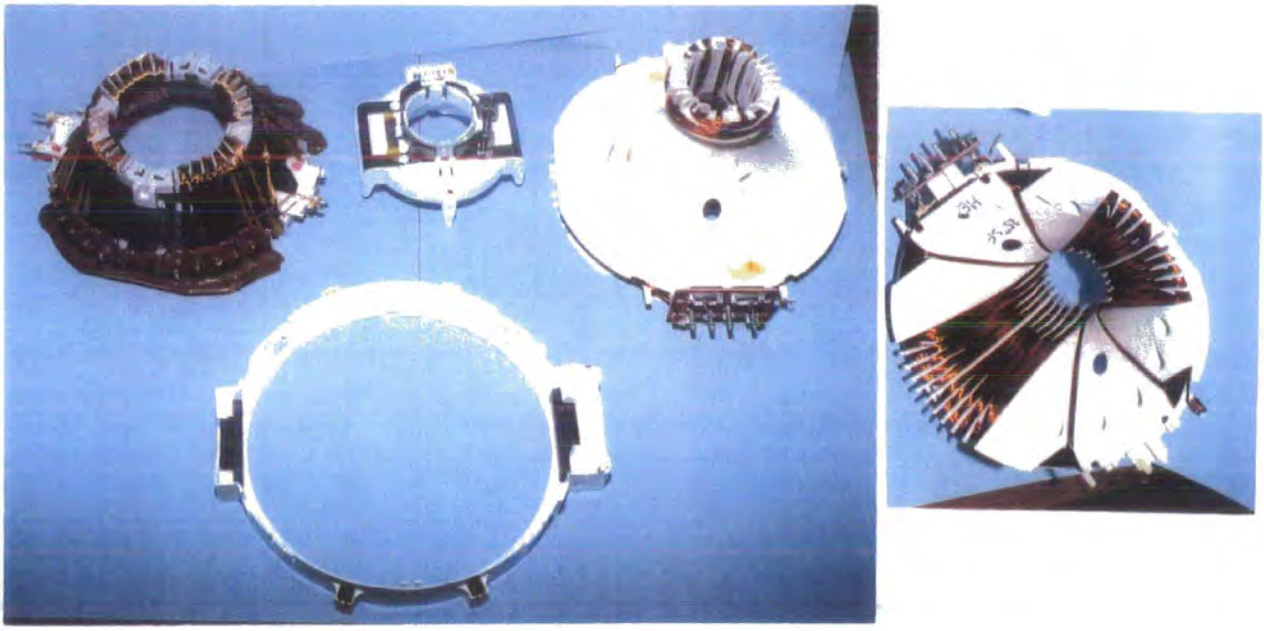

Diagram 13: Photograph of Slot Wound Product Design

1.4. Correction Methods for Colour Display Systems

1.4.1 Introduction to Terminology used to Evaluate System Performance

The magnetic deflection of three beams in colour picture tubes can be treated as a problem of minimizing the 'spot distortion' by designing magnetic deflection fields to achieve the least amount of aberration error. In an 'in-line' system, the guns red ***R***, green ***G*** and blue ***B***, as detailed in Diagram 14, are orientated to ensure convergence of the three beams in the undeflected state at the centre of the screen. Geometrical errors are defined for the central green beam ***G***. Convergence is defined as the requirement of each of the three colour beams to focus at the central screen position and all surrounding screen points. If the three fail to converge particularly at the transition of the colour beams, colour fringing on the screen will become visible.

Convergence errors defined for the ***R, G and B*** beams are: Astigmatism (half the vector difference of the deviations GR and GB) and Coma (half the vector sum GR and GB).

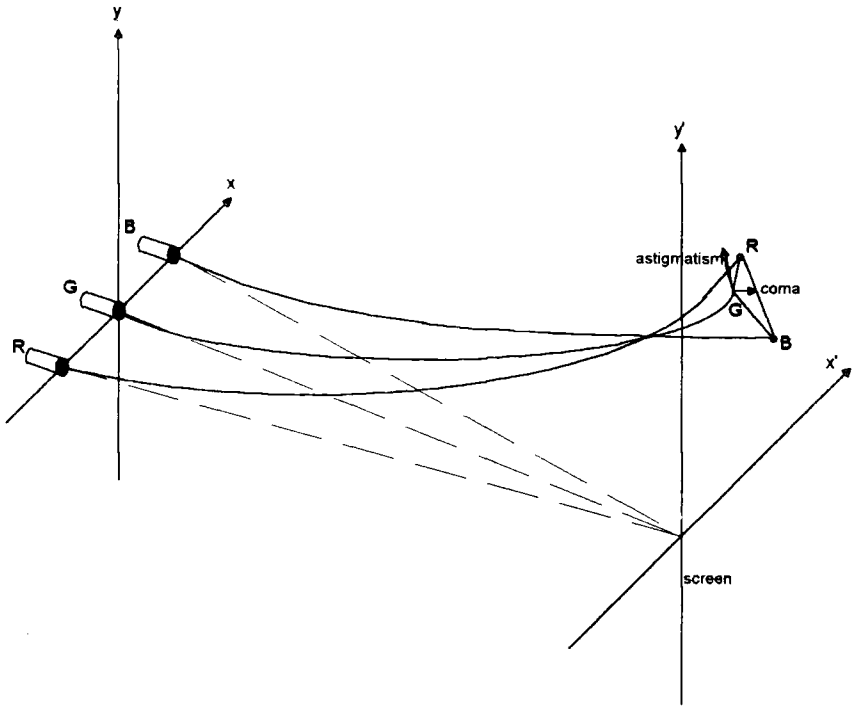

Diagram 14: In line system (Astigmatism and Coma Errors)

Raster distortion is observed when both the horizontal and vertical deflection fields are operating simultaneously and is primarily a result of the flatness of the screen or the shape of the deflection fields. On the display screen, a rectangular image may be reproduced as a barrel or a pincushion configuration due to raster distortion.

The required performance specification can be achieved by careful design of the deflection system, commonly requiring the addition of correction plates, such as coma, astigmatism, and raster plates attached to assist in achieving the correct convergence levels and overall raster shape on the display.

Further correction techniques may be essential to meet system requirements. Convergence/raster errors may result from the tube/gun combination which would necessitate supplementary components added to the deflection unit, such as multipole rings for adjusting static convergence, placed directly onto the unit or incorporated as

a separate subassembly. The compensation of deflection unit performance limitations may be overcome by correction components incorporated into the tube itself, such as coma correction plates or coma rings placed within the gun assembly.

A major prerequisite of this product design within a production/manufacturing environment is indeed the ability to control errors resulting during the control of the manufacturing processes, such as variational spread, diagonal asymmetry effects (due to piece part variation, etc.).

1.4.2. System Performance Criteria

The performance of a deflection system is determined and defined by two criteria; the degree of intersection of the three beams, 'convergence' at various measuring points specified on the T.V. screen, and raster distortion, the degree of deformation of the scanned pattern on the screen, i.e. the error shown within certain horizontal and vertical bands on the screen. The convergence and raster levels at various test points define the general specification for the deflection system performance. The measuring positions on the screen are defined by Philips, as follows:

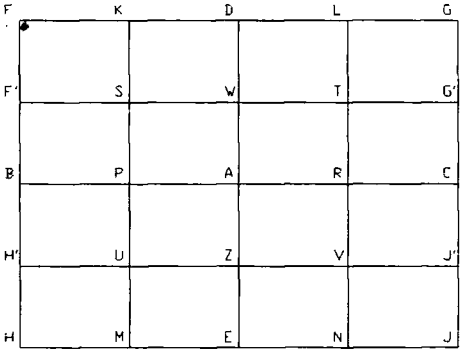

Diagram 15: Screen Measurement Positions

The lines BC and DE are called the line and frame axis respectively, where the distance between each of the test points is dependent upon the relevant screen size.

This comprehensive and generic referencing technique for the full evaluation of deflection system performance is an important measuring standard.

A common indicator of performance is the quality factor, represented by the Q number, which provides a weighted average of all convergence system parameters. Various points on the screen are weighted according to their respective spatial locations with less stringent demands being made on corner point convergence as compared to point axis or off-axis points on the screen. This ranking of importance is therefore selectable to bias the chosen performance specification as calculated by the Q number.

1.5 Conventional Product Design Cycle for Deflection Units

The development of a deflection system design would conventionally sub-divide the design based tasks into distinct transitional phases as detailed in Diagram 16. The initial phase would utilise DUCAD-Y, a software package specifically developed to aid deflection unit development, to determine a preliminary assessment of the systems' requirements. This appraisal would consider such information/detail as the lengths and overall dimensions of the line and frame coils; the yoke ring requirements, the global winding distributions of both line and frame coils, initial indications of coil/tube interface application aspects, and matching sensitivities.

The second phase would utilise DUCAD-C, a more detailed simulation package to address the design of mandrel components for saddle/mussel pin-fired coil winding, to undertake a more detailed and thorough evaluation of the system A full appraisal of the design, to component level is studied. A degree of hardware prototype development would be introduced to authenticate the proposed design plus resolve any issues of mechanical interfacing. The following issues would be realised;

- definition of copper volumes of both the line and frame coil (L/R filling, wire diameter)
- wire distribution

- mandrel design and profiles
- material and thickness of yoke ring determined
- plastic separator design
- additional component design parts

The third phase would embrace the design concept and incorporate any possible design alterations to accommodate high volume manufacture of the product design and compatibility of mass manufacture. The practicability and feasibility of design is closely reviewed in addition to the convergence and raster behaviour, closely studied on larger batch sample sizes.

The proposed design is examined with greater attention to the coil/tube application interface requirements. These would include specific product design issues such as environmental testing and physical properties. On a more global manufacturing base an appreciation of the anticipated yield of the product would be ascertained (Cpk > 1.3, where Cpk is the capability index of the manufacturing process).

The fourth and final phase would verify the calculated product design performance sensitivities considered in Phase 1. Much of this effort would require the involvement of the tube customer to determine the critical parameters within the manufacturing/design process, such as mechanical design issues, circuit demands and tube/coil combination issues (industrial aspects/equipment and matching method). Many mechanical issues directly related to the tube factory, setmaker and any tube development would be clearly resolved during this phase.

Within this development project the initial design phase is fully studied and considered to determine the authenticity and accuracy of DUCAD-Y predictions in ascertaining the performance of a slot based deflection system. The categorical dependency on DUCAD is clear, it is the first stage in the development process, upon which all other subsequent actions rely.

Preliminary Studies - Design Acceptance

Feasibility study for potentially new product design

Ducad-Y
Ducad-C

2-3 Months

PHASE 1&2 -Design phase

Objectives such as product performance, cost, investment timescales, etc., are defined on completion of this design phase
A product design is proposed

Provisional component tooling
Detailed design work and component selection
Hardware prototype development

2-3 Months

PHASE 3 - Design Consolidation

Complete demonstration that prototypes of the design proposal satisfy product demand, utilising actual component parts, equipment & standard factory process techniques

Order main design components
Finalised hardware trials

2-3 Months

PHASE 4 - Design Release

Total Development Time - ***12 Months***

Diagram 16: Design Process

2. CHAPTER TWO

PREVIOUS RELEVANT WORK

To consider a new product design utilising simulation software tools and mechanical hardware prototypes requires a clear understanding of the theoretical methods applied to the design and development of the product in question. In addition, the techniques by which the products are assessed, i.e. with respect to the systems' performance/quality, are important considerations.

During this study it was evident that the theoretical methods utilised to generate a deflection unit design could be divided into the following process steps; the calculation methods and associated techniques to determine the magnetic field strength of the deflection system and secondly the trajectory behaviour of electron beams within the established magnetic environment. Both these considerations are a prerequisite to ascertaining the deflection aberration errors present on the display. E. F. Ritz, Jnr , Tektronix, Inc., [1] provides a thorough analysis of the currently utilised techniques for the analysis, simulation and design of electron deflection systems. His paper highlights the importance of numerical computational methods, particularly attributable to the onset of numerous highly proficient computer simulation techniques. Basab B. Dasgupta, RCA Consumer Electronics, [2] introduces an analytical method of calculating the magnetic field produced by a deflection system expressing the field components as angular Fourier expansion terms. In exploiting Fourier analysis, this development process enables a design system to be analysed and thereafter evaluate the parameter constraints and restrictions of prominence to the overall coil system design. Much research work has studied the design processes and stages associated with the development of the deflection unit. W.A. L. Heijemans et al, Philips Eindhoven, [3] describe the techniques involved in accurately realising the required magnetic field behaviour and their relationship with the design of a deflection system, and introduce the concept of 'multipoles' when investigating the

magnetic deflection fields. T. Nakagawa et al, Mitsubishi Electric Corporation, Japan, [4] analyse the effect of magnetic plates attached to a deflection coil and calculate the magnetic fields combining a surface method with a finite difference method using Fourier transformation. This work introduces the influence of additional correction plates to the deflection design performance. Considering the direct relationship between coil design and manufacture, Basab. B. Dasgupta, RCA Consumer Electronics, [5] introduces the Fourier analysis technique in describing the winding distributions of a magnetic deflection coil, and thereafter explains the dependence of the generated harmonics on various design parameters.

During the early 1970's, many organisations began developing a specific tool configured to aid the deflection system design process. Many simulation tools emerged to quickly and effectively determine the deflection space within the tube via lengthy numerical calculations. Of consideration at this time was a deflection system with a slot based construction. T. Nakagawa et al, Mitsubishi Electric Corporation, Japan, [7] introduce a simulation tool which allows the calculation of the magnetic field levels, by extrapolation, of a slot product. The three dimensional magnetic field analysis program utilises the surface charge method for analysing the magnetic field generated by a deflection unit. The calculated values were compared with the measured values of tests deflection units and the calculated values for magnetic deflection fields were found to be 2% larger than the measured values. This program was proved to be efficient in designing a slot based product design. In addition Makato Watanabe et al, Sony Corporation, Japan, [8] introduce a computer simulation package which allows small windings to be incorporated into the base deflection coil. The subsequent effect on convergence errors and overall system performance is studied. The majority of developed computer system design aids therefore calculate the magnetic field of the deflection unit and the associated trajectories of the electron beams, to optimize the winding distribution.

The overall design performance of a deflection system is discussed by M. Watanabe et al, Hitachi, Ltd., [6] considering the calculations required to achieve field curvature,

astigmatism, distortion and misconvergence of a CRT electron beam from the deflection field strengths.

Philips, Eindhoven documented in 1987, [9] a design for an electromagnetic deflection unit wound directly onto the plastic separator support. Both the vertical and horizontal coils are wound around the plastic separator, the first set for line deflection directly wound on the inside of the support whose turns each run through the radial grooves in the flanges. The second set for the frame deflection are directly wound onto the support, where the turns run through the radial grooves in the flange.

Considering slot winding as applied to the design of CRT deflection coils, Matsushita Electron Corporation, Osaka, Japan [10] document a patent detailing a slot wound product, where both the horizontal and vertical coils are wound into slots arranged onto the plastic separator. A pincushion free system (refers to raster distortion) achieved for a 107cm 110 degree product requiring coma correction and two multipole coils to achieve further convergence performance levels. M. Ide et al., Kumamoto Electronic Components Div., considers the design of a slot wound deflection unit. They also adopt a system design where both the horizontal and vertical coils are slot wound and are able to achieve an optimized design and overall performance stability.

A further study documented by Murata details winding the frame coils in slots [11]. Plastic end sections are added onto both ends of the yoke ring and the wire is wound into these grooves. This method of manufacture can potentially impact upon the spread of the winding wire, particularly at high winding speeds around the yoke ring.

Much effort appears directed into defining an effective method of calculating the magnetic field strengths using computer techniques. Much work defines the effects which specific components within the system have upon the overall performance, components such as yoke rings, plates, magnets, etc. It is clear that good correlation between the predicted performance and the actual performance achieved from hardware prototypes is

determined. However, many state that within the complete design cycle, the software tool is used as one important step in the design process and is not considered to be an isolated design procedure, meeting all design criteria. Other design activities are required such as hardware modification and validation to fully optimize the product design.

Philips have invested greatly in developing a simulation tool specifically to aid the deflection unit design process. DUCAD, the simulation package, was evolved to allow the electron-optical designer to influence the design characteristics and behaviour via the multipole Fourier theory. This methodology allows the generated magnetic strength of a coil to be directly related to the winding process required for coil manufacture. This allows the designer to manipulate the design and its overall generated performance in a realistic and practical framework of design for manufacture.

3. CHAPTER THREE

Theory of Deflection Systems

3.1. Introduction

To accurately and precisely design a deflection system requires electro-optical and electromagnetic design techniques. The wire distribution of the deflection coils plus the incorporation of any correction components, magnetic yoke rings, magnets, etc. must be considered to assess their impact upon the overall magnetic fields generated, and thereafter upon the systems' performance.

It is important therefore to understand the function of each design component and the influence created upon the magnetic field generated. The initial objective in any deflection design study must be the full optimisation of individual vertical and horizontal deflection coil designs. Most designs however demand additional correction methods, such as plates and magnets to achieve the required performance levels due to the inherent limitations determined by both the winding technology and manufacturing processes.

As described previously, for a CRT system three electron beams are passed through the deflection systems' magnetic field to create the T.V. picture. To determine the overall 'performance' of a deflection system, it is necessary to consider the electron beam trajectories as they traverse through the deflection volume created by the deflection unit. (The deflection volume is the area which influences the electron trajectories due to the magnetic fields created by the deflection system). The path of the three electron beams determine their resultant spatial position on the display screen and using this information, the relationship between the magnetic field generated, its influence upon the electron trajectories and thereafter the systems' performance indicated visually on the screen can be assessed. When considering the main physical concepts relating to magnetic field deflection as generated by a deflection system, it is important to understand the theoretical basics.

3.1.1. Deflection in a Uniform Magnetic Field

A magnetic field can be described as a condition of space caused by the presence of (electric) currents or by any magnetic substance, characterised by a magnitude (field strength) and a magnetic field direction at any point in space.[17] A magnetic field can be depicted by multipole diagrams which show the shape and direction of the magnetic field.

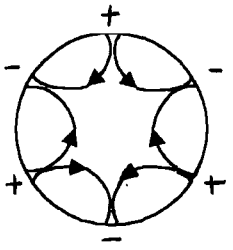

Diagram 17: Representation of a Multipole Diagram

Multipole drawings represent the magnetic scalar potential over a circle, concentric with the axis of the multipole. Characteristic field lines are drawn, depicting the flux lines running from + to -.

Magnetic fields are generated in this discussed application by the following sources; electric currents driven through the horizontal and vertical deflection coils; induced magnetisation of materials such as yoke rings (ferromagnetic); soft plasto-ferrite magnetic field spoilers and permanent magnets.

A highly idealised magnetic deflection field configuration consists of an uniform field transverse to the axis of the undeflected electron beams existing over a finite volume of space. In this uniform field region the path of the electrons are circular leaving the magnetic region at a tangent to the circle at its end.

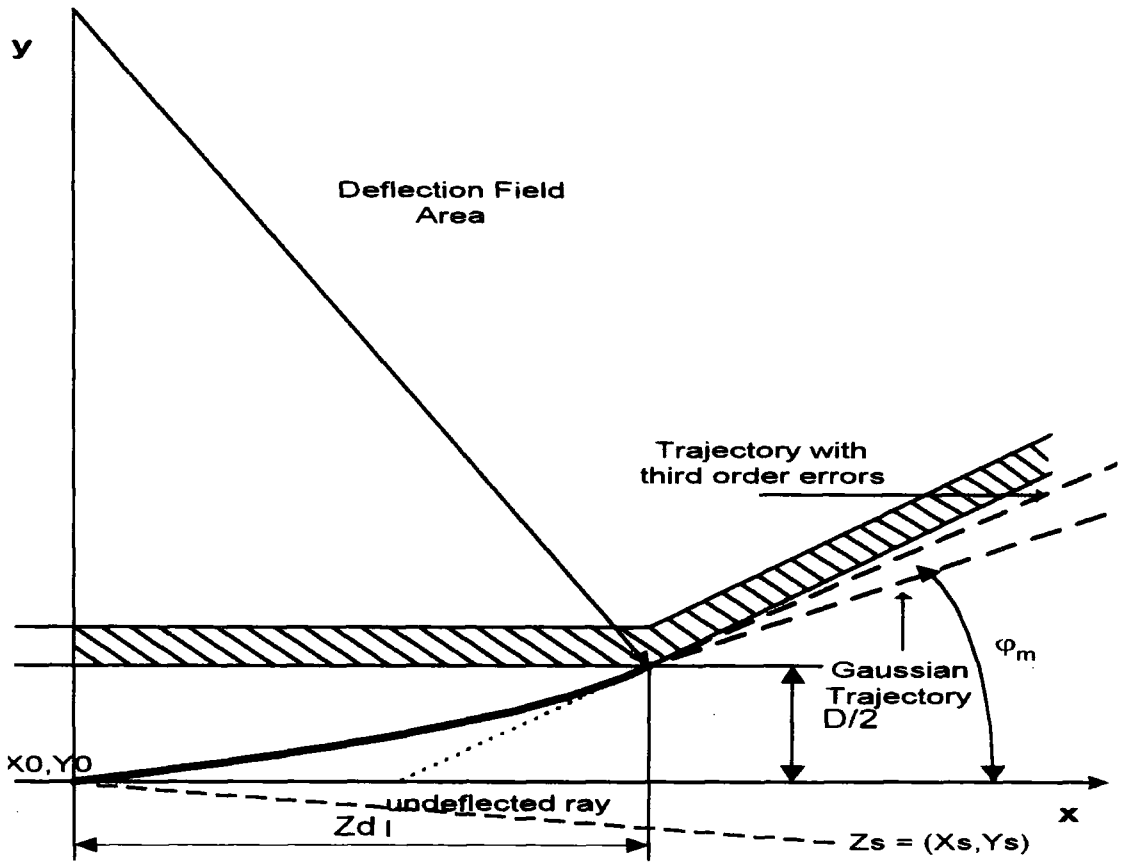

Diagram 18: Deflection of an Electron Beam in an Uniform Magnetic Field

The position and direction of travel of the electrons in the deflection space is determined with reference to screen position (X_s, Y_s), the point at which the undeflected electron path intersects with the screen. By continuing the undeflected electron path to intersection with the screen at point Z = Zs, the following beam parameters are defined, X_s, Y_s, $X_s = dX/dZ$, $Y_s = dY/dZ$. If the deflection field and the beam parameters are given, the electron path will be fixed. The equation of motion for the electron is called the *Gaussian Path* in the deflection space.

Gaussian deflection is defined as the first correction to the landing point of the undeflected electron beam rays and as such the electrons are only very slightly deflected on entering the deflection space parallel to the x-axis. On leaving the deflection space the electron path becomes straight. The 'deflection point' is the point from where the electron beams leave the region apparently in a straight line, the point

of intersection with the z-axis called the 'Gaussian deflection point' (z_d). If considering the deflection system in T.V. applications, the requirement for the deflection point and the exposure point of the green gun to coincide is crucial to obtaining maximum purity levels. This principle is now considered theoretically.

An angle of deflection ϕ is formed between this tangent and the undeflected electron beam; their point of intersection defined as the deflection point. (z_d). The deflection angle ϕ can be expressed as:

$$\sin \phi = l \, . \, |B| \, \sqrt{(e / 2 E_b m)}$$

where l length of the uniform field region

B magnetic flux density vector

e and m charge and mass of an electron

E_b CRT accelerating anode potential , with respect to the cathode.

The magnetic flux density **B** is proportional to the deflection current I and to the number of turns N. (The inductance L of the deflection coil is proportional to N squared.)

Small angle deflection theory is based on a power series expansion around the axis of the CRT of the equation of motion of an electron beam in an electromagnetic field. This equation is given as:

$$m \, dv/dt = e \, . \, \mathbf{E} + e (v \times \mathbf{B})$$

where v the electron velocity at the time t

E the electric field

m, e the mass and charge of an electron

B Magnetic Flux Density Vector.

The electron beam trajectory can be calculated by solving the second order simultaneous differential equations which are derived from Eulers equations using Fermats principle of optics. This principle is equivalent to *Newton's equation of motion by the Lorenzian force.* Considering horizontal X direction deflection only, the equations of motion can be written as

$$d^2 X/ dt^2 = e \mu_o / m \; v \; \mathbf{H}_y (Z)$$

$$d^2Y/dt^2 = 0 ; \quad d^2Z/ dt^2 = 0$$

Then $dX/dt = dX/dZ \; . \; dZ/dt = v \; dX/dZ$

$$d^2X/dt^2 = d/dt \; (dX/dt) = d/dZ \; (v \; dX/dZ) \; . \; dZ/dt$$

$$= v^2 \; d^2X/dZ^2$$

$$\Rightarrow \quad d^2X/ dZ^2 = k \; \mathbf{Hy} \; (Z)$$

(where $k = e \mu_o / m \; v = \mu_o \sqrt{(e/(2m \; U_o)}$

U_o defines the electrostatic potential with respect to the cathode

μ_o defines the permeability of vacuum).

This path equation may be solved by integration to give the Gaussian slope as follows:

$$X_g (Z) = \int_{Z_m}^{Z} d^2X_g (\xi) / \; d \xi^{\, 2} \; d \xi \; + X_s$$

$$= k \int_{Z_m}^{Z} \mathbf{Hy} (\xi) \, d \xi \; + \; X_s$$

where Z_m is the start of the deflection space and ξ an integration variable. Since we assume that no deflection occurs in the gun space, we may state,

$$X_g(Z) = k \int_{-\infty}^{Z} \mathbf{Hy}(\xi)\, d\xi + X_s$$

The Gaussian slope on the screen ($Z = Z_s$) is

$$X_{gs} = k \int_{-\infty}^{Zs} \mathbf{Hy}(Z)\, dZ + X_s$$

For Gaussian deflection on the screen it then applies (by replacing the integration variable by Z), that X_{gs}, the line deflection

$$X_{gs} = k \int_{-\infty}^{Zs} (Z_s - Z)\, \mathbf{Hy}(Z)\, dZ + X_s$$

Hence, the Gaussian deflection is exactly linear with magnetic field strength. As magnetic field strength is linear with the current through the coil, the Gaussian deflection will be linear with the current and can consequently be used as a measure of the amplitude of the deflection (metres) instead of the current (amps). Refer to Appendix A.

In practise actual deflection units do not generate perfectly uniform magnetic fields, nor do they provide a field having discrete boundaries. However, the above derivation gives an approximation to the deflection system performance.

3.1.2. Application to CRT Deflection Systems

When considering a CRT deflection system, magnetic deflection fields are generated by the electric currents in the horizontal and vertical coils situated around the neck of the CRT. The following schematic diagram shows the coils and their nominal position with respect to the utilized co-ordinate system. In order to accomplish symmetrical deflection in two perpendicular directions, each pair of coils requires symmetry in shape as well as in position, and the two coils forming a pair must be fed with the same current.

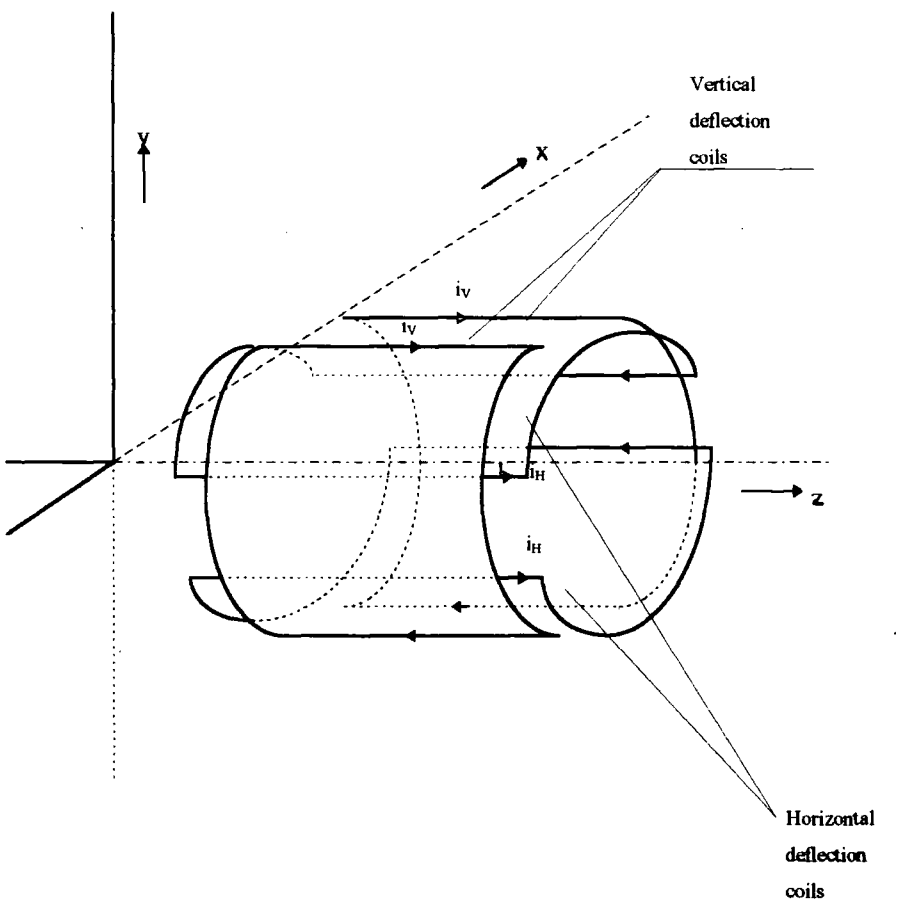

Diagram 19: Schematic Representation of a Deflection Unit.
The current I_H produces a deflection field in the positive y direction, the current I_V gives a field in the positive x direction.

Within the practical constraints of the practised winding methods and manufacturing processes this exact symmetry is not possible. As a result certain asymmetries in

picture performance occur due to the shape/position of the two coils forming the pair plus any additional components necessary to generate the required field distribution. Positional errors in deflection system fabrication may cause the incoincidence of the planes of symmetry of the horizontal and vertical deflection fields, generating further sources of errors.

The presence of the earth's magnetic field or the fringe area of adjacent focusing fields may produce further unwanted effects. Due to these inherent errors from the ideal state Gaussian deflection theory utilises the electron beam expressions and creates first and subsequently higher order approximations. If the solutions to these higher order equations deviate from the Gaussian deflection, the differences are referred to as aberrations of the same order. More detail shall be given to the deflection aberration errors later within this study.

3.2. *Calculation of the Magnetic Field of a Deflection System*

Due to the complicated geometry of the systems horizontal and vertical deflection coils and to the presence of a magnetic yoke material, it is extremely difficult to solve this three-dimensional field problem analytically to obtain the field strength of the magnetic deflection coil system. The three dimensional magnetic field distribution can be computed using the *Biot and Savart Law*, integrating over the current carrying conductor volume. Neglecting the conductor cross-sectional area the Biot and Savart law may be expressed as an integral equation to evaluate analytically certain conductor shapes (straight line and arc, for example). [1] To compute the magnetic field outside the curved conductors, the conductor can be represented as an array of straight line segments and numerical integration can be employed.

[1] $H(r_P) = 1/4\pi \int I\, dr_Q \times \dfrac{(r_p - r_Q)}{|r_p - r_Q|^3}$

where r_p and r_Q denote respectively the position vectors of the field point P, and the variable point Q describing the location of the current carrying conductor, I is the total current carried by the conductor, and dr_Q represents a differential line segment at Q.

To simplify matters, the 3- dimensional current distributions can be replaced by two dimension conduction currents sheets. In this representative model, the unit is assumed to be infinitely long and the magnetic yoke core is rotationally symmetric and of constant permeability ; permeability, μ, refers to the magnetic conductance of the material, where $\mathbf{B} = \mu \mathbf{H}$. Due to the rotational symmetry of the core and deflection coil form, the deflection unit is described in the cylindrical co-ordinate system (R, θ , Z) in which the Z-axis coincides with the yoke axis.

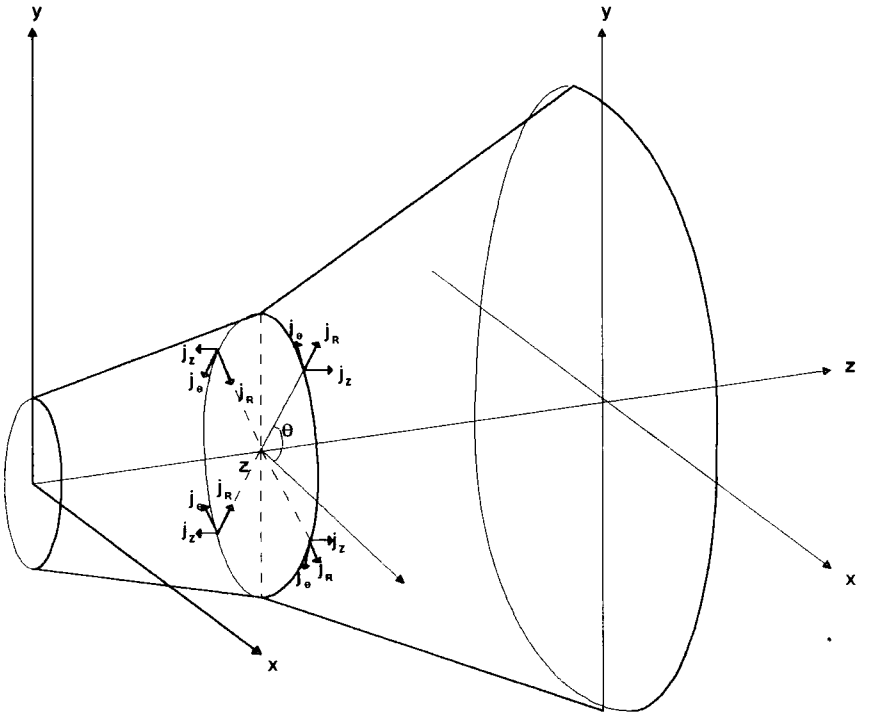

Diagram 20: Four Quadrant Symmetry of a Line Coil

The nominal design system has 2 planes of symmetry and its axis coincides with the picture tube axis, therefore the deflection currents and the generated magnetic field can be sufficiently described in one quadrant. By a suitable choice of the θ- origin (x-axis for line (horizontal) coils and Y-axis for frame (vertical) coils), a Fourier expansion of the components of current density vector **j** on the circle (R, Z) may be expressed.

Knowing the magnetic field distribution the electrical performance per unit length of the yoke may be determined, and thereafter the inductance, the stored magnetic

energy, the hysteresis losses, etc., of the deflection coils. In addition, the electron optical influences of differing design parameters and alterations can also be assessed.

3.3. Calculation of the Magnetic Field of a Saddle Shaped Line Coil

The magnetic field due to a saddle shaped line coil can be calculated by considering the field due to the main body of the deflection system, which is assumed to be a current sheet with a certain surface current density distribution determined by the actual angular distribution of the wires in the coils.

The main deflecting part of the unit a current sheet symmetric about the Z-axis has a profile similar to the profile of the neck of the cathode ray tube, and is expressed by a polynomial function in Z. The surface current density on the sheet is

$\mathbf{j}\,(R_o\,,\,\theta\,,\,Z)$ $\mathbf{a_k}$ has a magnitude which can be expressed as a Fourier series:

$$\mathbf{j}\,(R_o,\,\theta,\,Z) = \frac{\mathbf{I}\lambda(\theta,Z)}{R_0(Z)} = \frac{\mathbf{I}}{R_0(Z)_m} \sum_{m=1,3,5,\ldots} f_m(Z)\cos m\theta$$

$\mathbf{I}$ is the current in each turn of the coil and $\lambda\, d\theta$ is the number of turns passing between the angles θ and $\theta + d\theta$ at a cross section located at Z. The direction of the current density expressed by the unit vector $\mathbf{a_k}$ is assumed to be given by

$$\mathbf{a_k} = \frac{(\cos\theta R_o' a_x + \sin\theta R_o' a_y + a_z)}{(1+R_o)^{1/2}}$$

where a_X, a_Y, a_Z, are unit vectors along the x, y, z axes. (A prime indicates the derivative with respect to Z.) Physically this signifies the current flowing along the profile of the coil sheet in the (R, Z) plane and along the radial lines in the (x, y)

planes. The magnetic field at an arbitrary point (R , θ , Z) due to this current sheet can be obtained by applying the *Biot-Savart Law*,

$$\mathbf{H}\ (R,\ \theta\ ,Z) \quad = \quad \int \frac{\mathbf{j}\,(R_0, \theta_0, Z_0)}{4\pi R^3} \times \mathbf{R}\ ds$$

ds is an element of surface area located at (R_o, θ_o, Z_o) on the current sheet, and given by

$$ds \quad = \quad R_0\left(1 + R_0`(Z_0)^2\right)^{1/2}\, d\theta_0 dZ_0$$

$$\mathbf{R} \quad = \quad \left(R\cos\theta - R_0\cos\theta_0\right)a_x + \left(R\sin\theta - R_0\sin\theta_0\right)a_y + \left(Z - Z_0\right)a_z$$

$$\mathbf{R}^2 \quad = \quad R^2 + R^2 - 2RR_0\cos\left(\theta - \theta_0\right) + \left(Z - Z_0\right)^2$$

The cylindrical components of **H** may be calculated by extending the Z_o integrals from the rear-end to the front-end of the deflection unit. The magnetic field components can be given as follows:

$$\mathbf{H_R}(\ R,\ \theta\ ,Z\ ) = \sum_{n\ =\ 1,3,\ldots} H R^n\ (R,Z)\ \sin(n\,\theta\ )$$

$$\mathbf{H_\theta}\ (\ R,\ \theta\ ,Z\ ) = \sum_{n\ =\ 1,3,\ldots} H \theta^n\ (R,Z)\cos(n\,\theta\ )$$

$$\mathbf{H_z}(\ R,\ \theta\ ,Z\ ) = \sum_{n\ =\ 1,3,\ldots} H Z^n\ (R,Z)\ \sin(n\,\theta\ )$$

The use of Fourier transform techniques to calculate the Fourier expansion of a magnetic field as created by three dimensional wire distributions is inherent in the Biot and Savart method where each magnetic field components (wire distribution, correction component parts), must be analysed in small segment sample points, at each point of interest in the (R, θ, Z) region. [2]

The current distribution can be expanded however as a Fourier series defining one or more rotationally symmetric current sheets allowing calculation effort to be reduced. The matrix relation between the Fourier components of the current density and those of the field can then be assessed. Employing the Fourier transformation technique allows analytical expressions for each field harmonic to be developed. This produces data which is in a form more easily understood, enabling systems design criteria to be defined as a direct and more understandable influence upon the harmonic content of the winding distributions, and subsequently upon the overall performance of the deflection coil system.

3.4. Calculation of the Magnetisation Field of a Deflection System due to the Introduction of a Ferromagnetic Object.

The magnetic field produced by a ferromagnetic object in the presence of conduction current sheets may be determined using differential or integral methods. Differential methods require the deflection space to be discretised into small segments whereas, integral methods permit a limitation on the discretisation to the permeable region only. This avoids imposing 'far-field' boundary conditions as required in differential methods.

Since the ferrite core is assumed to have infinite permeability the magnetic field inside the core is identically zero.

---

[2] The deflection magnetic scalar potential on the circle (R, Z) is given by
$\phi (R, \theta, Z) = \sum_{n = 1,3....} \phi n (R, Z) \sin (n \theta)$

If we consider the effect of the core, (our discussions up to now have not included this), this changes the magnetic field generated substantially. The relative permeability of the typical core material is quite high, of the order of 1000, and can be assumed to be infinity for all practical purposes.

An accurate calculation of the magnetic field can be carried out by assuming infinite permeability of these objects. Under this assumption, the boundary of each magnetic material is an equipotential surface and the application of the integral form of *Coulombs Law* yields the scalar potential distribution ϕ_m that satisfies the *Fredholm Integral Equation*:

$$\phi_i = \frac{1}{4\pi} \int_{S_m} \frac{\sigma_m(r`)dS`}{|r - r`|} + \phi_c(r)$$

$\sigma_m(r_Q)$ is the surface magnetic charge density at Q, and S_m is the total surface of the magnetic material, ϕ_c is the scalar potential in current free region, r and r` are position vectors of the field and magnetisation points respectively.

Solutions to Fredholm's integral equation require knowledge of the scalar potential of the incident field on the surface of all magnetic objects. In addition, the surface charge density must be consistent with requirements imposed by the conservation of magnetic charges. This relation must be satisfied separately on each permeable object boundary. If there are a total of M different permeable objects, the Fredholm integral equation generates M auxiliary equations that must be solved in conjunction with equation

$$\int_{Si} \sigma_m(r`)\, dS` = 0$$

in order to obtain the magnetic potentials and charge distributions on all the magnetic objects surfaces.

By a suitable choice of the θ-origin and due to the symmetry of the deflection field, the Fourier expansion of the surface charge density σ_m on the circle (R_Q, Z_Q) can be written as

$$\sigma_m (R_Q , \theta_Q , Z_Q) = \sum_{n = 1,3,...} \sigma_{m,n} (R_Q, Z_Q) \sin (n \theta_Q)$$

We obtain, by Fourier expansion, and integration over θ_Q , the magnetisation scalar potential ϕ_m at point P situated on the core surface created by the surface magnetic charge density σ_m

$$\phi_m (R_p , \theta_p , Z_p) = \sum_{n = 1,3,...} \phi_{m,n} (R_p, Z_p) \sin (n \theta_p)$$

The Fourier expansion of the core magnetisation potential can thus be deduced directly from the Fourier expansion of its surface magnetic charge density σ_m. If the deflection systems core is the only permeable object present in the configuration, separation of variables will reduce the Fredholm integral equation to an integral equation involving separate equivalent magnetic charge distributions for each winding harmonic.

The following diagrams, 21 and 22, depict the influence the yoke ring has upon the magnetic fields generated by the line and frame coils respectively. Note that the line field is short-circuited by the yoke ring and the frame field has an equal proportion which is stray.

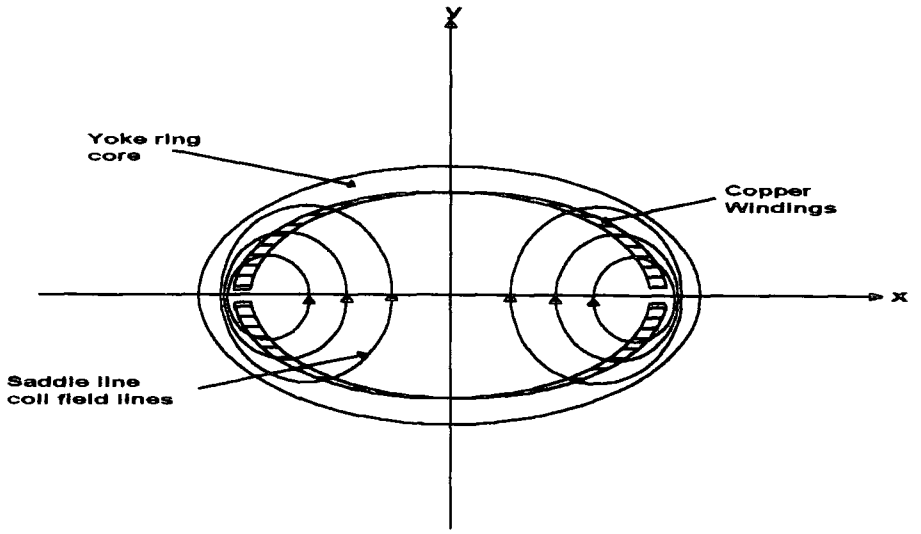

Diagram 21: Line Coil Magnetic Field Lines

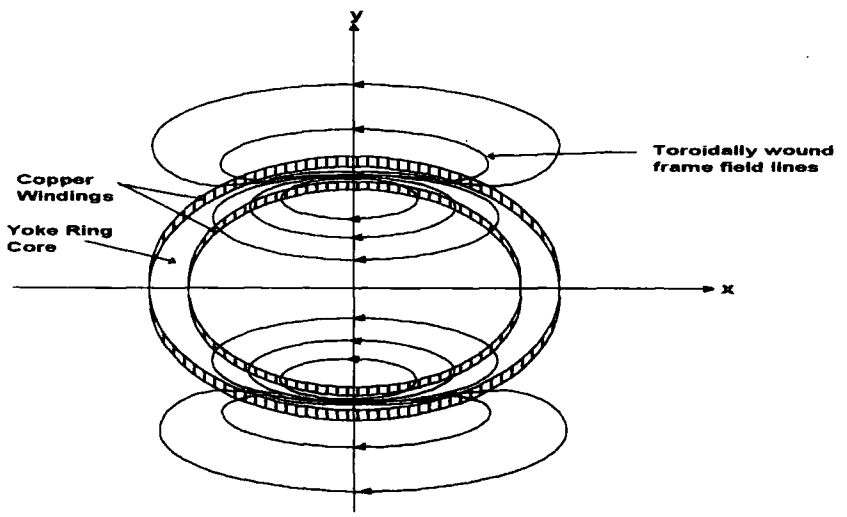

Diagram 22: Frame Coil Magnetic Field Lines

3.5. Deflection System with one or more Magnetic Components

The deflection unit system may contain one or more magnetic components and to calculate their contribution the total field is described as the superposition of the incident field created by the currents and the magnetisation field created by all the magnetic bodies present. The incident field can be calculated using the following equation.

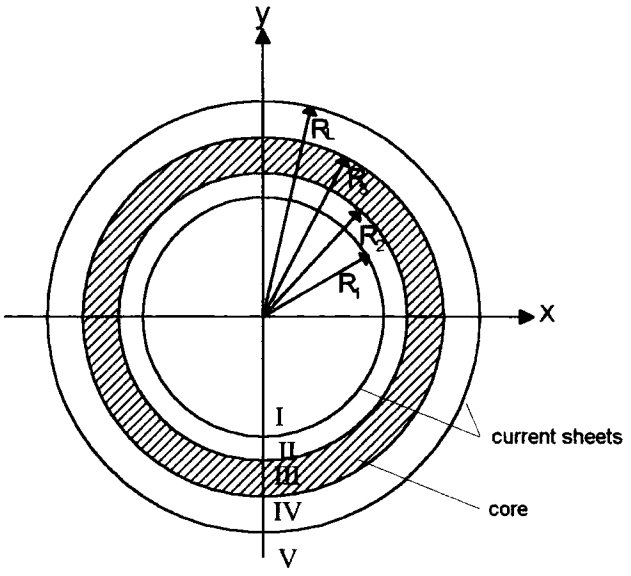

Diagram 23: Two Dimensional Model of a Deflection Unit consisting of an Annular Core of radii R_2 and R_3, and 2 Current Sheets of Radii R_1 and R_4.

$$\phi\ (R, \theta) \quad = \quad \sum_{n=1,3,\ldots} -\frac{i}{2n}\left(\frac{R_1}{R}\right)^n \sin(n\theta) \qquad : \quad R > R_1$$

Provided the permeability is constant, the magnetisation of each permeable body can be modelled by a simple layer distribution of surface magnetic charges. These charges can be calculated using the boundary conditions expressed on the surface of each magnetised body. The magnetisation field of the core is created by two layers of magnetic charge densities σ_2 and σ_3, distributed on the circle of radii R_2 and R_3 respectively. The boundary conditions on the surface of the core are the continuity of the tangential component of the field strength and the normal component of magnetic induction.

The magnetic scalar potentials multipole expansion of the circle (R, Z) is given by

$$\phi\ (R, \theta, Z) \quad = \quad \sum_{n = 1,3,\ldots} \phi_n (R, Z)\ \sin (n\theta).$$

where ϕ_n (R, Z) is the amplitude of the potential harmonic *n* on the circle (R, Z).

The magnetisation scalar potential ϕ_m created by a charge density σ_m (σ_2 or σ_3) distributed on the circle of radius R_m (R_2 or R_3) must remain finite throughout the two dimensional space, and satisfy

$$\phi_m(R, \theta) = \sum_{n=1,3,\ldots} \left[\frac{\sigma_{m,n} R_m}{2n}\right]\left(\frac{R}{R_m}\right)^n \sin(n\theta) \quad : \quad R < R_m$$

$$\phi_m(R, \theta) = \sum_{n=1,3,\ldots} \left[\frac{\sigma_{m,n} R_m}{2n}\right]\left(\frac{R_m}{R}\right)^n \sin(n\theta) \quad : \quad R > R_m$$

with $\sigma_m(\theta) = \sum_{n=1,3,\ldots} \sigma_{m,n} \sin(n\theta)$

ϕ_m is obtained by satisfying the boundary conditions at the surface of the core. The magnetisation potential can also be obtained via the magnetic equivalent of *Amperes Theorem*. The scalar magnetic potential, mostly used to calculate magnetic deflection field, can only be defined in current-free regions. This explains why in these calculations, deflection coils are reduced to current sheets of infinitesimal thickness. The vector potential of the two dimensional deflection model, has only one component normal to the plane considered. Using the vector potential allows the thickness of the deflection coils to be considered, and to evaluate the field inside the deflection coil itself allowing an estimation of the dynamic losses (eddy currents) associated with the system.[15]

3.5.1. Fourier Expansion of the Deflection Coil Field

By adding the contributions of all the magnetic conductors of the deflection system, we can obtain the Fourier expansion for the resulting deflection field. Because of the four-quadrant symmetry of the deflection coil, the first quadrant conductors are only detailed. This yields

$$\mathbf{H}\ (R_P,\ \theta_P,\ Z_P) = \frac{1}{\pi^2}\sum_i \int_{C_i} \frac{ds}{D^3}\sum (e_r, e_\theta, e_z)\begin{bmatrix} h_{R,n}\sin(n\theta_P) \\ h_{\theta,n}\cos(n\theta_P) \\ h_{Z,n}\sin(n\theta_P) \end{bmatrix}$$

where e_r, e_θ, e_z are unit vectors along the R, θ, and Z axes at the field point defined at R_p. C_i denotes the curve representing the location of conductor i, s denotes the parameter describing the current point location. The summation is done over all conductors situated in the first quadrant.

(note: $D^2 = (R_P + R_Q)^2 + (Z_P - Z_Q)^2$).

3.6. *Harmonics Of Winding*

The current distribution in the horizontal and the vertical coils are expanded as Fourier series in polar angle θ about the yoke axis. Knowing the n^{th} Fourier coefficients of the currents, the n^{th} coefficients of the magnetic field components and hence the total magnetic field can be determined. The harmonic coefficients of the coils wire distribution can be calculated by means of *Fourier Analysis*, allowing examination of the cross-sectional profile thickness for the proposed coil design.

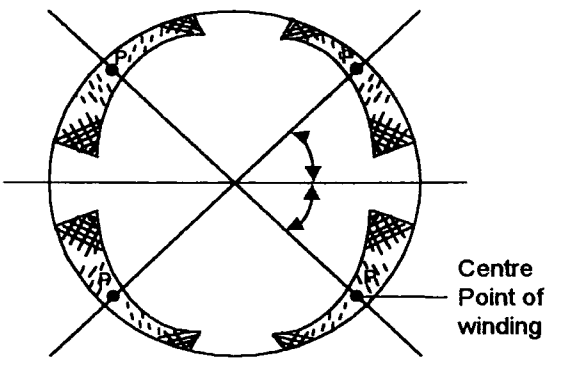

Diagram 24: Cross-Sectional View of a Toroidal Frame Coil.
The angle θ determines the shape of the resultant magnetic field.

If $f(\theta)\, d\theta$ is the number of ampere-turns between the angles θ and $\theta + d\theta$ at an arbitrary cross-section of a planar wound vertical coil, θ the polar angle measured from the horizontal axis, the Fourier expansion for $f(\theta)$ can be derived;

$$f(\theta) = \sum f_m \sin m\theta \qquad m = 1,3,5,...$$

Between the modulation levels, the wire density assumed to vary continuously with θ, will be defined. The current density vector $\mathbf{K}(R, \theta, Z)$ can be deduced using the representation (R(s), Z(s)) of the current sheet and the winding density $N_w(\theta, s)$.
If $\mathbf{I}$ is the current flowing through each winding, the relation
$R\, K_R(R, \theta, Z) = N_w(\theta, s)\, \mathbf{I} R'$; $R\, K_Z(R, \theta, Z) = N_w(\theta, s)\, \mathbf{I} Z'$
(Prime indicates derivative with respect to s, Nw expressed in turns per radian)

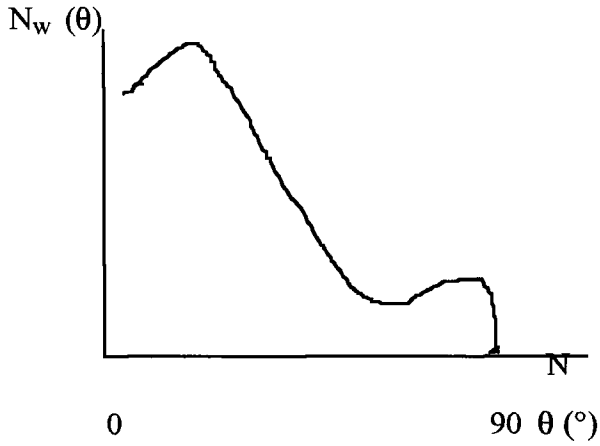

Diagram 25: Wire Density at various Modulation Levels - Continuous Function of the angle.

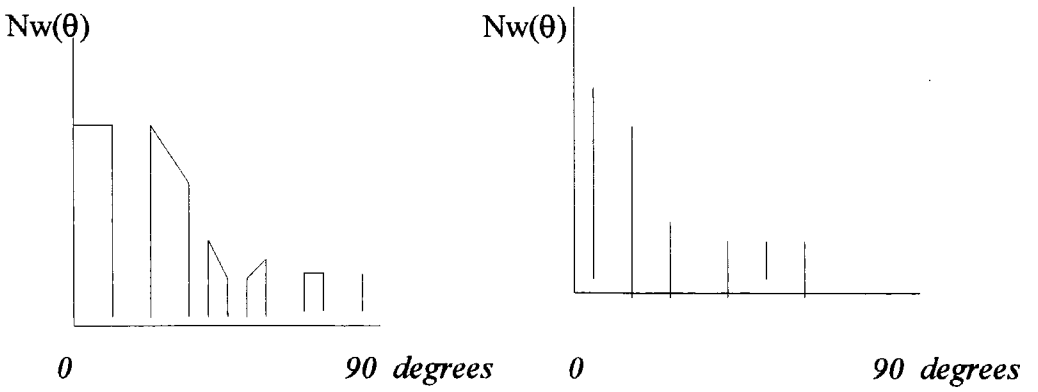

Diagram 26: Wire Density at various Modulation Levels - Discrete Function of the angle when the wires are grouped in slots.

The wire density is supposed to a) vary linearly within each slot, or b) is represented by Dirac's delta function, when we neglect slot width.

3.6.1. Description of a Deflection Coil

The winding distribution of a deflection coil can be defined as a revolving surface, where a certain number of cross sections called 'design modulation levels' are defined. The thickness of the coil is negligible, however by expressing the wire density at each modulation level in terms of the polar angle θ, and simulating the winding process between the different cross-sections, the deflection coils configuration can be defined. This can be formulated for continuous and discrete current distributions.

The current carrying conductors are grouped into slots at defined angular positions at the modulation levels. The array of slots may start at some non-zero position and may extend to $\pi/2$. Every wire package is reduced to its centre line and is described in cylindrical co-ordinates.

It is important to be able to solve the direct problem of defining the wire distribution of a coil in angular harmonics as well as the inverse problem of constructing the wire distribution from its Fourier series. The solution of this direct problem is a straight forward Fourier series analysis, however, in contrast, the inverse problem is complicated as the solution is limited to an 'windable' space, determined by the winding technology and electrical specifications of the deflection coil.

Excluding current reversals between 0 and $\pi / 2$, the problem of synthesis is formulated to calculate the positive wire distribution $N_w(\theta , s)$ is defined

$$N_w (\theta , s) = \sum_{n = 1,3,...} a_n (s) \cos (n \theta)$$

where

$$a_n (s) = 4/ \pi \int_0^{\pi/2} N_w (\theta , s) \cos (n \theta) d\theta$$

The continuous function $N_w (\theta , s)$, can be determined for both continuous and discrete wire distributions. Note that for the discrete wire distribution the Fourier series expansion is calculated for each of the slots comprising the winding pattern.

It is important to note that for design purposes other conditions are imposed upon the overall wire density. For example, in order to ensure proper tensioning and feeding of the wires during the winding process, or to avoid ringing problems between line and frame coils, is may be desirable to consider windings whose densities fall within definite limits. Technological constraints can also be imposed which require careful consideration.

3.7. Deflection Aberrations

The differences which occur between the originally transmitted picture and the picture reproduced on the T.V. screen are deflection aberrations, defined such that if each aberration was present alone it would describe a characteristic effect.

There are two types of *geometrical aberrations*, firstly, non-linearity of the deflection, due to the flatness of the screen. This can be separately observed when only one deflection field is present. A pattern of originally equidistant lines appears on the screen compressed at the centre and expanded at the edges. This error can be eliminated by modifying the currents through the deflection coils to be slightly S-shaped instead of a pure saw-tooth. The second geometric aberration is raster distortion, which is observed when both deflection fields are operating simultaneously, and is due to the flatness of the screen or to the shape of the deflection field.

Spot distortion may also result due to the finite cross section of the electron beams. These distortions are known as astigmatism, curvature of the field and coma errors. Astigmatism occurs when the deflection field affects the focus of the electrons in different axial planes and axial distances and the spot on the screen of a rotationally-symmetric beam becomes elliptical. Astigmatism may be divided into isotropic astigmatism, caused by line or frame fields separately and anisotropic astigmatism which can only occur if both fields are operating simultaneously.

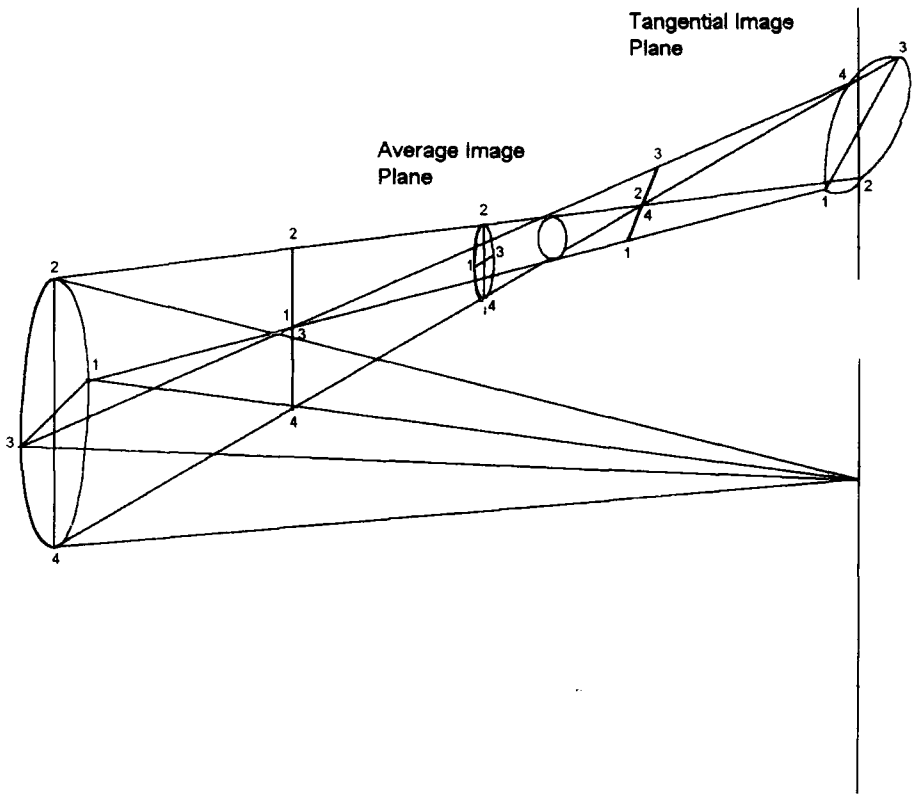

Diagram 27: Aberration due to Astigmatism and Curvature Distortion of the Spot

The image plane on the screen will have its spot horizontally in focus. Self convergence on the three in-line beams will occur maintaining each beam horizontally in focus. But the vertical images converges behind the screen, resulting in an overfocused vertical beam images as depicted.

If the deflection field focuses points off the axis on planes different from those on the axis, the focused image of a flat object will be on a curved surface whose curvature will vary with the field shape. The image will appear sharp all over only where the screen has the correct curvature.

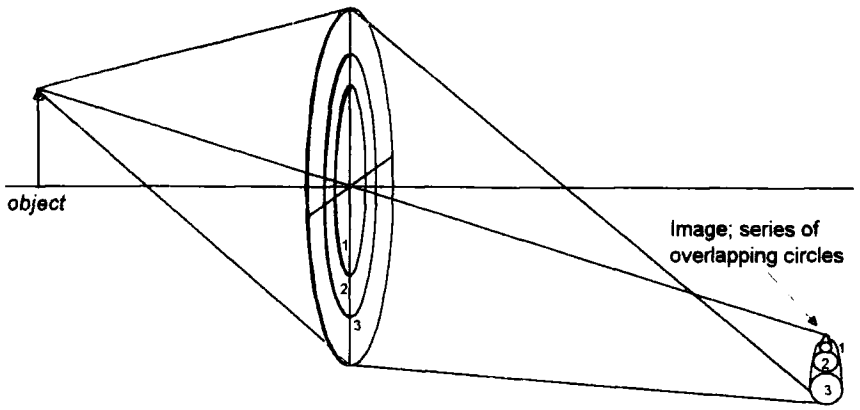

Diagram 28: Coma Distortion

Contrary to the ellipses obtained in the case of astigmatism errors, the ellipses obtained for coma errors are all on one side. The edge beams are situated towards one side, forming a 'haze'.

Coma distortion gives a comet-like appearance to the electron beam spot. The rays from the object point close to the axis form an image of that point in the image plane. Rays which come from points off the axis may be brought to another focus in the image plane but the focal length around the ray varies with the height. The intersection of the rays with the screen therefore forms a circle, the centre shifted with respect to the axis. The image consists of a sharp point with a series of overlapping circles increasing in radius with their distance from the axis. Coma distortion is divided into isotropic coma caused by the line and frame coils separately and anisotropic coma observed only when both the line and frame fields are operating simultaneously.

As previously considered, the Gaussian deflection model can be represented by a first order approximation of the electron deflection system. Any higher order approximations produce solutions of third order, etc., which are important in the development of a self-converging deflection system. (A self-converging deflection system is the minimisation of 'spot distortion' by achieving deflection fields of least amount of aberrations via the design of the deflection system). The approach taken in this study correlates the various harmonics and the performance characteristics of the deflection system to achieve an optimised deflection system.

The following theory considers certain categories of error patterns with specific types of coil asymmetry, and includes the even-order terms which are zero for a perfectly symmetric coil, and terms up to the fourth order. Third-order aberration theory is valid for deflection angles up to about 50 degrees. and the fifth order aberration theory is valid up to almost 90 degrees. In modern television sets the CRT's used for deflection angles of 90-110 degrees may be approximated by this theoretical application however corner regions are less reliable.

As established X_{gs} and Y_{gs} (line and frame currents respectively) vary linearly with deflection in the case of Gaussian deflection (ideal case), but screen deflection is not linear with Gaussian deflection. The additional deviations, such as astigmatism and coma effects, are therefore important in order to determine the screen deflections of a deflection system as a function of the Gaussian deflection. The beam parameters X_s, Y_s, X'_s, and Y'_s give the position and slope of the non-deflected beam at the screen, and are all equal to zero when the beam enters the system across the axis.

The principle of deriving raster and non-linearity distortion from screen deflection errors may also be applied to astigmatism and coma aberrations errors. For non-zero beam parameters, astigmatism and coma errors occur. Astigmatism errors are associated with odd-degree terms of the beam parameter, whilst coma errors are associated with even-degree terms of the beam parameters.

Astigmatism terms, such as X_s; Y_s; $X_{s'}$; $Y_{s'}$; X_s^3; $X_s^2 Y_s$; ....

Coma terms, such as X_s^2; Y_s^2; X_s^2; Y_s^2; $X_s^2 Y_s^2$;.....

In third order theory, all terms higher than the third degree in the power series expansion of the equation of motion are neglected and the resultant differences from Gaussian deflection are known as third-order errors. The magnitude of these errors are dependent upon the following; deflection amplitude, beam initial conditions (eccentricity and slope), deflection field distribution, and screen form and position. From the symmetry properties of the deflection field, the power series expansion contains no terms that are of even degree in the currents and the slopes together.

Third order errors are classified according to the powers of the slope of the undeflected beam; *s-distortion*, independent of the slope but proportional to the third power of the deflection currents; *curvature of the field and isotropic astigmatism* proportional to the square of the deflection currents; and *coma* proportional to the deflection current and to the square of the slope. When the beam is deflected in both directions, two additional third order errors occur proportional to the product of the two deflection currents, *raster distortion* and *anisotropic astigmatism.*

Diagram 29 details the geometrical errors of the third order. An 'ideal' rectangle undergoes s-distortion (X_S, Y_S), EW-distortion (ΔX_{EW}) and NS-distortion, (ΔY_{NS}). On account of this s-distortion, X is no longer proportional to Ih, or Y to Iv. In this diagram if ΔX_{EW} and ΔY_{NS} are positive, the distortion is called 'pincushion' and when ΔX or ΔY are negative, the distortion is called 'barrel'.

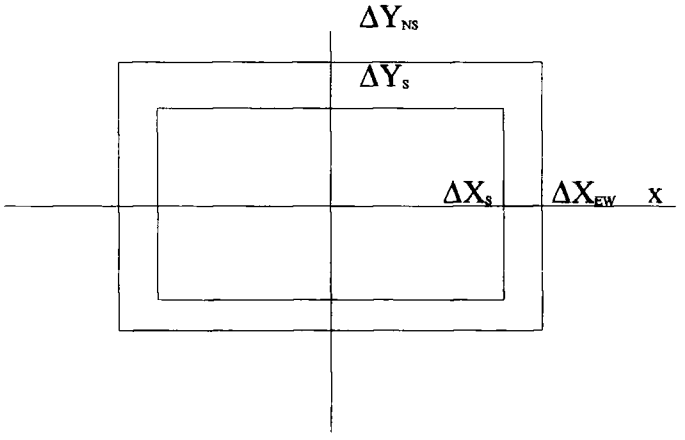

Diagram 29: Geometrical Errors

The green beam defines raster within certain horizontal and vertical bands on the screen as detailed in Diagram 30. If the green beam hits the screen right of a raster line, the distance for the corner point (e.g. F, G, H, J) is called positive raster error. The usual definition of NS raster distortion is:

$$\frac{2\,(a+b)}{FH+GJ} \times 100\%$$

and for EW raster distortion is:

$$\frac{2\,(c + d)}{FG + HJ} \times 100\%$$

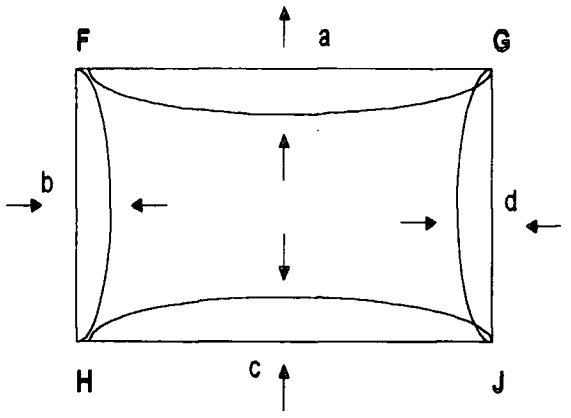

Diagram 30: Raster Distortion

Further approximations of the equations of motion result in a series of contributions known as the fifth order errors. In each term, the powers of the undeflected beam slope and the deflection current add up to five. Terms in which the third or higher powers of the slope occur are discarded because of the fairly small slopes encountered in practise. The fifth order errors are; *geometrical distortion* proportional to the fifth power of the horizontal or vertical deflection currents (S-distortion), or to the fifth-degree products (raster distortion); *astigmatism* proportional to the slope and to the fourth power of the deflection currents (isotropic) or to the fourth degree products (anisotropic); *coma* proportional to the square of the slope and to the third degree products of the two deflection currents.

In self convergent in line CRT's, convergence is achieved by proper design of the deflection unit, gun and additional tube magnetic pole pieces driven by external circuitry that depends on the deflection currents. Self convergence is difficult to achieve. Ordinary deflection systems with homogeneous fields cause three beams to cross and diverge before reaching the screen. If we consider deflection in a dipole field for both horizontal and vertical deflection fields, the intersection of two deflected

beams in either field occur inside the tube, not on the screen. Pure dipole modulation gives severe horizontal astigmatism errors, both for horizontal and vertical deflection. To correct this horizontal deflection, the outer beam must be deflected more strongly than the inner one; the field must be 'pin-cushion' shaped. For vertical deflection, the beams must be deflected more towards the outside in a dipole field, the line field must be 'barrel-shaped'. Utilising the Fourier series composition of multipoles, the superposition of a dipole and a six-pole can produce either pin-cushion or barrel shaped fields dependent upon the direction of the magnetic fields involved as detailed in Diagram 31. Therefore the need for higher order multipole modulation is necessary to determine an acceptable design performance.

This defect is partially corrected by giving the horizontal deflection field a pincushion shape and the vertical field a barrel shape and is achieved by introducing a large third order harmonic component into the angular distribution of the winding current of each axis of deflection. Their associated strengths can be adjusted to remove horizontal red-to-blue mis-convergence at the ends of the x and y axes on the screen.

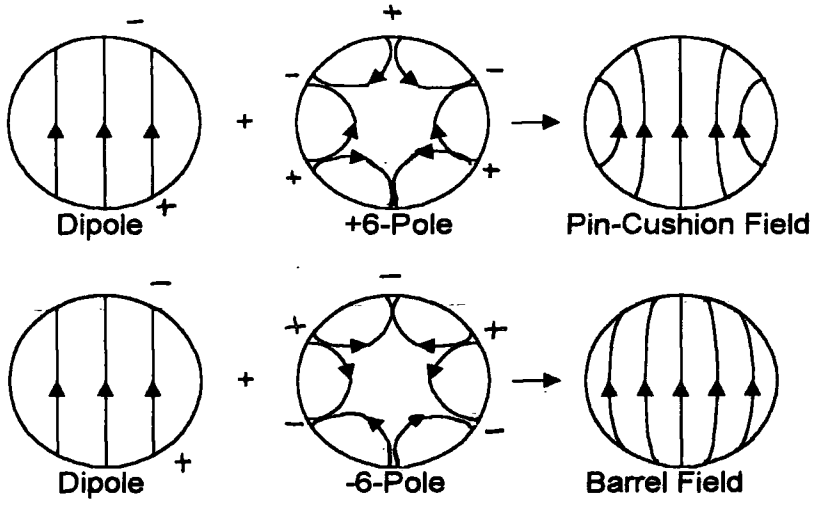

Diagram 31: Superposition of a Dipole and Six-pole to determine Desired Field Shape.

This multipole technique offers two advantages. Firstly, the design can be evolved in steps because a multipole has no effect on deflection errors of lower order than its multiplicity (the principal action of a 2n pole is its influence on nth order errors, all

subsidiary effects are always of higher order.) Pure dipoles therefore produce deflection with resultant third order errors which are corrected by six-pole modulation. The correction of remaining fifth order errors therefore is achieved by ten-pole modulation. Secondly, multipole and wire distributions are related such that if the density of the current perpendicular to the R, Ψ plane is expanded into a Fourier series in Ψ , each harmonic excites the corresponding multipole. To produce a 2n pole with a given coil, we must therefore alternately concentrate and thin out the wire windings along the circumference , with a periodicity of $(2\pi /n.)$

To summarise, the use of six-pole modulation, either to produce pin-cushion or barrel shaped fields are important in minimising the convergence errors which result from a dipole modulated field. Diagram 32 depicts specific areas within a coil where certain convergence aberrations are more sensitive to the effects of six-pole modulations. In the third order aberration theory, this also removes horizontal R-B mis-convergence in the corners, but leaves a vertical R-B mis-convergence due to astigmatism errors. Coma errors are also present, causing the green beam to land inward from the average position of the red and blue spots.

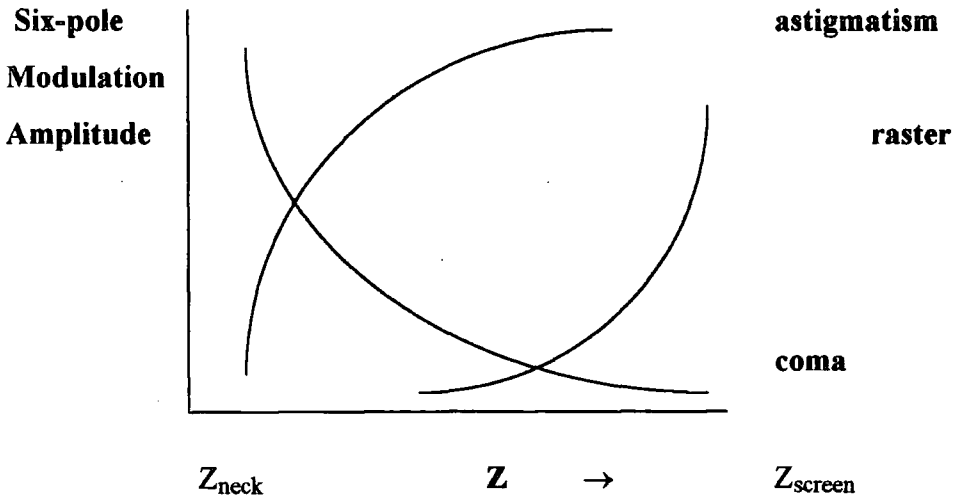

Diagram 32: The Effect of Six-pole Modulation on Convergence/Raster Errors

Astigmatism is affected most strongly by the amount of third order harmonic at the mid-section of the deflection unit while coma is affected most strongly at the entrance, with opposite sign. Consequently, by having an amount of third harmonic in the windings change sign from the front to the rear, both astigmatic and comatic mis-convergence can be removed at the ends of the X and Y axes, although the vertical astigmatic mis-convergence between red and blue remains in the corners. All of these conclusions follow from the third order aberration theory.

To explain in terms of multipole theory, specifically, at each point of the deflection space the field strength of a line multipole varies in proportion to III and the field strength of the frame multipole varies in proportion to IV. This is still true if the field is distorted by the ferrox magnetic yoke ring of the unit. Permanent magnets also effect the multipole distribution, such that a static 2(n+1) pole is equivalent to the sum of a dynamic line 2n-pole and a dynamic frame 2n pole.

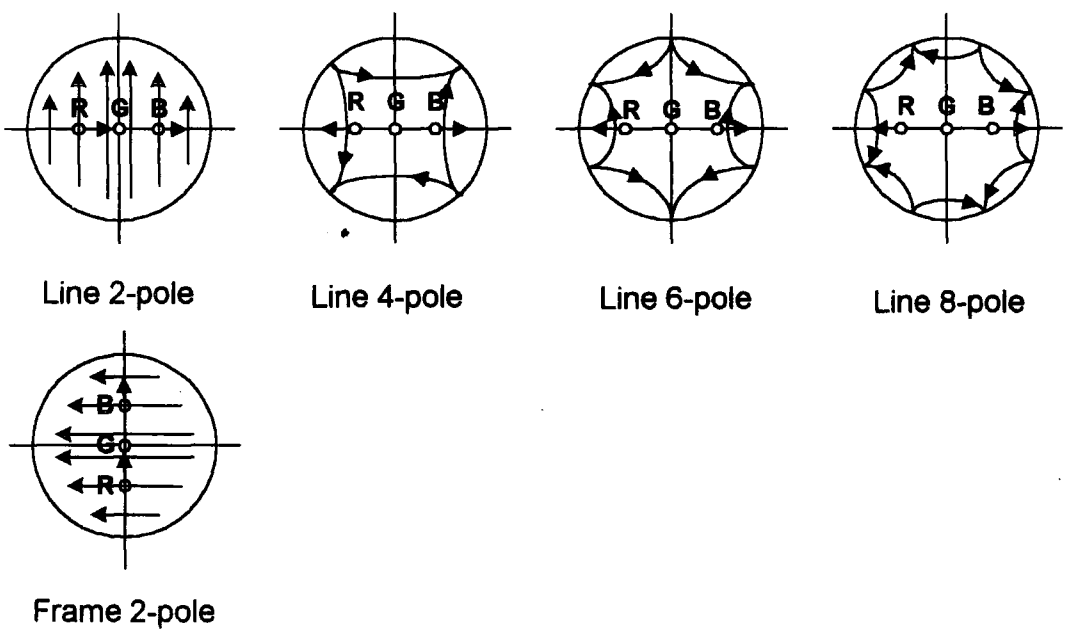

Diagram 33: Multipole Diagram for line dipole, 4-pole, 6-pole and 8-pole. Frame dipole only detailed, note 90 degrees in rotation to line dipole.

The magnetic field variation for the simplest multipoles are line and frame dipoles, four-poles and six-poles. The number of north poles (or periods), n, is the multiplicity of a 2n pole. The dipole **H**1 is the principal component of the line coil field and the dipole **V**1 is the principal component of the frame coil field. The amplitude of each multipole is a function of z; in designing a deflection unit each multipole must maintain the correct amplitude function, to achieve acceptable convergence and raster errors.

For the horizontal astigmatism errors from pure dipole modulation, a positive **H**3 and negative **V**3 are required between the screen side and the centre of the coil. Other effects result. The coma produced by the six-poles at the centre can be corrected by an opposing six-pole near the neck. In a saddle line coil, the wiring towards the screen flare side must therefore be more concentrated around the horizontal plane than the wiring for pure dipoles. At the neck the wiring must be concentrated around the 60 degrees plane from the horizontal.

To consider the design of a saddle/toroidal deflection system, we therefore require to generate specific magnetic field shapes. The toroidal frame coil requires to generate a positive pincushion field at the neck of the coil and a barrel shaped negative field at the screen side of the coil. The resultant frame coma errors are compensated for by more positive six-pole fields at the neck. To achieve this six-pole field requires the wire near the neck of the coil to be concentrated strongly around the vertical plane, and the wiring near the centre concentrated around the 60 degrees plane to the vertical. This is a difficult design to achieve successfully using the practical limitations of toroidal winding.

The software simulation package employed in this thesis specifically concerns this interpretation of magnetic deflection fields to assist in determining a deflection unit design. Computer modelling is increasingly being used in recent years for computing deflection errors generated by a wide angle deflection coil. It is possible therefore to obtain from the series multipole expansion of the deflection fields generated, a Fourier

expansion of the deflection coil field which may be transposed into a winding distribution for coil manufacture. Using this simulation tool therefore, Fourier expansion as applied to multipole theory is employed as a language to manipulate and develop the design solutions.

4. CHAPTER FOUR

DUCAD - Y: Computer Simulation of a Magnetic Deflection System

4.1. History

The computer simulation model employed in this investigation has been developed by Philips, Eindhoven specifically for T.V. deflection system design applications. This computer aided design tool allows the computer simulation of magnetic deflection derived from a deflection unit system. It involves the computation of the deflection field, the calculation of the electron beam trajectories, and the determination of the resultant design performance. The simulation model allows different aspects of the design of a product to be analysed, and for predictions of the performance of the yoke design to be obtained.

4.2. Deflection System Model

This deflection coil CAD program allows accurate modelling of a deflection coil system and the calculation of the magnetic fields created by this system in the region where the electron beams are located. DUCAD-Y (deflection unit CAD program) simulates the above criteria via a standard set of programs.

The magnetic field of a deflection system can be considered as the superposition of the incident fields created by the current distribution, and the magnetisation fields of the core and other permeable objects. The magnetic fields created by the current distribution are directly calculated using the Biot and Savart Law. In determining the magnetisation fields, an integral equation method, based on the surface magnetic charge concept is used.

The deflection system model initially consists of a basic coil geometry, such as line coils, frame coils, and yoke ring components. Any further components in the base design, such as astigmatism plates, coma plates, etc. should be included. Refer to

Diagram 34. The modelling system considers the winding pattern of the deflection coils starting with cross-sectional wire distributions at a finite number of design levels, called modulations levels. Information concerning the winding technology and the deflection coil cross-sectional profiles are required in order to realistically connect the modulation levels and to describe the wire distributions accurately upon a revolving surface.

The current distribution is Fourier-transformed and the magnetic field harmonics are calculated using a boundary integral method. The trajectory of an electron is computed in three-dimensional space considering, for a given deflection current, the magnetic field generated by the yoke and the field correcting components. By specifying the cathode ray tube geometry, the electrons may be trajected at any point (normally at the end of the gun), and thereafter their deflection to a desired location at the screen may be analysed.

The motion of the electron beams through this magnetic field is calculated with the overall performance on the screen being determined. At this stage, an optimization routine is necessary to allow the development of a deflection coil with an improved performance to be achieved.

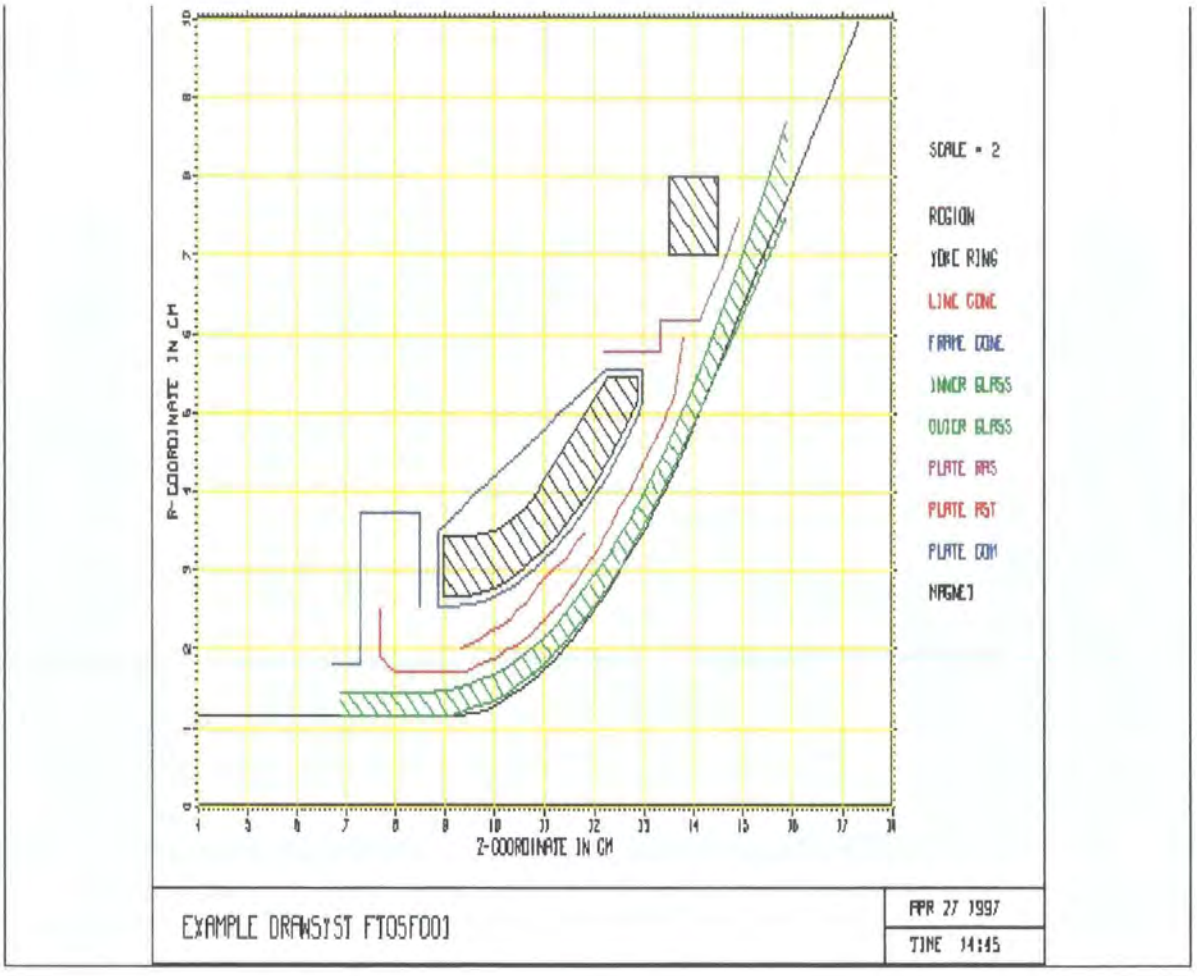

Diagram 34: Plot of Defined Geometry of Deflection Unit and Associated Components in DUCAD-Y

The following components are defined; line cone, frame cone, inner and outer glass profiles, astigmatism, coma and raster plates, and magnets

4.3. Mechanics of Operation

The analytical Fourier integration method calculates the Fourier components of the primary fields of the region, yoke ring and plate(s) from the rotational symmetrical current distribution. The magnetic charge on the surface of the yoke ring is calculated using this primary field and the region field is calculated as the sum of the primary field and the secondary field resulting from the yoke ring.

In DUCAD -Y, all currents are assumed to lie on two rotationally symmetric sheets, which run parallel to the outside contour of the glass tube, called line and frame cones. The sheets are defined by a set of (Z, R) co-ordinates which define, by rotation, a series of rings; therefore cylindrical co-ordinates (Z, R, θ) describe the system.

A coil is specified by defining the current distribution at these rings, or modulation levels. A number of 'slots' at each modulation level are defined at certain angles. Assuming no current reversals within the defined quadrant of the coil (this is referred to as the 'positive current' requirement), there is only one way of connecting adjacent modulation levels. This is done by connecting the slots with wires, which lie on the revolving surface and using these winding connections, the wire distribution on every ring of the cone can be calculated. In this way the current distribution of the coil is defined by the slots of the cones at the modulation levels. The deflection coil is therefore described by a sequence of straight-line wires and the Fourier components of the fields are obtained by summing the contributions of all the wire sections.

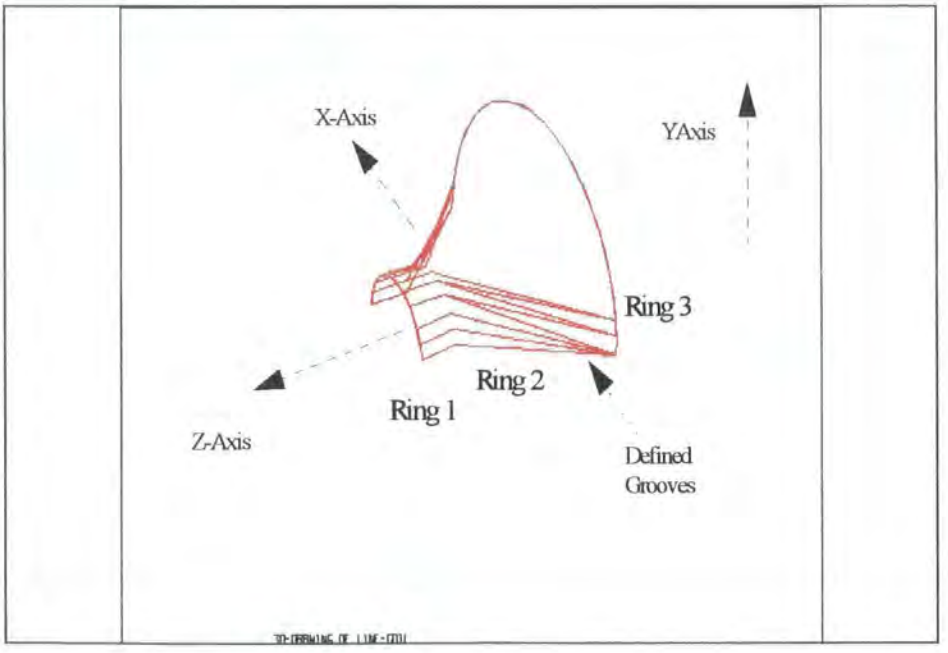

Diagram 35: Plot of Defined Line Coil Slot Positions in DUCAD-Y

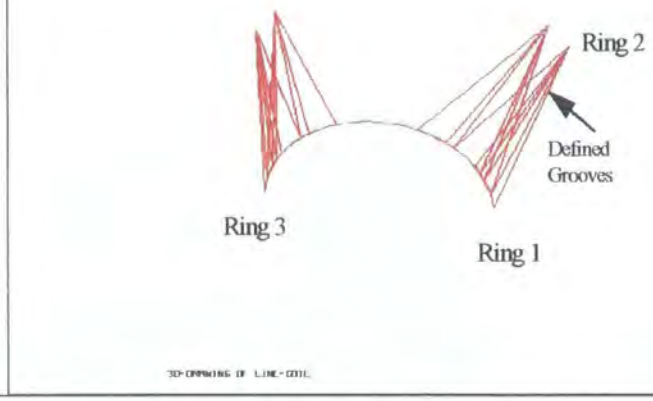

Diagram 36: Plot of Defined Frame Coil Slot Positions in DUCAD-Y

4.4. Computation of Magnetic Field Calculations

4.4.1. Line and Frame Coil Deflection Fields Discussion

Due to the symmetry of the deflection coils, the currents have to be defined in one quadrant of the coil only, and in terms of multipoles, this symmetry leads to the contribution of only odd multipoles.

The currents $I(\theta_i)$ through a slot at an angle θ_i can be expressed in the multipole strengths a_n of multipole n.

For the line coil:

$$I(\theta_i) = I_t \; \pi/2S \sum_{n=0}^{M-1} a_{2n+1} \cos[(2n+1)\theta_i] \text{ where}$$

$$a_{2n+1} = 1/I_t \; 4/\pi \sum_{i=0}^{S-1} I(\theta_i) \cos[(2n+1)\theta_i]$$

For the frame coil:

$$I(\theta_i) = I_t \ \pi/2S \sum_{n=0}^{M-1} a_{2n+1} \cos[(2n+1)(\theta_i - \pi/2)] \text{ where}$$

$$a_{2n+1} = 1/I_t \ 4/\pi \sum_{i=0}^{S-1} I(\theta_i) \cos[(2n+1)(\theta_i - \pi/2)]$$

Here S denotes the number of slots in one quadrant and M the number of multipoles used. [1]

The coil description details a number of multipole strengths at the differing modulation levels and the program calculates the current distribution through the slots from the multipole requirements. The winding distribution of the complete coil on every cone ring is calculated from these currents. The winding distribution on every ring can be converted back into a multipole description on every ring to aid design interpretation.

The magnetisation of permeable objects is represented by a magnetic surface charge, which is used to determine the field outside the object. If the permeability of the object is infinite, the edge of the object is an equipotential surface. The potential of the region is used to calculate the distribution of magnetic charges on a surface just outside the region called the source. Refer to Diagram 37. At the source of the magnetic field, the wires and the magnetisation are replaced by a magnetic charge distribution. The magnetic charge distribution on the source is used to calculate the potential in the deflection volume and to determine the overall magnetic field.

[1] It should noted that these relations are valid of the positions of the slots are given by

$\theta_i = (2i + 1)\ \pi/4s$

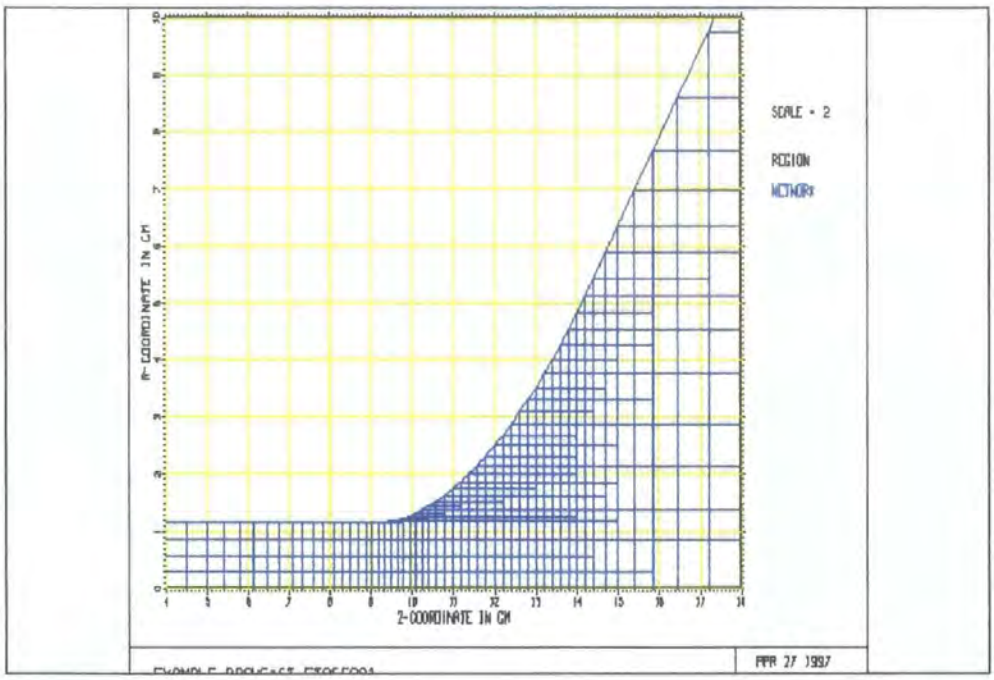

Diagram 37: Plot of Defined Region and Network Spaces in DUCAD-Y

This procedure is performed for every multipole separately. The potential at every node circle j in the deflection volume, resulting from a strength of multipole n at ring position r at the cone and can be written as

$$\Phi_j{}^n(\theta) = M_{j,r}{}^n a_n(r) \begin{bmatrix} \sin(n\theta) \\ \cos(n\theta) \end{bmatrix}$$

where **M** is a matrix that depends on the geometry of the line and frame cone.
On initial creation of a deflection system design in DUCAD-Y, both the region and source fields are calculated based on initial coil geometry data inputted by the user.

4.4.2. Magnetisation Field of a Permeable Object of Arbitrary Shape

To calculate the magnetisation field of permeable objects DUCAD-Y discretises the straight line segment boundaries, and numerically superposes these contributions by the surface charge method to determine the overall magnetisation field. The number of segments N defined depends upon the length of the discretisation segments, the number of multipoles wanted, and the accuracy required. A system of equations is generated which permits the unknown magnetic charge density distributions and total

scalar potentials on the surface of the field shapers to be obtained. The magnetic charges of the yoke ring plus field shapers must be assessed (if both components are present) to determine any field interactions.

The systems of equations permit the surface charge harmonics distributions of the core, the magnetic charge density distribution and the scalar potentials on the surface of the field shapers to be calculated. All matrices involved do not depend on current harmonics but include plate to plate magnetic interactions. Once the solution is found, the magnetisation potential can be determined at any point in space and thereafter the Fourier magnetic expansion.

4.5. Beam Trajectories

The integration of the electron path equations requires knowledge of the magnetic field strength along the electron beam trajectory. Biot and Savart law and the magnetic equivalent of Coulomb Law can be applied to calculate the incident and magnetisation fields at each electron position during the integration. Many trajectories have to be determined with this approach for each deflection yoke design and during the development of a deflection yoke, several designs may have to be optimized. DUCAD-Y calculates the Fourier expansion for the magnetic scalar potential at the node of a network and by interpolation techniques, calculates the field at any point along the electron path. A matrix relation can then be established between the nodes of the network and those of the grids defined on the currents sheet profile and on the core contour.

To calculate the electron beam trajectory in a tube, the magnetic field must be known at arbitrary points along the beam. The magnetic field at any point is calculated by interpolation of the field in a number of fixed points on the grid surrounding the point in question. A program *TRAJECT* calculates the electron trajectories from the gun to the screen. During trajectory, the electrons are under the influence of one or more magnetic fields. The field strengths for points of the electron trajectory are calculated through interpolation of the field strengths at points of the network around the concerning point. The calculation for the electron trajectory takes place through

solving the trajectory equations with the help of the field strengths and the numerical Runge-Kutta technique. Refer to Appendix A for derivation.

On the screen, a square grid of points is defined, denoted by $(X_s(i), Y_s(j))$. These screen positions can be reached by the beam by varying the current through the deflection coils. The current $X_g(i)$ through the line coil which is necessary to reach the point $(X_s(i), 0)$ on the line axis is determined iteratively. Thereafter, the current $Y_g(i)$, necessary to reach the point $(0, Y_s(i))$ on the frame axis is determined. Any non-linearity within the system on the line or frame axes is compensated for by varying the current through the coils non-linearly.

The electron trajectory calculations are repeated for each of the three beams in the CRT; the middle beam (the green beam because it is supposed to strike the green phosphors), and the 'red' and 'blue' beams which are located symmetrically to the sides of the green beam. The three beams are statically converged which means that without any deflection field they would strike the same point in the middle of the screen. For the non-axis positions, the 'green' beam is traced with a current $(X_g(i), Y_g(j))$ through the coils. Usually the point reached on the screen by the 'green' beam (G_x, G_y) will not be equal to the grid point $(X_s(i), Y_s(j))$. The difference between the actual points reached and the grid points is termed raster distortion X_r and Y_r.

In order to determine the convergence errors the currents are determined for the 'green' beam to land on the grid point $(X_s(i), Y_s(j))$. This is done for every grid point separately; $G_x = X_s(i)$ and $G_y = Y_s(i)$. These currents are determined by iteration. With the same currents, the 'blue' and 'red' beams are traced and the points of intersection with the screen of the 'red' beam (R_x, R_y) and the 'blue' beam (B_x, B_y) are determined. Differences between these points of intersection will be denoted with two letters, e.g. $B_{gx} = B_x - G_x$. From the points of intersection the convergence errors can be determined. These can be separated into asymmetrical and symmetrical errors:

Coma: $X_c = (BG_x + RG_x)/2$ and $Y_c = (BG_y + RG_y)/2$

Astigmatism: $X_a = (BG_x - RG_x)/2$ and $Y_a = (BG_y - RG_y)/2$

4.6. Optimization Method

4.6.1. Optimization Algorithm

A 'defect function', a design dependent function, is defined with the aim of minimization, via evaluating and comparing the relative quality of deflection unit design in a quantitative manner. This optimization process involves the control of the following; the starting point, which is defined by a standard configuration (i.e. tube profile, etc.), the design constraints, which directly/indirectly limit the range of the adjustment of the design variables, and the variation in design parameters to allow sufficient optimization. The optimization algorithm determines the necessary design parameters to satisfy the imposed constraints and minimise the defined defect function.

The minimization optimization algorithm used in DUCAD-Y uses the sectioning method, generating a new deflection system design by estimating the optimal linear combination of parameter alterations to determine the minimization parameters required. This is dependent upon the system inhibits and variants available within the optimization process. This process is continuously repeated until a satisfactory end point has been reached, i.e. acceptable product design performance. A vector Xo of the aberrations per screen points is calculated, the modulus of this vector being a measure of coil quality. The weighting factors for points on the screen, the various target values for aberrations levels at various points on the screen plus the weighting factors for the various aberrations per screen point may be defined. Quality factors summarising the designs overall performance are calculated per screen co-ordinate, (Xs, Ys), and the following aberration levels are defined; Raster Distortion, X_r, Y_r ;

Astigmatism, RB_X, RB_y; Coma, X_{coma}, Y_{coma}. The overall raster and convergence errors are combined into one quality factor Q, defining the defect function to be optimized.

$$Q = \frac{\sum_{i=1}^{N} [X_R(i)/w_{xR}(i)]^2 + [Y_R(i)/w_{yR}]^2 + [X_A(i)/w_{xA}(i)]^2 + [Y_A(i)/w_{yA}(i)]^2 + [X_C(i)/w_{xC}(i)]^2 + [Y_C(i)/w_{yC}(i)]^2}{\sum_{i=1}^{N} [X_R(i)/w_{xR}(i)]^2 + [Y_R(i)/w_{yR}]^2 + [X_A(i)/w_{xA}(i)]^2 + [Y_A(i)/w_{yA}(i)]^2 + [X_C(i)/w_{xC}(i)]^2 + [Y_C(i)/w_{yC}(i)]^2}$$

Here N is the number of screen points, and w indicates the relevant weighting of the point. This can be adjusted according to the importance of a certain performance effects. Q can be split up into values for raster Q_R, astigmatism Q_A, coma Q_C and the colour Q_K. The equation to derive Q_K from Q_A and Q_C is as follows:

$$Q_K = \sqrt{\left((Q_A \cdot Q_A)/2 + 2 \cdot (Q_C \cdot Q_C)/3 \right)}.$$

4.6.2. Parameter/Constraints of the Deflection Model

The design parameters (design variables) are individual elements in a group of dependent (or independent) parameters that uniquely define the deflection coil design. They may represent the wire distribution at the modulation levels, the length and positions of the deflection coils with respect to the picture tube, gun position, position and shape of correction plates (field shapers), the screen form, etc.

Design parameters including coil length and position, picture tube envelope, screen form, etc. have great influence on the electrical coil performance, total pull-back, raster distortion and convergence. Selection of design parameters to determine the optimum has to be made very carefully.

Deflection aberrations are functions of the design parameter values, the defect function being the sum of all the relevant design parameters, formulated to describe the functional relationship between the various design variables. The most important electron-optical design parameters relate to the wire distributions on the modulation levels. As the number of wires at discrete angular positions is an important design parameter, the number of possible mutations is very large, having similar screen effects. Using the Fourier components of the wire, a complete set can be defined, i.e. every current mutation can be described as the sum of harmonic mutations.

The design space, which is the total domain defined by all design parameters is usually limited by constraints imposed by the winding technology used and the specifications wanted. It is possible to define equality constraints, or inequality constraints, such as the conservation of the number of turns between the different coil modulation levels (equality), and the total system pullback, which has a lower limit defined by the system tolerances and upper limit defined by the deflection sensitivity (inequality). All these conditions can be translated into conditions of the Fourier harmonics of the wire density.

4.6.3. Optimization Technique

The resulting defect function has its minimum at or near the constrained minimum of the design function. The technique for optimization is complex, and to obtain a true minimum of the defect function is not an easy process. The greater the number of correction plates that are included into the design, the more the likelihood for non-linear behaviour during an optimization run. If this occurs, it is necessary to return to a point in the optimization process where linear behaviour was present.

Optimization procedures can be formulated in terms of more than one measure of merit, which may conflict (e.g. optimizing both electro-optical performance plus sensitivity simultaneously). If more than one measure of merit exists, it is necessary to establish priorities and assign weighting factors for each measure of merit, and regardless of the form it takes, the defect function must be a unique function of the design variables. Qualitative factors such as customer satisfaction, simpleness and aesthetic appeal are difficult to include into an optimization scheme/process.

4.7. Determination of Performance

A *CVRSLF LxFx* file, detailed in Diagram 38, is produced on executing the *DEFLECT-Y* program. *DEFLECT-Y* is an executable program which calculates the magnetic field (if desired) by means of calling a number of programs and executables, to generate electron trajectories and derive system aberrations. The *CVRSLF* file contains information about the raster, astigmatism and coma distortion at various screen points defined as Xs and Ys positions.

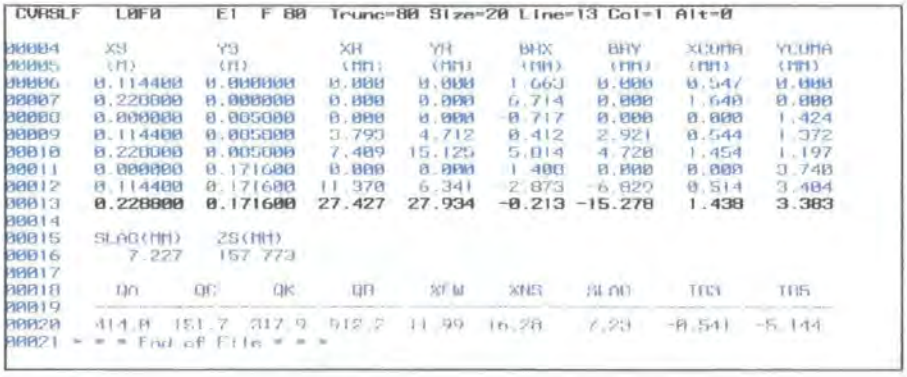

```
CVRSLF    L0F0      E1   F 80   Trunc=80 Size=20 Line=13 Col=1 Alt=0

00004     XS        YS          XR        YR        BRX       BRY       XCOMA     YCOMA
00005     (M)       (M)         (MM)      (MM)      (MM)      (MM)      (MM)      (MM)
00006   0.114400  0.000000    0.000     0.000     1.663     0.000     0.547     0.000
00007   0.220000  0.000000    0.000     0.000     6.714     0.000     1.640     0.000
00008   0.000000  0.085000    0.000     0.000    -0.717     0.000     0.000     1.424
00009   0.114400  0.085000    3.793     4.712     0.412     2.921     0.544     1.372
00010   0.220000  0.085000    7.489    15.125     5.014     4.728     1.454     1.197
00011   0.000000  0.171600    0.000     0.000     1.400     0.000     0.000     3.748
00012   0.114400  0.171600   11.370     6.341    -2.873    -6.829     0.514     3.404
00013   0.220000  0.171600   27.427    27.934    -0.213   -15.278     1.438     3.383
00014
00015   SLAG(MM)    ZS(MM)
00016      7.227     157.773
00017
00018     Q0        QC        QK        QD        %FM       XNS       SLOP      TRC       TRS
00019   ------------------------------------------------------------------------------------
00020   414.8     151.7     317.9     512.2     11.99     16.28     7.23     -0.541    -5.144
00021  * * * End of File * * *
```

Diagram 38: CVRSLF Convergence/Raster Output File Example

XS and YS, the co-ordinates of the screen points are defined
XR and YR detail the raster distortion belonging to each screen point
XA and YA details the astigmatism distortion belonging to each screen point.
XC and YC detail the coma distortion belonging to each screen point.
In addition, information is given detailing the pull-back, third and fifth order trilemma and Q value data.

The performance of a deflection system may be separated into various characteristics.

1. Quality Factor, Q, as discussed previously;

2. Stored magnetic energy and self-inductance of the deflection system;

3. Total pullback, an important concern during the tube/coil matching process;

4. Systems' resistance;

5. Systems' colour purity, also an important consideration during matching.

4.8. Practical Application

Much effort is required to initially define the required input files and determine the basic geometry to determine an initial 'starting point' for optimization . The optimization procedure is complex to realize an acceptable design solution. The DUCAD-Y technique relies on the user to drive the requirements of the optimization and the preferred method by which this achieved. Initially attention is set around determining the line and frame coils modulation fields. An important factor in

realizing a viable design within DUCAD is its high dependency upon the practical knowledge of the deflection unit designer.

The DUCAD-Y modelling system is limited in only being able to simulate rotationally symmetric models. As one can appreciate from the theory of an deflection system, to model a perfectly symmetrical model and calculate the magnetic field generated is complex enough, therefore the introduction of asymmetry into a magnetic model would be an extremely complex and time-consuming computational task.

CHAPTER 5

Design Investigation

5.1. Introduction - Deflection Unit Design

The objective of this study was to investigate the accuracy of the simulation package DUCAD-Y in predicting the performance of a slot wound deflection unit as applied to T.V. manufacture. The product type investigated was 59FS, a mid sector product of screen diagonal dimension of 59 cm. A secondary aim of this study was utilising the information from both the hardware and software manipulation of data to design a 59FS slot based deflection unit achieving an acceptance performance specification.

The proposed overall design for the 59 FS slot product was based upon slot wound line coils and toroidally wound frame coils. The approach to designing this new product was considered from first principles using DUCAD-Y, electron optical theoretical techniques and knowledge gained from existing product designs.

The feasible electron-optical performance capabilities using this technique of winding, whereby the wire is actually wound directly onto the plastic carrier is constrained by the available winding equipment. It was important therefore to concisely analysis all aspects of the slot winding process, to determine subjectively the inaccuracies, for example, of this technique, and any possible characteristics inherent in the manufacturing process, i.e. independent of the simulation techniques of DUCAD-Y.

It was anticipated that the design would require coma, astigmatism and N/S Raster correction on the deflection unit to meet the required performance levels. To determine an optimized geometrical design of the separator, attention was paid to the following parameters; the overall deflection, scanning with the correct horizontal frequency; the convergence/raster specification; the geometrical correction for north-south and east-west pincushion distortion; electrical parameters in the integrated

electrical circuit; defocusing of the electron beams, the trade-off between deflection sensitivity and electron beam spot size; adaptability in the overall tube system; tiltability for optimum convergence; achievable stroke movements for optimum colour purity; existing knowledge of the techniques of slot winding, and the deflection units' capability for high volume manufacture.

5.2. DUCAD-Y Simulation Approach

5.2.1. General Introduction

The simulation approach initially considered a 'base design' , i.e. a deflection system containing only line and frame coils. Using DUCAD-Y, this system was optimized fully to a linear degree, from which the performance characteristics for this optimized system could be determined. Once reached, this design was realized in hardware and measurements were undertaken to assess the degree of cross-correlation between the hardware and software findings.

This 'base design' was modified, by modifying such control parameters as the wire distribution to assess the degree of sensitivity in the product design (derived from DUCAD-Y), and the degree of correlation each modification had upon the software predictions. This approach identified the critical design areas within the separator design.

The addition of extra components to the product design such as astigmatism plates, magnets, etc., ultimately improved the overall performance of the design. DUCAD-Y was employed to determine the 'best' design and this was verified via hardware representations of this design being analysed. The theoretical understanding of the effect of overall performance was assessed with regard to each additional component upon its introduction.

Finally, each run of the optimization process was repeated to determine the linearity of this design. The greater the number of piece parts inherent in the product design effects the repeatability and linearity of the overall system performance. This manifests itself with regard to variation in component positional errors, manufacturing assembly processes, winding processes, measurement equipment stability (whether mechanical/electrical). This approach highlighted critical process parameters and identified areas within the manufacturing process or product design less desirable with regard to achieving product yield levels and product quality.

The initial step in the process to optimize the deflection coil system involved generating various input files defining the base geometry of the deflection system. From this data, various output files were generated by running set programs. The following flowchart in Diagram 39 documents the procedure/process carried out within DUCAD-Y.

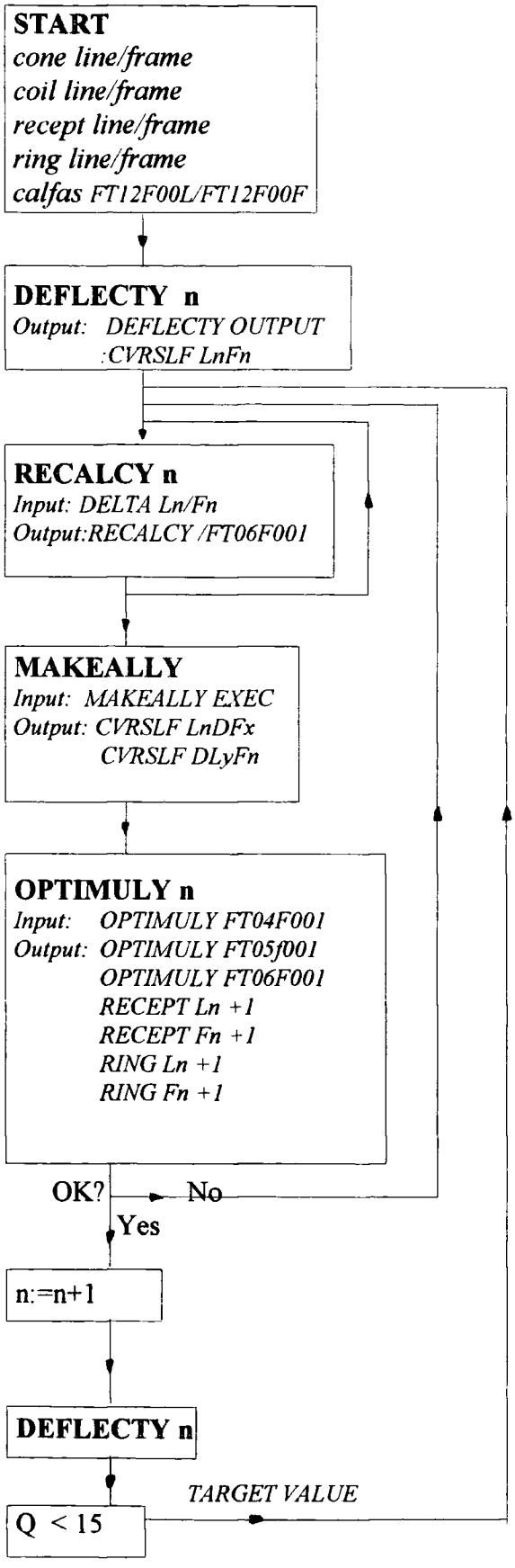

Diagram 39: Flow Chart for Design Optimization

5.2.2. DUCAD-Y Programming Structure

Once the individual input files have been created, the program *DEFLECTY* is run which generates an overall base coil, L0F0. *DEFLECTY* is an executable which calculates the magnetic field behaviour by means of calling many other programs, which ultimately generate electron trajectories to derive the inherent design aberrations. This is the building block to optimize the design. Various input files are modified, via the *RECALCY, MAKEALLY* process. *RECALCY* checks the line and frame coils on stated deltas in the input file *DELTA* Lx/Fx and checks against the allowed maximum and minimum current amplitudes to avoid negative currents being calculated. For each given multipole delta, one delta recept file is created. For each ring delta, one delta ring file is created. *MAKEALLY* is called for the number of defined deltas subsequently calling the executable *DEFLECTY. OPTIMULY* program assesses the overall effect of each of the deltas (whether they are wire or components changes (position, size, etc.)).

There are many input files for the *OPTIMULY* program which comprise of a vector Xo of aberrations per screen point. Xo is a measure of the coil quality. The following input files need to be created; *OPTIMULY FT02F001*, containing the weighting factors for the points on the screen.

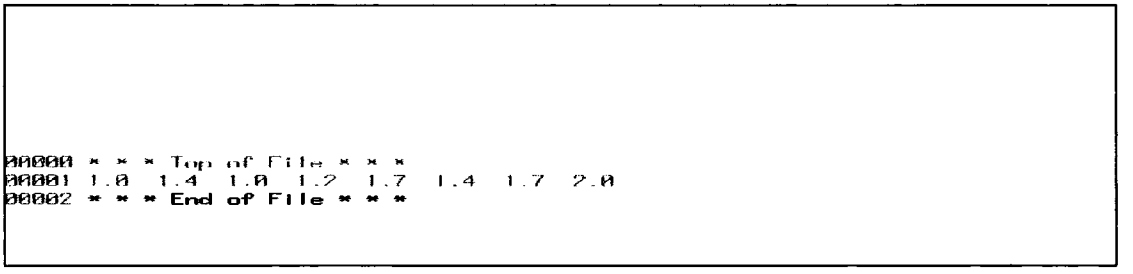

Diagram 40: OPTIMULY FT02F001 Input File

File is composed of WF (i) = i = 1, NSP

where WF(i) = weighting factor for screen point i

NSP is the number of screen points.

Diagram 41: Measuring Points for a 59FS Screen

OPTIMULY FT03F001 file contains the target values for the various aberrations. If minimal aberrations are required, zeros are stated.

```
OPTIMULY FT03F001 E1  F 80  Trunc=80 Size=12 Line=8 Col=1 Alt=0

00000 * * * Top of File * * *
00001  EXAMPLE OPTIMUL FT03F001
00002
00003  RBX          RBY          XCOMA        YCOMA        XRASTER      YRASTER
00004
00005  0.000        0.000        0.000        0.000        0.000        0.000
00006  0.000        0.000        0.000        0.000        0.000        0.000
00007  0.000        0.000        0.000        0.000        0.000        0.000
00008  0.000        0.000        0.000        0.000        0.000        0.000
00009  0.000        0.000        0.000        0.000        0.000        0.000
00010  0.000        0.000        0.000        0.000        0.000        0.000
00011  0.000        0.000        0.000        0.000        0.000        0.000
00012  0.000        0.000        0.000        0.000        0.000        0.000
00013 * * * End of File * * *
```

Diagram 42: OPTIMULY FT03F001 Input File

Weighting Factors per screen point:

RBX, RBY;	Weighting Factor for X and Y Astigmatism
XCOMA, YCOMA;	Weighting Factor for X and Y Coma
XRAST, YRAST;	Weighting Factor for X and Y Raster Distortion

OPTIMULY assesses each of the proposed changes to assess the effect each individual effect would have upon the required performance aberrations, as set by the various *OPTIMULY* inputs files. The optimization procedure is then expanded into higher order levels to generate a more 'realistic' coil. *OPTIMULY FT05F001* is the main

input file for this command; it activates the deltas which have been created and sets the maximum and minimum magnitude limits.

```
OPTIMULY FT05F001 E1   F 80  Trunc=80 Size=20 Line=10 Col=1 Alt=0

00001 EXAMPLE OPTIMUL FT05F001 E WITH CODE=DESIGN
00002 3
00003 'DESIGN'
00004 11111100000000000000000000
00005 11111100000000000000000000
00006 00000000000000000000000000
00007 0 0 0 0
00008 .0010
00009 0.00 20
00010 5 20
00011 0  0  0  0  0  0  0  0  0  0  0  0  0  0  0  0
00012 50 50 50 50 50 50 50 50 50 50 50 50 50 50 50 50
00013 -2 -2 -2 -2 -2 -2 -2 -2 -2 -2 -2 -2 -2 -2 -2 -2
00014 +2 +2 +2 +2 +2 +2 +2 +2 +2 +2 +2 +2 +2 +2 +2 +2
00015 0  0  0  0  0  0  0  0  0  0  0  0  0  0  0  0
00016 50 50 50 50 50 50 50 50 50 50 50 50 50 50 50 50
00017 -2 -2 -2 -2 -2 -2 -2 -2 -2 -2 -2 -2 -2 -2 -2 -2
00018 +2 +2 +2 +2 +2 +2 +2 +2 +2 +2 +2 +2 +2 +2 +2 +2
00019 -2 -2 -2 -2 -2 -2 -2 -2 -2 -2 -2 -2 -2 -2 -2 -2
00020 +2 +2 +2 +2 +2 +2 +2 +2 +2 +2 +2 +2 +2 +2 +2 +2
====>
                                                    XEDIT  1 File
```

Diagram 43: OPTIMULY FT05F001 Input File

General Input File which controls the *OPTIMULY* program
15 numbers for the line, frame and special deltas can be either set to 1 of 0. A 1 indicates that the delta file is included into the *OPTIMULY* calculation; a 0 indicates it is switched off.

The absolute maximum and minimum limits which OPTIMULY may use each delta is detailed in lines 00013 to 00020.

5.3. General Product Description

The 59FS slot product was simulated on the Philips 59FS tube. Information concerning the tube specification and the required deflection system specification was drawn from the design specification of the 59FS product design. This defined the starting point of the following design study.

5.3.1. Deflection System Geometry

Screen and tube profile data was transferred into the TRAJECT input file in DUCAD-Y. The *TRAJECT* input file details general information on the gun/tube structure, such as the screen form/position, gun position, magnet strength, if applicable, coma ring RB size and position, static correction, etc.

Data for the screen cone is taken from the 110 deg. (45AX) tube profile detailed as a polynomial function to allow definition of the inner and outer glass profiles. The screen centre was defined in DUCAD-Y co-ordinates and the data for the screen cone was taken from the 110- degree (45AX) F disk already created for 59FS. The position of the gun was additionally defined in the relevant co-ordinates.

```
 TRAJECT  FT05F001 E1  F 80  Trunc=80 Size=58 Line=10 Col=1 Alt=0

00001 'SCHOEN'
00002 0.354000
00003  0.279891D+00
00004 -0.343346D+00
00005 -0.756164D+00
00006 -0.380023D+01
00007 -0.263289D+00
00008 -0.761500D+01
00009  0.680735D+02
00010  0.763576D+01
00011  0.349959D+01
00012  0.113351D+03
00013 'GUN'
00014 0.0065 0.04600
00015 'ENTER'
00016 'LINE',11,'LINE'
00017 10101010100000
00018 00000000000000
00019 'ENTER'
00020 'FRAME',12,'FRAME'
 TRAJECT  FT05F001 E1  F 80  Trunc=80 Size=58 Line=30 Col=1 Alt=0

00021 00000000000000
00022 10101010100000
00023 'ENTER'
00024 'STATIC',14,'STATIC'
00025 01010101000000
00026 00000000000000
00027 'FIELDMUP'
00028 4
00029 'STATIC'  2  0.0   1.900
00030 'STATIC'  4  0.0   1.900
00031 'STATIC'  6  0.0   1.900
00032 'STATIC'  8  0.0   1.900
00033 'ENDREG'
00034 0.260
00035 'TOL'
00036 1.E-3  1.E-4
00037 'COMAND'
00038 0.05000  0.05000
00039 'COMB-A'
00040 0. 0. 0. 0.
====>
 TRAJECT  FT05F001 E1  F 80  Trunc=80 Size=58 Line=50 Col=1 Alt=0

00041 'CHECK-A'
00042 'COEF-SC'
00043   TEKST COUF-SC
00044   6
00045   0.11440  0.00000  0.10974  0.00000  1.24213  0.00000  0.00000  1.00000
00046   0.22800  0.00044  0.10370  0.00000  1.97424  0.00000  0.00000  1.00000
00047   0.00000  0.08580  0.00049  0.07944  1.00000  0.00000  0.00000  1.14720
00048   0.11440  0.08580  0.10869  0.08001  1.25320  0.04350  0.07935  1.12067
00049   0.22880  0.08580  0.18026  0.08091  2.05671  0.16901 -0.02106  1.07357
00050   0.00000  0.17160  0.00000  0.14538  1.00000  0.00000  0.00000  1.46032
00051   0.11440  0.17160  0.10581  0.14976  1.26871  0.02075  0.14564  1.34977
00052   0.22000  0.17160  0.17000 -0.15220  2.20477  0.24073 -0.16540  1.13015
00053   GLASS'
00054   SLAB'
00055   0.23000  0.19440  0.17615  0.16504  2.43100  0.24713 -0.15004  1.13652
00056 'SENSITIV'
00057   0.2300  0.1000  27
00058 'END'
00059 * * * End of File * * *
```

Diagram 44: *TRAJECT FT05F001* Input File

5.3.2. Line Coil Definition

The *LINE CONE* was constructed, based on the 59FS tube profile, primarily setting the profile of the line separator. The G3/G4 gun position determined the start position for the line coil. The line coil winding was taken to be at the average line of the separator profile (accommodating clearance, etc.) All information for system co-ordinates was inputted as (Z, R) co-ordinates. The plastic separator and therefore the line coil were constructed parallel to the outer glass contour. The average winding position of the line coil is situated at a distance of 1.5 mm to the outer glass contour. Sufficient clearance was left for the line coil to allow for optimization possibilities. The two dimensional structure of the line coil is detailed within the *GEOMETRY* file which sets the (Z, R) co-ordinates (2D model) for all components within the deflection system.

A *RING LINE* file was created corresponding to the line coil geometry information. A number of rings were defined referring to the levels of multipole modulation. A number of slots were defined for each ring position, which detailed the position (angle subtended) at which the wires of the coil may be positioned. i.e. the number of grooves in the ring and the associated angle of the grooves in the ring.

```
00000 * * * Top of File * * *
00001     3
00002      5   14   50
00003      6    6   10
00004    8.000  24.000  38.000  57.000  72.000  84.000
00005    8.000  24.000  38.000  57.000  72.000  84.000
00006    3.000  11.000  16.000  22.000  27.000  32.000  39.000  46.000  52.000
00007   70.000
00008 * * * End of File * * *
```

Diagram 45: DUCAD Input File Ring L26 File

Line 0001 Number of Rings
Line 0002 Ring Positions specified as a z position on the line cone
Line 0003 Number of Slots per ring
Line 0004 - 0007 Angle of slots per ring

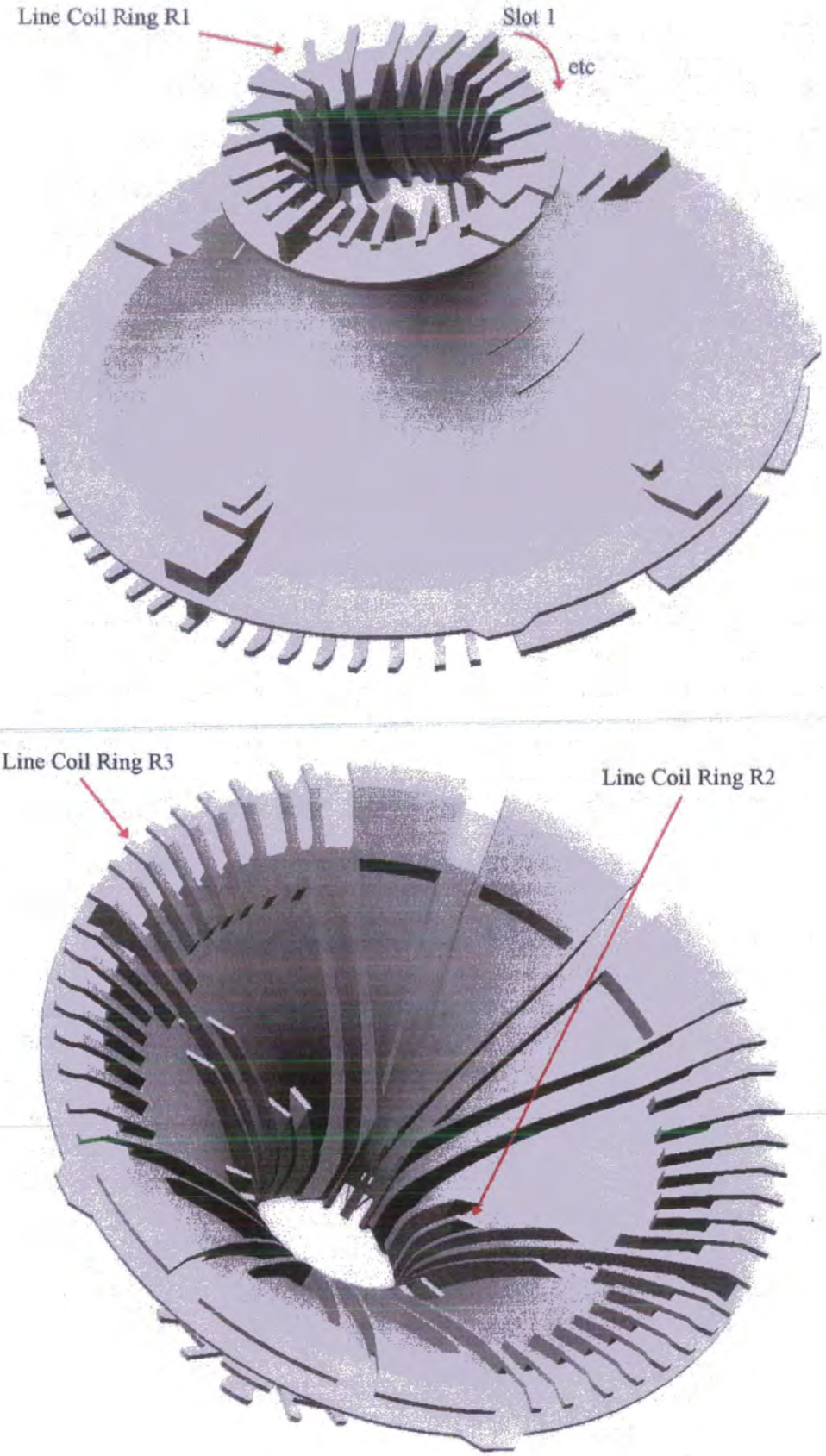

Diagram 46: Diagrammatic Representation of Line Coil angles and Ring Definitions.

Cross-comparison with competitor slot products designed to similar tube profiles and specifications was used as an initial design estimate. In addition experience of the currently produced 59FS double mussel product indicated where likely levels of modulation would be required to achieve the necessary magnetic deflection fields. At this stage, the position of the yoke ring and hence the frame coil was considered to determine the 'best' positioning for the frame modulation levels, plus any necessary optimization reserve.

A *COIL LINE* file was generated detailing the winding pattern for the line coils and the total number of wound turns per coil.

```
COIL     LINEE    E1  F 80  Trunc=80 Size=5 Line=6 Col=1 Alt=3



00000 * * * Top of File * * *
00001 ********* SLOT HYBRID 59 FS  LINE      *********
00002 'LINE',9
00003 0,2
00004 1,1,2,2, 120,'REAL'
00005 2,2,3,3, 120,'REAL'
00006 * * * End of File * * *
```

Diagram 47: DUCAD Input File COIL LINE file

Line 00002 Type, number of multipoles
Line 00003 No of sections per line cone
Line 00004 No. of first ring, level of first ring total, no of wire turns
Line 00005 No. of second ring, level of second ring total, no of wire turns

5.3.3. Yoke Ring Definition

The yoke ring selected was a 27V product yoke ring. This was a currently available component therefore a frame clamping tooling existed to wind the yoke rings on a development universal machine. This yoke ring was chosen, as it was readily available for hardware samples, and approximately provided the necessary length and profile. This information was included in the *GEOMETRY FT05F001* file. The yoke ring, and hence the frame coil windings were positioned to locate practically upon the separator main body. The decision not to manufacture a new yoke ring was taken due to the

lack of understanding of the slot winding process at the outset of the investigation. It was felt that a full determination of a slot wound line coil was required prior to any attempts to create a yoke ring fabrication tool for a 'live' cost effective 59FS slot product.

5.3.4. Frame Coil Definition

The *FRAME CONE* was constructed, based on data available on the yoke ring. The *frame cone* was situated 3.5 mm away from the line cone and 2 mm from the yoke ring profile. The *GEOMETRY FT05F001* file included (Z, R) information on both the frame coil and yoke ring. A nominal clearance was given for the packages of the frame coil, sufficient clearance for the yoke ring to the line separator, adequate space for the astigmatism plate, and additional room for optimization possibilities. As detailed in the line coil, *RING FRAME* file and *COIL FRAME* files were created, as per the line coil structure.

```
00000 * * * Top of File * * *
00001    3
00002     1   41   67
00003     9    7    9
00004   35.000  40.000  45.000  50.000  55.000  60.000  65.000  70.000  75.000
00005   25.000  30.000  35.000  45.000  55.000  65.000  75.000
00006   35.000  40.000  45.000  50.000  55.000  60.000  65.000  70.000  75.000
00007 * * * End of File * * *
```

Diagram 48 : DUCAD Input File Ring F26 File

Line 0001 Number of Rings
Line 0002 Ring Positions specified as a z position on the frame cone
Line 0003 Number of slots per ring
Line 0004 - 0007 Angle of slots per ring

```
00000 * * * Top of File * * *
00001 ********* HYBRID 59 FS  SLOT          *********
00002 'FRAME',9
00003 0,2
00004 1,1,2,2, 400,'REAL'
00005 2,2,3,1, 400,'REAL'
00006 * * * End of File * * *
```

Diagram 49: DUCAD Input File COIL FRAME File

Line 00002 Type, number of multipoles
Line 00003 No of sections per frame cone
Line 00004 No. of first ring, level of first ring total, no of wire turns
Line 00005 No. of second ring, level of second ring total, no of wire turns

5.3.5. Plate Correction and Geometry

The program SEGMENT divides a correction plate into sections and subsequently divides each section into segments. A 'section' is defined as a plated piece between a cone point and the next cone point between two defined angles.

The level of accuracy of these component simulations is heavily dependent upon the degree of segmentation of defined points in the input *SEGMENT AST/COM/RAS* input files.

```
SEGMENT  AST24    E1  F 80  Trunc=80 Size=10 Line=7 Col=1 Alt=0


00000 * * * Top of File * * *
00001 SLOT ASTIB. PLATE  AST24 Standard Wings
00002   8
00003 7 43.28 90
00004 8 42.82 90
00005 09 43.52 90
00006 10 44.20 90
00007 11 26.89 90
00008 12 26.89 90
00009 13 26.89 90
00010 14 26.89 90
00011 * * * End of File * * *
```

Diagram 50: SEGMENT AST24 Input File

Plate defined by 8 segments; e.g. segment 7: plate section subtended between 43.28 deg. and 90 deg.

```
SEGMENT  COM1     E1  F 80  Trunc=80 Size=25 Line=9 Col=1 Alt=0

00000 * * * Top of File * * *
00001 SLOT COMA PLATE With Cut-out No Pole Shoe
00002  23
00003 7 35.83 69.0
00004 8 30.77 69.0
00005 9 28.79 69.0
00006 10 26.34 69.0
00007 11 24.28 69.0
00008 12 0 40.03
00009 13 0 37.02
00010 14 10.5  34.48
00011 15 10.0  32.28
00012 16 9.50  30.0
00013 17 9 30.0
00014 18 9 30.0
00015 19 9 30.0
00016 20 9 30.0
00017 21 9 30.0
00018 22 9 30.0
00019 23 9 30.0
====>
```

Diagram 51 : SEGMENT COM1 Input File

```
SEGMENT  RAS1     E1  F 80  Trunc=80 Size=17 Line=10 Col=1 Alt=0

00001 SLOT RASTER PLATE ras1 dia 60   std. Pole Shoe
00002 14
00003 1 0.0 68.2
00004 2 0.0 68.2
00005 3 0.0 68.2
00006 4 0.0 68.2
00007 5 0.0 68.2
00008 6 0.0 68.2
00009 7 22.84 68.2
00010 8 23.57 67.9
00011 9 25.6 65.98
00012 10 25.6 70.98
00013 11 25.6 70.98
00014 12 25.6 70.98
00015 13 25.6 70.96
00016 14 25.6 70.28
00017 'END',0,0
00018 * * * End of File * * *
```

Diagram 52: SEGMENT RAS1 Input File

5.4. Overall Design Requirements

5.4.1. Introduction

During the design process all possibilities for wire modulation in both the line and frame coils were considered. Full exploitation was made of all multipole modulations in order to achieve the desired line and frame magnetic modulation fields. An important constraint in determining acceptable line and frame modulation was the manufacturing processes utilised, typical limitations which are inherent in all coil manufacturing processes. Much use was made of 6 and 10 multipoles to realize suitable convergence and raster behaviour. The use of multipole expansions from the Fourier theory as applied in the DUCAD-Y simulation process allowed a self converging unit to be realized.

5.4.2. Astigmatism Correction

In order to achieve zero frame astigmatism within an in-line tube, a strong barrel-shaped field in the middle of the coil is required. This negative six-pole field can be realized if the average position of the winding turns are centralised within the middle section however this field shape is a difficult characteristic to achieve on the flare side of a toroidally wound frame coil. The toroidal method of winding subtends both the upper (neck) and lower ring of the frame coil (flare) at the same angle and therefore does not allow negative and positive modulations to be achieved in the same winding turn. In addition, deeper modulation on the neck side is not possible due to the clamping mechanism of the winding machine.

Astigmatism plates are therefore required to correct the actual six pole fields to minimise frame astigmatism errors and improve the convergence errors along the edges of the screen. Astigmatism plates are positioned in the primary field of the frame coils and in the secondary field of the line coils, between the line and frame coils at North/South locations. The plates approximately follow the direction of the frame coil

field lines and as the magnetic resistance of the plates are considerably lower than that of air, the field lines run through the plates, consequently disappearing from the deflection zone. The remaining field lines in the tube spread over this zone, producing a strong barrel-shaped six-pole field. The plates effectively cancel the field lines in the middle of the plates and concentrate them at the edges as defined in Diagram 53.

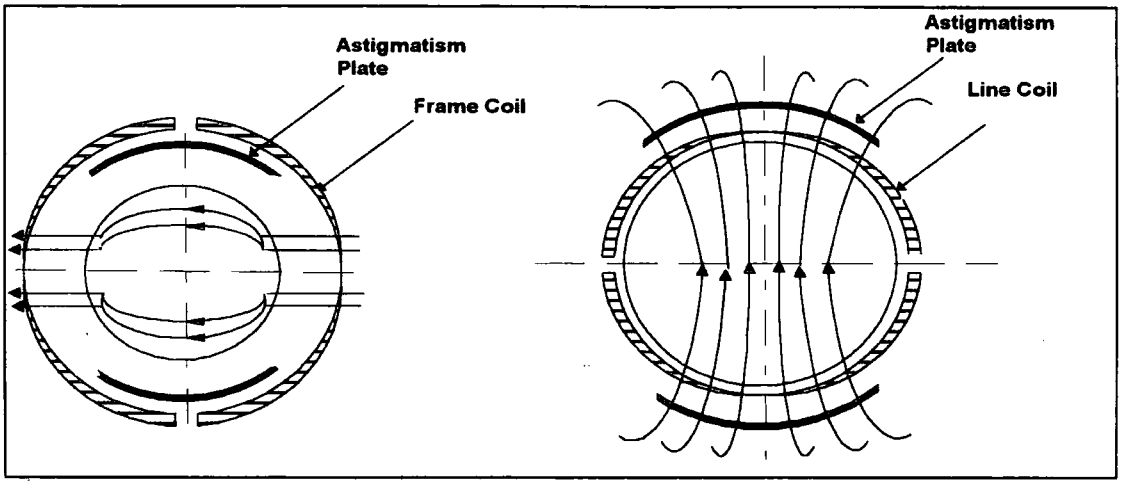

Diagram 53: Frame and Line Field Lines with Astigmatism Plates.

A simplistic astigmatism plate was initially chosen, and during the software optimization process modifications to the plate were made, resulting in the astigmatism plate, as defined in *SEGMENT AST24* file. (Refer to Diagram 50).

Anisotropic coma effects and the ratio between tails (BRx astigmatism errors) and crossings(BRy astigmatism errors) can be affected by the shape of this plate, plus East/West raster distortion by up to approximately 15%.

5.4.3. Coma Correction

To sufficiently correct coma errors, both a COMA-RB ring in the tube and a coma plate in the simulation design were introduced.

Coma correction rings are placed around holes in the bottom plate of the G4 cup in the tube through which the red and blue outer beams pass. The frame field is diverted by these rings which causes no deflection of the outer beams. When running through the rest of the coil fields this lagging behind of the outer beams deflection is compensated for. Positive anisotropic coma Y may arise in the corners of the screen as the three beams are no longer passing through the fields of the deflection unit in one plane due to the modified dipole field. The green beam is more deflected in the Y-direction on the neck side, and when applying the line deflection, this extra green deflection is reversed due to the strong positive line six-pole introduction. The influence upon line coma and spot distortion by employing a coma plate in the tube are unavoidable side-effects. The coma-RB correction in the unit was initially employed, set at an initial length of 3mm.

Coma plates are positioned on the neck side of both the line and frame coils of the deflection unit, enabling the correction of frame coma errors with the desired pincushion six-pole field. The correction occurs due to the diversion and strengthening of the stray frame field lines emitted by the yoke ring. There are two main disadvantages in using coma plates: firstly, eddy currents are generated due to the position of the plates within the flange of the line coil; secondly, correction of the frame coma is taking place very far back in the unit, resulting in the convergence problem of anisotropic coma (green droop).

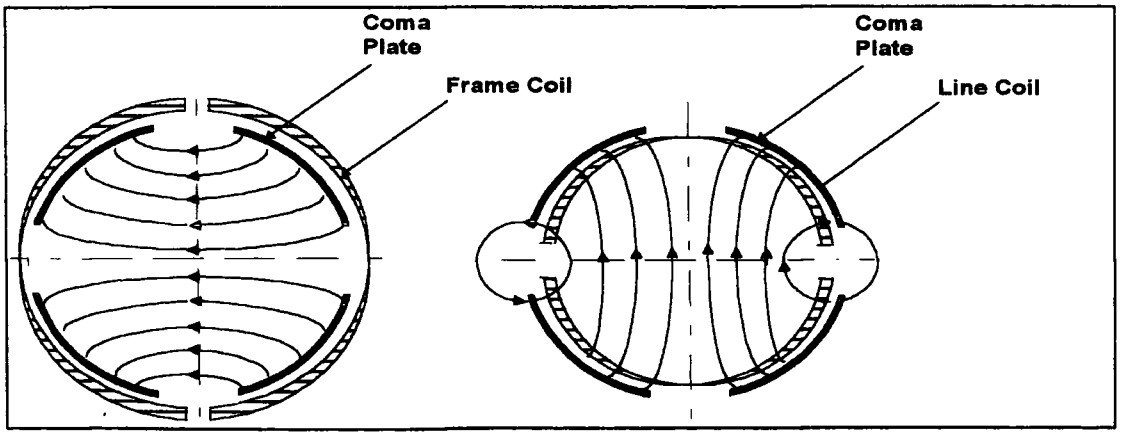

Diagram 54: Frame and Line Field Lines with Coma Plates

A further characteristic of coma plate correction is the inherent interference with frame astigmatism levels created by the astigmatism plate (play against one another). The plate must be shifted towards the screen to obtain zero frame astigmatism levels, which forces the E/W raster to be pincushion shaped. Therefore with an improvement on frame coma levels the side effects are more positive crossing behaviour and a more barrel shaped NS raster shape. The dimensions of the coma plate were varied to optimize these associated aberration levels.

5.4.4. Raster Correction

In all product designs in the mid-sector range, raster correction is an issue. Stronger field modulation at the flanges of the line coil flare can reduce some of the raster distortion by modulating the flange around 55 degrees. The elimination of seagull wing distortion is therefore possible, however this results in a unusually shaped flare flange which is difficult to control in the winding process. To reduce the inherent raster distortion occurring in the deflection coils requires additional components in the overall design. The residual raster distortion in this design was corrected by N/S static magnets and raster plates.

Static magnets are used to correct pincushion and seagull North/South raster shapes. There are two main disadvantages in using magnets; firstly, purity suffers, focus is difficult to achieve due to the local field generated by the magnet; and secondly, convergence problems result, such as astigmatism, crossing and tails. As previously discussed, wire materials generate odd multipole modulations, as per the Fourier expansion. Magnets generate even multipoles such as 4 (2nd order), 8 (4th order) and 12 (6th order) poles. Two N/S magnets produce 8 and 12 poles static fields which compensate a parabolic N/S pincushion distortion and a N/S seagull wing distortion.

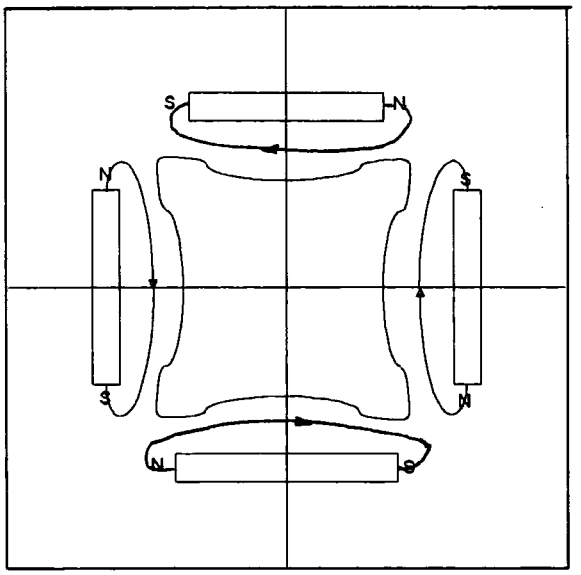

Diagram 55: Field Lines with N/S and E/W Static Magnets

The strength of the magnets were initially set to 1.2 and optimized to 1.9 . The position of the magnets were estimated from prior design models, the available space and possibilities available in the separator design.

Initially no raster plates were incorporated, however, during the optimization process, the need for further raster correction became an obvious requirement.

Raster plates consist of two main sections; the collector plate, positioned near to the yoke ring to charge the plate, and the pole shoes, which determine the alternative correction field shape. The multipole fields generated by this section may be altered by minor modifications to their form, position and length in the z direction. The smaller the distance between the two pole shoes, higher order multipoles will be charged (+ 6 pole, + 10 pole, + 14 pole) and become effective. The larger the distance of this gap ensures that only positive six poles will be affected. The deflection point of the deflection system moves as the plates move the field forward.

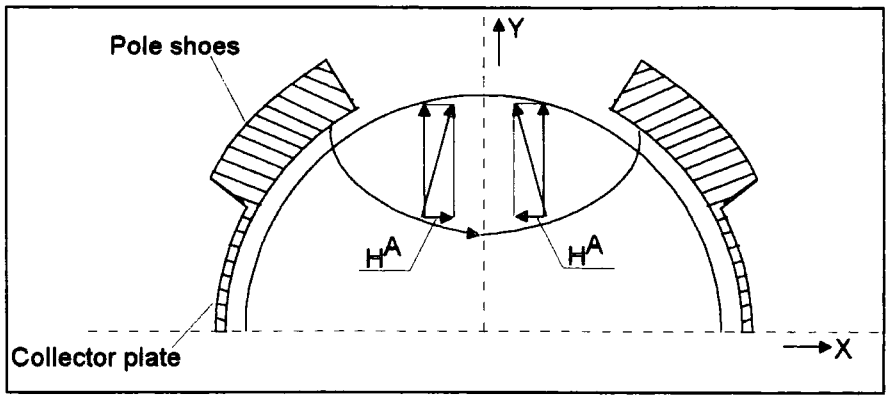

Diagram 56: Magnetic Field Lines with Raster Plates

Raster plates mainly assist N/S raster distortion however the poleshoes effectively balance the N/S and E/W raster relationships. The amount of pincushion can be corrected by modulating the supply voltage. The maximum correction possible in E/W is about 6% and in N/S 2% can be obtained with raster plates, the penalty is a deterioration in the convergence performance.

During the software development procedure, raster plates were positioned East and West around the separator to achieve the desired raster shape.

5.5. Deflection Unit Line Coil Separator Design

5.5.1. Separator Design

The general deflection system design was initially considered; firstly, the picture tube profile; secondly, the horizontal and vertical deflection coil positions with respect to the screen, and with respect to each other; and thirdly, the distribution of the deflection field. All the tube design parameters were predefined therefore it was necessary to optimize the second and third issues to obtain the best picture performance. As previously discussed the most important method to minimize deflection aberrations within the allowable limits is to obtain proper shaping of the deflection field itself. This depends not only on the wire distribution of the deflection coils but also on the form and position of any extra components (magnets, plates, etc.).

A separator is a plastic moulding which in pin-fired technology, due to the deflection coils being the formed components, is primarily used for electrical separation of the line and frame coils. However, in slot winding, the separator is actually the carrier for the line coil winding and subsequently plays a far more important design role.

The main design philosophy for the 59FS slot product was to develop a saddle-type separator to act as the line coil support. This separator comprised of flare and neck end sections, with various rows of grooves extending from either end of the coil winding supports to allow the wire to be wound in a continuous manner to form the saddle-type line coil. Also designed into the separator are grooves which, on their extension from the neck, met crossover grooves at the mid-section of the coil which extend further to the flare. These have been incorporated to give maximum opportunities for modulating the wire distribution in order to optimize the performance of the coil.

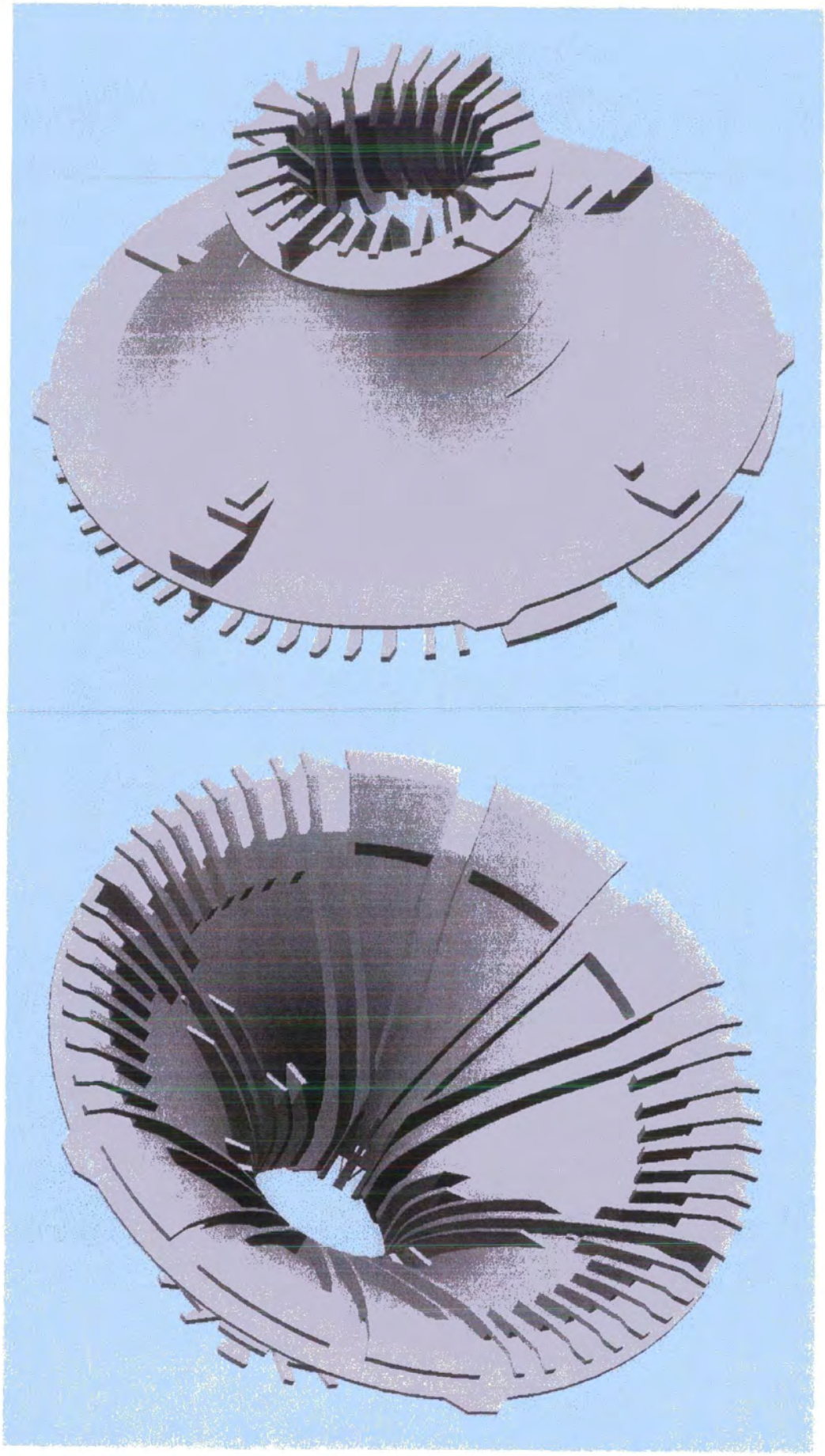

Diagram 57: Separator Design

The profile of the separator was defined from the Philips 59FS tube curvature with the outer and inner flanges at the neck and flare defining the length of the saddle coil, and hence the coils' focal length.

DUCAD-Y was used to determine the optimized lengths of the neck to mid section, and mid to flare section of the saddle slot coil and to provide an indication of wire distributions. These design parameters principally affect convergence, stroke and sensitivity however, additionally important are the implications upon the pullback parameter. From the position where the deflection unit rests against the glass, the unit must be shifted , in mm, towards the neck until the beams hit the glass, with deflection towards the corners. This space is called the total pullback. A large pullback results in a relatively low deflection unit sensitivity. Approximately, it can be stated that one millimetre of additional pullback requires 5% to 10% more deflection energy (type dependent). If the coil was lengthened at the neck side, the pullback would be reduced. The sensitivity of a toroid is less than that of a saddle coil caused not only by the leakage field created by the outer windings and opposite to the deflection, but principally by the stray fields generated outside the yoke which are not contributing to the deflection. The definition of the length of the line coil in conjunction with the length of the frame coil is an important issue.

At this stage, the design parameters considered within the systems overall performance were pullback and trilemma, design parameters which indicate if sufficient coil length is available to provide the magnetic deflection/sensitivity required, and secondly to ensure sufficient scope for adjustment and modification in the final design proposal. Trilemma error is a further design function utilised and is defined as the difference between line astigmatism error and frame astigmatism error plus the corner astigmatism levels. The introduction of astigmatism errors as detailed is a result of inherent line and frame six-pole modulation. This definition is utilised to assist in determining the start position for the line and frame deflection specification , i.e. coil lengths to achieve a self-converging system.

The proposed deflection unit separator consisted of a support with a flange at either end with grooves running in the radial profile of the separator. Two sets of deflection coils are directly wound onto the support. The coil turns run through the radial grooves in the inner profile, then around the tangential grooves at the neck and flare flanges. The choice of wire position was not restricted to straight wire runs from the screen to the neck but was able to alternatively run at an angle controlled by the separators grooves. The wire distribution therefore could be freely modulated as a function of position along the direction of the longitudinal axis. Performance characteristics such as North/South raster can be achieved by ensuring the length of the line coil is longer at the flare end than at the frame coil. The wire slots detailed within the inner profile of the separator were designed to provide a number of electro-magnetic possibilities to allow the correction of convergence and raster errors to be accomplished.

Additional design features were incorporated into the separator to ensure adequate functionality for practical winding samples and prototypes. These included fixtures to aid accurate positioning of the yoke rings. Small keyways on the separator outer profile were added to aid mutual positioning of the line and frame coils which is known to significantly influence the orthogonality of the deflection unit. In addition reference markings were added to assist in reproducibly locating various correction plates to the separator body. Lead out partitions were added to channel the line and frame coil wires to the PCB connections. It was important to optimize the length of routing travel of the lead outs for minimum influence on line balance distortion and bending effects.

An important consideration in the design of the separator was the requirements imposed by the winding process upon the plastic separator. As the wire is directly wound in and around the separator certain process criteria are imposed onto the separator design. Issues such as the shape, dimensions and profile of the neck/flare fingers and the separator material, both of which are crucial to a smooth winding process. It was preferable to provide as sharp an edge on the leading edge of the slot finger to aid the natural slippage of the wire into the grooves. A tapered edge on the

opposite return side of the finger, in the direction of the winding, aids positioning the wire into the grooves, reducing the possibility of damaging the wire and excess travel in the wire path.

It was thought preferable to maintain the finger dimensions protruding at the neck and flare end sections as broad as possible to maintain its rigidity and overall strength. If the fingers are too weak, damage to the wire will result, or even snapping of the cap fingers. However, to counteract this argument, any increase in the slot width is at the expense of coil sensitivity thus limiting the L/R ratio possibilities. Ideally, it was considered advantageous to vary the length of the slot fingers from the central panel to the outermost edges to lessen the winding difficulty at the extremes of the coil, with the principle being that a shorter finger required less hooking angle on the nozzle feed.

The overall three dimensional shape of the slots was important to repeatable winding of the wire. It is of benefit that the thickness of the horizontal deflection coil decreases as it departs from the central package. A step wise decrease in the depth of the slots from the central section to the outermost slot provides two advantages. Firstly, repeatable positioning of the wire. Since the groove shape is tapered, the wire slips into the corners of the groove initially, and subsequent windings fill the grooves in a more repeatable manner. Secondly, the shaping of the wire packages greatly impacts upon the generated electromagnetic field. The overall dimensional shape of the slot can provide more negative and/or positive characteristics to the electromagnetic field.

Material choice for the separator was 35% glass filled polycarbonate. It was necessary to incorporate a high proportion of glass within the material composition to re-inforce the overall structural strength of the cone. The wall thickness was set at 1mm to ensure adequate separation between the line and frame coils.

A soft tool (not case-hardened to allow for tool modifications) of the separator design was fabricated to allow hardware validation of the software predictions. Using the line coil definition, the proposed design model was fully optimized using DUCAD-Y to determine an overall system performance.

Once the base design for the line coil was set, the frame coil and yoke ring were introduced, and the overall system was simulated and optimized.

5.5.2. Electrical Considerations

Electrical design issues considered include the electrical stored energy and the inductance/resistance (L/R) ratio of the line and frame deflection coils. Diagram 58 depicts a line drive circuit where L represents the inductance of the line coil, C_s the s-correction capacitance and C_{fb} the fly-back capacitance. During flyback the switch, usually a combination of a transistor and a diode, is open and the current oscillates with a flyback frequency $(1/2\Pi \sqrt{(L C_s . C_{fb} / (C_s + C_{fb})})$. Subsequently, the line scan is started by closing the switch. This changes the oscillating frequency to the much lower frequency $(1/2\Pi \sqrt{L C_s})$. Both Cs and Cfb are designed to comply with the line scan frequency, screen curvature and circuit (voltage) restrictions.

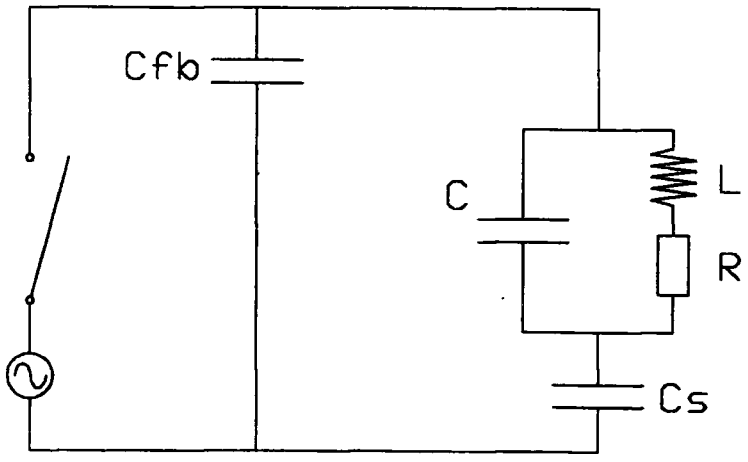

Diagram 58: Line Drive Circuit with a Lumped RCL Model of a Deflection Unit

The current through the line coil is sawtooth shaped. The output stage is basically an electronic switch which periodally connects the line coil to a certain voltage. The current through the coil can then be determined by solving the following differential equation.

$$E = L\,dI/dt + I\,R \quad \text{and} \quad I = E/R\,(1 - e^{-R/L\,t})$$

For deflection in the vertical direction the current through this coil is approximately sawtooth shaped dependent upon the deflection angle and curvature radius of the tube. The deflection frequency is 50 Hz, the trace a duration of approximately 19 ms and the flyback approximately 1ms.

The stored energy of the horizontal coil is a key design characteristic of all deflection units. Its design should be fabricated to minimise the stored energy to reduce the voltage across the transistor on the deflection circuit during this flyback period. This assists in extending the deflection circuit lifetime and its overall reliability. During each cycle of an alternating current through the horizontal coil, this energy is transferred back and forth between the magnetic field and the source of the current. Each harmonic of the winding distribution contributes independently to the stored magnetic energy. In most practical situations, the dipole contribution dominates. During this process some of the energy is lost. By minimising the stored energy one can reduce these losses as well as the power requirements resulting in a more energy-efficient television set.

The L/R ratio affects the non-linearity of the coils performance and the heat generated within the line coil. The values of L and R may be altered with a variation in the number of wire turns per slot and the type of wire employed. For slot winding, it is thought preferable to employ F grade specification wire, grade 1, to provide the required strength of insulation on the wire. The manipulation of the wire around the separator slots necessitates a high specification to reduce the risk of insulation breakdown and short circuit failures owing to the variation of the stretching force acting on the winding wire as it is wound the wire is displaced and biased in a

particular direction. This variation in wire displacement is reduced as the width of the coil grooves are narrowed. However coil sensitivity and performance deteriorate with respect to the L/R ratio. The depth of the slots must provide sufficient L/R ratio and so adequate filling factor for the required application. Filling factor is the ratio between the total volume of winding wire and the available volume within the separator (or lower and upper jigs if pin-fired technology). The turns of wire within the separator slots are not compressed as in conventional bonding deflection unit manufacturing methods therefore the net space factor is considerably reduced. Oblique winding of the wire into the separator slots may potentially reduce the potential filling of the coil.

5.5.3. Application Issues on Product Design

5.5.3.1. Introduction

Due to the use of hybrid technology within this product design, there was an inherent need for additional correction plates (primarily due to the limitation on the frame coil winding technique). To reduce convergence and raster errors, correction plates such as coma plates and raster plates were employed. It is necessary to further investigate their possible impact upon the important product design application considerations.

5.5.3.2. Temperature

All deflection units generate heat, but the operating temperature of all consumer systems lies below 100°C at a room temperature ambient. As the horizontal frequency increases, further heat is generated for the hysteresis losses in the yoke core and the increased coil resistance produced by the skin effect. This heating produces two undesirable consequences; high power consumption and deterioration of tube circuitry reliability.

In particular, the correction plate components in the proposed design due to their function and location within the frame and line fields absorb a proportion of this field. This can significantly add to problems in temperature levels created over extensive

switch on times. This may be reduced by careful choice of the component material, such as black anodised raster plates.

The energy loss in the line coil is considerable particularly at higher frequencies such as 100Hz. This phenomenon occurs due to the current passing through the wire finding itself in the alternating magnetic field generated by the current through the wires. This phenomenon which is caused either by the current in its own wire (skin effect) or by currents in other wires (proximity effect) is a quadratic function of the frequency. A frequency of 100Hz of a hybrid design is possible, however this is the limit to a design using raster plates. The addition of raster plates causes trapezoidal raster distortion at 32kHz.

The additional frequency responses of the line coil may affect the energy levels associated, however litz wire may improve this characteristic. Litz wire consists of many small gauge wires stranded in a particular way. The use of litz wire in coil windings reduces the skin effect increasing the active cross-sectional area, thus reducing the effective resistance.

There are various sources of dissipation present in the deflection coil; the temperature determined by the ambient temperature in the set; dissipation in the line and frame coils and yoke ring; and the dissipation in the picture tube. (The use of special ferrites with lower hysteresis losses is a possible aid to reduce the heat generated in the defection system).

The effect on line coil scanning frequency affects the performance of the coil, therefore in any design, the objectives are to optimize power consumption, linearity, resonance frequencies and temperature rises within the deflection unit.

5.5.3.3. Sensitivity/Pullback

The sensitivity of the optimized slot product was measured as approximately 1 with the pullback measuring approximately 2mm.

The pullback levels of this design would be unacceptable for a manufacturing product solution as the pullback would provide insufficient adjustability during tube matching.

5.5.3.4. Ringing

Ringing in the case of hybrid units refers to an oscillation produced in the frame coil by the line flyback. Ringing is the appearance of vertical 'kinks' in the raster lines on the left hand side of the CRT screen due to resonance of the winding inductance's and floating capacitance. Ringing is more significant for deflection units requiring higher scan frequency and those with lack of overscan possibilities.

To maintain ringing behaviour to acceptable levels it is preferable to design the slot separator to have adequate separation between the different slot segments for the wire windings. This is of course restricted by the requirements of convergence performance of the deflection unit and other system refinements.

5.5.3.5. Drift/Noise

It is important to consider if any distortion of the separator windings results during the temperature cycle that this does not relax the wire windings of the coils, causing either convergence/raster drift during the temperature cycle, or relaxation of the separator on cooling of the line coils. In addition, it is also worth considering that during the winding process, the separator may be stressed and weakened. This may impact upon its behaviour during any temperature increases. Therefore, it is important to assess the deformation of both convergence and raster behaviour from the nominal.

For the optimized product design there is a need to closely assess the level of noise generated. For high frequency applications for line coils, plated designs, particularly those including astigmatism plates and raster plates, contribute significantly to the inherent rattle in the system. This is a specific characteristic of this design type which should be carefully evaluated and minimized.

5.6. Optimization Procedure

5.6.1. Initial Set-Up

The initial geometry of the slot based 59FS product type was created, based on existing designs and the design specification for the 59FS double mussel. This data giving the geometrical information defining the make-up of the base design was inputted into the relevant input files of DUCAD-Y. The finalised design model comprised of two line coils carried upon the slot separator, toroidally wound frame coils wound around a yoke ring, (note not specifically designed for this design), astigmatism plates, coma plates, magnets, coma correction in the tube, and raster plates. This optimization was successfully extended using DUCAD simulation technique to achieve a Q_K of 25, with East/West raster distortion at 3.7%. However, it was noted through further simulation studies that a better overall performance could have been achieved if a dedicated yoke ring was fabricated, providing greater frame coil modulation and overall system sensitivity.

5.6.2. Optimization Strategy and Starting Point

The overall optimization objective was to fully minimise the Q_K (Colour Quality Factor) of the deflection system, whilst ensuring that third order trilemma, total coil pullback, convergence, and raster performance levels are sufficiently maintained.

Initially, the lengths of the line and frame coils were determined by the third order trilemma. Thereafter, the raster and convergence errors were optimized, together with

further fine tuning of the coils dimensions, using 6 and 10 pole modulations, plus additional correction plates. To close, 10 , 14 and 18 pole correction component modifications were included to achieve an acceptable specification.

During the optimization process, greater emphasis was placed upon the input files of the *OPTIMULY* program which defines the design parameters/characteristics of most significance. During the first cycles, the optimization procedure considered convergence errors only. Weighting factors were used. The optimization was limited up to the third harmonic, and then up to the fifth harmonic of wire modulation. Diagram 59 shows the *RECEPT* fields and Diagram 60 shows the *DRAWSECT* diagrams (deflection coil configuration and winding connections) after the optimization process.

```
RECEPT   F2       E1  F 80  Trunc=80 Size=5 Line=6 Col=1 Alt=0



00000 * * * Top of File * * *
00001    2   8
00002     1.006085    0.352521    0.152521    0.000000    0.000000    0.000000
00003     0.000000    0.000000
00004     1.093200    0.400000    0.200000    0.000000    0.000000    0.000000
00005     0.000000    0.000000
00006 * * * End of File * * *
```

Diagram 59 : RECEPT File (typical)

Line 00001 Number of modulation levels and number of multipoles

Line 00002 - 00005 Multipole coefficients of first and second levels.

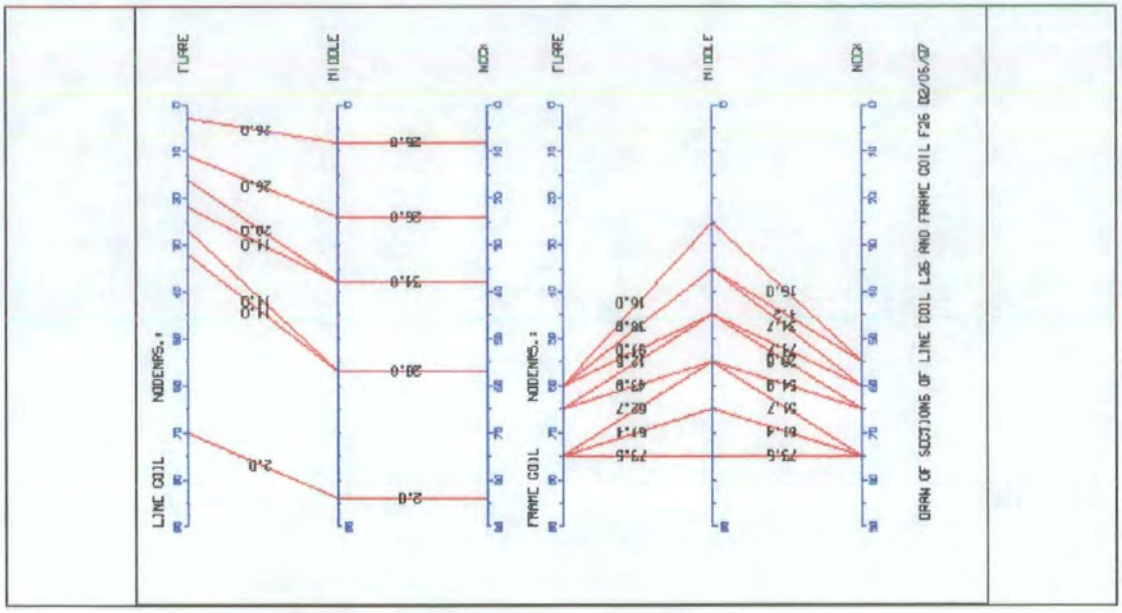

Diagram 60 : DRAWSECT file L26F26

Throughout the optimization process coil dimensions, mechanical wire distributions, wire density distributions, plus component alterations were modified with the objective of minimising the aberration errors.

Initially in the optimization process, a pure dipole was introduced at all three modulation levels (rings) of both the line and frame coils. Both astigmatism and coma plates were introduced at this stage however their effect was only realised on the introduction of higher order modulations other than pure line and frame dipoles. ASTx and COMx are the associated segmentation files, x referring to the desired level of plate modification. An initial Q_K of 317 was realised.

From this point, wire deltas were introduced (minor modifications to the multipole distributions) in both the line and frame coils, plus special deltas (all other changes, other than multipole alterations, such as component position and size, magnet strength, etc.). In this pass, only four special deltas were introduced, varying the number of wound turns in three of the crucial slots within the separator, slots 1, 5 and 6, plus an alteration to the magnet strength.

Changes to the system were made based on the *RECALCY, MAKEALLY, OPTIMULY* process of alteration.

5.6.3. Detailed Study of Design Optimization Procedure

Level L1F1 Coil Design

L1F1 coil was created, adding a small amount of six pole modulation. Only approximately half the estimated available modulation space was introduced at this stage of the process. This was to maintain sufficient optimization space for later steps to prevent DUCAD-Y optimizing to a local minimum. The six pole modulation fields of the line and frame coils were coupled to some 10 pole modulation, to further reduce Q_K to approximately 175.

L2F2

Further wire deltas were implemented; the six and ten poles were de-coupled in their modulation to achieve reasonable convergence behaviour in order to introduce higher order multipoles (10, 14 and 16 poles). Introduction of excessive higher order modulation may result in spot performance deterioration, therefore their introduction was carefully studied.

L3F3

More six pole modulation in the line field was obtained using a small amount of coupled 10 pole modulation. This reduced the Q_K to 126. At this point in the optimization the sign of some wire deltas were changed to achieve positive modulation of the line/frame fields to give sufficient space for optimization deltas to work and so ease the astigmatism error levels.

14 pole modulation was added at this stage to the front screen ring of the line coil, in the hope of influencing the tails behaviour. Only dipole, six and ten pole modulation was present on ring R1 to limit the overall modulation of the line coil. Note that on the introduction of 14 pole modulation, the 10 pole was de-coupled from the six-pole modulation. In order to achieve the positive current levels required, recalculation of the modulation contributions was undertaken after each wire delta. Modifications were make to the *OPTIMULY FT04F001* file to decrease the optimization weighting of the BRx errors, in the hope of allowing further optimization of other coil parameters.

A new coma plate was introduced with pole shoes, COM2. A new astigmatism plate AST2, was introduced, with a section removed from the neck and added to the midsection of the plate.

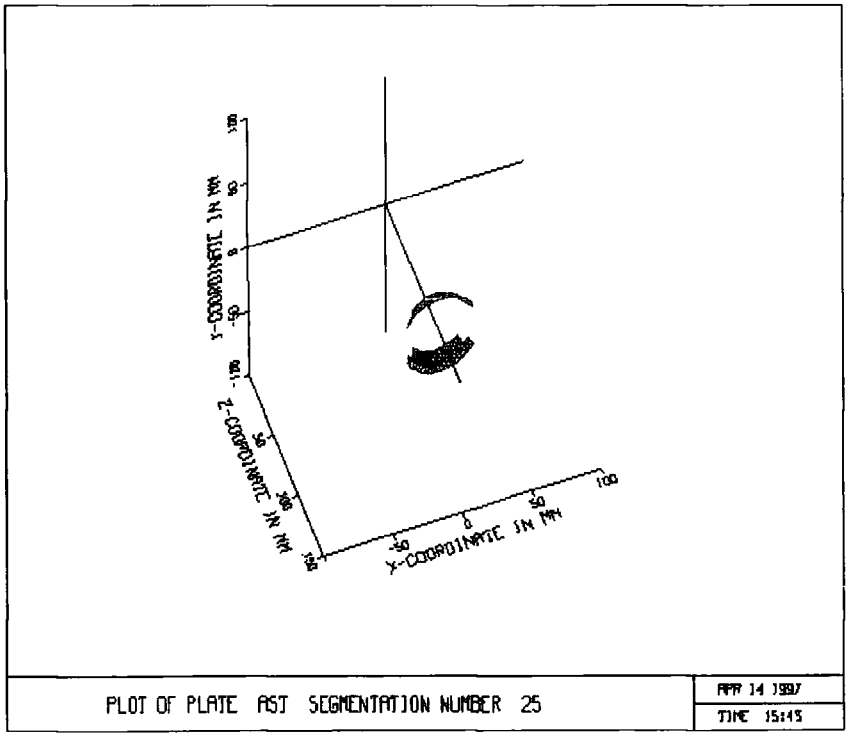

Diagram 61: Modification to Astigmatism Plates

Neck section reduced, midsection of plate increased in height.

The astigmatism effectively screens the field line underneath the plate, and amplifies the field surrounding the plate edges. A small astigmatism plate therefore makes all multipoles more negative, and a plate with a large subtended angle makes multipoles of lower order more negative and those of higher order more positive. Therefore the astigmatism plate is primarily used to determine the required sign of six-pole modulation around the mid section of the coil, and additionally effect tails and crossing behaviour by the shape and dimensions of the side sections of the plate.

In addition, the plate was moved forward to help influence frame astigmatism levels. However, on performing this operation, the tails behaviour deteriorated drastically, and BR_x/BR_y performance became positive/negative opposite in sign. When attempting to reduce the level of BR_x/BR_y it is beneficial to maintain the same signs of the coil errors to aid the general convergence optimization approach.

L5F5

To recovery from this deterioration in performance, a 6 pole offset was performed to restore some stability to the line coil. A Q_K of 114 was restored.

L6F6

The astigmatism and coma plates, COM1 and AST1 were restored into the design model. A further repair loop was introduced and de-coupled to reduce the instability influence of the correction plates. There are three main reasons for implementing a repair loop in the optimization process. Firstly, *OPTIMULY* may predict a performance result based upon a modification to the line/frame multipole strengths and/or multipole signs. Due to the defined system geometry, primarily the number of line/frame slots defined and/or the position of the slots within the coil rings, the realised multipoles may differ from the requested ones, causing an offset between the results. Secondly, the linearity of the requested delta may be poor. This is indicated when a delta is employed to further improve the design, however a different strength

of delta is used causing a further difference in the realised results. This can be corrected by changing the sign and the strength of the deltas created and repeating the delta implementation. Thirdly, a repair loop is often required due to the instability in the system when utilising astigmatism and coma plates in the design. If a mixture of geometry deltas is implemented, for example a coil ring position and/or a plate modification simultaneously, non-linearity of the system will result, due to the interaction of the plate with the field lines running underneath and in the vicinity of the plate section. This is more often required when introducing modifications to the astigmatism plate due to its location between both line and frame fields. This effects mainly higher order multipole deltas , particularly when employed +1 times, as compared to the *OPTIMULY* output file which may indicate a smaller magnification of change of multipole strength.

L7F7

In this move both *OPTIMULY FT04F001/FT05F001* files were modified. Further wire and special deltas were created.

L8F8

At this stage, higher order deltas were introduced on the line coil at the front side to reduce the influence on tails/crossings, etc., plus any corner effects. To reduce the large corner coma errors, higher order multipoles were required, modifications were made to the *OPTIMULY* file to reflect this requirement.

In addition, wire and special deltas were carried out on the magnet size and strength, and to the position and size of both astigmatism and coma plates. However, with a resultant Q_K of 69.4, with Qc at 59.7, it was recognised that to achieve a reasonable coil design of Q_K approximately < 30, additional coma correction was required, via a coma ring in the tube.

The DUCAD-Y model simulates a COMA -RB, a metallic plate shielding field around the gun area, by killing all local fields from the outer beams, red and blue guns, over the distance specified in the TRAJECT FT05F001.

L9F9

A new astigmatism plate design was introduced. However, a 6 pole error pattern appeared. The dipole strength was varied to allow sufficient room for the higher order modulations. A Q_K of 59 was realised.

L10F10/L11F11

A negative 10 pole modulation was introduced on the front ring of the line coil. The weighting of the F_{ast} errors were increased, from 1.0 to 1.4, to rectify the excessive tails behaviour. Frame wire deltas were created.

L12F12

On the initial run of this level, Q_K was 48.7. Anisotropic coma was -1.142mm. Deltas were created on both the magnet and coma shunt. The frame coil was creating anisotropic coma effects, F_{ast} weighting level was increased in an attempt to eliminate.

The following course of action was considered at this stage; move the astigmatism plates towards the screen, and increase the size of the T-wings of the plates; modify the separator design to allow more wire modulation within the first slot position; increase the angle at which this slot is subtended; design a specific yoke ring to better fit the separator profile. (The current yoke ring and hence the frame coil suit the 27V hybrid design, however, if a yoke ring could be fabricated to suit the 59FS profile, better modulation of the frame coil could be achieved.) In this case, the position of R2 could be modified with respect to R1 and R3, to increase the modulation at the neck to reduce coma distortion.

The optimization procedure continued, with a Q_K of 60.9 being realised. Line astigmatism at -0.855 mm, frame astigmatism at 1.616 mm. The main errors still present were large crossing and tails distortion.

L13F13

To try to eliminate the tails/crossing errors, a new astigmatism plate was introduced, AST5, with larger wing sections. However, this change seemed too large, L13F13 became unstable (flipping deltas), and the L12F12 coil design was returned to. Flipping deltas is an indication of system instability, and occurs for example if removing one turn from a slot indicates in OPTIMULY a certain behaviour, and on re-calculating with the opposite move, i.e. adding one turn to the slot, a linear relationship is not achieved. This is an indication that the optimization has become unstable and a local minima in the optimization map has been entered. The method of recovery is to switch off all the suspect wire and special deltas and re-continue.

L14F14

The smaller astigmatism plate was introduced AST10, to effect the tails and anisotropic errors resulting, and return the optimization model to more linear and stable behaviour. In addition, the magnet strength and size were altered to control the tails/crossing behaviour. (In *TRAJECT FT05F001* the magnet strength is defined as an arbitrary value which during hardware/software validation requires definition).

L15F15

At this stage, a raster plate was introduced into the design, RAS1. -10 mm of YR barrel existed. (YR defines the amount of raster distortion in the Y-direction at the corners of the screen). To compensate for this pincushion raster profile, the magnet strength was reduced, which introduced a slight barrel shape raster.

The raster plates were introduced to achieve the required raster behaviour, as defined in the design specification. Due to the design limitations of the saddle/toroidal concept, the need for raster plates to tackle the raster distortion was evident. The raster plate effectively increased the contribution of six pole modulation on the flare side of the line coil.

L16F16

Further wire and special deltas were carried out to optimize the coil design. A Q_K of 42.4 was realised.

L17F17

Further wire and special deltas were carried out to optimize the coil design. Further 10 pole modulation was introduced. A Q_K of 40.8 was realised.

L18F18

Further wire deltas were carried out, with the design containing AST10, COM1 and RAS1. The Q_K of 39.1 was realised. At this stage in the optimization run, much work was required to achieve significant improvement. E/W raster remained high, at Q_R of 260.

L19F19

Special deltas were carried out on the astigmatism plate to reduce the tails and crossings behaviour. On reducing the size of the wing sections of the plate, the anisotropic effects were reduced by 0.2 mm.

L20F20

Modifications were made to the coma plate shoes. Other deltas were carried out on the number of turns per separator slot, on the COMA RB size, etc. A Q_K of 44.9 was realised.

L21F21/L22F22

Further line and frame wire deltas were introduced to this design make-up. A Q_K of 28.6 was realised.

L23F23

On the neck screen side of the frame coil, six pole modulation was added, in the hope to overcoming the non-linear behaviour. Further modifications were made to the raster plate pole shoes and coma plates. A Q_K of 27.7 was realised, with much improved tails behaviour.

L24F24

This level of optimization includes AST10, COM1 and RAS1. In ensure that the correction methods, such as astigmatism, coma plates and COMA RB rings are influencing the overall field modulations in a stable and reliable manner, deltas are carried out omitting each in turn, to ensure that their influence is as expected.

Omitting COMA RB ring, greatly influenced the level of anisotropic coma, frame coma and tails effects, influencing 1.6mm in frame coma levels, and 1.5 mm in anisotropic coma.

Omitting the coma plate, greatly influenced the level of anisotropic coma, frame coma and tails effects, influencing 0.9 mm in tails, and 1.3mm in frame coma levels , and 1.3 mm in anisotropic coma.

Omitting the astigmatism plate increased frame coma by 2.6mm, whilst giving 7 mm of BRx errors. The frame field was shortened, indicated by third order trilemma, which resulted in a -0.5 value. This may indicate that the plate is too large for the frame design.

Without the raster plate, X_R increased to 4 mm, whilst Y_R increased to 10.2 mm. The magnets and raster plates greatly affected tails behaviour, giving

-0.994 mm and 1.524 mm

-0.989 mm in BRx 1.761mm in BRy errors

Without the N/S magnets, of strength 1.8, 4.99mm in X_R error and 15.8 mm Y_R resulted.

L25F25

Further wire deltas were carried out, plus alterations to the OPTIMULY FT04F001 weighting file. A Q_K of 28.2 was realised.

5.6.4. Finalised Design Solution: L26F26

In this final design level the following correction means were utilised;

N/S magnets, of strength 1.9;
Coma RB, size 3mm;
Astigmatism Plates, *SEGMENT AST24*;
Coma Plates, *SEGMENT COM1*;
Raster Plates, *SEGMENT RAS1*.

A Q_K of 25.5 was realised, with Q_C at 13.2, Q_A at 32.7, and Q_R at 220.5. The raster performance was mainly as a result of E/W behaviour, which could be compensated for within the circuitry of the tube/set. Therefore a reasonable design was achieved, however some possible performance improvements to the design could be made, particularly the raster shape and ease at which coma correction is obtained, i.e. perhaps without the need for a coma ring within the tube.

CVRSLF L26F26 E1 F 80 Trunc=80 Size=20 Line=13 Col=1 Alt=0

	XS (M)	YS (M)	XR (MM)	YR (MM)	BRX (MM)	BRY (MM)	XCOMA (MM)	YCOMA (MM)
	0.114400	0.000000	0.000	0.000	0.216	0.000	0.128	0.000
	0.228800	0.000000	0.000	0.000	0.002	0.000	0.451	0.000
	0.000000	0.085800	0.000	0.000	-0.119	0.000	0.000	0.580
	0.114400	0.085800	1.866	1.502	-0.080	-0.116	0.063	0.491
	0.228800	0.085800	2.930	2.595	-0.473	0.711	0.271	0.376
	0.000000	0.171600	0.000	0.000	0.622	0.000	0.000	1.662
	0.114400	0.171600	4.185	0.263	-0.040	-0.249	-0.166	1.294
	0.228800	**0.171600**	**8.477**	**-0.211**	**-1.131**	**0.940**	**-0.079**	**0.790**

SLAG(MM)	ZS(MM)
4.705	155.295

QA	QC	QK	QR	%EW	%NS	SLAG	TR3	TR5
37.6	53.2	50.9	221.6	3.70	-0.12	4.71	0.219	-2.016

* * * End of File * * *

Diagram 62 : CVRSLF L26F26, without COMA RB

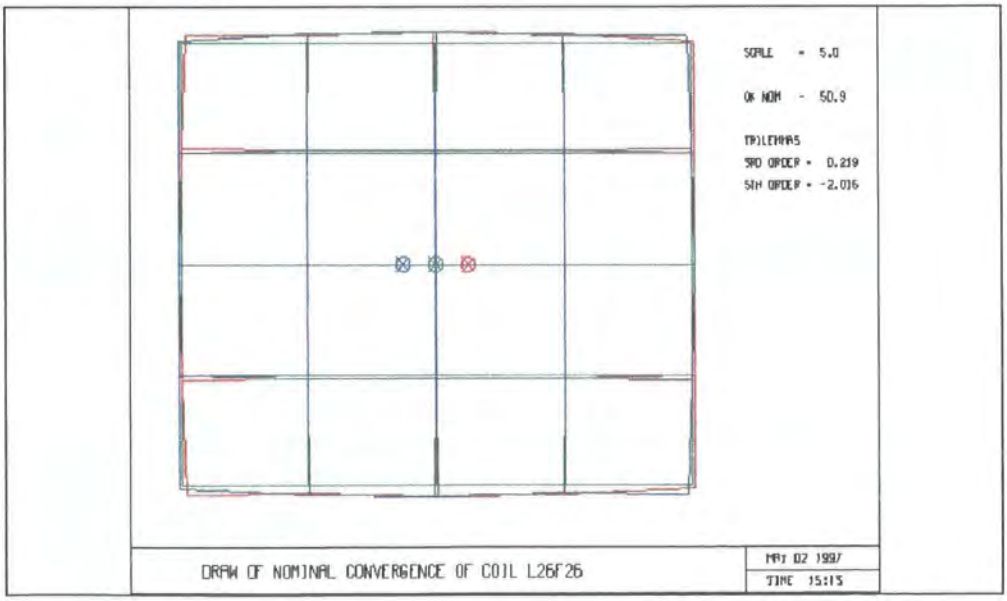

Diagram 63: Diagrammatic Representation of CVRSLF L26F26 Convergence Behaviour, without COMA RB

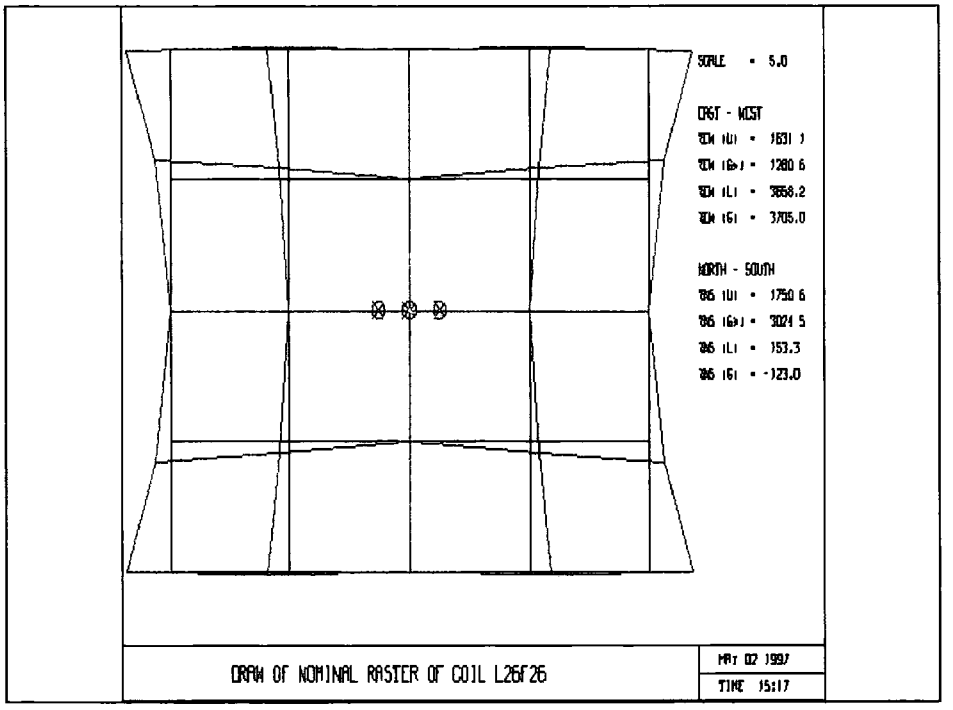

Diagram 64: Diagrammatic Representation of CVRSLF L26F26 Raster Behaviour, without COMA RB

6. CHAPTER SIX

Validation Of Software Simulation Model Via Hardware Experimentation

6.1. Introduction

To check the accuracy and validity of the DUCAD-Y simulation model hardware validation of the optimized product design was performed. In any design process of this nature it is considered prudent to realize the generated software design solution via practical prototyping methods to confirm the degree of correlation between the analytically derived results and the experimentally gained equivalent data. In this development study on realising the software design, hardware validation was used to finally optimize the design. At this stage within the development cycle less time and effort was essentially involved in the implementation of minor modifications to the product design.

Assembly errors and inaccuracies are obviously inherent in any hardware prototype model, therefore to minimize the degree of inaccuracy between hardware and software results a number of samples were fabricated to average out the anticipated inaccuracies.

6.2. Measurement Equipment

The measuring equipment employed in this study is referred to as a MOM, an accurate method of measuring small convergence and raster errors at all screen positions by means of an automatic moving camera. The camera is placed in front of the green tube (special CRT), and a computer operates the camera movement. Each position on the screen is located and the camera sequentially switches on the green, red and blue guns to identify the errors. The output signal of the camera is monitored and its position is adjusted to place the green spot at the centre of its measuring field. The position of each electron

beam is determined by averaging the output signal over the central part of the spot. The equipment is able to measure accurately to the order of μ mm.

For additional visual verification, a manual monitor was used which allowed individual samples to be visually analysed.

6.3. Methodology

Many magnetic interactions occur in the proposed design due to the number of included correction components, therefore to accurately determine the proposed design solution the hardware design was fabricated as a complete solution. On creation of the complete hardware design, the correction components were removed one at a time. By adhering to this methodology, the individual component parts could be assessed to determine their individual influence. The individual harmonic field potentials were considered to note any convergence shifts or distortion. The analysis of the performance plots, etc., aided optimizing the hardware model against the software ideal. Thereafter the hardware samples were optimized to an acceptable design solution.

Not considered in the hardware replication from the DUCAD-Y model was the introduction of the tube coma ring (COMA RB). This fabrication would have required alterations to the tube geometry and gun configuration, and was beyond the scope of this study.

6.4. Fabrication of the Hardware Components of the DUCAD-Y Design Solution

6.4.1. Line and Frame Coils Hardware Replication

6.4.1.1. Introduction and Method of Manufacture

For initial design verification, the line and frame coils were considered in isolation and fabricated to establish a degree of confidence in the DUCAD-Y simulation geometry's, etc. The line coils were manufactured using a Sony slot winding machine. The frame coils were wound using a standard universal frame winding machine. Refer to appendix C for manufacturers literature on the Sony winding machine.

The Sony winding machine employs the winding technique depicted in Drawing 62. Two hooks are mounted at the neck and flare sections around the separator to manipulate the wire. The wire is fed through a nozzle which runs vertically to the separator. The circular motion in Slot Winding process pushes and pulls the wire around the separator to create a complete turn of wire. The two hooks therefore hold the wire at either the neck and flare, and after indexing the separator, one hook releases the wire to allow the respective hook to take over. The tension alternates to different levels pulling and pushing the wire at different points around the separator. The higher the tension, the more compacted and settled the wire is within the slot grooves.

Inherent in the slot winding process is asymmetry from the left side of the wound coil to the right side. This is indicative of the inherent pulling and pushing of the wire, creating high and low tension levels around the separator. The asymmetry of the winding process is particularly noticeable at the neck and flare sections of the wound separator.

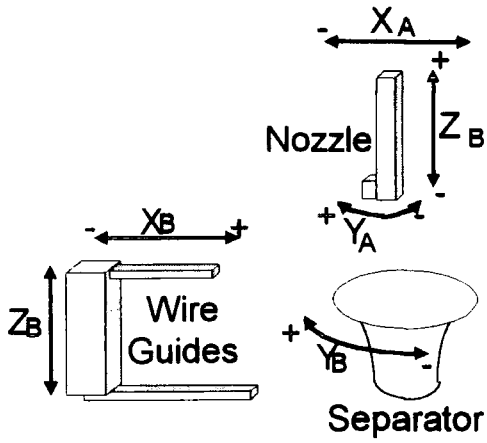

Diagram 65 : Winding Methodology of the Sony Slot Winding Machine

The impact of this in product performance was assessed by carrying out process capability trials to assess the level of spread against the nominal design errors. It is shown to be an acceptable working amount, therefore in the following trials, the anticipated spread in main axis convergence was assumed to be negligible. The anticipated diagonal asymmetry due to the winding process was studied and shown not to be significant.

6.4.1.2. Generation of Accurate Winding Specifications for the Line and Frame Coils

Frame Coil

Manufacturing Process

The vertical coil is constructed by splitting a ferrite core into two halves and separately winding the coil distribution on each half of the core using a standard universal winding machine. The yoke rings are clamped into the winding machine thereby leaving some unwindable spaces on the yoke ring. Refer to Diagram 66 for detail of the mechanical frame winding arrangement.

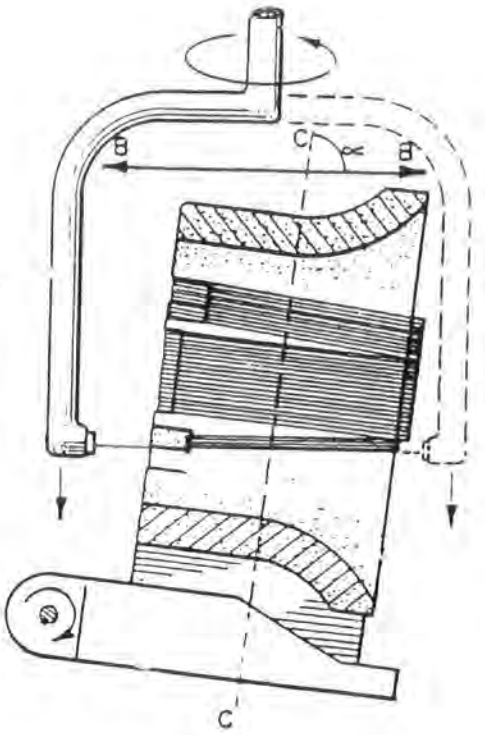

Diagram 66: Diagram of Frame Coil Winding Mechanical Arrangement

To achieve a good windable coil, a winding program was written to minimize the frequency of stops in a winding run and any reversals of winding direction, in order to increase the overall accuracy and precision of wire positioning. The two halves are then reassembled on the plastic line separator using a metallic spring clip. After winding, the two halves are then reassembled on the plastic line separator using a metallic spring clip.

The DUCAD generated wire distribution for the frame coil can be digitised into various cross-sectional turns of wire around the yoke ring.

Neck Section

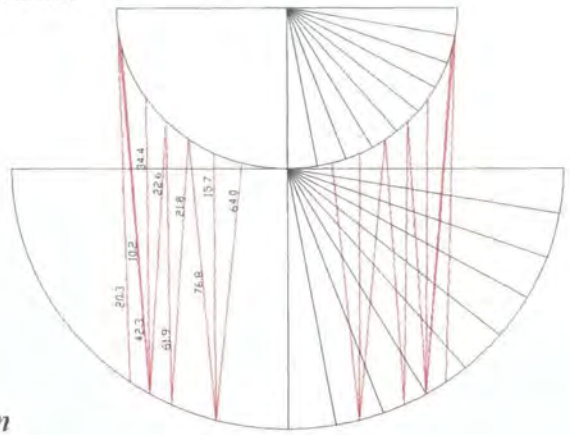

Flare Section

Diagram 67 : Actual Wire Distribution across the Toroidal Frame Coil

Diagram 68 details the wire distribution for the frame coil as a harmonic analysis of the winding pattern, allowing the frame winding program to be more easily created.

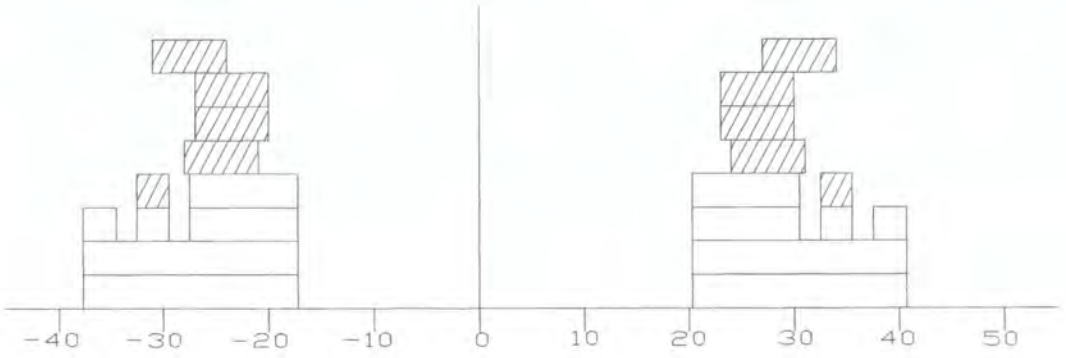

Diagram 68: Wire Distribution - Harmonics of Winding Pattern

The above diagram depicts the position and density of winding across the frame coil. The hashed sections refer to wire positions with a slant angle of greater than 20 degrees. The large oblique winding slants were incorporated to reduce the level of frame coma errors present.

6.4.1.3. Electrical Considerations for the Line and Frame Coils

Introduction

In addition the deflection systems magnetic field distributions and its visual performance on the CRT display screen, the electrical interfacing of the deflection unit and the CRT circuitry must be considered.

Two of the primary electrical considerations are stored energy and the inductance/resistance (L/R) ratio, the stored energy of the horizontal coil being a key design characteristic of the deflection unit. During each cycle of the horizontal current the stored energy is transferred back and forth between the magnetic and electric field where it is stored as $CV^2/2$, C being the capacitance and V the voltage difference across the retrace capacitor. An optimized design should aim to minimize the stored energy to reduce the voltage V across the transistor in the deflection circuit during the flyback period, otherwise the deflection circuits' lifetime and reliability is reduced (or a higher specification of transistor is required). The L/R ratio is an important circuit parameter for both deflection coils and is prescribed by the circuit designer. It affects the non-linearity of the raster from one side to the other and the amount of heat generated for a given L. The values of L and R can be varied independently by simultaneously changing the wire size and number of turns whilst keeping the cross-sectional area constant.

Frame Coil Electrical Design

The maximum permissible voltage during flyback and the $1/2\ L\ I^2$ term determine the self-inductance of the frame coil. The required electrical parameters for a toroidally wound frame coil for a 59FS tube chassis are based upon a flyback time of the order of 0.8 ms. Due to the inherent necessity for low coil impedance, the toroidal coil demands a very high current, of the order of 3.9A, which can lead to high heat dissipation.

For this development application, a comparatively higher coil impedance was chosen to provide some relief from the high current levels to reduce the heat dissipation. (This is a disadvantage of the toroidal coils as opposed to double mussel wound coils).

The target electrical values were set as; Lv = 6.4 mH, and Rv = 3.2 ohms, giving a peak current Iv of 2.62A edge to edge at 27kV, assuming a flyback time of approximately 1.1 ms. To achieve an acceptable nominal setting, and further scope for wire distribution flexibility, the number of turns were set to 400. The frame coil wire diameter was selected, 0.355 mm diameter (Grade 1, specification wire) based on the designed length of copper per coil and the target impedance level.

The sensitivity levels (L/R ratio) is a crucial factor in determining an ideal frame coil. It is clear that for higher frequency applications the toroid coil has inherent design limitations due to the shorter flyback period (0.45ms) required. A flyback period of 0.45 ms imposes a reduction in coil inductance levels to approximately 0.5 mH resulting in an unacceptable peak deflection current, exceeding the 'safe' maximum of approximately 2.5A.

Line Coil Electrical Design

Manufacturing Process

Horizontal deflection consists of two line coil halves having the same winding direction. The line coils were fabricated from the designed separator, the winding process directing the wire into the grooves of the plastic separator. Wire tension was an important factor influencing the performance of the coil, the higher the tension, the more compacted the wire became within the slot grooves. This increased the compression of the wire within the slot grooves directly affecting the magnitude of the generated electromagnetic horizontal field.

The created DUCAD-Y file *CALFAS FT12F00L* detailed in Diagram 69, defined the winding distribution for the line coil.

```
CALFAS   FT12F00L E1  F 80  Trunc=80 Size=19 Line=9 Col=1 Alt=0

00000 * * * Top of File * * *
00001 'BOUNDS'
00002  37.0    0.0      0.0     0.0    10.0    4.0
00003  37.0  120.0    120.0   120.0    10.0    4.0
00004 'END'
00005 'BOUNDS'
00006  37.0    0.0      0.0     0.0    10.0  4.0
00007  37.0  120.0    120.0   120.0    10.0  4.0
00008 'END'
00009 'BOUNDS'
00010  37.0    0.0      0.0     0.0    10.0  4.0
00011  37.0  120.0    120.0   120.0    10.0  4.0
00012 'END'
00013 'BOUNDS'
00014  37.0     0.0    0.0     0.0     0.0   0.0     0.0     0.0   10.0  4.0
00015  37.0   120.0  120.0   120.0   120.0 120.0   120.0   120.0   10.0  4.0
00016 'END'
00017 'END'
00018 'END'
00019 FEND'
====>
                                                          XEDIT 1 File
```

min. number of turns per slot

max. number of turns per slot

slot overlap definition for R2 to R3

Diagram 69: CALFAS FT12F00L File

Due to the inherent electrical losses in this particular application, an important objective is the reduction of current in the deflection coils. This in practice imposes high voltage characteristics, of the order of 1200-1600 V. The line voltage and sensitivity of the deflection unit ($1/2\ LI^2$) combine to determine the self-inductance of the coil, using $E = - L\ dI/\ dt$. The line coil resistance is commonly determined by the requirements for deflection linearity and heat economy.

Four 0.375 mm diameter wires, Grade 1 insulation specification were wound in parallel to determine the necessary line coil inductance levels. The line coils were subsequently connected in series. As initially determined by DUCAD-Y 60 turns were wound per each line coil half and the optimized line coil had the following electrical values;
L_L (inductance) = 1.85 mH and R_L (resistance) = 1.80 ohms.

Refer to Appendix B for the *DRAWSECT L26F26* output file detailing the winding specifications for the line and frame coils. The line coil winding information was easily transposed into the number of turns per slot in the separator, and thereafter preset in the Sony machine winding variables.

6.4.1.4. Assembly Method

The wound line coil plus the two yoke halves of the frame coils were assembled. The line coils were series connected and the frame coils parallel connected, the wire lead outs were terminated on the termination board to the front of the deflection unit. The units were thereafter tinned and coupled. Coupling refers to the extent an a.c. voltage applied to the line coils results in an induced a.c voltage in the frame coils. A 1V a.c. signal was applied to the line coils, and the resultant voltage across the frame coils was read using a volt meter. The yoke ring was then rotated to ensure that the vertical and horizontal axes are at 90 degrees with respect to each other, achieved if there is no voltage induced in the frame coil, i.e. 0V a.c..

Once the correct alignment of the line and frame coil positions was determined, the unit was glued into position to retain the coupled set-up.

6.4.1.5. Discussion of DUCAD-Y Predictions

The following section discusses the magnetic field distributions predicted by DUCAD-Y when only the optimized line and frame coils are present. The angles refer to the position of the wire of the line and frame coils, as defined in the Theory Section.

Line Magnetic Field Distributions (Line and Frame Coils Only)

Refer to Appendix B for the line and frame magnetic field distribution plots.

Studying the multipole distributions at the neck and flare of the designed line coil, it is noted that a barrel shaped six pole field is generated peaking at approximately 18 degrees, together with a pincushion six pole field, of larger magnitude, peaking at 45 degrees.

Ideally for a line coil deflection ten pole modulation should be negative at the neck side and positive at the flare of the coil. Wire placed at 36 degrees around the coil is very suitable to generate a negative 10 pole. A positive ten pole field is generated at 15 degrees of small magnitude, accompanied by a larger peak at 45 degrees. Ten pole modulation is important as it primarily influences raster distortion. The undesirable 'seagull raster distortion' is caused by positive line ten pole field modulation.

From studying the line distribution plots it is clear that the six-pole neck modulation does not create sufficient barrel-shaped field , and there is an overcompensation of the positive pincushion field at the screen side of the line coil. Therefore, a less than ideal six-pole field shape is generated at the neck and insufficient positive ten pole is generated at the flare.

Frame Magnetic Field Distributions (Line and Frame Coils Only)

For the optimized frame coil, a negative barrel shaped dipole field is generated at 45 degrees, with a slight pin cushion field at the front of the frame coil.

For six-pole modulation, a positive pincushion field is generated at the neck, at approximately 20 degrees necessary to limit the amount of frame coma errors. A six pole barrel field, of greater strength, peaking at 45 degrees, is generated at the flare. A barrel ten pole field is generated at both the neck and flare of the frame coil.

Note that in this design the necessary E/W correction is high. To minimize this effect, the six pole frame field at the extreme screen side requires further positive modulation. To generate positive six-pole pincushion at both the neck and flare sections of a toroidal coil is extremely difficult, due to the inherent limitations of the winding method.

The *L26F26 CVRSLF* output performance file for the optimized line and frame coils is detailed in Diagram 70.

```
 CVRSLF   L26F26   E1  F 80  Trunc=80 Size=20 Line=13 Col=1 Alt=0

00004     XS         YS          XR       YR       BRX      BRY     XCOMA    YCOMA
00005     (M)        (M)         (MM)     (MM)     (MM)     (MM)    (MM)     (MM)
00006    0.114400   0.000000    0.000    0.000    0.779    0.000    0.096    0.000
00007    0.228800   0.000000    0.000    0.000    1.852    0.000    0.413    0.000
00008    0.000000   0.085800    0.000    0.000    1.655    0.000    0.000    0.025
00009    0.114400   0.085800    3.448    3.334    3.256    1.278   -0.031   -0.149
00010    0.228800   0.085800    4.384    7.988    6.314    3.736    0.272   -0.342
00011    0.000000   0.171600    0.000    0.000    5.605    0.000    0.000    0.476
00012    0.114400   0.171600   13.067    7.493    9.344    0.916   -0.488   -0.178
00013    0.228800   0.171600   17.698   19.911   18.919    7.933   -0.195   -1.040
00014
00015    SLAG(MM)    ZS(MM)
00016       8.560    116.440
00017
00018      QA      QC      QK      QR      XEW     XNS     SLAG      TR3      TR5
00019     ------------------------------------------------------------------------
00020     505.2    28.8   358.0   665.2    7.74   11.60    8.56     0.402    2.929
00021 * * * End of File * * *


====>
```

Diagram 70: CVRSLF L26F26 Line and Frame Coils only

6.4.2. Fabrication of Astigmatism Plates to overall Hardware System Replication

6.4.2.1. Introduction

The proposed astigmatism plate as detailed in file *SEGMENT AST24* was fabricated. In addition other astigmatism plates available, of different shape and size were tested during hardware optimization to assess their characteristics to determine if a potentially better system performance could be realized using different correction plates to those specified by DUCAD-Y.

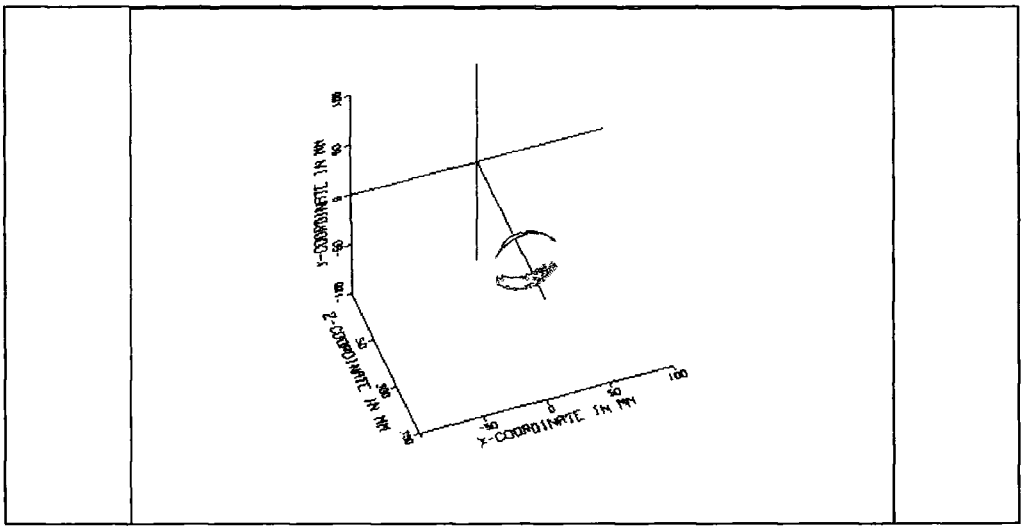

Diagram 71: SEGMENT AST24 Plot

By varying the subtended angle of the astigmatism plates it is possible to obtain certain ratios between the multipoles. Small plates at north and south positions make all multipoles more negative, whereas plates with a larger subtended angle make lower order multipoles more negative and those of a higher order more positive. Therefore, by dividing the plate configuration into several sectional parts with different subtended angles, fine adjustment of the multipoles is possible.

6.4.2.2. Generation of Hardware Profile for Astigmatism Plate

From the *SEGMENT AST24* file, an engineering drawing was created from which a small quantity of hardware components were fabricated to this specification. The CVRSLF L26F26 performance, line and frame coils, plus AST24 plates is detailed in Diagram 72.

```
CVRSLF   L26F26   E1  F 80  Trunc=80 Size=20 Line=13 Col=1 Alt=0

00004    XS        YS         XR       YR       BRX      BRY     XCOMA    YCOMA
00005    (M)       (M)        (MM)     (MM)     (MM)     (MM)    (MM)     (MM)
00006   0.114400  0.000000   0.000    0.000    0.779    0.000   0.096    0.000
00007   0.228800  0.000000   0.000    0.000    1.852    0.000   0.413    0.000
00008   0.000000  0.085800   0.000    0.000   -1.234    0.000   0.000    1.175
00009   0.114400  0.085800   4.715    4.093   -0.267   -1.732   0.070    0.982
00010   0.228800  0.085800   7.553   10.461    1.171   -1.286   0.329    0.673
00011   0.000000  0.171600   0.000    0.000   -5.555    0.000   0.000    3.089
00012   0.114400  0.171600  16.761    8.871   -3.595   -6.700  -0.067    2.498
00013   0.228800  0.171600  26.662   24.365    0.679   -5.257   0.153    1.482
00014
00015   SLAG(MM)   ZS(MM)
00016      7.944   122.056
00017
00018     QA      QC      QK      QR      %EW     %NS     SLAG     TR3      TR5
00019    ------------------------------------------------------------------------
00020    242.7    99.7   190.0   887.6   11.65   14.20    7.94    0.281   -3.452
00021 * * * End of File * * *
```

Diagram 72: CVRSLF L26F26 Line and Frame coils, plus AST24 Plates

6.4.2.3. Assembly Method

Reference lines in both the horizontal and vertical plane were engineered into the separator profile to assist in positioning the astigmatism plates in the north and south locations. It is highly important to accurately locate the astigmatism plates as this may lead to increased spread on frame astigmatism levels and crossings/tails behaviour, terms referring to the blue-to-red Y and X errors respectively. The correct position for the astigmatism plates was derived from the DUCAD-Y geometry file given in (Z,R) co-ordinates.

6.4.2.4. Discussion of DUCAD-Y Predictions

Refer to Appendix B for the line and frame magnetic field distribution plots.

Line Magnetic Field Distributions due to the Introduction of Astigmatism Plates

The astigmatism plates located perpendicular to the line field lines will only have any significant effect to line magnetic distributions if the subtended angle of the plate is large.

Therefore, on introduction of the astigmatism plate, there appears little affect upon the line dipole modulation characteristics. Too strong a dipole field is generated at the neck with insufficient six pole barrel modulation and positive pincushion ten pole being realized at the neck section of the line coil.

Frame Magnetic Field Distributions due to the Introduction of Astigmatism Plates

For the frame magnetic distribution, early negative dipole modulation was present at 20 degrees. Pincushion shaped six-pole modulation had been reduced by introducing the astigmatism plates and the negative barrel shape of the six-pole profile had increased in magnitude by a factor of two, at 30 degrees. Small additional bumps in the six-pole amplitude profile indicated a barrel field appearing at 45 degrees.

Introducing the astigmatism plate generated a negative ten-pole modulation field at 30 degrees and a pincushion field at 45 degrees. The astigmatism plate does not appear to have affected the magnitude of this secondary peak, but has introduced a negative field at 30 degrees (solely due to the astigmatism plate).

Therefore, for frame field modulation there was too much dipole field generated at the flare, too much six pole positive pincushion realized, and insufficient positive pincushion 10 pole realized to create a high performing design.

6.4.3. Fabrication of Coma Plates for overall Hardware System Replication

6.4.3.1. Introduction

The segment file defining the proposed coma plate was fabricated as detailed in file *SEGMENT COM1.*

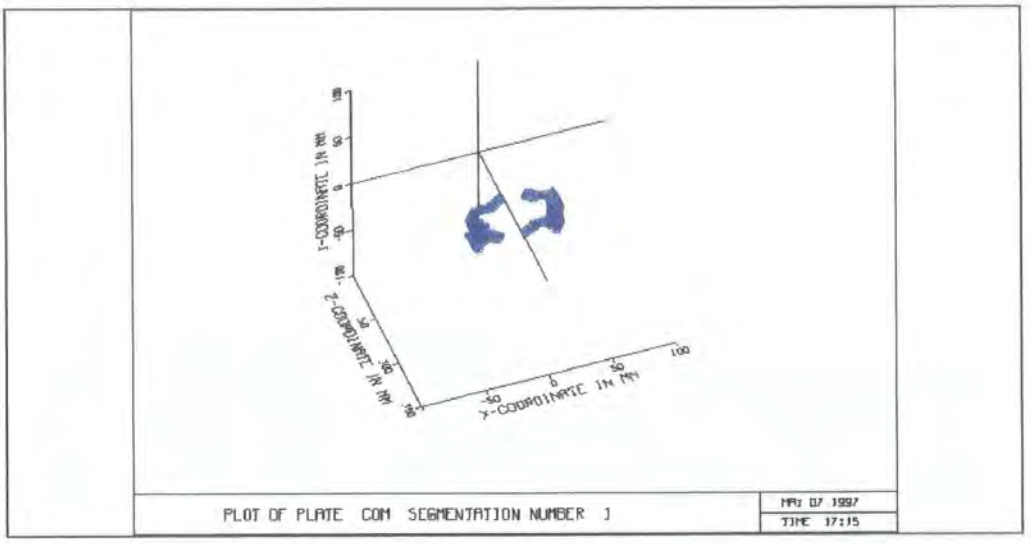

Diagram 73: SEGMENT COM1 Plot

6.4.3.2. Generation of Hardware Specification

From the *SEGMENT COM1* file detailing the dimensions and profile of the coma plate, an engineering drawing was created from which a small quantity of hardware components were fabricated to this specification. The CVRSLF L26F26 performance, line and frame coils, AST24 and COM1 plates is detailed in Diagram 74.

CVRSLF L26F26 E1 F 80 Trunc=80 Size=20 Line=13 Col=1 Alt=0

	XS (M)	YS (M)	XR (MM)	YR (MM)	BRX (MM)	BRY (MM)	XCOMA (MM)	YCOMA (MM)
00006	0.114400	0.000000	0.000	0.000	0.779	0.000	0.096	0.000
00007	0.228800	0.000000	0.000	0.000	1.852	0.000	0.413	0.000
00008	0.000000	0.085800	0.000	0.000	-1.133	0.000	0.000	0.655
00009	0.114400	0.085800	4.762	3.894	-0.142	-1.561	0.006	0.528
00010	0.228800	0.085800	7.603	9.785	1.382	-1.015	0.250	0.360
00011	0.000000	0.171600	0.000	0.000	-5.185	0.000	0.000	1.978
00012	0.114400	0.171600	16.941	8.501	-3.155	-6.203	-0.324	1.454
00013	**0.228800**	**0.171600**	**26.929**	**23.225**	**1.409**	**-4.539**	**-0.178**	**0.675**

	SLAG(MM)	ZS(MM)
00015	SLAG(MM)	ZS(MM)
00016	7.832	122.168

	QA	QC	QK	QR	XEW	XNS	SLAG	TR3	TR5
00018	QA	QC	QK	QR	XEW	XNS	SLAG	TR3	TR5
00020	223.1	59.4	165.8	874.8	11.77	13.53	7.83	0.351	-3.046

00021 * * * End of File * * *

Diagram 74: CVRSLF L26F26 performance, Line and Frame Coils, plus AST24 and COM1 Plates

6.4.3.3. Assembly Method

The correct position for the coma plates was derived from the geometry file from DUCAD-Y, given in (Z,R) co-ordinates. The design of the separator enabled the coma plates to fit securely to the neck portion, in the east-west direction.

6.4.3.4. Discussion of DUCAD-Y Predictions

Refer to Appendix B for the line and frame magnetic field distributions for this system.

Line Magnetic Field Distributions due to the Introduction of Coma Plates

No additional effects were introduced into the line field modulation plots due to the introduction of the coma plates.

Frame Magnetic Field Distributions due to the Introduction of Coma Plates

There if no significant effect to the dipole modulation of the frame field on introduction of the coma plates. A small bump is noticed on the dipole distribution due to the dipole/six-pole interaction, attenuating the dipole field at the neck side of the frame field.

For the six pole modulation, the small positive pincushion at the neck of the coil is made more negative changing the field strength from 0.5 to -7. This peak also starts slightly earlier at 12 degrees instead of the previous 17 degrees. The six-pole barrel field at the middle/flare section is not affected by the coma plate.

A small negative ten-pole modulation is introduced at the neck portion with a relatively small increase in the positive ten-pole modulation at 35 degrees.

Little effect is evident on the higher order modulations. There is a slightly more prolonged negative modulation of the 12 pole at the neck, however the magnitude of modulation remained constant.

6.4.4. Fabrication of Raster Plates for overall Hardware System Replication

6.4.4.1. Introduction

The segment file defining the preferred raster plate profile was fabricated.

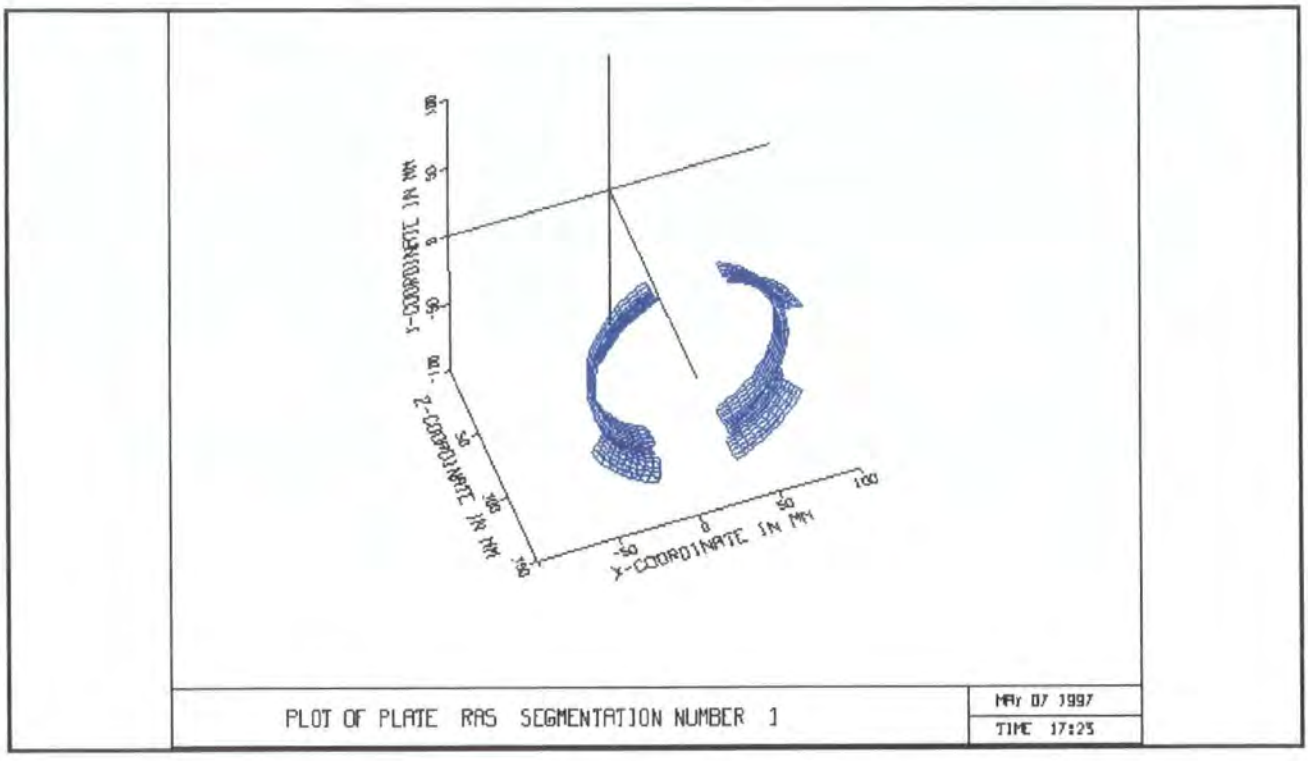

Diagram 75: SEGMENT RAS1 Plot

6.4.4.2. Generation of Hardware Specification

From the SEGMENT file detailing the dimensions and profile of the raster plates, an engineering drawing was created from which a small quantity of hardware components were fabricated to this specification. The CVRSLF L26F26 performance of the line and frame coils, AST24, COM1, and RAS1 plates combined system is detailed in Diagram 76.

CVRSLF L26F26 E1 F 80 Trunc=80 Size=20 Line=13 Col=1 Alt=0

	XS (M)	YS (M)	XR (MM)	YR (MM)	BRX (MM)	BRY (MM)	XCOMA (MM)	YCOMA (MM)
00006	0.114400	0.000000	0.000	0.000	0.779	0.000	0.096	0.000
00007	0.228800	0.000000	0.000	0.000	1.852	0.000	0.413	0.000
00008	0.000000	0.085800	0.000	0.000	-0.570	0.000	0.000	0.598
00009	0.114400	0.085800	3.228	3.170	0.400	-0.802	0.018	0.477
00010	0.228800	0.085800	4.125	6.943	1.798	0.377	0.267	0.340
00011	0.000000	0.171600	0.000	0.000	-2.051	0.000	0.000	1.776
00012	0.114400	0.171600	10.760	7.067	0.034	-3.486	-0.272	1.249
00013	**0.228800**	**0.171600**	**13.736**	**16.228**	**3.333**	**0.427**	**0.005**	**0.672**

SLAG(MM)	ZS(MM)
6.737	123.263

QA	QC	QK	QR	%EW	%NS	SLAG	TR3	TR5
128.2	53.3	100.6	552.2	6.00	9.42	6.74	0.547	-2.069

* * * End of File * * *

Diagram 76: CVRSLF L26F26 Line and Frame Coils, plus AST24, COM1 and RAS1 Plates

6.4.4.3. Assembly Method

The correct position for the raster plates was derived from the geometry file from DUCAD-Y, given in (Z,R) co-ordinates. The raster plates were positioned in the east-west position on the separator, secured in place with Loctite glue.

6.4.4.4. Discussion of DUCAD-Y Predictions

Refer to Appendix B for the line and frame magnetic field distributions for this system.

Line Magnetic Field Distributions due to the Introduction of Raster Plates

The function of the raster plates is to effectively increase the six-pole modulation levels on the flare side. Due to the separator design limiting the achievable modulation possibilities, only a small increase is achieved for the six-pole flare modulation. The negative six-pole field at the neck of the coil is increased in magnitude slightly. The positive field at the middle/flare is reduced in magnitude from 23 to 19 at the 45 degrees angle.

Frame Magnetic Field Distributions due to the Introduction of Raster Plates

To overcome the pincushion EW raster distortion ideally the frame field should generate a six-pole pincushion field at the flare and a stronger barrel-shaped field at the mid-section to successfully converge the blue and red beams.

For the six pole frame modulation a significant effect is created on introduction of the raster plates. The six-pole pincushion at the neck is unaffected alongside the barrel six-pole field at the middle of the coil. However a large pincushion six pole field is created at the extreme screen side of the coil at 50 degrees, of magnitude -17; previously this was a barrel field. This pincushion field is created to minimize the amount of E/W raster distortion.

A second pincushion ten-pole peak is generated at 55 degrees with no change to the magnitude of this deflection field. For sixteen pole modulation, a pincushion field is introduced at 50 degrees, the barrel field at the middle of the coil is unaffected. For

twenty-four pole, the barrel field at 45 degrees is increased in magnitude by a factor of 6. The peak of modulation appears thinner, maximising at 50 degrees instead of 45 degrees.

6.4.5. *Fabrication of static N/S magnets to overall hardware system Replication*

6.4.5.1. Introduction

The *STATIC FT05F001* file defining the preferred N/S magnets was validated. Refer to Diagram 77. Combinations of already available magnets were summed together to predict the magnet influence on the overall raster performance. Other available magnets of different shape, size and strength were tested to assess their characteristics and determine if a potentially better system performance could be realized using different magnets to those specified by DUCAD-Y.

The strength of the magnets were initially set to 1.90 units. (The exact definition of 1 unit of magnetic strength was determined in the hardware prototype study). The magnetic field generated by the influence of the magnets was optimized, the relationship between the individual multipoles being affected by adjusting the magnets overall dimensions and strength. This enabled a more confident correlation of the defined magnet strengths as defined in DUCAD-Y to that realized in hardware.

```
STATIC   FT05F001 E1  F 80  Trunc=80 Size=5 Line=6 Col=1 Alt=0



00000 * * * Top of File * * *
00001      MAGNET FILE STATIC FT05F001 E
00002 0.0  0.07500 0.14000 0.060 0.0100 0.0100
00003
00004 XCENTER, YCENTER, ZCENTER, XSIZE, zSIZE, ySIZE
00005
00006 * * * End of File * * *
```

Diagram 77 : STATIC FT05F001 File, detailing the N/S Magnets

Line 00002 defines magnets centre co-ordinates and dimensions in X,Y and Z

6.4.5.2. Generation of Hardware Specification

From the *STATIC FT05F001* file the overall dimensions of the N/S magnets were defined as 60 mm long by 10 mm high x 10 mm deep. The strength of the magnets were defined in the *TRAJECT FT05F001* file.

```
TRAJECT  FT05F001 E1  F 80  Trunc=80 Size=58 Line=32 Col=1 Alt=0

00023 'ENTER'
00024 'STATIC',14,'STATIC'
00025 01010101000000
00026 00000000000000
00027 'FIELDMUP'
00028 4
00029 'STATIC'  2  0.0   1.900
00030 'STATIC'  4  0.0   1.900
00031 'STATIC'  6  0.0   1.900
00032 'STATIC'  8  0.0   1.900
00033 'ENDREG'
00034 0.260
00035 'TOL'
00036 1.E-3  1.E-4
00037 'COMARR'
00038 0.05000  0.05000
00039 'COAR-A'
00040 0. 0. 0. 0.
00041 'CHECK-A'
00042 'COEF-SC'
```

Diagram 78 : TRAJECT FT05F001 File (section of)

Line 00029 to 00032 defines magnet strength 1.900

The *GEOMETRY FT05F001* file documents the optimized magnet position to be 10 mm away from the flare of the separator at the centre of line coil winding. The CVRSLF L26F26 performance of the line and frame coils, AST24, COM1, and RAS1 plates and N/S magnets combined system is detailed in Diagram 79.

```
 CVRSLF   L26F26   E1  F 80  Trunc=80 Size=20 Line=13 Col=1 Alt=0

00004    XS         YS         XR       YR       BRX      BRY      XCOMA    YCOMA
00005    (M)        (M)        (MM)     (MM)     (MM)     (MM)     (MM)     (MM)
00006   0.114400   0.000000   0.000    0.000    0.216    0.000    0.128    0.000
00007   0.228800   0.000000   0.000    0.000    0.002    0.000    0.451    0.000
00008   0.000000   0.085800   0.000    0.000   -0.119    0.000    0.000    0.580
00009   0.114400   0.085800   1.866    1.502   -0.080   -0.116    0.063    0.491
00010   0.228800   0.085800   2.930    2.595   -0.473    0.711    0.271    0.376
00011   0.000000   0.171600   0.000    0.000    0.622    0.000    0.000    1.662
00012   0.114400   0.171600   4.185    0.263   -0.040   -0.249   -0.166    1.294
00013   0.228800   0.171600   8.477   -0.211   -1.131    0.940   -0.079    0.790
00014
00015   SLAG(MM)   ZS(MM)
00016      4.705   155.295
00017
00018     QA      QC      QK      QR      %EW     %NS     SLAG      TR3      TR5
00019    ------------------------------------------------------------------------
00020     37.6    53.2    50.9   221.6    3.70   -0.12     4.71    0.219   -2.016
00021 * * * End of File * * *


====>
```

Diagram 79: *CVRSLF L26F26* Performance; Line and Frame coils, AST24, COM1, RAS1 plates and N/S magnets.

6.4.5.3. Assembly Method

The correct position for the N/S static magnets was derived from the geometry file from DUCAD-Y, given in (Z,R) co-ordinates. The magnets were positioned within plastic magnet holders in the north-south position on the separator and secured in place with Loctite glue.

6.4.5.4. Discussion of DUCAD-Y Predictions

The line and frame magnetic field distributions for this system are included in Appendix B.

If a product design includes magnets the analysis of the field distributions is complex. Magnets generate static fields in contrast to deflection coils and permeable components which produce dynamic fields. Hence, unlike that of deflection coils, even harmonics are relevant for magnets while odd harmonics indicate asymmetries in magnet location and/or strength.

6.4.6. Complete DUCAD-Y System Solution

The proposed complete system solution includes the previously detailed correction plates/magnets, plus the incorporation of a coma-RB, which requires major alterations to the tube geometry and settings. It was felt that a representative validation would be possible if the remaining correction pieces were prototyped in hardware to assess their level of accuracy.

6.4.7. Overall Discussion

The complete system solution was replicated in hardware including all the correction components (excluding COMA-RB). From initial studies it was clear that without any raster correction, i.e. NS-magnets or raster plates, the MOM would be unable to measure the complete screen size, i.e. all twenty-five positions. The measuring equipment would only be able to measure the main axis (line and frame) errors, and therefore would only give an indication of the strength and behaviour of the line and frame coils. This would be insufficient to determine the overall behaviour to the design and the various interactions of the designed components.

Therefore, the complete software solution was prototyped in hardware as the starting point for both design optimization and validation of the software modelling system.

6.5. *Validation of Software Simulation Model via Hardware Experimentation*

6.5.1. *Hardware Replication - Initial Validation*

6.5.1.1. Introduction

As an initial test of the simulation model, a simplistic hardware design model was fabricated, considering the line and frame coils only (note not the optimized design proposal). The line and frame coils were relatively simplistic to fabricate of homogeneous winding structure. The details of this design were inputted into a DUCAD-Y model to initially assess the level of cross correlation.

The line and frame coils were realized in hardware and measured. The line and frame axis measurements were taken, i.e., only five positions were considered to determine if the correct strength of coils had been realized via the line and frame astigmatism process parameters.

6.5.1.2. Methodology and Hardware Results

Line and Frame Winding Pattern

The winding pattern for this line coil was:

6-10	1T	5-9	0T
4-6	7T	4-5	7T
3-5	0T	3-4	7T
3-3	9T	2-2	10T
1-1	10T		

The frame coil winding was homogeneous with a total of 400 turns.

Refer to Appendix D for the hardware measurement and DUCAD-Y results.

6.5.1.3. Validation of Software DUCAD-Y Model

The hardware measurements were in agreement with the software model with respect to the line coil strength and coma behaviour. In hardware, the measured value for line astigmatism was 7.291 and 0.638 in Xcoma error. In the software model, the line astigmatism was determined as 7.137, and Xcoma error at 0.845. However, less agreement appeared between the frame coil parameters. In hardware the measured values for frame astigmatism was -0.292, and Ycoma at 2.754; in software, the value for frame astigmatism was -0.874 and Ycoma at 2.080.

The following alterations were made to the software model to determine if further improvements could be made to the definitions of the design model to reduce the level of discrepancy between the model and the hardware:

- The angle of the slots in all the ring positions of the line coil were altered slightly to assess whether the method of winding the wire into the slots was not ensuring a mean position of wire in each slot as defined in DUCAD-Y . The winding process employed does introduce some spread into the wire as it is wound into the separator, particularly in the mid-section of the cap, where there is no plastic sectioning of the slots at this point. The ring position of the ring 2 (mid-section) was particularly modified to assess its impact.

- The position of the yoke ring and the frame coil were modified to assess if there was discrepancy between the relative positioning of the line and frame coils in the hardware and software models. The yoke ring and hence the frame coil were moved in the R direction, nearer to the electron guns, initially by 1mm to assess its impact. This caused BRx errors at the corner positions to change by -1mm, and BRy by +1mm. This appeared too large a change, therefore the yoke ring and the frame coil was

moved 1mm nearer to the line coil. The yoke ring and frame coil were both moved by 5mm in the -R direction. This change influenced greatly the corner astigmatism levels, BRx changing by 2.3mm and BRy by -3.3mm. The angle subtended on Ring 2 of the frame coil was modified to investigate any sensitive areas in the design. However, an increase in all angles by 5 degrees merely affected corner BRx by 1mm and BRy by 0.9mm, with insignificant effects on all other parameters.

None of the above modifications determined the root cause of the problem as the main concern was the frame coma error which was too large in the simulation as compared to the model. In this experiment, reasonable proportions of error were achieved for both the line and frame coils, however, the simulation of the frame coil in its astigmatism and coma correlation was in less agreement with the line coil behaviour. However, sufficiently close agreement was suggested by this test experiment to continue the hardware design optimization procedure.

6.5.1.4. Overall Discussion

The simulated frame coil was generated on hardware, and the anticipated coma Y error of 0.48 was proved difficult to realize in the hardware samples based upon the derived winding specifications. The frame astigmatism level of 5.605 was achieved however this gave a Ycoma error of 1.79mm.

This discrepancy in frame coma may be caused by the nature of the simulation of the electron guns in DUCAD-Y. The grid G3a, a gun housing arrangement, is composed of a magnetic conductive material. Toroidal frame coils generate long magnetic fields and therefore a significant level of the field modulation is present at the grid G3a position. The electron gun, grid G3a, is made of magnetic conductive material to make the frame field ineffective.

This can be simulated by using the 'coma RB' option in the *TRAJECT FT05F001* file defining the coma ring between two z-positions, zmin RB and zmax RB.

Further experiments were carried out creating only line and frame base coil designs. An approximate design solution was realized, however the incorporation of the remaining correction plates, etc. was necessary to determine the overall 25 position behaviour of the design solution.

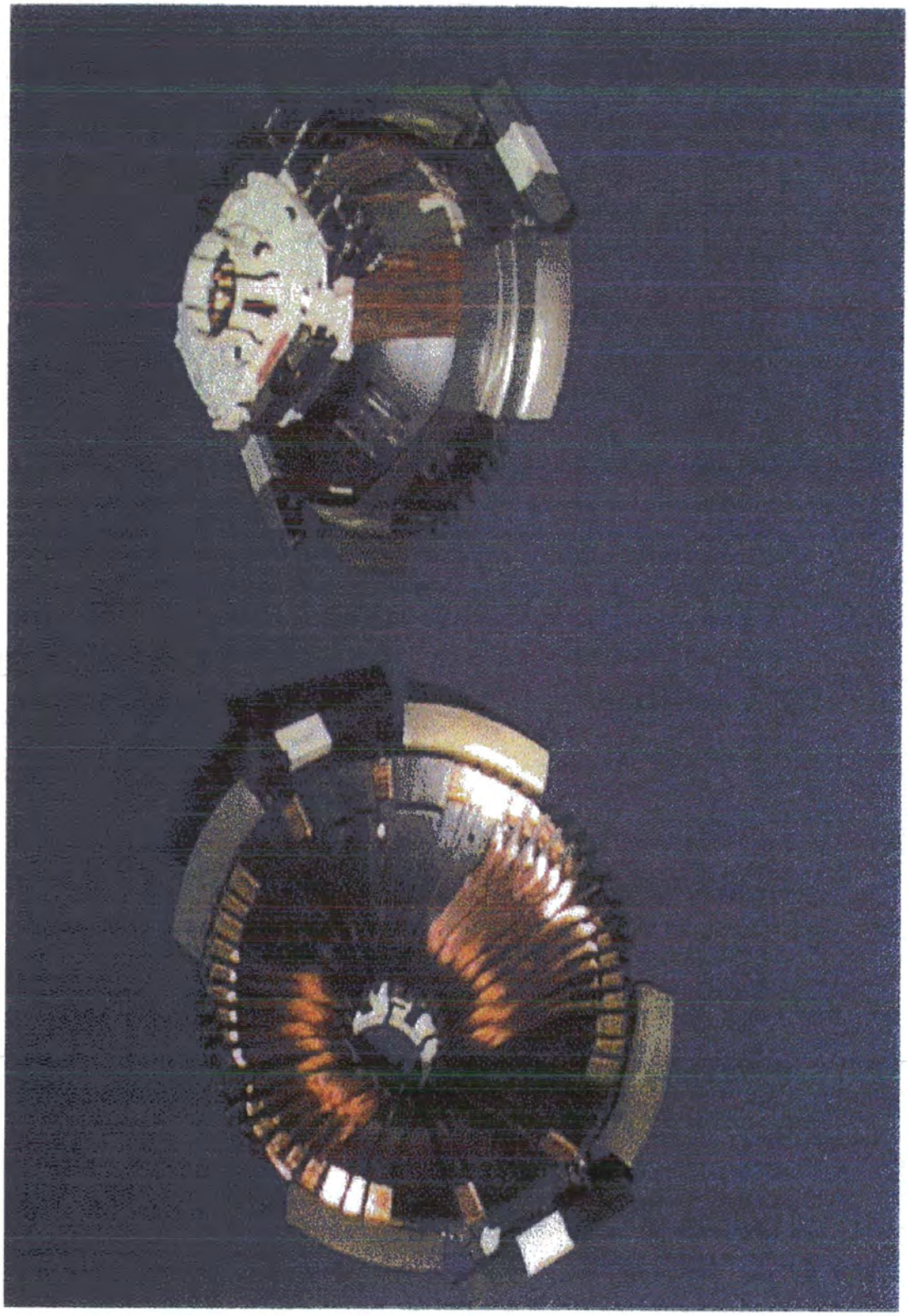

DIAGRAM 80a: COMPLETE SLOT WINDING DEFLECTION COIL DESIGN

Diagram 80a: Complete Slot Winding Deflection Coil Design

DIAGRAM 80b: COMPLETE SLOT WINDING DEFLECTION COIL DESIGN

Diagram 80b: Complete Slot Winding Deflection Coil Design

6.5.2. *Hardware Prototype approaching DUCAD-Y Optimized System Solution*

6.5.2.1. Introduction

The DUCAD-Y optimized line and frame winding patterns were studied to determine their feasibility in hardware samples. Potential difficulties were identified such as limitations in the filling density of particular slots (volume available), the practical limitations of the winding equipment and the need to create a stable and repeatable winding option.

6.5.2.2. Methodology

The following details the winding pattern for the line coil from the DUCAD-Y optimized winding pattern.

DUCAD-Y L26	**L26; Required Sensitivity**	**Hardware L26**
6-10 4T	6-10 2T	6-10 2T
5-9 10T	5-9 5T	5-9 5T
4-5 13T *(12/14)*	4-5 6/7T	4-5 6/7T
4-4 4T	4-4 2T	4-4 2T
4-2 26T	4-2 13T	*4-3* 13T
3-2 11T *(10/12)*	3-2 5/6T	3-2 5/6T
2-2 15T *(14/16)*	2-2 7/8T	2-2 7/8T
1-1 37T *(36/38)* *only whole turns possible*	1-1 17/18T	1-1 17/18T
Total No. of Turns: 120	Total No. of Turns: 57/61	Total No. of Turns: 57/61

To determine what was feasible in terms of winding the designed separator, the following trials were carried out. Of main consideration was the filling density of each slot whilst maintaining no damage to the separator during the winding process. In parallel to this activity, the degree of correlation with the software representations was studied.

6.5.2.3. Complete Hardware Design Solution

The complete product solution was replicated in hardware to gain actual measurements of the performance of the design. After assembly of the hardware prototype, large convergence errors were present of the order of 18 mm in the corner screen position. The MOM measuring system was unable to detect this magnitude of convergence error. Therefore the MECC manual monitor which allows a visual checking method of assessing product performance was employed. The unit was positioned on a 59FS tube to determine the extent of the convergence problems. Large tails behaviour was seen on the display, of the order of 20mm blue to red X errors, and large, but less significant crossing behaviour was also present. The remaining coil aberrations were reasonable, such as frame astigmatism, frame coma, line astigmatism and line coma.

Tails effect, as represented in Diagram 81, is the distance of the blue to red errors in the corners in the X-direction and can be correlated to the amount of line astigmatism, line 10 pole modulation, frame astigmatism and frame 10 pole modulation present in the design. Seagull distortion of the North-South raster occurs if two positive ten-poles are present at the line coil flare section. In addition, Y crossing and X corner errors, i.e. tails behaviour, is also commonly present.

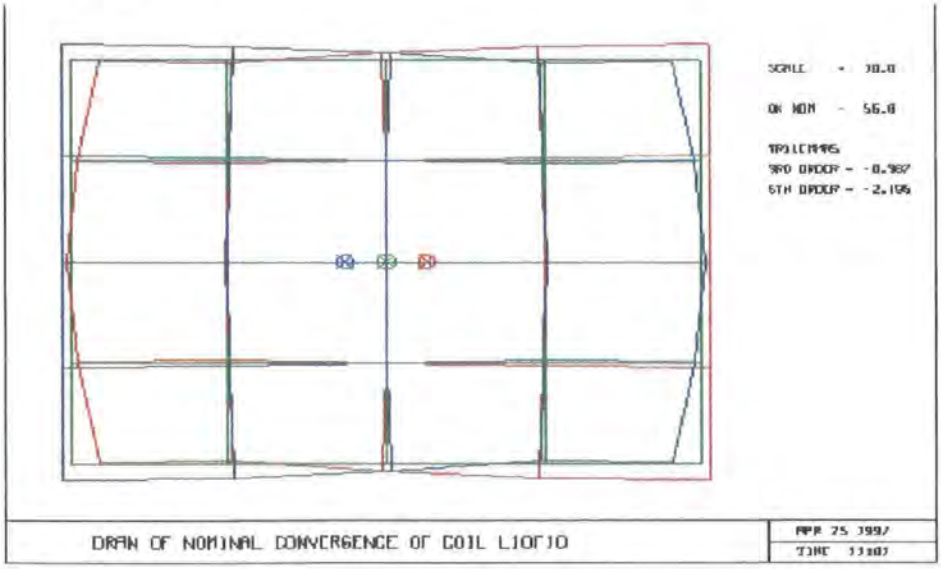

Diagram 81: Representative Performance of Hardware Samples (Tails Effect)

Negative ten-pole modulation is particularly sensitive at a subtended angle of 36 degrees around the line coil. This angle is approximately equivalent to the angle which slot 3 in the separator design allows wire to subtend at. To determine exactly the multipoles generated by the hardware prototype would require elaborate measuring equipment to measure specific multipole strengths. This would be able to compare more accurately the computational results of DUCAD-Y against those generated from the MOM measuring system. This equipment was not available during these investigations however.

6.5.2.4. Discussion of Results

The line coil astigmatism levels appeared to have an offset between hardware and software of 4 mm. Large errors in the tails and crossing behaviour made it impossible to measure on the MOM.

Initially the problem appeared to be caused by the long astigmatism plates in the design, i.e. the large subtended angle of the astigmatism plate tails. In hybrid designs, there is greater emphasis upon the length of the astigmatism plate wings, as this section of the plate is particularly sensitive to tails/crossing astigmatism aberrations. Conventionally, an astigmatism plate acts on the generated frame field which runs perpendicular to the astigmatism plate plane. However, if the wing portions of the plate extend too far, the plate becomes positioned within the generated line field which is then short-circuited by the plate. The plate effectively acts as a yoke ring thereby short circuiting the line field surrounding this area and redistributing it elsewhere. The generated line field therefore becomes more susceptible to any increase in the shape/size of the astigmatism plate.

This interaction between the astigmatism plate and the generated line coil field is not calculated in DUCAD-Y. A previous DUCAD-Y study (a 27V design for the American market), considered this line field interaction as their model appeared to indicate some inaccuracies between the predictions of DUCAD-Y and the hardware prototypes. A

DUCAD-Y program was created to calculate this interaction to assess its significance upon the overall system performance.

With the line interaction calculation not activated, no change to the generated magnetic field was seen on removal of the astigmatism plate from the product design. However with the line coil interaction calculation activated a difference to the generated line magnetic field was documented. This corresponded to a -0.347 mm effective difference for line astigmatism and -0.365 mm for line x coma.

The plates used in this development design had slightly longer astigmatism plate tails therefore, on assessment, it appeared that the calculated effect for the line field interaction should be slightly increased for this application. Therefore, approximately, the line astigmatism should be offset by -0.45 mm, and line x coma error by -0.46 mm. This offset needs to be included into the hardware/software correlation study.

To determine if the astigmatism plate indeed caused the large tails behaviour, another astigmatism plate design was employed. This action did reduce the level of tails errors, although not to the extent required. It was clear that another feature of the hardware model was causing the large tails behaviour. In addition, modifications were carried out to the frame coil winding pattern, but no relief was given to the tails distortion. A further area for improvement was the frame coil winding. Modifications were made to the frame ring file F26 to limit the possible maximum angle of wire modulation. This process was iterated a few times to create the frame coil F30. The *DRAWSECT* winding pattern and the *DRAWCVRS* convergence performance output file are included in Appendix D.

Greater attention was therefore placed upon the line coil design. In the line coil, the areas which greatly effect tails behaviour are around the flare slot positions 3 and 4, and slots 9 and 10. Within the optimized line coil winding, two turns were wound in slot 10 and 5 turns were wound in slot 9. 13 turns were wound in slot 3 and 2 turns in slot 4.

From this analysis, one particular slot behaviour was studied, slot 5 (neck) to slot 3 (flare). This pattern appeared to wind at a significantly larger subtended angle to its respective neighbours. The winding process appeared to cause the wire winding into this slot to roll creating a steep 'mountain' of wound copper. Therefore the smooth filling expected and simulated by DUCAD-Y, assuming a constant planar wound coil of constant filling factor was not replicated in the hardware prototypes.

To confirm this, a separator was wound with no wire turns in this suspect slot. This indeed eliminated the excessive tails behaviour and identified the root cause of the problem.

6.5.2.5. Conclusion

DUCAD-Y assumes a rotationally symmetric wire model and considers only current sheets subtending around a symmetrical co-ordinate system. Any deviation from this uniform filling of wire packages therefore will not be considered or identified by the simulation model. Clearly this detailed portion of the line coil, particularly sensitive to tails behaviour greatly impacted upon the predicted results and their correlation to the hardware prototypes.

6.5.3. Complete Hardware Prototype Optimized System Solution

6.5.3.1. Introduction

Due to the problems generated by manufacturing the DUCAD-Y final optimized design proposal, an alternative line coil design was sought, eliminating as far as possible the use of slot 5-3. Two base designs were fabricated in hardware minimising the number of turns of wire in slot 5(neck) to slot 3(flare) of the separator. This configuration was

fabricated in hardware and measured on the MOM to document the reduction in line astigmatism Y errors. The following optimization procedure was undertaken.

6.5.3.2. Optimization Procedure

Due to the inaccuracy in determining the exact strengths of the line and frame coils in the final optimization iteration in DUCAD-Y, the following design optimization procedure was undertaken at this stage.

Create a hardware model	simulating the *CALFAS* distribution for both the line and frame coil	plus all required correction plates.

Measure the hardware model

Input the measured aberration errors into the *CVRSLF* convergence performance output file, to create a new base coil in DUCAD-Y

Create new delta files using six and ten multipole modulations as wire deltas and optimize the new coil using these defined deltas.

Create a hardware model of this new winding pattern given by *CALFAS*

Repeat the above sequence until a fully optimized product design is achieved.

6.5.3.3. Re-set Base Hardware Line/Frame Coil Designs

Hardware modifications were carried out to the frame coil winding pattern to achieve an improved level for frame astigmatism. This however introduced further difficulties in the corners, especially large BRy crossing behaviour. The following line coil winding patterns were selected and fabricated in hardware.

Unit 1				Unit 2			
6-10	1T	5-9	0T	6-10	1T	5-9	0T
4-6	7T	4-5	7T	4-6	7T	4-5	7T
3-5	0T	3-4	7T	3-5	0T	3-4	7T
3-3	9T	2-2	13T	3-3	9T	2-2	13T
1-1	13T			1-1	15T		

The DUCAD-Y optimized design proposal was modified to reflect the above modifications. The predictions of the coil designs are included in Appendix F (Design L26F26)

6.5.3.4. Optimization Procedure - Hardware /Software Delta

A large discrepancy was still present in the tails and crossings distortion behaviour. A delta file was created, which detailed the actual errors between the DUCAD-Y predictions and the realized hardware measurements. DUCAD-Y was employed to further optimize the coil design. The hardware measurements were inputted as the base design performance and further wire deltas were carried out to improve the overall performance of the coil. This included line coil wire modifications and correction plate modifications.

The delta between the hardware and software aberration data was calculated and subsequently used throughout the following DUCAD-Y optimization process. This predicted delta was set against the 'new' optimized DUCAD-Y design to enable a more realistic performance to be determined, ensuring the winding process characteristics were fully incorporated into the optimization. Each slot in the line separator was studied and a delta was calculated to assess the impact of introducing a further turn into each slot individually. *OPTIMULY* was then used to select the preferred winding pattern to improve performance. The *OPTIMULY FT05F001* file was extensively used to ensure that realistic changes were being requested in the *OPTIMULY* program. DUCAD-Y optimized the product design to the following set-up.

Optimized Line Coil Winding Pattern:

6-10	1T	5-9	0T
4-6	7T	4-5	7T
3-5	0T	3-4	8T
3-3	10T	2-2	13T
1-1	16T		

In addition, the segment files defining the astigmatism and raster plates were modified to determine if a better design could be realized by minor modifications to the plates. Further sections were removed from the astigmatism plate to reduce the level of crossing and tails. Modifications were made to the raster plates however a limit was reached at which no further improvements were possible with any of the correction plates.

Based upon the initial design proposal, the *OPTIMULY* set-up requested a reduction in the width of the astigmatism plate by 2mm and an increase in height by 3mm at the top section. For the raster plates, the radial sections were reduced initially by 5 degrees and then by 8 degrees. The hardware model was replicated in DUCAD-Y. The predictions of this deflection systems' performance are detailed and the difference between the hardware prototypes and the DUCAD-Y predictions, referred to as delta files, are documented in Appendix D.

6.5.3.5. Interpretation of Hardware Measurement Results

General convergence errors as measured on the MOM were considered to determine the correlation with the hardware samples. (Note: East-West raster distortion can mostly be compensated by modulating the amplitude of the line current during the raster scan. Therefore, the E/W raster correction was set and the raster shape was visually inspected

against the DUCAD-Y model. No great attention was paid to the measured values for raster.)

General agreement was realized between the hardware and software proposal by carrying out the required wire and minor component alterations to the design to reflect the slot winding process characteristics. The DUCAD-Y predictions therefore enabled an indication to be given of the expected effect of any design and component alteration. Individual wire changes, for example the removal of one turn in a slot to introduce another showed good agreement from the hardware and software results.

6.5.3.6. Final Design Solution

Further hardware modifications were introduced to the line coil. The original winding pattern was returned to in order to improve overall convergence performance.

Optimized Line Coil Winding Pattern:

6-10	1T	5-9	0T
4-6	7T	4-5	7T
3-5	0T	3-4	7T
3-3	9T	2-2	13T
1-1	13T		

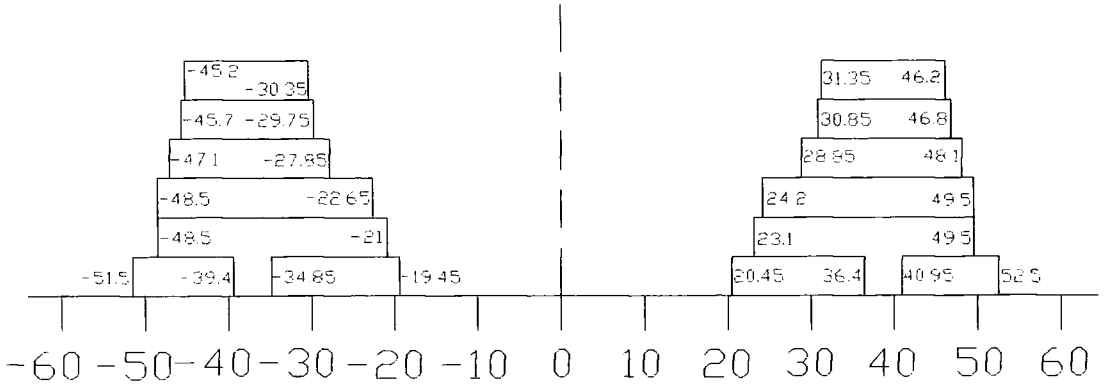

Diagram 82: Wire distribution from the frame coil DRAWSECT outputs - Harmonics of Winding Pattern

Optimized Frame Coil Winding Pattern

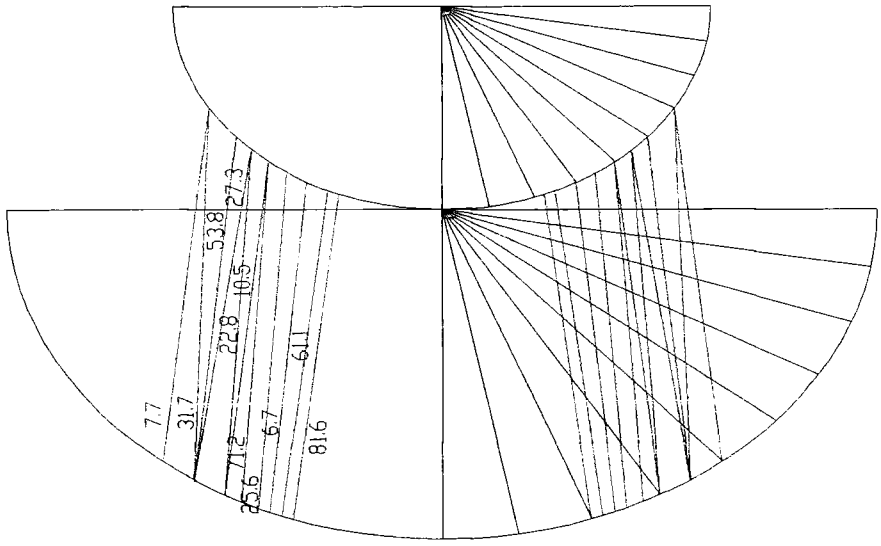

Diagram 83: Actual wire Distribution is digitised into various Cross-Sections of the Yoke Ring Profile

An acceptable product design solution was achieved by making a number of hardware modifications using general electron-optical hardware practice and techniques.

It was found easier and quicker at this stage in the optimization process to neglect the DUCAD-Y design model and concentrate on the physical performance as achieved in the hardware prototypes. Assembly errors and inherent errors were more easily minimized and controlled at this stage. Five samples of the finalised design were fabricated to identical product set-ups to minimize these indirect effects.

MEASURED

	BRX	BRY	XCOMA	YCOMA
R	0.212	0	0.625	0
C	1.079	0	1.266	0
W	-0.08	0	0	0.08
T	0.144	1.277	0.511	-0.062
G'	0.664	1.818	1.06	0.432
D	-1.277	0	0	0.419
L	-0.892	0.326	0.214	0.747
G	0.805	2.527	0.987	1.204

Diagram 84: Measurements of Hardware Prototype Samples of Optimized Design

An overall Qk value of approximately 40 was achieved, refer to Appendix G for detailed measurements. It can be seen that the convergence characteristics have improved remarkably and although the raster errors have not been considered to great detail in this study, the optimization process led to a much better north-south raster shape.

6.5.3.7. Generation of DUCAD-Y Model to Reflect Hardware Modifications/Optimization

The finalised hardware product design was simulated in DUCAD-Y, design L33F33. Appendix G details the differences recorded between the two sets of results obtained from hardware and software.

DUCAD RESULTS

	BRX	BRY	XCOMA	YCOMA
R	-0.006	0	0.566	0
C	1.311	0	1.115	0
W	-0.218	0	0	-0.201
T	-0.727	0.817	0.495	-0.005
G'	-0.404	-0.472	0.817	0.4
D	-0.662	0	0	-0.021
L	-3.627	1.728	0.422	0.52
G	-11	-4.566	0.977	1.898

Diagram 85: DUCAD-Y Predictions of Optimized Design

As documented, the results were in correlation with previously documented disagreement and misalignment.

	DELTA Ducad/ Measured			
	BRX	BRY	XCOMA	YCOMA
R	-0.218	0	-0.059	0
C	0.232	0	-0.151	0
W	-0.138	0	0	-0.281
T	-0.871	-0.46	-0.016	0.057
G'	-1.068	-2.29	-0.243	-0.032
D	0.615	0	0	-0.44
L	-2.735	1.402	0.208	-0.227
G	11.805	-7.093	-0.01	0.694

Diagram 86: Difference between DUCAD-Y Predictions and Hardware Measurements of Optimized Design

To assess the accuracy of individual components being simulated in DUCAD-Y, a series of hardware and software deltas were carried out. The impact on removal ,one at a time, of each component was documented, in both the hardware prototypes and the software

model. (This is an extremely important procedure to carry out particularly in respect to the static magnets. The strength of the magnet is detailed in *TRAJECT FT05F001* file in DUCAD-Y and the value detailed is an arbitrary figure. This comparison procedure of hardware against software enables a realistic value to be defined for the magnet strength (a component which greatly impacts upon the line coil behaviour).

6.5.3.8. Agreement of DUCAD-Y Model to Hardware Experiments

Good agreement was present between the hardware and software deltas on removing the raster plates from the optimized design. The direction of change and the magnitude of errors predicted for most of the convergence aberrations were in good correlation, however the magnitude of error of the BRx in G position was out by a factor of 2.

On removing the N/S magnets again the agreement between hardware/software deltas values was good, with the exception of points G' and G for BRx errors. All other documented errors were in close agreement. Alternative magnet strengths were simulated in DUCAD-Y by varying the static magnet value in *TRAJECT FT05F001*, in an attempt to achieve closer correlation. The magnet strength set at 1.0 achieved the best correlation. (note that this is different to the originally optimized value in L26F26 of 1.9).

The hardware and software deltas for the removal of the coma plates were less satisfactory. The biggest area of concern appear in the lack of DUCAD-Y to predict the 3 mm shift in frame astigmatism and the negative shift of BRy at screen position G of 4.7mm. In addition, the simulation of frame coma errors were also poor. The hardware model increased the frame coma errors by approximately 4.5mm on removal of the coma plate, but this was not simulated in DUCAD-Y.

The agreement between the hardware and software delta on removing the astigmatism plates was more satisfactory. The direction of change of most of the convergence

aberrations were generally in good agreement. The BRy simulated values appeared high by a factor of four, at position G. The BRx at screen position G was simulated high also, by a factor of 1.4. In this simulation change, the effect on frame coma error was too severe in the model when compared to reality.

The definition of the frame coil was adjusted to determine the sensitivity of the simulation. It was considered that the frame coil definition was not realistically charging up the coma plates and therefore incorrectly simulating the coma plate behaviour. The design, L100F100 was calculated, and software component deltas were investigated. Good agreement was present between the hardware and software deltas on removing the raster plates from the optimized design. The direction of change of most of the convergence aberrations were in good correlation however the magnitude of error of the Xcoma in G position was out by a factor of 2. All other magnitude of errors predicted were in extremely close agreement.

On removing the N/S magnets again the agreement between hardware/software deltas values was good, with the exception of points G' and G for BRx errors. All other documented errors were in close agreement.

The agreement between the hardware and software delta on removing the coma plates was more satisfactory than that realised from the previous definition of the frame coil. The direction of change of most of the effects on convergence aberrations was generally in good agreement. The BRx at screen position G was simulated high at a factor of 2.5. The largest disagreement, however, was at L position for a Ycoma error of the order of 5mm. All other values were in good agreement.

The hardware and software deltas for the removal of the astigmatism plates were less satisfactory. The biggest area of concern appears in the excessive prediction of a 20mm shift in corner BRx errors. A 20mm effect on BRx corners is not feasible with a normal sized plate design. The prediction of all BRx errors in the DUCAD-Y model on removal

of the astigmatism plate were all excessively too positive by a high order of magnitude. In addition there was a discrepancy of 4mm for BRy errors, in which DUCAD-Y was predicting too positive an error effect.

6.6. Results

During the optimization procedure changing the weighting factors in *OPTIMULY FT04F001* for coil aberration parameters, such as astigmatism, was found to modify the level of astigmatism error merely to introduce additional coma errors. It was noticed that the winding patterns for both designs were relatively constant. There appeared an inherent error within the design system which could be present in either astigmatism or coma behaviour. The Q factor may therefore be the more realistic measure of coil performance at this stage, rather than individual convergence effects.

The wire packages are assumed to connect each of the defined modulation levels with a uniform cross sectional wire distribution. The thickness of the coil is not taken into account, and the current sheet is assumed to lie at the average of the winding distribution. The assumption is valid provided the thickness of the coil is small with respect to its radius and the current sheet is placed at its centre of gravity. This avoids the necessity of specifying and dealing with discrete wire locations in space for coils with a large number of turns.

The *scalar magnetic potential*, used in this package to calculate the magnetic deflection fields, can only be defined in current-free regions. Therefore, in all calculations, the deflection coils are reduced to current sheets of infinitesimal thickness. The vector potential of the 2 dimensional deflection yoke model has only one component normal to the plane considered. If we wish to consider the thickness of the deflection coils, the preferred method is using the *magnetic vector potential* which can be defined everywhere. The evaluation of the field inside the deflection coil itself, makes further possible the

estimation of the dynamic losses (eddy currents, etc.) in the coil. The model is then able to replace the cylindrical currents sheet by cylindrical shells of finite thickness.

In a paper by Dasgupta (1983) the effect of finite winding thickness upon the generated field is analysed. This is undoubtedly an important question because ordinarily it is assumed that the windings can be represented by sheet currents in magnetic field calculations. Analytical calculations for infinite cylindrical cylinder deflection designs are used. It is found that the higher multipole contents of the field (i.e. the coefficients of higher order terms in a Fourier expansion about the coil's axis) decrease by progressively larger percentage amounts compared to their values for a coil of zero thickness. Therefore, for thicker windings the higher harmonics of the field have smaller amplitudes than in the thinner winding case.

The deflection system model must closely relate to the technology used in order to permit a direct and accurate translation of the computer results and predictions into practical designs.

Initial inaccuracies are introduced by the assembly process. Samples were fabricated to identical set-ups, and errors (discrepancy) resulted between each sample generated. This is due to the prototype nature of many of the utilised components in the design. There were few locations points and reference lines to accurately and repeatedly locate components. Therefore, when the magnitude of errors for convergence is so small the effect of these assembly errors are magnified.

The winding process has inherent spread associated with it. For the line coil, this could have been reduced by designing the separator to have slot channels for the wire to be more accurately positioned. However this would be achieved at the expense of wire modulation possibilities. For the particular winding machine utilised in this investigation, the method of winding has a section of the winding cycle where the tension in one section of the winding cycle is zero. Therefore the wire is at that point under no control. This

introduced a diagonal problem in the wound coil, and increased the height variation throughout the fabricated coil manufacture.

For the frame coil, the introduction of castellations (plastic formers positioned at the neck and flare end sections of the yoke ring to reduce the natural slippage of the wire during winding) in the frame coil design could reduce the level of spread in this winding process. This was attempted during the hardware optimization and was found to help significantly. However, for this design there was severe limitations in the height available between the neck and flare of the separator. Therefore the space available for the frame coil was small which lead to modulation limitations.

Discrepancies were identified specifically concerning the simulation of the correction plates included in the proposed design. It is clear that the accuracy of the simulation model is unclear, and much further work is required to determine conclusively the source of this inaccuracy. The DUCAD-Y model in this study proved weak in realistically simulating plates with the design. It was certainly clear that the inclusion of plates greatly reduced the stability in design optimization. However, due to the large number of plates (greater than two), there may exist an overlap in plate cone definitions, which can cause instability in making the matrix calculations. It is clear that the definition of plates cones is extremely critical and should not be defined with gaps between any of the defined plates segments. Indeed the definition of plate positions, their angles of subtension and possible interaction issues with other design components must be carefully assessed.

The attachment of the magnetic plate to the deflection system causes a change in the inductance of the coil nearby. The measurement shows a significant change of the inductance and the resulted coil current. This effect may not be accurately accounted for in the simulation calculations. In addition, the leakage flux of the horizontal deflection field is about one order of magnitude weaker than the leakage flux of the vertical deflection field. This weakness may cause the loss of significant digits in computation.

In addition, there are errors inherent in the computer simulation calculation (discretisation error, the difference between the initial equation and the discrete model simulation), and quantization error, (inaccuracy due to number truncation in the optimization computations). Therefore, the above error processes are important and the results generated by any simulation tool should be examined critically. The validity of any simulation results may easily be improved by intuition and experience, obtained by a large number of practical example.

Due to the rotationally symmetric structure of the model, the correction plates and wire models can only be defined as curved, rotationally symmetric structures. Therefore, the flat details of the raster plate, such as the collector section can not be realistically reproduced in the DUCAD environment. This inaccuracy between hardware and software predictions has been considered in past DUCAD-Y studies and found to be minimal. It was therefore felt that this inaccuracy would not affect the design validation process in any significant way.

6.7. *Possible Design Improvements*

6.7.1. *Improvements to Current Product Design*

In designing the proposed deflection system, one of the main objectives was the removal of severe East-West raster distortion whilst maintaining acceptable convergence levels. For acceptable convergence of red and blue electron beams the line magnetic field requires a pin-cushion shape and the frame field requires a barrel-shape. In order to converge the green beam with the remaining two requires opposite modulations at the neck. Such a practical design therefore has straight north-south raster and a pin-cushion shaped east-west raster. For toroidally wound frame coils., the east-west raster correction is corrected within the deflection circuitry, called an RCF-system (Raster Correction Free).

6.7.1.1. Separator Design

Modifications were made to the DUCAD-Y simulation model of the 59FS slot based design to identify potential improvements to the line coil design, and hence the separator design. At the end of this investigation, there was a far clearer appreciation of the issues impacting upon the separator design. This was due to the extended use and familiarity with the slot winding process and equipment.

Specifically in relation to electron-optical product performance, the simulation model showed that improved line coil behaviour could be achieved by varying the slot angles on the line neck and flare portions. This would greatly enhance the ability to create the desired pincushion and barrel shaped fields required for a self-converging system. Additional improvements could be gained by varying the lengths of R1 to R2 (neck length) and R2 to R3(mid-section to flare section of separator) to achieve improved raster/convergence behaviour and possibly more give in the pullback criteria. (This would have to be fully evaluated on determining the exact preferable length for the frame coil).

Slots 9 and 10 of the separator were designed to reduce the tails/crossing convergence behaviour, however their position was found to be slightly out when utilising slot winding as a manufacturing method . Experiment showed the preferred positions for slots 9 and 10 to be nearer to the line axis (less subtended angle).

To achieve greater flexibility during optimization, it would have been advantageous to have greater depth in the slots in the separator to allow for a greater variation in the filling factor. However, this was not always possible. During our investigation into slot winding as a manufacturing process it was noted that the winding process achieved low overall spread in convergence values if the slots were wound at 100% filling factor. Therefore it would have been preferable during the hardware optimization to have filling flexibility. However if the design was to be transferred into a production environment, the separator would benefit from 100% filling of the slots. Increasing the filling of the slots increases

the distance of the unit from the glass of the tube. This may slightly affect the sensitivity and pullback characteristics of the deflection system design, however assumptions can be made concerning its influence. Furthermore, the ability to increase the number of turns in the slots in the separator would greatly aid the initial hardware evaluation of the design.

At the outset of the separator design, the central slots were detailed as open portions to maintain wire modulation flexibility. However, during the production of hardware prototypes, it was evident that greater support of the wire at these portions would have reduced the convergence spreads experienced during the hardware optimization procedure. This impacted upon the accuracy and reliability of the hardware. This may lead to a reduction in the deviation noticed with the software to hardware results.

6.7.1.2. Frame Coil Design

The frame coil employed in this investigation employed a non-specific yoke ring, not DUCAD-Y derived. The employed frame coil is therefore not fully optimized to the requirement of the 59FS slot design. This therefore limited the possibilities in achieving a design proposal which met the requirements of the product specification. If the following recommendations are carried out, however, the optimized product design would achieve reasonable convergence performance.

Because of the extended stray field, a toroidal frame coil must remain short at the gun side in order to guarantee a minimum total pull back. The 27V frame coil was too long for this design geometry ,and this hampered the degree of pullback available. A frame coil was designed to achieve positive /negative six pole modulation, producing a narrow flare modulation and wide neck modulation packages. It is possible to reduce the available height for the yoke ring to suit line coil referencing. The 27V yoke ring profile was very thick and this increased the problems experienced in lowering the seating of the frame coil. It would be preferable to be able to lower the height of the frame coil to achieve a greater pullback availability.

6.7.1.3. Automatable Design Base

The achievement of a design solution using increased automation by slot winding techniques would provide more options in the generation of an integrated product.

With reference to a patent detailed by Philips and other non-Philips companies, design possibilities are available to determine both a line and frame slot wound product. This would have the advantages of minimising component and labour/assembly costs, and lead to the more focused and compacted manufacturing approach.

In addition, the termination of the lead outs could be undertaken by the winding machine, Automatic wire wrapping and wire termination is becoming a more viable manufacturing technique and manufacturers are identifying its potential within this highly competitive market sector. The PCB could be positioned at the neck or the flare of the separator. Quick fixing top and bottom component covers would ease the assembly of the unit. Correction components such as magnets and coma plates could be secured within the plastic support covers. This would allow a minimal assembly process to be proposed.

7. CHAPTER SEVEN

Discussion

In this investigation, the development and optimization of a magnetic deflection system for CRT has been considered. A computer aided design method plus theoretical electron-optical theory thereafter, allowed a product design to be realized. Of prime consideration in this study was the validation of DUCAD-Y to precisely model and accurately determine the many performance characteristics of a deflection unit system.

The mathematical methods utilised by the DUCAD system in conjunction with Fourier expansions of the segmented current elements was the basis under which the software model developed a representation of a deflection unit. DUCAD-Y defines the system solution by changing the realistic three dimensional problem into a superposition of two dimensional problems by means of Fourier expansion techniques. Two dimensional techniques were considered such as harmonic analysis of the current density to explain simplistically the influence of the shape and position of current elements on the magnetic deflection field and hence the electron optical performance of the system. The harmonic winding density expresses graphically this relationship between magnetic field generated and associated performance characteristics in a comprehensive form.

In this study the software optimization of a deflection coil system was undertaken. The DUCAD-Y simulation package considers each package of wire approximately as one infinitesimally thin wire tightened between two slots on neighbouring multipole modulation rings. This 'thin wire' follows the line and frame coil profiles along their surface, with the current proportional to the number of wires in the package. The required basic geometry of the system was defined and the understood constraints of the relevant manufacturing processes and system component parts were identified. The optimization

technique in DUCAD-Y , *OPTIMULY* , allowed iterative steps to be executed until no further electron-optical performance could be gained or recovered.

The software design optimization utilised an optimization algorithm to determine the minimum objective function for the overall system performance governed by the user defined limits and system constraints. An example of a system design constraint is the region boundaries which should not be exceeded, a criteria defined to limit the electron beams hitting the glass profiles. This occurs primarily at the outset of an optimization cycle whilst the main dimensions of the coils are being determined. Once overall system stability is achieved (indicated by an acceptable level of design unit pullback), this constraint can predominantly be neglected. The optimization procedure necessitates the user to continually assess the output performance data at various optimized levels and thereafter manually vary the input design parameters. Much use is made of the *CVRSLF* convergence/raster performance files, multipole fields measurements, and various other design aids.

During this software development phase, non-linearity of the optimization process would commonly occur. This symptomatic behaviour was dependent upon the interaction of the numerous correction plates and the associated plate interactions with the line and frame wire distribution interactions. The introduction of any design modification whether a plate or wire change would commonly influence the stability of the optimized system. A limitation imposed by the use of saddle/hybrid design techniques is its inherent limitation in wire modulation options which greatly restricts the ability to realize an adequate frame field by coils alone. Therefore in using toroidal winding, a higher number of correction plates was incorporated into the design proposal to achieve the required performance specification. The associated increase in components parts, and their inherent field interactions therefore imposed much additional work onto the manipulation of DUCAD to realize a stable design proposal.

This system was replicated in hardware to allow cross correlation of results to authenticate the DUCAD-Y predictions. During hardware optimization, practical theoretical understanding was applied to optimize the product design. This included such methods as the harmonic theory of winding and multipole theory, particularly the imposed requirements of six-pole and ten-pole modulation at various portions of the deflection unit. This was an important aspect of the development process as it not only validated the software design study but additionally considered any limitations in physically creating the proposed design.

Much additional design effort was required in the hardware optimization of the design as the use of DUCAD and the theoretical evaluation of the system imposed practical limits on an acceptable system being achieved. The need to fully optimize and minimise all system aberrations imposed a heavy dependency upon the hardware prototyping phase which was carried out in order to merge any process/machine limitations to create a physically optimized design proposal.

A delta file was created (the difference between the DUCAD-Y and hardware results) and this was employed to realize a reasonably performing product design. The latter stages of the optimization process were carried out manually, introducing minor hardware modifications to component sizes and position to determine the best solution. The adoption at the latter stages of the process to hardware optimization of the product design minimised the duration of this stage of work. This allowed a sample of prototypes to be developed and measured.

The large inconsistency between the DUCAD-Y predictions and the hardware results was caused primarily by the assumption that the deflection coil represents a rotationally symmetric current element of uniform density. The technique of slot winding causes an uneven and inclined slope to the wire within the separator slots and this was particularly the case for the 'open slots' towards the centre of the separator. The concept of open

mid-sections was introduced into the separator design principally to allow for a greater extent of wire modulation freedom during product optimization.

To determine the associated influence upon the generated magnetic field and the deflection unit performance, the unequal graduation of wire as it lies within the line coil slot was simplistically simulated in DUCAD-Y. Modifications were made to the *GEOMETRY FT05F00L* file in an attempt to simulate the offset in the assumed position of the copper wire in the line coil. To alter one particular section of the line coil definition would require defining the line cone as a discontinuous element, a function not allowed within the DUCAD design 'rules'. Therefore, the complete height of the line coil was displaced by 2 mm from its original position to assess the sensitivity of this design. This modification affected the BRx errors by -1mm in the corner positions, reflecting the prototype measurement results experienced.

Comparing the hardware and software performance results, the main discrepancy was documented as the excessive tails distortion principally created by the uneven distribution of successive wire windings within the separator slot. The particular portion of the line coil of concern is a particularly sensitive and susceptible area to higher order multipole influence, indicative of the excessive BRx convergence errors experienced in the screen corners. To accurately simulate the unsymmetrical winding nature as created within the hardware prototypes would be a complex task. The DUCAD-Y format would require further complicated calculations specifically dealing with certain portions of the line coil and the realized variation in the height and shape of the wire packages within the slot. Each of the wire packages would need to be segmented and separate calculations carried out to determine individual package influence thereby increasing the number of numerical calculations enormously.

DUCAD-Y was able to simulate more effectively however the 'channelled' slots in the separator; i.e. the wound slots which approach more closely a rotationally symmetric system. As the wire model definition for the deflection coil neglects the overall coil

thickness, it can only be considered to be a very simplistic representation. The inaccuracies in the hardware to software measurements may be indicative of the single wire model where the current flows in an infinite thin layer positioned on the cone surface. The height of the wire package is ignored; hence the coil sensitivity. The resultant data from DUCAD-Y can therefore only be considered as a starting point in the development of a hardware coil and therefore to obtain an optimized design, a measure of hardware optimization must be maintained.

It must be questioned that the current approach is the 'best', as this assumption of rotationally symmetry can restrict the electron-optical designer in some applications in realizing a more suitable design solution. This 'restriction' may potentially reduce the number of available design solutions, for example designs incorporating uneven components shapes/sizes. DUCAD, specifically written for rotationally symmetric systems, would have to be modified in its calculation approach to allow individual segmentation of wound slots to more representably reflect a slot wound product.

Individually each of the correction plates and static magnets were removed to document their contribution to the overall system performance. On initial pass of this process, the effect of the coma plate was poorly simulated in the DUCAD-Y model. The position of the plate was altered, a move which we know in hardware to cause large shifts in coma correction levels. This was not reflected in the software model. The DUCAD-Y definition of the frame coil was modified and the software deltas were re-calculated to ensure the yoke ring was 'charging up' via the frame coil currents, as required. On this evaluation of the component parts the coma plates were well simulated, however this appeared to effect the simulation of the astigmatism plates in the DUCAD-Y model.

Neglecting the above documented discrepancy, in all investigated cases, the comparison between the computational and measurements results were satisfactory to a level however alarming differences were often visible for some aberrations. Commonly it was experienced that the relative differences between the hardware and software values

became larger on component modification and wire pattern changes, i.e. the agreement between DUCAD and hardware became poorer. However, the overall aberration Quality factor Qk, remained a good measure of the global design performance of the deflection unit. DUCAD appeared more capable of determining the overall quality performance of a design proposal, although the realisation of exact aberration errors was not so precise . A further possible reason may be due to winding tolerances as a result of the winding pattern introducing unexpected effects.

During the software development of the product, it became clear that modifications could be made to the separator to improve the overall product performance highlighting the inherent restrictions DUCAD-Y has in accurately realising a superior product design. A great level of involvement with component suppliers was an important aspect within the design and development processes. A more comprehensive understanding of the possibilities and limitations in separator design were understood from discussions with the plastic supplier. These issues included material requirements and specification, complexity of tooling, and the possibility of design modifications during development phase.

DUCAD-Y requires and is heavily dependent upon a large amount of initial information to begin any simulation study. By this very design approach, if a design concept is inputted into DUCAD-Y the optimization calculations will attempt to produce a design maintaining closely to the initial constraints, believing that the information provided is the 'best' starting point. Often, however in development processes of this nature the starting point is a guesstimate allowing the design process to commence. The final product design optimized in this investigation gave an acceptable design performance, however, it could certainly be improved. The next step would be to re-start the simulations study including the design improvements raised from the initial study.

The process of optimization is highly dependent upon the skills of the DUCAD user, and the likelihood of determining the overall system global minima is very much down to experience. The probability of optimizing to a local minima within the system objective

function is more common, and there always remains the doubt that a 'better' more improved and stable design solution could be possible. The current optimization process often led to an unstable solution following from variation in the definition of certain design parameters. Indeed, a continuous optimization run was seldom achieved. One must indeed question if the minima being directed towards in the optimization process is indeed a global system optimum or a local minimum in the system.

In manufacturing design systems, the need to define a stable minima is crucial i.e. if a component position is altered/mis-aligned, it is preferable that this variable should not be highly sensitive to the optimized system performance. High volume production scenarios required a highly stable system to attain acceptable product yields and quality levels. These issues can be much aided if the chosen optimization system parameter definitions are not sensitive to minor variations.

In current use, there is a need for the DUCAD-Y design proposals/solutions to be continually considered by the electron-optical designer, who is able to restrict the development of certain design proposals which appear less practical. An example of this is the frame winder where mechanical stops restrict winding angles greater than 55 degrees. This is a physical restriction which can be inputted into the simulation package, however it is for the DUCAD-Y operator to control and manage.

Of prime concern is the current level of user interaction required to manipulate the mechanics of the system. An improved procedure would allow a set of design variables and constraints to manage the optimization process and eliminate the need for expertise in the process. From this study, it is necessary to limit the number of optimization stages purely in order to maintain control of the simulation process. To realize a more memory-based optimization cycle with improved response variables would undoubtedly improve subsequent design constructions, and improve the ability to locate the global system optimum.

The use of the DUCAD-Y simulation model certainly assists in developing a product design to achieve reasonable performance, however further investigation is required to fully assess the extent of the inaccuracies which are certainly present. These inaccuracies certainly appear more affected by any increase to the number of additional correction components.

By employing a computer aided engineering tool, electron-optical designers can analyse the dependence of deflection system performance without the requirement to generate time-consuming hardware prototypes. This is particularly important if the designer does not have all the required technical specifications, and the customer requires the 'best' solution to the problem. Then the designers' time and expertise is more effectively generating an adequate computer model of the deflection system.

The discrepancies between the actual winding relationship between machine and separator design are now well understood. Subsequent slot based designs would therefore be better placed to more closely predict the achievable convergence/raster behaviour. By investigating a potential slot wound design this could produce a more competitive and viable financial solution to the current Philips method of pin-fired winding which require the fabrication of expensive machine tooling. Slot winding is viewed as a more accessible method of manufacture but a prime consideration is its impact upon product performance. If applied to the mid-range product category where premium performance is not as critical as other product specifications, slot winding could be seen as a complementary design technology.

A particularly weak limitation of the DUCAD-Y software simulation is that the practical restrictions in product coil manufacture are difficult to realize in the computational assessment of a product design. The main point to examine closely is that any simulation technique approximates a real system and in so doing will achieve at best minimized errors across the system range.

It can be concluded that DUCAD-Y provides an initial iterative design step certainly eliminating many initial steps within the design cycle, however it is important to incorporate hardware prototyping in any development study of this nature. Further refinement of the model may improve the correlation between hardware and software, however in reality the designer would resort to hardware optimization as it is a more effective and speedy process at this stage in the design cycle.

A complete understanding of any simulation tool must extend to the overall design process, in addition to the product being designed. The design concept may start as a customer request but as it proceeds through many activities, product definition (type design/manufacturing), prototype for manufacture, design and manufacture, generally the cost of each activity is greater than that of the one before. Defining the specification, generating the design and demonstrating the solution are technical tasks which must be undertaken at minimal cost (in both time and capital) to the development cycle. If the design concept is accepted, an increasing sequence of costs is generated, proving that the product meets the initial customer specification is at least one of these and the ability to exploit this form of design technique should not be underestimated. Therefore, a knowledge of the costs for prototyping and testing design concepts should discipline a formal design procedure where the involvement of technical aids, such as DUCAD are important in supporting the entire design cycle.

Good approximations to system outputs for a variety of inputs are required. Models may be used to test the effect of various inputs to the real system by observing the models' outputs. This is desirable for many reasons, but fundamentally because diagnostic testing on real systems is costly and impractical. Firstly, as with many software simulation aids, the finalised results are only as consistent as the input data, therefore an experienced electron-optical designer is required to operate the system. Secondly a valuable starting point is extremely advantageous to provide a 'good' design. This can however be achieved by many iterative runs of the optimization program to gradually improve the designs' performance and capability. In general, simulation techniques are advantageous

within a design cycle, however it is important to realize its limitations in a development programme. Although good modelling techniques may be in place, the need for validation against the real system should not be neglected (input/output checks should be performed regularly). Undoubtedly, the documented discrepancies revealed in this investigation test the validity of the assumptions made and the working mechanics of operation of the DUCAD-Y package. Further work is required in determining more accurate deflection unit performance predictions which more closely correlate to hardware trials.

8. CHAPTER EIGHT

Conclusion

Omitting the discrepancy in precisely modelling a slot wound product design as described, there exists fundamental inaccuracies in effectively calculating the interaction of correction components and their multiple impact upon the overall deflection system modelled within DUCAD-Y. Further investigation is required to thoroughly assess the shortcomings of this numerical optimization technique.

DUCAD-Y can be seen to be a valuable tool at the outset of the development design cycle. Its ability to calculate the optimized lengths of deflection coils is accurate and particularly effective, and in this regard DUCAD-Y achieves a valuable starting point in the product design cycle. However, DUCAD-Y is limited in its true scope, producing notable disparities to reality even disregarding the peculiarities of the slot winding process.

An overall system performance using the DUCAD-Y optimization technique was difficult to achieve and the emerging system aberrations became more understandable, determined by the detailed interactions of the conceptual design. Further system optimization beyond this conceptual design stage required hardware manipulation of the designed components. Within this design phase, hardware optimization was a more flexible development approach, excluding the complexities of the DUCAD-Y manipulation. A systems view of the complete product throughout the design period proved an essential consideration. It proved extremely important to thoroughly define such factors as the manufacturing and winding processes to allow an accurate software model to be realized and increase the level of accuracy between the hardware and software measurements. Not withstanding this however, the findings of this DUCAD-Y study emphasised the need to carefully validate the accuracy of DUCAD-Y in its prediction of deflection unit performance.

Optimization Techniques are widely employed in a varied range of engineering applications to achieve the 'best' solution to a particular design scenario. The strategy for product design through analytical engineering optimization tools is beneficial in many aspects, however, as highlighted in this design study it has limitations and restrictions, and conventional methodologies should not be excluded. One can conclude however, that the DUCAD-Y simulation tool is important in deflection unit design processes, and plays an important role in this specialised field.

APPENDIX A - ELECTRON TRAJECTORY CALCULATION

APPENDIX A - ELECTRON TRAJECTORY CALCULATION

During the numerical integration procedure of ray tracing, the magnetic field is needed along the complete electron path. The trajectory calculation is carried out on a flat, imaginary screen, from which the landing positions of the beams in the mask surface and fluorescent surface are obtained.

Fermats principal in geometric optics can also used in electron optics where the electron path between two points P_1 (on cathode) and P_0 (on screen) states

$$\partial \int_{P_0}^{P_1} \left(\mathbf{U} - \sqrt{\left(\frac{e}{2m}\right)} (\mathbf{A} \bullet \mathbf{s}) \right) ds = 0$$

where
- **U** static electric potential,
- **A** magnetic vector potential,
- e electron charge
- m electron mass,
- **s** unit vector tangent to the trajectory.

The transformation of the Euler equation above is carried out by substituting the following independent variables

$$d/dz \left(x' / \sqrt{(1 + x'^2 + y'^2)} \right) = k \left(-y' H_z + H_y \right)$$

$$d/dz \left(y' / \sqrt{(1 + x'^2 + y'^2)} \right) = k \left(x' H_z - Hx \right)$$

$$K = (e/2 m U)$$

Using the *Runge-Kutta Method* to solve the first order simultaneous equations

$$dx/dz = \xi$$

$$dy/dz = \eta$$

$$d\xi/dz = (1 + \xi^2 + \eta^2)^{1/2} \left((1 + \xi^2) g + \xi \eta h \right)$$

where $g = k (-\eta Hz + Hy)$

$h = k (\xi Hz - Hx)$

The position where the electrons beams meet the shadow mask can be obtained by solving the first order equations under the initial conditions determined by constants such as the gun co-ordinates of the picture tube, the position of the mask, and the pitch of the fluorescent paint, etc. (vectoral position and slope at cathode)

The curve surface equation of the shadow mask is given by:

$$\mu_1 (x, y) = \left[\left((R_v^2 - y^2)^{1/2} - (R_v - R_n) \right)^2 - x^2 \right]^{1/2} + z_c$$

On the surface of the fluorescent light emitting screen, the equation is:

$$\mu_2 (x, y) = \left[R_p^2 - x^2 - y^2 \right]^{1/2} + z_d$$

where

R_v is the radius of curvature in the vertical direction of the mask.
R_H is the radius of curvature in the horizontal direction of the mask.
R is the radius of curvature of the fluorescent surface.
Z and Z are constants that show the relative positions between the mask and the fluorescent surface.

The rays whose plane of convergence is parallel to the plane of deflection converge more rapidly due to different path lengths in the field than rays with planes of deflection and convergence perpendicular. Consequently screen colour errors results and a change in focus voltage can only exaggerate rather than remedy this defect. Since an increase in beam current to obtain a high brightness results in a larger beam cone vertex angle, the effect of greater spot growth on deflection for a brighter image is readily explained.

APPENDIX B - DUCAD-Y SIMULATION PERFORMANCE DATA

- Finalised DUCAD-Y design L26F26 with COMA-RB correction
- Line and Frame Magnetic Field Distributions for each multipole

RASTER AND CONVERGENCE ERRORS OF COIL L26F26
8 POINTS

XS (M)	YS (M)	XR (MM)	YR (MM)	BRX (MM)	BRY (MM)	XCOMA (MM)	YCOMA (MM)	
0.114400	0.000000	0.000	0.000	0.219	0.000	0.066	0.000	
0.228800	0.000000	0.000	0.000	0.019	0.000	0.277	0.000	
0.000000	0.085800	0.000	0.000	-0.062	0.000	0.000	-0.135	
0.114400	0.085800	1.866	1.501	-0.012	-0.182	-0.028	-0.094	
0.228800	0.085800	2.930	2.595	-0.394	0.565	0.097	0.118	
0.000000	0.171600	0.000	0.000	0.780	0.000	0.000	0.091	
0.114400	0.171600	4.185	0.263	0.181	-0.398	-0.260	0.098	
0.228800	0.171600	8.477	-0.211	-0.897	0.672	-0.273	0.323	

SLAG(MM)	ZS(MM)
4.986	155.014

QA	QC	QK	QR	%EW	%NS	SLAG	TR3	TR5
33.2	13.2	25.8	221.5	3.70	-0.12	4.99	0.099	-1.971

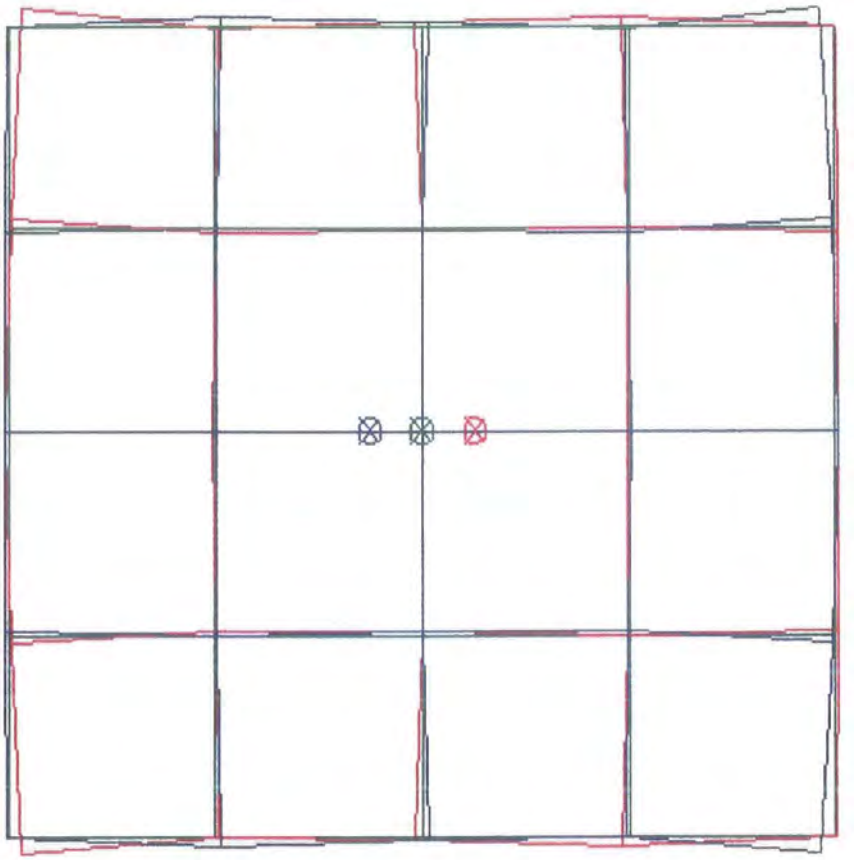

DRAW OF NOMINAL CONVERGENCE OF COIL L26F26

DEC 16 1996
TIME 12:59

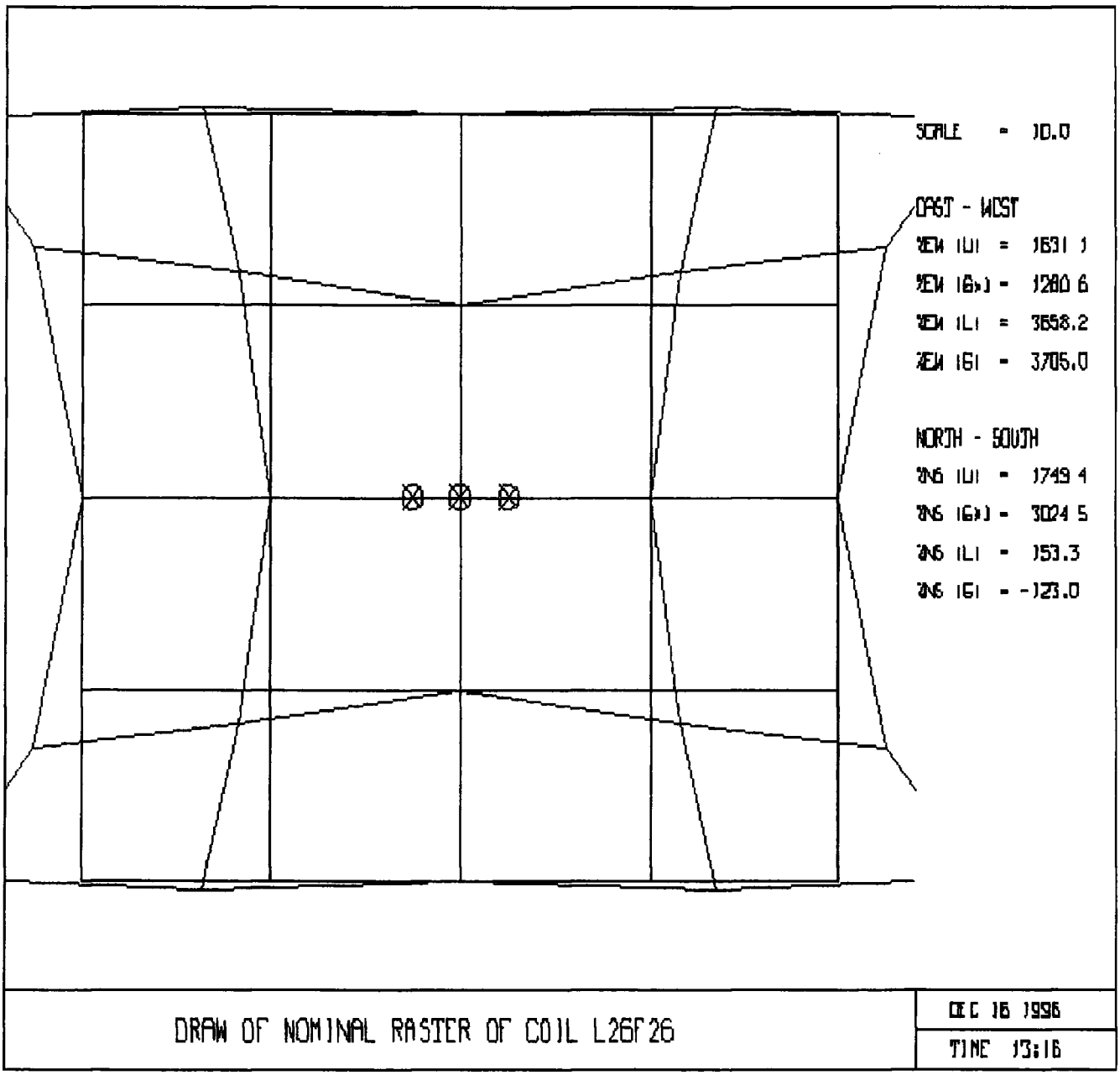
SCALE = 10.0
EAST - WEST
NORTH - SOUTH
DEC 16 1996
TIME 13:16
DRAW OF NOMINAL RASTER OF COIL L26F26

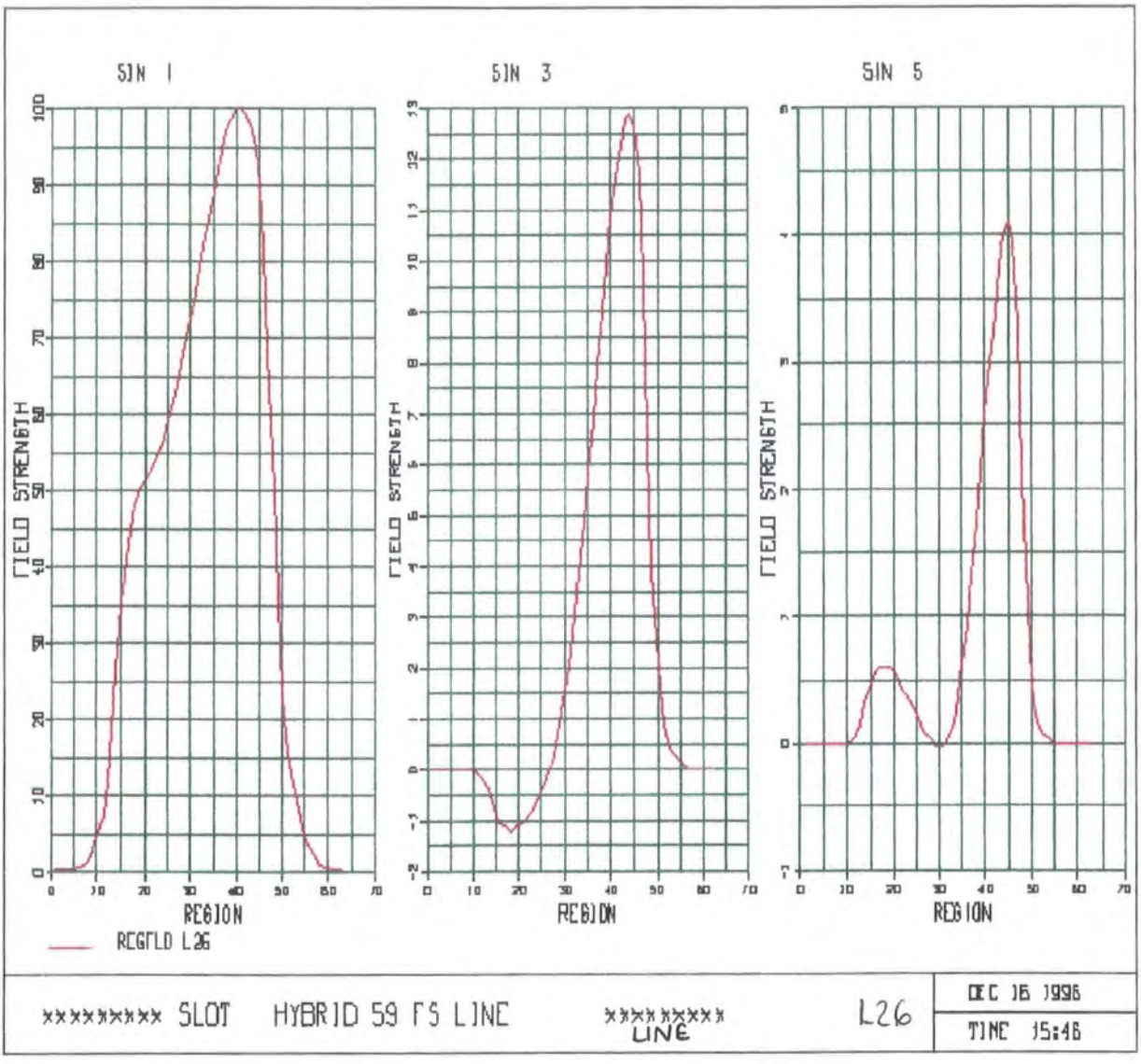
SIN 1
SIN 3
SIN 5
FIELD STRENGTH
REGION
REGFLD L26
********* SLOT HYBRID 59 FS LINE
********* LINE
L26
DEC 16 1996
TIME 15:46

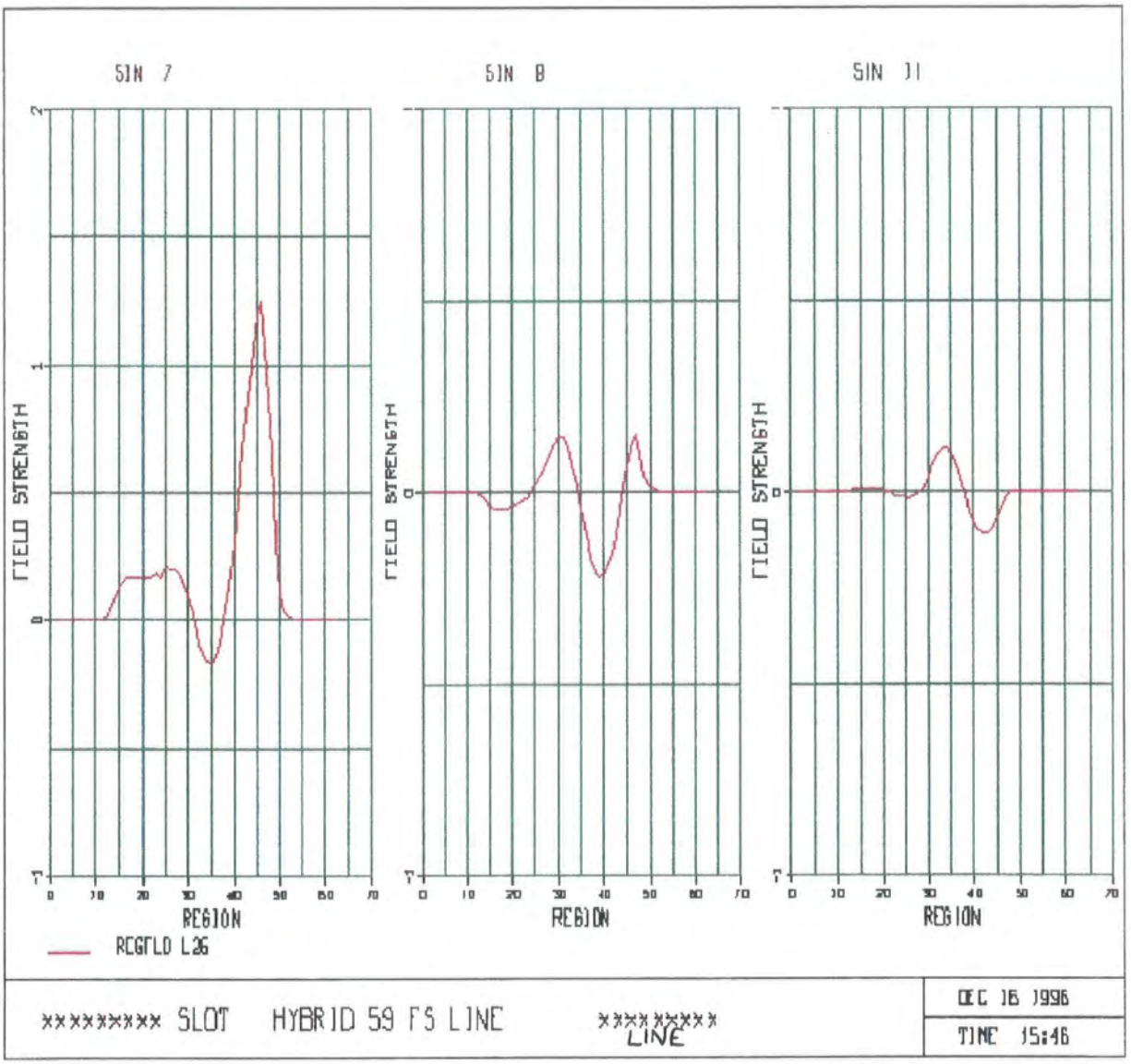
SIN 7
SIN 8
SIN 11
FIELD STRENGTH
REGION
REGFLD L26
********** SLOT HYBRID 59 FS LINE **********
LINE
DEC 16 1996
TIME 15:46

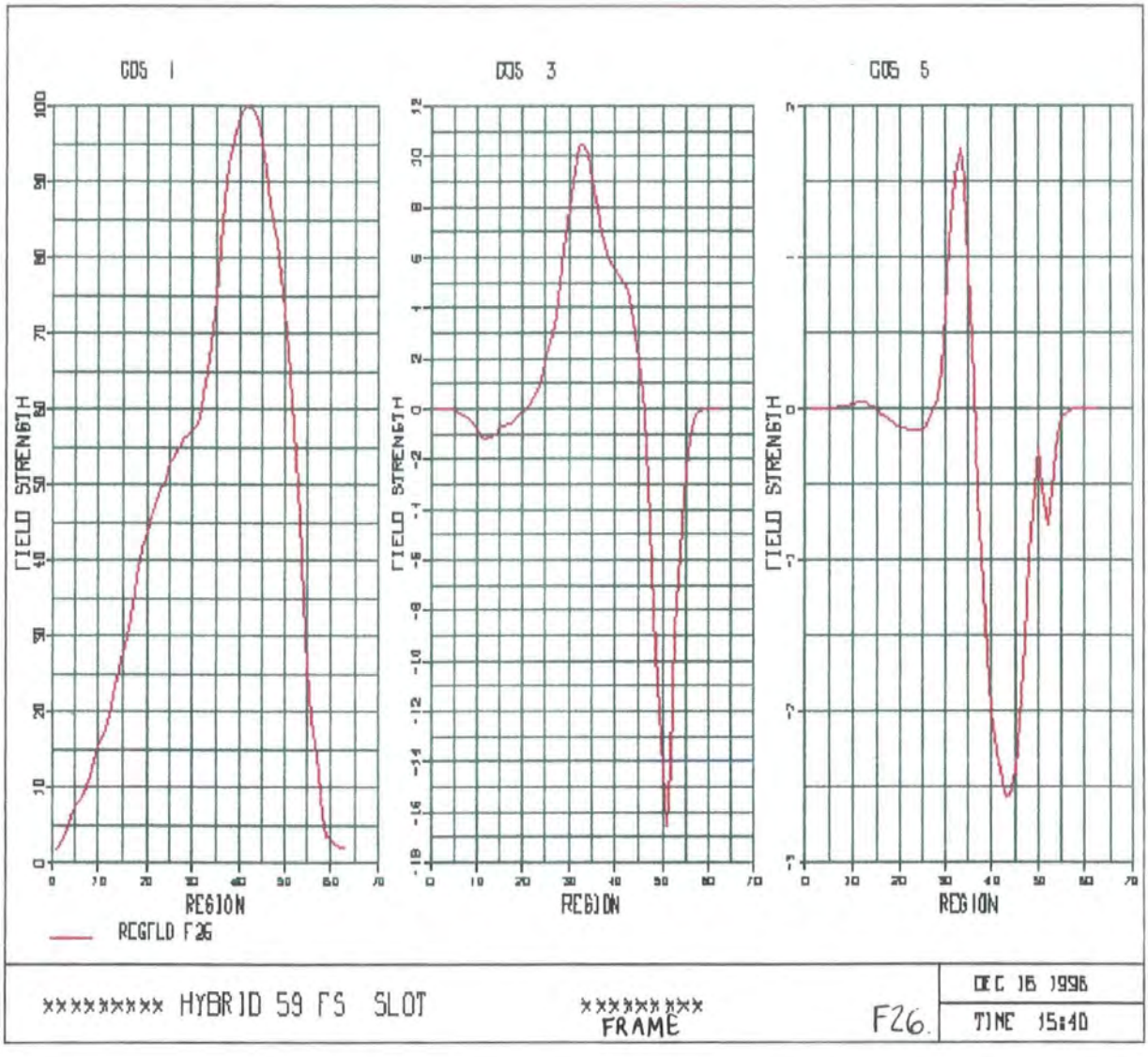
COS 1
COS 3
COS 5
FIELD STRENGTH
REGION
REGFLD F26
********** HYBRID 59 FS SLOT
********** FRAME
F26.
DEC 16 1996
TIME 15:40

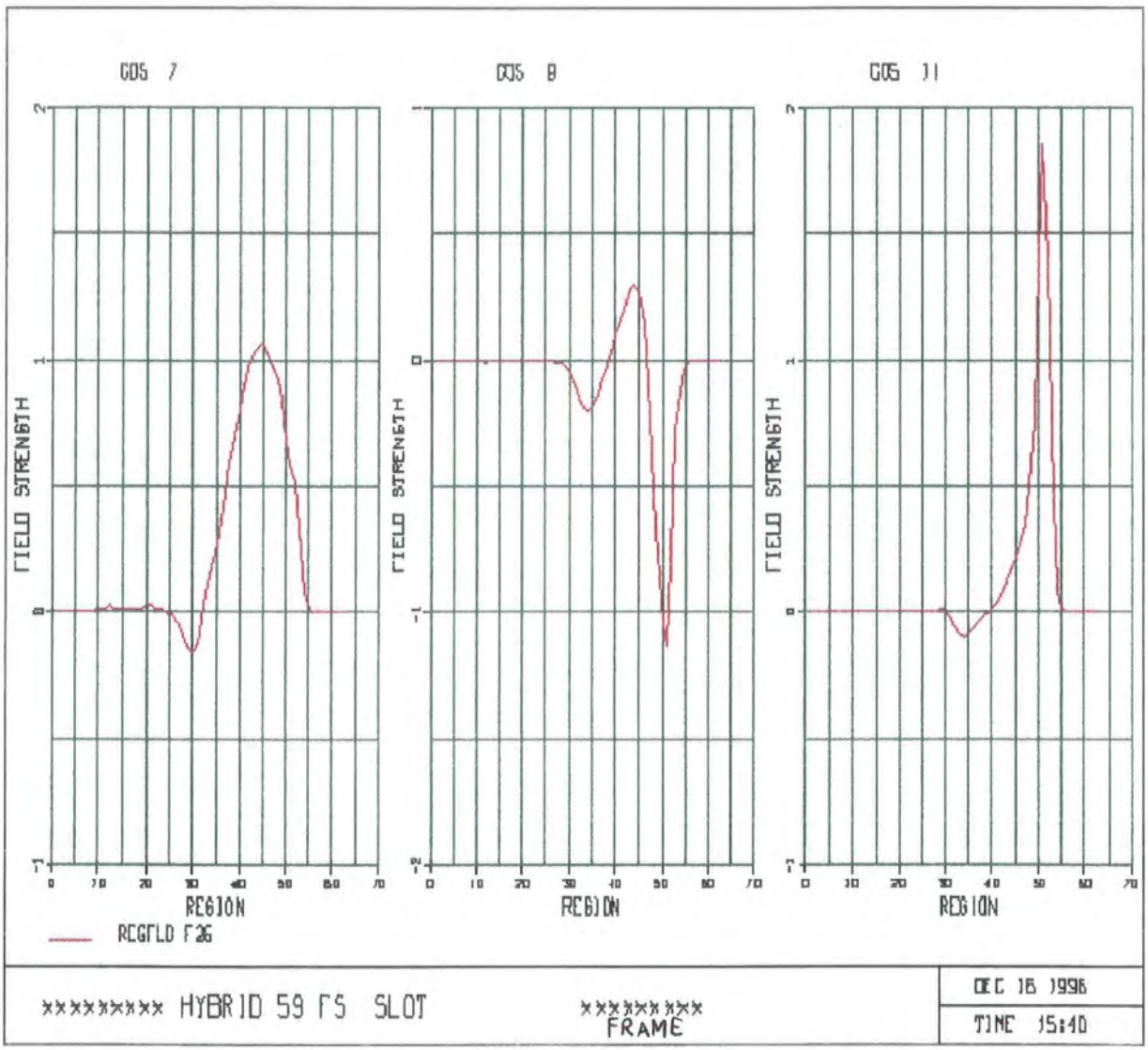
COS 7
COS 8
COS 11
FIELD STRENGTH
REGION
REGION
REGION
REGION 26
********* HYBRID 59 FS SLOT
********* FRAME
DEC 16 1996
TIME 15:40

APPENDIX C - HARDWARE REPLICATION - Sony Winding Machine Specification

SONY

Deflection Yoke Winding Machine

YD-1100

Applicable to non-divided separator

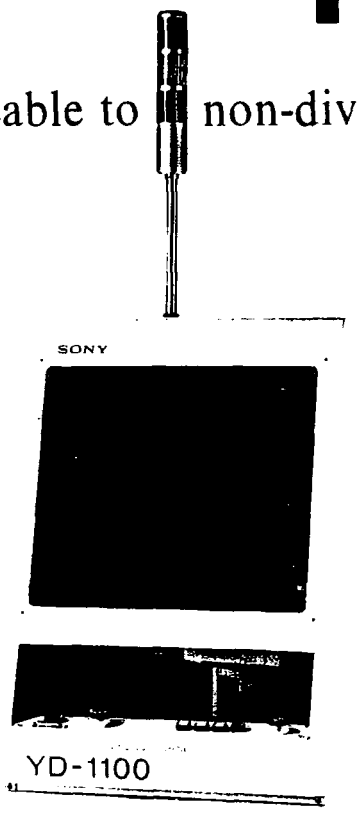

- To realize highly precise winding through guiding wire by hook.
- Applicable to all kinds of deflection yoke.
- Small, light-scale and space-saving type.

SonyFA

Features

- Capable of precise winding through guiding wire by hook.
  Capable of winding exactly in gutter
  Capable of winding exactly in circumference gutter
  Capable of decreasing deformation of separator
- Applicable to all kinds of deflection yoke by change of program and holder.
- Capable of winding twisted wire or single wire
- Capable of winding clockwise or counter-clockwise continuously by turn of guide.

clockwise

counterclockwise

Application of separators	● Non-devided separator ● Devided section separator ● Maximum diameter : ϕ230mm ● Minmum inside diameter : ϕ22.5mm ● Maximum height : 120mm
Application of wires	● Twisted wire : ~ϕ0.15×49 ● Single wire : ~ϕ0.40

[Outline of wining]

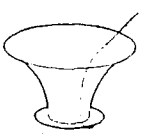

Winding up in gutter

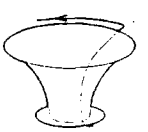

Winding in large circumference gutter

Winding down in gutter

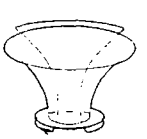

Winding in small circumference gutter

SPECIFICATIONS	
EXTERIOR DIMENSION	490×960×1,500(W×D×H)mm
WEIGHT	Approx.400kg
POWER SUPPLY	1ϕAC200V±10% 50/60Hz
POWER SUPPLY CAPACITY	Appox.5KVA
AIR PRESSURE	0.5MPa 5kg f/cm²
AIR CONSUMPTION	Appox.20 ℓ/min

*Design and specifications are subject to change without notice

Sony Corporation
FA & Precision Products Group
FA Overseas Marketing Division
6-7-35, Kitashinagawa
Shinagawa-ku, Tokyo 141 Japan
Tel: 03-5448-2805
Fax: 03-5448-2959

APPENDIX D - HARDWARE REPLICATION - INITIAL VALIDATION

BASIC LINE AND FRAME WINDING FORMAT

- *CVRSLF L62F62* Anticipated DUCAD-Y Performance Output
- *DRAWSECT L62F62* Plot
- Example of 'Special Delta' carried out to improve hardware/software correlation
- Example of Hardware Measurement File, as measured on the MOM

RASTER AND CONVERGENCE ERRORS OF COIL L62F62
8 POINTS

XS (M)	YS (M)	XR (MM)	YR (MM)	BRX (MM)	BRY (MM)	XCOMA (MM)	YCOMA (MM)
0.114400	0.000000	0.000	0.000	1.654	0.000	-0.261	0.000
0.228800	0.000000	0.000	0.000	7.137	0.000	-0.845	0.000
0.000000	0.085800	0.000	0.000	0.079	0.000	0.000	0.685
0.114400	0.085800	5.289	4.170	1.754	-1.429	-0.275	0.593
0.228800	0.085800	9.811	12.263	7.282	-2.256	-0.882	0.373
0.000000	0.171600	0.000	0.000	-0.874	0.000	0.000	2.080
0.114400	0.171600	18.683	7.953	1.172	-5.092	-0.392	1.656
0.228800	0.171600	34.646	24.439	7.004	-6.820	-0.969	0.991

SLAG(MM)	ZS(MM)
8.387	121.613

QA	QC	QK	QR	%EW	%NS	SLAG	TR3	TR5
324.6	73.3	237.2	1021.5	15.14	14.24	8.39	0.146	-2.422

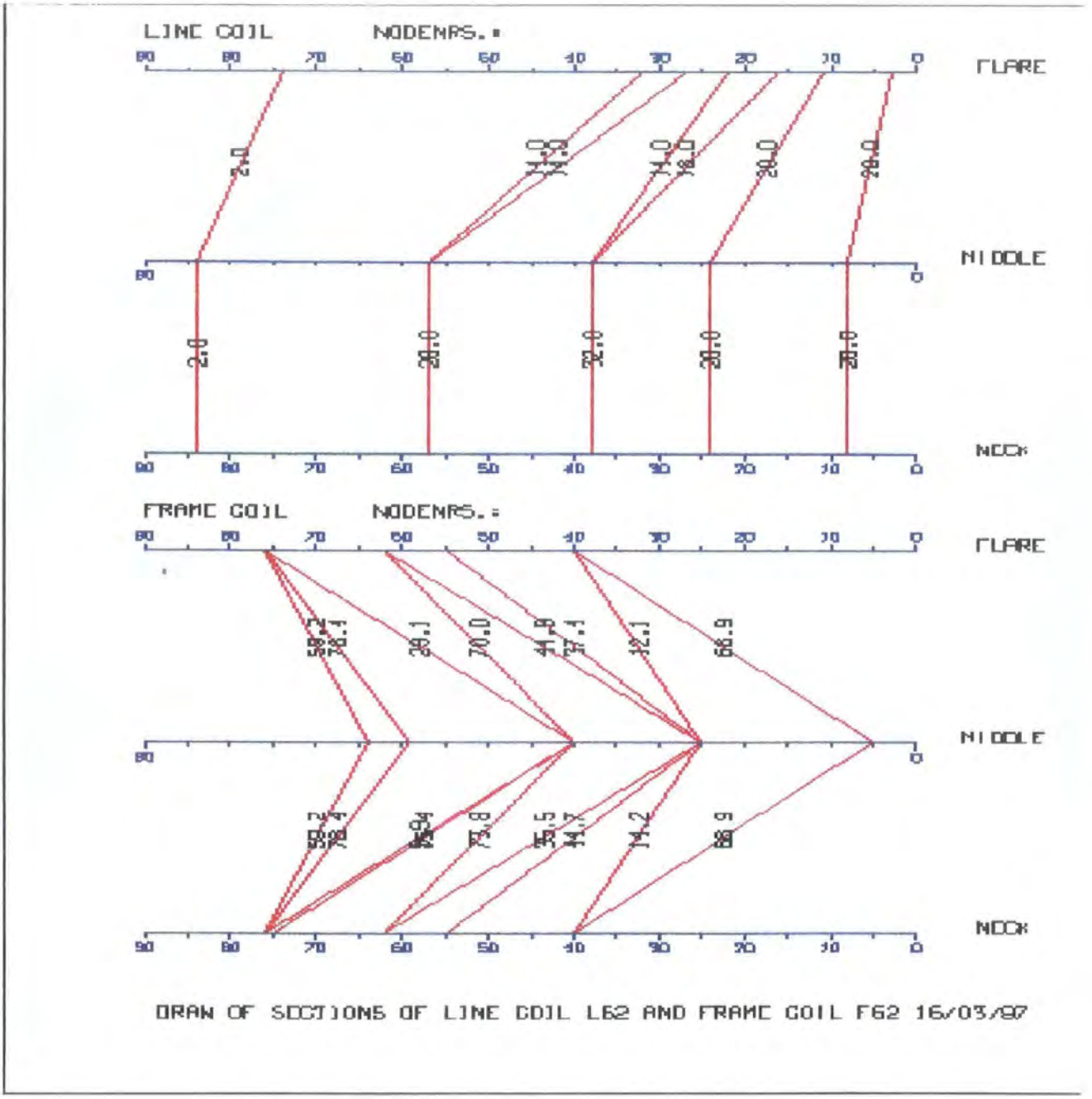
LINE COIL NODENRS.=
FLARE
MIDDLE
NOSE
FRAME COIL NODENRS.=
FLARE
MIDDLE
NOSE
DRAW OF SECTIONS OF LINE COIL L62 AND FRAME COIL F62 16/03/97

RASTER AND CONVERGENCE ERRORS OF COIL S62D1
8 POINTS

XS (M)	YS (M)	XR (MM)	YR (MM)	BRX (MM)	BRY (MM)	XCOMA (MM)	YCOMA (MM)
0.114400	0.000000	0.000	0.000	1.519	0.000	-0.188	0.000
0.228800	0.000000	0.000	0.000	6.597	0.000	-0.678	0.000
0.000000	0.085800	0.000	0.000	-0.324	0.000	0.000	0.947
0.114400	0.085800	5.688	4.161	1.245	-2.228	-0.268	0.802
0.228800	0.085800	10.695	11.941	6.367	-3.475	-0.817	0.522
0.000000	0.171600	0.000	0.000	-3.215	0.000	0.000	3.060
0.114400	0.171600	20.205	8.054	-0.956	-7.677	-0.647	2.298
0.228800	0.171600	37.557	23.843	4.717	-10.080	-1.277	1.300

SLAG(MM)	ZS(MM)
7.759	122.241

QA	QC	QK	QR	%EW	%NS	SLAG	TR3	TR5
362.7	98.5	268.8	1072.8	16.41	13.89	7.76	-0.385	-3.451

RASTER AND CONVERGENCE ERRORS OF COIL L62F62
8 POINTS

XS (M)	YS (M)	XR (MM)	YR (MM)	BRX (MM)	BRY (MM)	XCOMA (MM)	YCOMA (MM)
0.114400	0.000000	0.000	0.000	1.654	0.000	-0.261	0.000
0.228800	0.000000	0.000	0.000	7.137	0.000	-0.845	0.000
0.000000	0.085800	0.000	0.000	0.079	0.000	0.000	0.684
0.114400	0.085800	5.300	4.177	1.756	-1.432	-0.275	0.594
0.228800	0.085800	9.827	12.277	7.286	-2.259	-0.882	0.373
0.000000	0.171600	0.000	0.000	-0.872	0.000	0.000	2.078
0.114400	0.171600	18.686	7.960	1.175	-5.091	-0.392	1.655
0.228800	0.171600	34.649	24.436	7.001	-6.822	-0.969	0.992

SLAG(MM)	ZS(MM)
8.388	121.612

QA	QC	QK	QR	%EW	%NS	SLAG	TR3	TR5
324.6	73.3	237.2	1021.9	15.14	14.24	8.39	0.143	-2.417

DELTA EFFECTS
8 POINTS

XS (M)	YS (M)	XR (MM)	YR (MM)	BRX (MM)	BRY (MM)	XCOMA (MM)	YCOMA (MM)
0.114400	0.000000	0.000	0.000	-0.135	0.000	0.073	0.000
0.228800	0.000000	0.000	0.000	-0.540	0.000	0.167	0.000
0.000000	0.085800	0.000	0.000	-0.403	0.000	0.000	0.263
0.114400	0.085800	0.388	-0.016	-0.511	-0.796	0.007	0.208
0.228800	0.085800	0.868	-0.336	-0.919	-1.216	0.065	0.149
0.000000	0.171600	0.000	0.000	-2.343	0.000	0.000	0.982
0.114400	0.171600	1.519	0.094	-2.131	-2.586	-0.255	0.643
0.228800	0.171600	2.908	-0.593	-2.284	-3.258	-0.308	0.308

QA	QC	QK	QR	%EW	%NS	SLAG	TR3	TR5
126.3	28.3	92.2	70.8	1.27	-0.35	-0.63	-0.528	-1.035

iwQAC7064L 59FS SLOT WINDING, CMR 1989. A
IEAD 2 UNITS 1-10 OLD CLAMPING JIG.
Measured on mom v11 conv. only untranslated.
5.2.97

5 0 10 1 0 DATE: 7-FEB-97 08:23:11 L.Q.

LINE-EFF.

NR	AST	COY	COX	SYM	BAL	TWI	ASCOY	ASCOX
0001	7.352	0.044	0.636	1.765	-0.003	0.150	-0.145	-0.370
0002	7.081	0.093	0.572	-1.268	-0.249	0.196	-0.116	-0.188
0003	7.330	0.087	0.733	1.779	-0.037	0.192	-0.139	-0.295
0004	7.270	0.099	0.566	2.756	-0.553	0.250	-0.152	-0.248
0005	7.439	0.065	0.667	0.358	-0.446	0.250	-0.120	-0.091
0006	7.327	0.041	0.522	-1.058	-0.559	0.087	-0.157	-0.208
0007	7.186	0.044	0.654	-0.106	-0.106	0.116	-0.147	-0.321
0008	7.294	0.032	0.487	1.384	0.085	0.050	-0.124	-0.282
0009	7.451	0.062	0.859	-0.154	-0.322	0.151	-0.127	-0.185
0010	7.179	0.110	0.687	1.896	-0.653	0.237	-0.205	-0.371
MEAN	7.291	0.068	0.638	0.735	-0.284	0.168	-0.143	-0.256
RANGE	0.370	0.078	0.372	4.024	0.738	0.200	0.089	0.280
ST.DEV	0.116	0.028	0.109	1.369	0.263	0.069	0.026	0.089

FRAME-EFF.

NR	AST	COY	COX	SYM	BAL	TWI	ASCOY	ASCOX
0001	0.032	2.682	-0.010	0.930	-3.007	0.182	-0.273	-0.531
0002	-0.630	2.800	0.040	1.073	-0.806	0.319	-0.283	-0.114
0003	-0.227	2.691	0.038	0.686	-3.040	0.255	-0.298	-0.464
0004	-0.300	2.772	0.066	0.925	-3.100	0.311	-0.352	-0.449
0005	-0.366	2.750	0.041	1.128	-1.663	0.188	-0.409	-0.268
0006	-0.449	2.809	0.018	1.195	-0.630	0.109	-0.393	-0.091
0007	-0.238	2.768	0.042	0.530	-1.689	0.149	-0.262	-0.223
0008	-0.122	2.691	0.035	0.246	-2.758	0.206	-0.213	-0.402
0009	-0.455	2.824	0.056	1.416	-1.920	0.405	-0.394	-0.315
0010	-0.160	2.753	0.052	1.020	-3.008	0.342	-0.406	-0.464
MEAN	-0.292	2.754	0.038	0.915	-2.162	0.247	-0.328	-0.332
RANGE	0.662	0.142	0.076	1.170	2.470	0.296	0.196	0.440
ST.DEV	0.191	0.051	0.021	0.343	0.952	0.095	0.071	0.155

APPENDIX E - HARDWARE REPLICATION -

Hardware Optimized Prototype System Solution

APPENDIX E - HARDWARE REPLICATION -

Hardware Optimized Prototype System Solution

Line Winding	Line Astig. Measured	Xcoma Measured	Line Astig. Simulated	Xcoma Simulated	Line Astig. Delta	Xcoma Delta
1-1 13T 2-2 5T 3-3 4T 3-4 12T 3-5 2T 4-5 5T 4-6 6T 5-9 4T 6-10 2T	9.356	0.736	13.855	1.877	4.499	1.141
1-1 15T 2-2 5T 3-3 4T 3-4 12T 3-5 2T 4-5 5T 4-6 7T 5-9 4T 6-10 2T	6.967	-0.044	11.484	1.015	4.517	1.059
1-1 15T 2-2 6T 3-3 4T 3-4 12T 3-5 2T 4-5 5T 4-6 7T 5-9 4T 6-10 2T	7.079	-0.128	11.031	0.892	3.952	1.020
1-1 15T 2-2 8T 3-3 4T 3-4 12T 3-5 2T 4-5 5T 4-6 7T 5-9 4T 6-10 2T	6.228	-0.381	10.176	0.658	3.948	1.039
1-1 15T 2-2 12T 3-3 4T 3-4 12T 3-5 2T 4-5 5T 5-9 4T 6-10 2T	-1.740	-2.661	2.595	-1.844	4.335	0.817

Line Winding	Line Astig. Measured	Xcoma Measured	Line Astig. Simulated	Xcoma Simulated	Line Astig. Delta	Xcoma Delta
1-1 15T 2-2 7T 3-3 4T 3-4 12T 3-5 2T 4-5 5T 4-6 2T 5-9 4T 6-10 2T	-0.053	-2.206	4.189	-1.417	4.242	0.789
1-1 17T 2-2 12T 3-3 4T 3-4 12T 3-5 2T 4-5 5T 4-6 3T 5-9 4T 6-10 2T	-1.438	-2.677	3.439	-1.634	4.877	1.043
1-1 15T 2-2 7T 3-3 4T 3-4 12T 3-5 2T 4-5 5T 4-6 2T 5-9 4T 6-10 2T	1.841	-1.595	6.200	-0.720	4.359	0.875
1-1 15T 2-2 7T 3-3 4T 3-4 12T 3-5 2T 4-5 5T 4-6 3T 5-9 4T 6-10 2T	2.794	-1.323	7.147	-0.395	4.353	0.928
1-1 17T 2-2 7T 3-3 6T 3-4 12T 4-5 8T 4-6 3T 5-9 5T 6-10 2T	3.001	-1.252	7.528	-0.170	4.521	1.082
1-1 17T 2-2 8T 3-2 6T 4-4 2T 4-5 6T 5-9 5T 6-10 2T	0.263	-1.657	3.033	-0.610	2.770	1.047

APPENDIX F - HARDWARE REPLICATION -

Re-Set Base Line/Frame Coil Designs

1. Modified Line Coil winding; L26F26

- *DRAWSECT L26F26* Plot
- *CVRSLF L26F26* Convergence Output Plot

2. Modified Frame Coil Winding; L27F27

- *DRAWSECT L27F27* Plot
- *CVRSLF L27F27* Convergence Output Plot

3. Modified Frame Coil Winding; L30F30
(reduction in the winding angle of frame coil (R2 definition)

- *DRAWSECT L30F30* Plot
- *CVRSLF L30F30* Convergence Output Plot

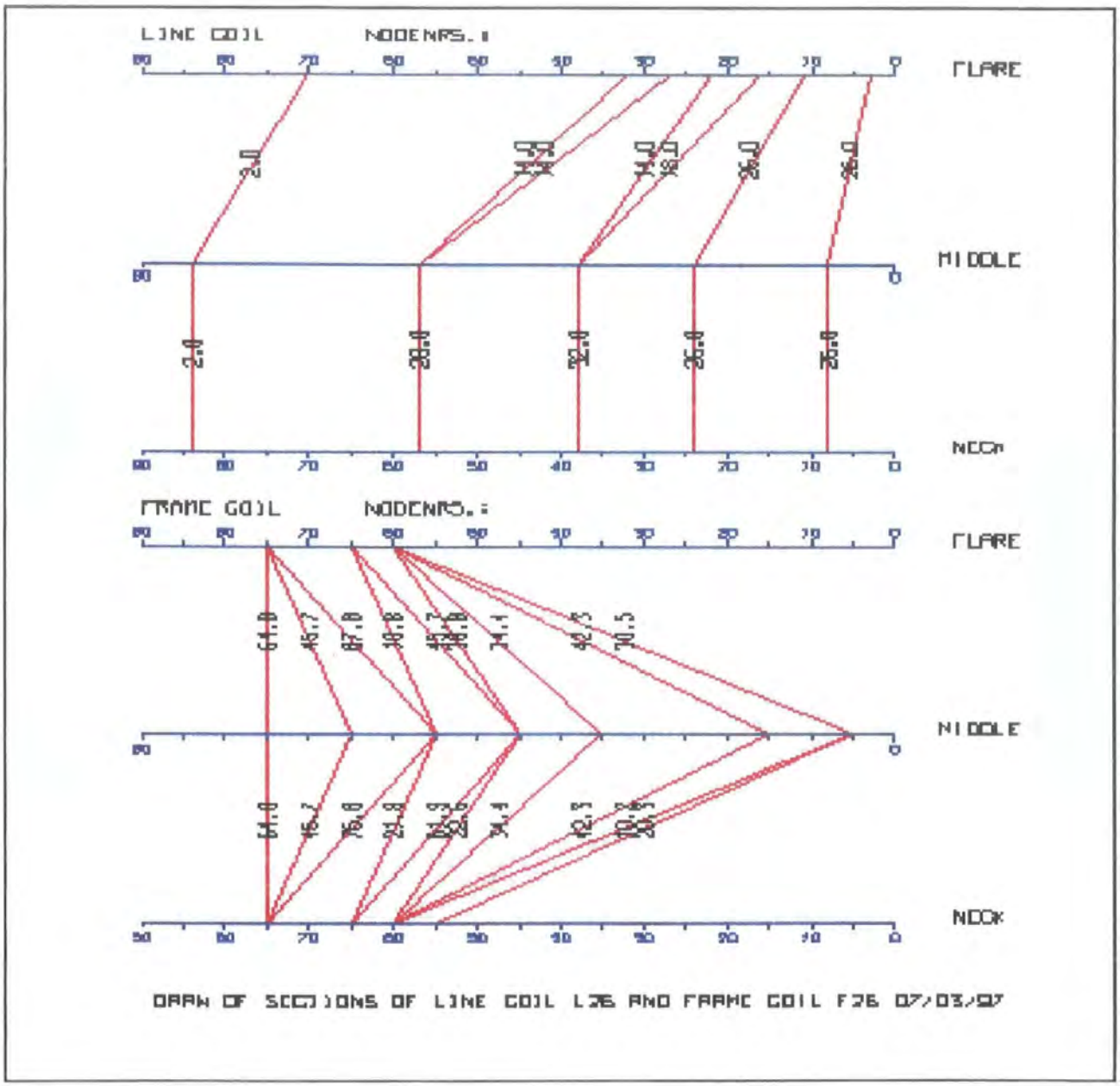

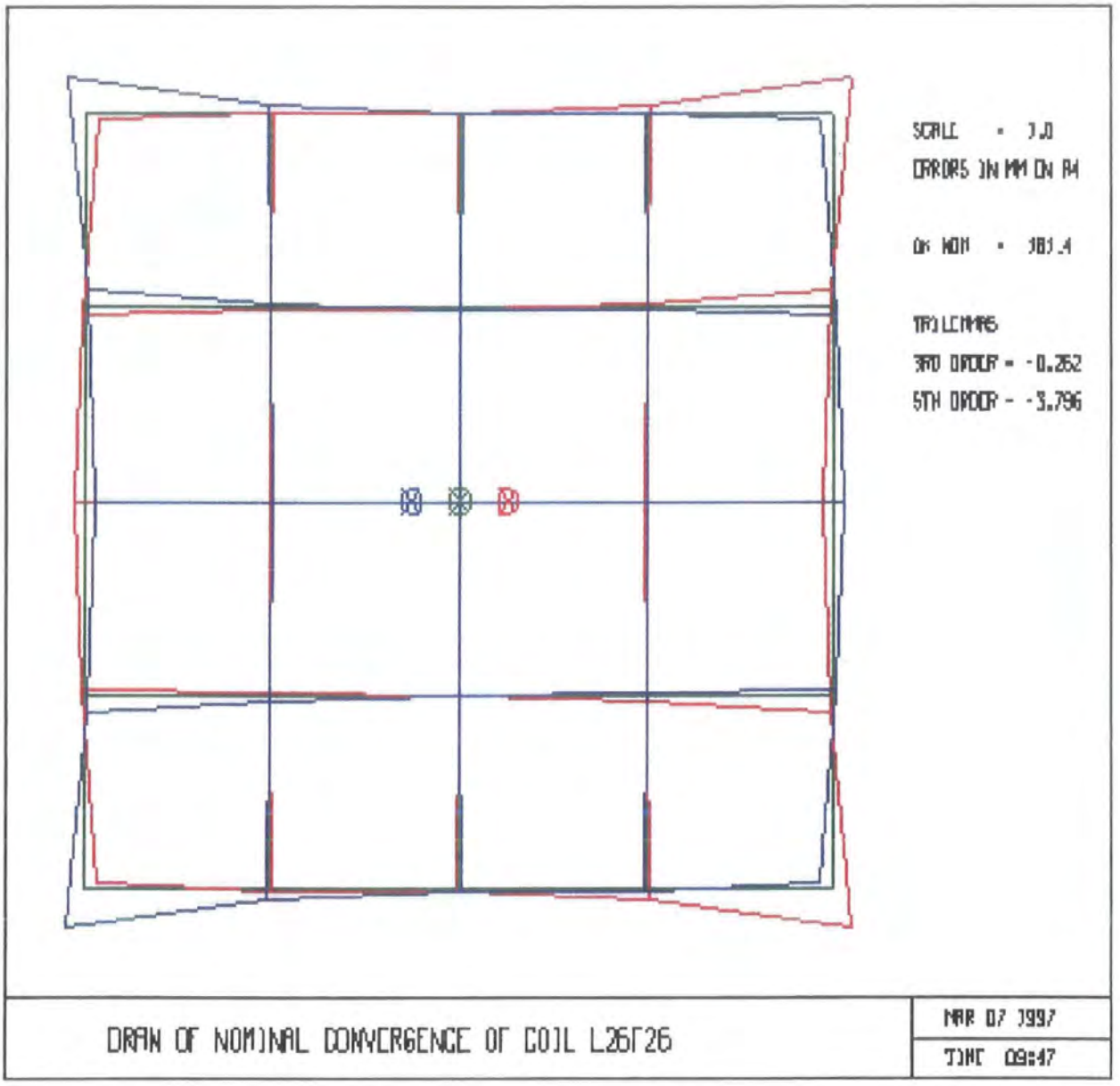
SCALE = 1.0
ERRORS IN MM ON R4
DX MIN = 381.4
TRILEMMAS
3RD ORDER = -0.262
5TH ORDER = -3.796
DRAW OF NOMINAL CONVERGENCE OF COIL L26F26
MAR 07 1997
TIME 09:47

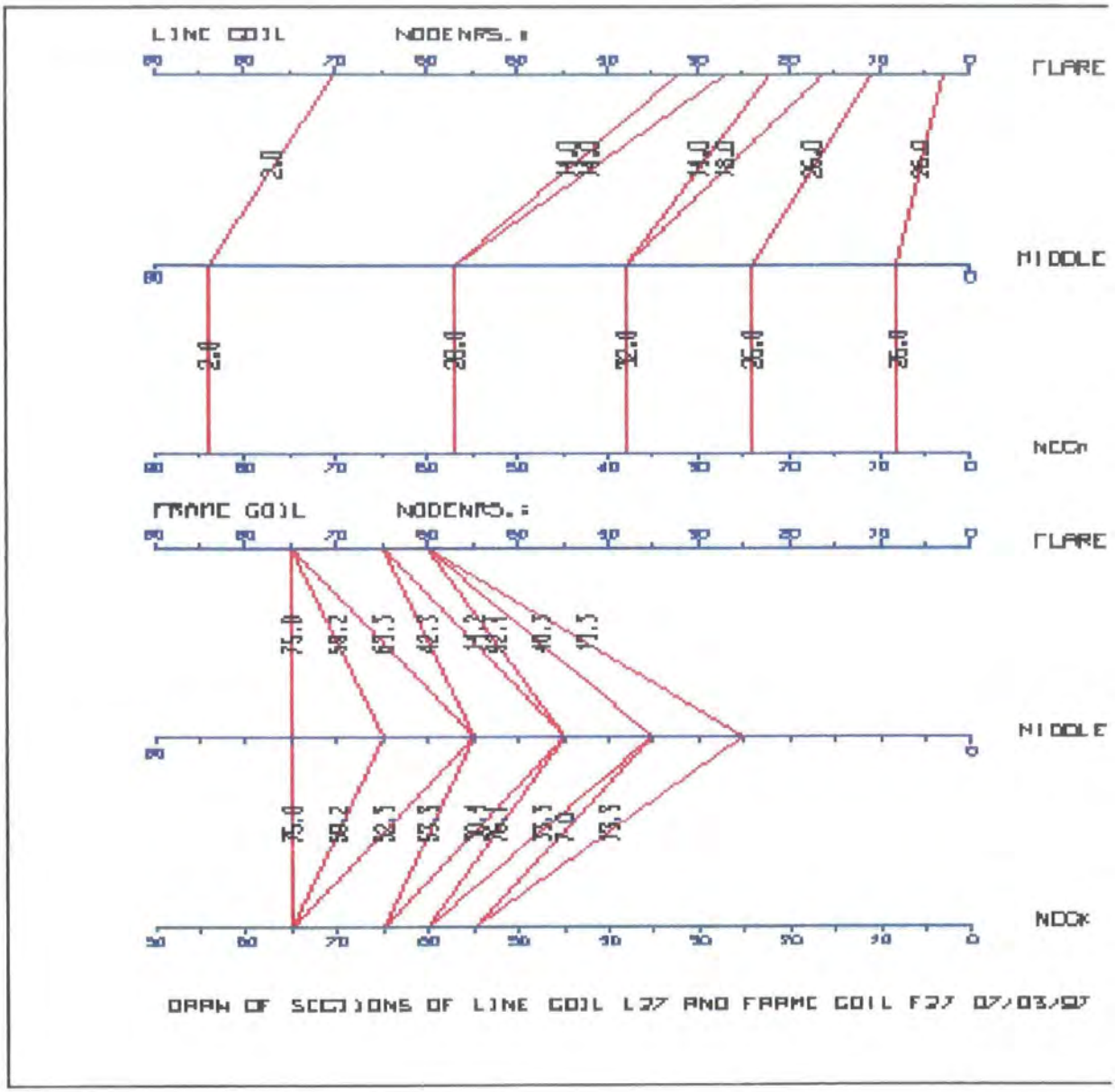

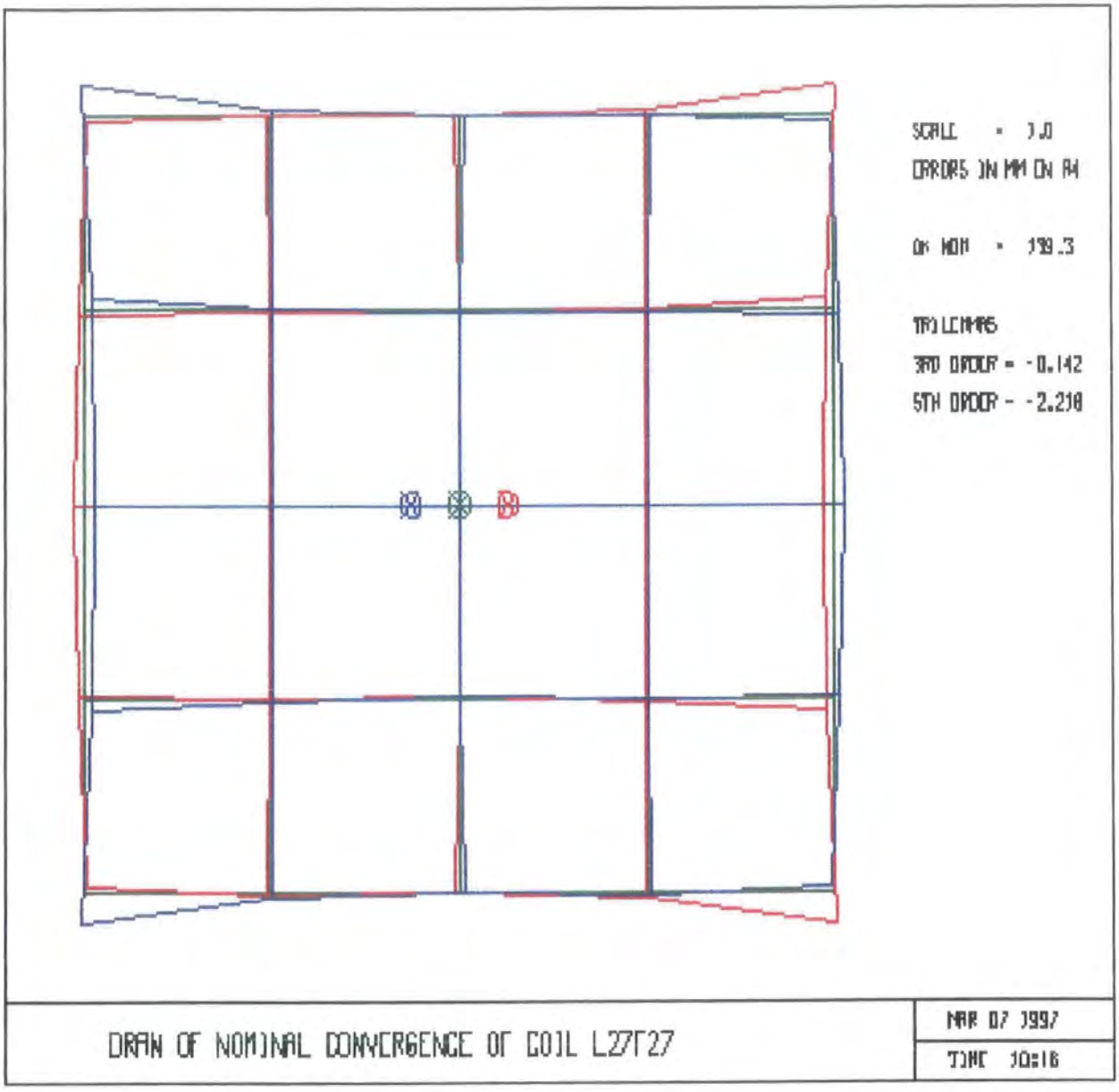
SCALE = 1.0
ERRORS IN MM ON R4
ON MON = 199.3
TRILEMMAS
3RD ORDER = -0.142
5TH ORDER = -2.210
DRAW OF NOMINAL CONVERGENCE OF COIL L27T27
MAR 07 1997
TIME 10:16

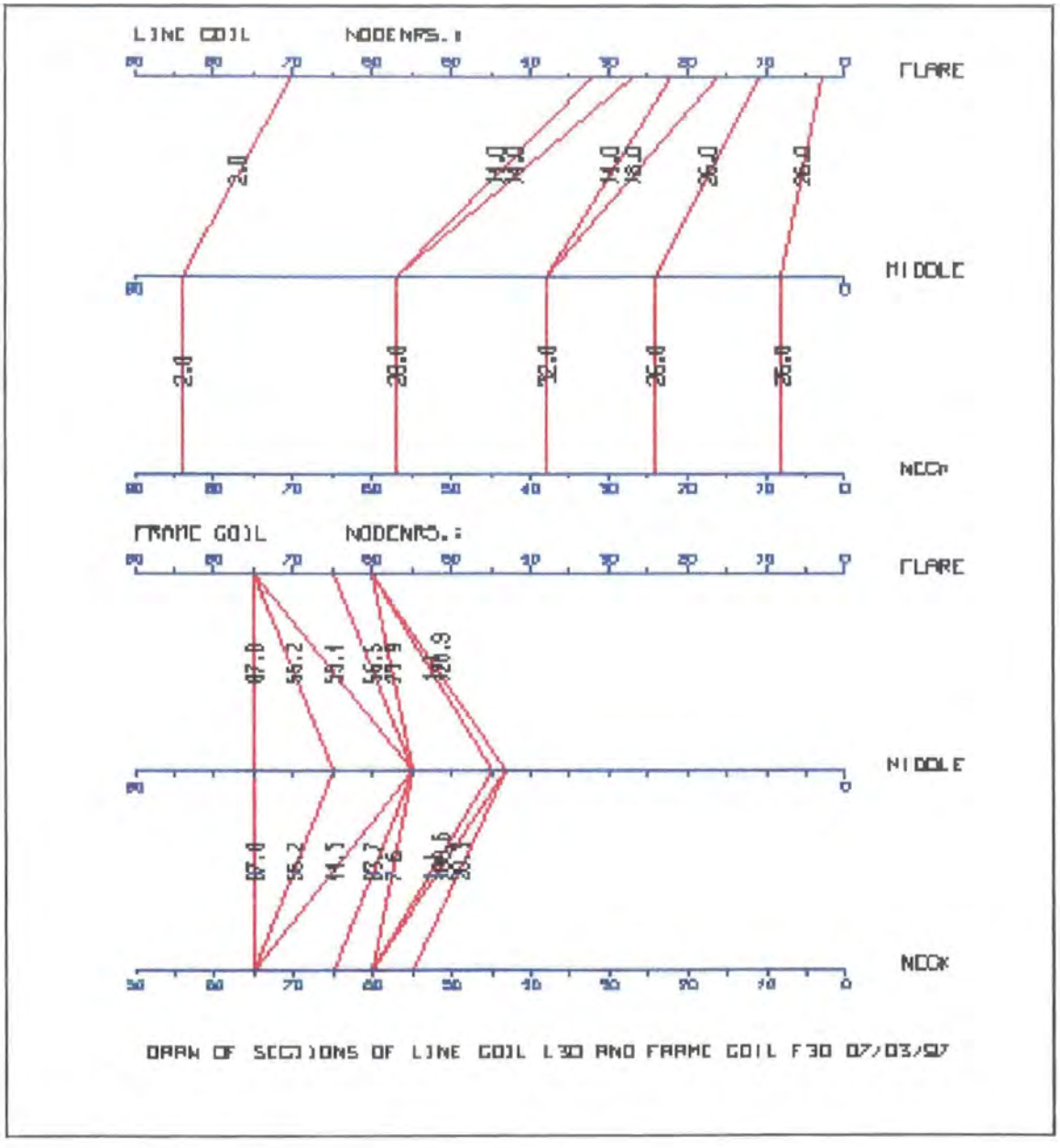
LINE COIL NODENRS.:
FLARE
MIDDLE
NECK
2.0
11.0
14.0
16.0
26.0
26.0
2.0
20.0
32.0
26.0
26.0
FRAME COIL NODENRS.:
FLARE
MIDDLE
NECK
87.0
55.2
53.1
56.5
120.9
87.0
55.2
14.5
DRAW OF SECTIONS OF LINE COIL L30 AND FRAME COIL F30 07/03/97

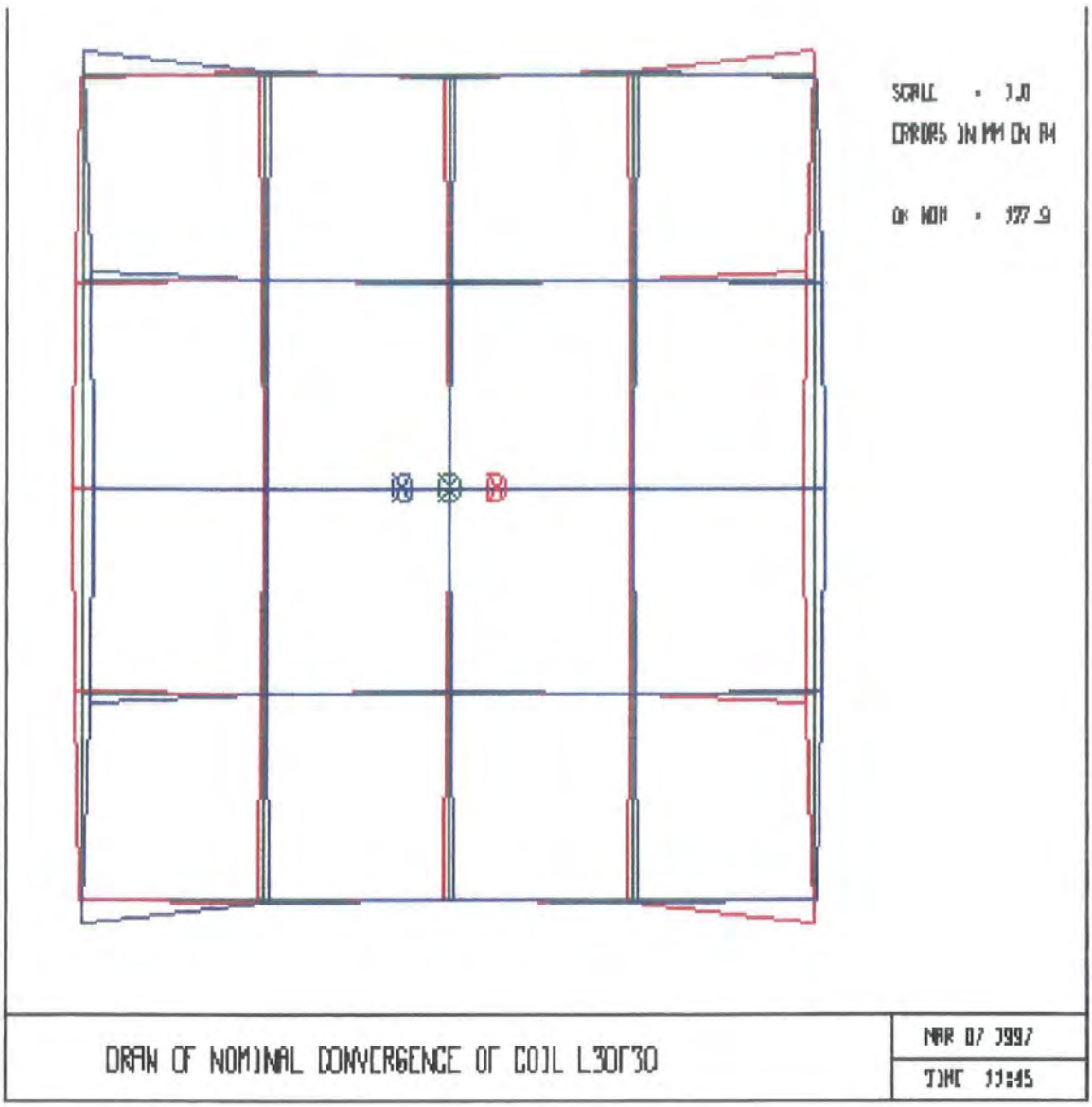

APPENDIX G - HARDWARE REPLICATION

- **Optimization Procedure in DUCAD-Y - Simulation Results of Hardware Optimized Design (Design L33F33)**

- **DUCAD-Y results compared to hardware measurements for the following conditions:**

  Base line coil (Set-Up ONE)

  Variation from base line coil (modification to winding pattern) (Set-Up TWO)

  Optimization Procedure (Set-Up THREE)

  Variation from base frame coil (modification to winding pattern) (Set-Up FOUR)

- **Hardware Measurement Data**

  Base Design vs. Design without Raster plates
  Base Design vs. Design without Magnets
  Base Design vs. Design without Coma plates
  Base Design vs. Design without Astigmatism plates

- **Agreement between Hardware/Software Deltas Carried out on Individual Components**

  Case 1 - Original Yoke Ring Definition
  Case 2 - Modified Yoke Ring Definition

  Hardware Delta/Software Delta : Raster Plates (Case 1)
  Hardware Delta/Software Delta : Magnets (Case 1)
  Hardware Delta/Software Delta : Coma Plates (Case 1)
  Hardware Delta/Software Delta : Astigmatism Plates (Case 1)

  Hardware Delta/Software Delta : Raster Plates (Case 2)
  Hardware Delta/Software Delta : Magnets (Case 2)
  Hardware Delta/Software Delta : Coma Plates (Case 2)
  Hardware Delta/Software Delta : Astigmatism Plates (Case 2)

L33F33 DESIGN OPTIMIZATION PROCEDURE

	DUCAD PREDICTIONS			L33F33
	BRX	BRY	XCOMA	YCOMA
R	0.322	0	0.182	0
C	3.795	0	-0.116	0
W	-0.08	0	0	-0.218
T	-0.564	0.332	0.183	0.038
G'	-0.017	-2.271	-0.107	0.626
D	-0.065	0	0	-0.071
L	-3.382	1.258	0.22	0.569
G	-12.826	-4.912	0.641	2.012

	HARD WARE MEASUREMENTS			
	BRX	BRY	XCOMA	YCOMA
R	0.536	0	0.375	0
C	3.014	0	0.493	0
W	0.053	0	0	-0.273
T	0.576	0.93	0.265	-0.062
G'	2.148	1.098	0.468	0.44
D	-0.88	0	0	0.614
L	-0.534	-0.812	-0.139	0.901
G	2.606	0.563	0.098	1.11

Design	Set-Up	
Winding	Pattern	
Slot 1-1	13T	AST26
Slot 2-2	13T	RAS4
Slot 3-3	10T	COM1
Slot 3-4	8T	mag (1.9)
Slot 3-5	7T	Frame coil
Slot 4-5	7T	Modified
Slot 4-6		
Slot 5-9		
Slot 6-10	1T	

DELTA
DUCAD
TO
HARDWARE

BRX	BRY	XCOMA	YCOMA
-0.214	0	-0.193	0
0.781	0	-0.609	0
-0.133	0	0	0.055
-1.14	-0.598	-0.082	0.1
-2.165	-3.369	-0.575	0.186
0.815	0	0	-0.685
-2.848	2.07	0.359	-0.332
-15.432	-5.475	0.543	0.902

			Set-Up	Number	ONE	Base	Line	Coil
MEASURED		RESULTS			DUCAD	RESULTS		

	BRX	BRY	XCOMA	YCOMA	BRX	BRY	XCOMA	YCOMA
R	0.615	0	0.381	0	0.307	0	0.352	0
C	3.211	0	0.536	0	4.848	0	0.37	0
W	0.326	0	0	-0.364	-0.094	0	0	0.644
T	0.958	1.153	0.35	-0.164	-0.124	-0.881	0.276	0.777
G'	2.394	1.457	0.697	0.379	1.365	-2.728	0.213	1.03
D	0.192	0	0	0.177	0.369	0	0	1.998
L	1.201	0.124	-0.021	0.404	-0.564	-2.632	0.034	2.082
G	4.605	2.293	0.542	0.647	-2.597	-7.919	-0.072	2.628

DELTA	Ducad/	Measured	
BRX	BRY	XCOMA	YCOMA
0.161	0	-0.029	0
1.737	0	-0.166	0
-0.172	0	0	-0.085
-0.573	-0.819	-0.074	-0.061
0.01	-3.017	-0.484	-0.06
0.403	0	0	-0.857
-1.907	0.94	0.055	-0.663
-9.335	-5.503	-0.614	0.231

Design	Set-Up	
Winding	Pattern	
Slot 1-1	13T	AST24
Slot 2-2	13T	RAS1
Slot 3-3	9T	COM1
Slot 3-4	7T	mag (1.9)
Slot 3-5	7T	
Slot 4-5	7T	
Slot 4-6		
Slot 5-9		
Slot 6-10	1T	

			Set-Up	Number	TWO	Variation	from base	coil
MEASURED		RESULTS			DUCAD	RESULTS		
	BRX	BRY	XCOMA	YCOMA	BRX	BRY	XCOMA	YCOMA
R	0.253	0	0.632	0	0.388	0	0.412	0
C	1.417	0	1.293	0	2.887	0	0.692	0
W	0.405	0	0	-0.382	0.154	0	0	-0.449
T	0.846	1.788	0.548	-0.196	0.151	0.835	0.394	-0.249
G'	1.774	2.907	1.239	0.231	1.395	-0.334	0.682	0.213
D	0.494	0	0	0.15	0.595	0	0	-0.68
L	1.603	1.291	0.109	0.324	-0.768	1.885	0.278	-0.287
G	5.152	4.526	0.741	0.47	-4.382	-2.068	0.798	0.82

DELTA	Ducad/	Measured	
BRX	BRY	XCOMA	YCOMA
0.135	0	-0.22	0
1.47	0	-0.601	0
-0.251	0	0	-0.067
-0.695	-0.953	-0.154	-0.053
-0.379	-3	-0.557	-0.018
0.101	0	0	-0.83
-2.371	0.594	0.169	-0.611
-9.534	-6.594	0.057	0.35

Design	Set-Up	
Winding	Pattern	
Slot 1-1	15T	AST24
Slot 2-2	13T	RAS1
Slot 3-3	9T	COM1
Slot 3-4	7T	mag (1.9)
Slot 3-5	7T	
Slot 4-5	7T	
Slot 4-6		
Slot 5-9		
Slot 6-10	1T	

Set-Up Number THREE OPTIMIZATION PROCEDURE

DUCAD PREDICTIONS ANTICIPATED VALUES

	BRX	BRY	XCOMA	YCOMA	BRX	BRY	XCOMA	YCOMA
R	0.202	0	0.543	0	0.072	0	0.763	0
C	1.899	0	1.085	0	0.429	0	1.685	0
W	0.154	0	0	-0.449	0.404	0	0	-0.389
T	0.039	1.071	0.506	-0.261	0.729	1.971	0.656	-0.211
G'	0.91	0.258	0.992	0.157	1.29	3.458	1.552	0.159
D	0.595	0	0	-0.68	0.494	0	0	0.15
L	-0.8	2.275	0.362	-0.301	1.6	1.675	0.192	0.309
G	-4.214	-1.52	0.949	0.79	5.286	4.98	0.889	0.44

DELTA Ducad/ Measured

BRX	BRY	XCOMA	YCOMA
0.13	0	-0.1	0
1.47	0	0.05	0
-0.25	0	0	-0.06
-0.69	-0.9	-0.01	-0.05
-0.38	-3.2	-0.5	-0.002
0.101	0	0	-0.83
-2.4	0.6	0.02	-0.61
-9.5	-6.5	-0.5	0.35

Design	Set-Up	
Winding	Pattern	
Slot 1-1	16T	AST24
Slot 2-2	13T	RAS1
Slot 3-3	10T	COM1
Slot 3-4	8T	mag (1.9)
Slot 3-5	7T	
Slot 4-5	7T	
Slot 4-6		
Slot 5-9		
Slot 6-10	1T	

			Set-Up	Number	FOUR	Frame	Coil	Modified
MEASURED		RESULTS			DUCAD	RESULTS		
	BRX	BRY	XCOMA	YCOMA	BRX	BRY	XCOMA	YCOMA
R	0.212	0	0.625	0	-0.006	0	0.566	0
C	1.079	0	1.266	0	1.311	0	1.115	0
W	-0.08	0	0	0.08	-0.218	0	0	-0.201
T	0.144	1.277	0.511	-0.062	-0.727	0.817	0.495	-0.005
G'	0.664	1.818	1.06	0.432	-0.404	-0.472	0.817	0.4
D	-1.277	0	0	0.419	-0.662	0	0	-0.021
L	-0.892	0.326	0.214	0.747	-3.627	1.728	0.422	0.52
G	0.805	2.527	0.987	1.204	-11	-4.566	0.977	1.898

DELTA	Ducad/	Measured	
BRX	BRY	XCOMA	YCOMA
-0.218	0	-0.059	0
0.232	0	-0.151	0
-0.138	0	0	-0.281
-0.871	-0.46	-0.016	0.057
-1.068	-2.29	-0.243	-0.032
0.615	0	0	-0.44
-2.735	1.402	0.208	-0.227
11.805	-7.093	-0.01	0.694

Design	Set-Up	
Winding	Pattern	
Slot 1-1	16T	AST25
Slot 2-2	13T	RAS3
Slot 3-3	10T	(4 deg. cut)
Slot 3-4	8T	COM1
Slot 3-5	7T	mag (1.9)
Slot 4-5	7T	
Slot 4-6		cast.
Slot 5-9		frame coil
Slot 6-10	1T	modified

		HARD	WARE	MEAS	URE	MENT	DATA		
	BASE	DESIGN	REAL			DESIGN	WITHOUT	RASTER	PLATES
	BRX	BRY	XCOMA	YCOMA		BRX	BRY	XCOMA	YCOMA
R	0.536	0	0.375	0		0.568	0	0.356	0
C	3.014	0	0.493	0		3.345	0	0.425	0
W	0.053	0	0	-0.273		-0.634	0	0	-0.173
T	0.576	0.93	0.265	-0.062		-0.412	0.3	0.293	0.056
G'	2.148	1.098	0.468	0.44		0.53	-0.554	0.428	0.599
D	-0.888	0	0	0.614		-3.376	0	0	0.783
L	-0.534	-0.812	-0.139	0.901		-3.677	-1.832	-0.832	1.059
G	2.606	0.563	0.098	1.11		-2.851	-2.059	-2.059	1.311

Design	Set-Up	
Winding	Pattern	
Slot 1-1	13T	AST25
Slot 2-2	13T	RAS4
Slot 3-3	10T	(5 deg. cut)
Slot 3-4	7T	COM1
Slot 3-5	7T	mag (1.9)
Slot 4-5	7T	cast.
Slot 4-6		
Slot 5-9		
Slot 6-10	1T	

DELTA

BRX	BRY	XCOMA	YCOMA
0.032	0	-0.019	0
0.331	0	-0.068	0
-0.687	0	0	0.1
-0.988	-0.63	0.028	0.118
-1.618	-1.652	-0.04	0.159
-2.488	0	0	0.169
-3.143	-1.02	-0.693	0.158
-5.457	-2.622	-2.157	0.201

HARD WARE MEAS URE MENT DATA

	BASE	DESIGN	REAL	
	BRX	BRY	XCOMA	YCOMA
R	0.536	0	0.375	0
C	3.014	0	0.493	0
W	0.053	0	0	-0.273
T	0.576	0.93	0.265	-0.062
G'	2.148	1.098	0.468	0.44
D	-0.888	0	0	0.614
L	-0.534	-0.812	-0.139	0.901
G	2.606	0.563	0.098	1.11

	DESIGN	WITHOUT	MAGNETS	
	BRX	BRY	XCOMA	YCOMA
R	0.865	0	0.354	0
C	4.353	0	0.439	0
W	-0.685	0	0	-0.154
T	0.158	0.251	0.248	0.027
G'	2.253	0.188	0.414	0.541
D	-4.245	0	0	0.89
L	-2.128	-2.559	-0.094	0.912
G	0.96	-0.18	0.553	1.22

Design	Set-Up	
Winding	Pattern	
Slot 1-1	13T	AST25
Slot 2-2	13T	RAS4
Slot 3-3	10T	(5 deg. cut)
Slot 3-4	7T	COM1
Slot 3-5	7T	mag (1.9)
Slot 4-5	7T	cast.
Slot 4-6		
Slot 5-9		
Slot 6-10	1T	

DELTA

BRX	BRY	XCOMA	YCOMA
0.329	0	-0.021	0
1.339	0	-0.054	0
-0.738	0	0	0.119
-0.418	-0.679	-0.017	0.089
0.105	-0.91	-0.054	0.101
-3.357	0	0	0.276
-1.594	-1.747	0.045	0.011
-1.646	-0.743	0.455	0.11

		HARD	WARE	MEAS	URE	MENT	DATA		
	BASE	DESIGN	REAL			DESIGN	WITHOUT	COMA	PLATES
	BRX	BRY	XCOMA	YCOMA		BRX	BRY	XCOMA	YCOMA
R	0.536	0	0.375	0		0.597	0	0.441	0
C	3.014	0	0.493	0		3.477	0	0.575	0
W	0.053	0	0	-0.273		-1.189	0	0	1.819
T	0.576	0.93	0.265	-0.062		-0.876	-0.816	0.47	1.811
G'	2.148	1.098	0.468	0.44		0.528	-1.626	0.603	1.722
D	-0.888	0	0	0.614		-4.188	0	0	4.966
L	-0.534	-0.812	-0.139	0.901		-3.868	-4.145	0.385	-1.222
G	2.606	0.563	0.098	1.11		-2.187	-4.168	0.447	3.551

Design	Set-Up	
Winding	Pattern	
Slot 1-1	13T	AST25
Slot 2-2	13T	RAS4
Slot 3-3	10T	(5 deg. cut)
Slot 3-4	7T	COM1
Slot 3-5	7T	mag (1.9)
Slot 4-5	7T	cast.
Slot 4-6		
Slot 5-9		
Slot 6-10	1T	

DELTA

BRX	BRY	XCOMA	YCOMA
0.061	0	0.066	0
0.463	0	0.082	0
-1.242	0	0	2.092
-1.452	-1.746	0.205	1.873
-1.62	-2.724	0.135	1.282
-3.3	0	0	4.352
-3.334	-3.333	0.524	-2.123
-4.793	-4.731	0.349	2.441

		HARD	WARE	MEAS	URE	MENT	DATA		
	BASE	DESIGN	REAL			DESIGN	WITHOUT	ASTIG.	PLATES
	BRX	BRY	XCOMA	YCOMA		BRX	BRY	XCOMA	YCOMA
R	0.536	0	0.375	0		0.566	0	0.379	0
C	3.014	0	0.493	0		3.232	0	0.561	0
W	0.053	0	0	-0.273		1.168	0	0	-0.592
T	0.576	0.93	0.265	-0.062		2.124	1.905	0.292	-0.41
G'	2.148	1.098	0.468	0.44		4.869	2.829	0.626	0.058
D	-0.888	0	0	0.614		2.294	0	0	-0.107
L	-0.534	-0.812	-0.139	0.901		4.156	0.986	-0.268	-0.029
G	2.606	0.563	0.098	1.11		9.833	3.805	-0.081	-0.097

Design	Set-Up	
Winding	Pattern	
Slot 1-1	13T	AST25
Slot 2-2	13T	RAS4
Slot 3-3	10T	(5 deg. cut)
Slot 3-4	7T	COM1
Slot 3-5	7T	mag (1.9)
Slot 4-5	7T	cast.
Slot 4-6		
Slot 5-9		
Slot 6-10	1T	

DELTA

BRX	BRY	XCOMA	YCOMA
0.03	0	0.004	0
0.218	0	0.068	0
1.115	0	0	-0.319
1.548	0.975	0.027	-0.348
2.721	1.731	0.158	-0.382
3.182	0	0	-0.721
4.69	1.798	-0.129	-0.93
7.227	3.242	-0.179	-1.207

CASE 1		HARD	WARE	SOFT	WARE	DELTA		RASTER	PLATES
	HARD	WARE	DELTA			SOFT	WARE	DELTA	
	BRX	BRY	XCOMA	YCOMA		BRX	BRY	XCOMA	YCOMA
R	0.032	0	-0.019	0		-0.573	0	0.072	0
C	0.331	0	-0.068	0		-1.945	0	0.012	0
W	-0.687	0	0	0.1		-0.148	0	0	0.143
T	-0.988	-0.63	0.028	0.118		-0.63	-0.546	0.057	0.105
G'	-1.618	-1.652	-0.04	0.159		-2.908	-1.107	0.114	0.11
D	-2.488	0	0	0.169		-0.944	0	0	0.469
L	-3.143	-1.02	-0.693	0.158		-0.638	-1.7	-0.037	0.241
G	-5.457	-2.622	-2.157	0.201		-3.768	-0.251	0.187	-0.081

Design	Set-Up	
Winding	Pattern	
Slot 1-1	13T	AST25
Slot 2-2	13T	RAS4
Slot 3-3	10T	(5 deg. cut)
Slot 3-4	7T	COM1
Slot 3-5	7T	mag (1.9)
Slot 4-5	7T	cast.
Slot 4-6		
Slot 5-9		
Slot 6-10	1T	

DELTA
SOFTWARE
TO
HARDWARE

BRX	BRY	XCOMA	YCOMA
-0.605	0	0.091	0
-2.276	0	0.08	0
0.539	0	0	0.043
0.358	0.084	0.029	-0.013
-1.29	0.545	0.154	-0.049
1.544	0	0	0.3
2.505	-0.68	0.656	0.083
1.689	2.371	2.344	-0.282

CASE 1		HARD	WARE	SOFT	WARE	DELTA		MAGNETS	
	HARD	WARE	DELTA			SOFT	WARE	DELTA	
	BRX	BRY	XCOMA	YCOMA		BRX	BRY	XCOMA	YCOMA
R	0.329	0	-0.021	0		0.977	0	-0.067	0
C	1.339	0	-0.054	0		2.627	0	0.031	0
W	-0.738	0	0	0.119		-0.761	0	0	-0.009
T	-0.418	-0.679	-0.017	0.089		0.705	-0.871	-0.064	-0.074
G'	0.105	-0.91	-0.054	0.101		3.3	0.309	0.071	-0.152
D	-3.357	0	0	0.276		-4.311	0	0	0.06
L	-1.594	-1.747	0.045	0.011		-0.777	-4.193	0.107	-0.119
G	-1.646	-0.743	0.455	0.11		5.929	0.099	0.342	-0.357

Design	Set-Up	
Winding	Pattern	
Slot 1-1	13T	AST25
Slot 2-2	13T	RAS4
Slot 3-3	10T	(5 deg. cut)
Slot 3-4	7T	COM1
Slot 3-5	7T	mag (1.9)
Slot 4-5	7T	cast.
Slot 4-6		
Slot 5-9		
Slot 6-10	1T	

DELTA
SOFTWARE
TO
HARDWARE

BRX	BRY	XCOMA	YCOMA
0.648	0	-0.046	0
1.288	0	0.085	0
-0.023	0	0	-0.128
1.123	-0.192	-0.047	-0.163
3.195	1.219	0.125	-0.253
-0.954	0	0	-0.216
0.817	-2.446	0.062	-0.13
7.575	0.842	-0.113	-0.467

CASE 1		HARD	WARE	SOFT	WARE	DELTA		COMA	PLATES
	HARD	WARE	DELTA			SOFT	WARE	DELTA	
	BRX	BRY	XCOMA	YCOMA		BRX	BRY	XCOMA	YCOMA
R	0.061	0	0.066	0		0.001	0	0.001	0
C	0.463	0	0.082	0		0.006	0	0.002	0
W	-1.242	0	0	2.092		-0.003	0	0	0.227
T	-1.452	-1.746	0.205	1.873		-0.066	0.05	0.016	0.199
G'	-1.62	-2.724	0.135	1.282		-0.226	-0.054	0.041	0.147
D	-3.3	0	0	4.352		0.103	0	0	0.54
L	-3.334	-3.333	0.524	-2.123		-0.155	0.353	0.014	0.441
G	-4.793	-4.731	0.349	2.441		-1.223	0.032	0.156	0.319

Design	Set-Up	
Winding	Pattern	
Slot 1-1	13T	AST25
Slot 2-2	13T	RAS4
Slot 3-3	10T	(5 deg. cut)
Slot 3-4	7T	COM1
Slot 3-5	7T	mag (1.9)
Slot 4-5	7T	cast.
Slot 4-6		
Slot 5-9		
Slot 6-10	1T	

DELTA
SOFTWARE
TO
HARDWARE

BRX	BRY	XCOMA	YCOMA
-0.06	0	-0.065	0
-0.457	0	-0.08	0
1.239	0	0	-1.865
1.386	1.796	-0.189	-1.674
1.394	2.67	-0.094	-1.135
3.403	0	0	-3.812
3.179	3.686	-0.51	2.564
3.57	4.763	-0.193	-2.122

CASE 1		HARD	WARE	SOFT	WARE	DELTA		ASTIG.	PLATES
	HARD	WARE	DELTA			SOFT	WARE	DELTA	
	BRX	BRY	XCOMA	YCOMA		BRX	BRY	XCOMA	YCOMA
R	0.03	0	0.004	0		0	0	0.006	0
C	0.218	0	0.068	0		-0.002	0	0.015	0
W	1.115	0	0	-0.319		1.877	0	0	-1.29
T	1.548	0.975	0.027	-0.348		2.266	3.448	0.029	-1.24
G'	2.721	1.731	0.158	-0.382		3.364	5.294	0.08	-1.127
D	3.182	0	0	-0.721		5.86	0	0	-3.397
L	4.69	1.798	-0.129	-0.93		7.001	8.592	0.225	-3.164
G	7.227	3.242	-0.179	-1.207		12.145	13.201	0.125	-2.892

Design	Set-Up	
Winding	Pattern	
Slot 1-1	13T	AST25
Slot 2-2	13T	RAS4
Slot 3-3	10T	(5 deg. cut)
Slot 3-4	7T	COM1
Slot 3-5	7T	mag (1.9)
Slot 4-5	7T	cast.
Slot 4-6		
Slot 5-9		
Slot 6-10	1T	

DELTA
SOFTWARE
TO
HARDWARE

BRX	BRY	XCOMA	YCOMA
-0.03	0	0.002	0
-0.22	0	-0.053	0
0.762	0	0	-0.971
0.718	2.473	0.002	-0.892
0.643	3.563	-0.078	-0.745
2.678	0	0	-2.676
2.311	6.794	0.354	-2.234
4.918	9.959	0.304	-1.685

CASE 2		HARD	WARE	SOFT	WARE	DELTA		RASTER	PLATES
			modified	yokering					
	HARD	WARE	DELTA			SOFT	WARE	DELTA	
	BRX	BRY	XCOMA	YCOMA		BRX	BRY	XCOMA	YCOMA
R	0.032	0	-0.019	0		0	0	0	0
C	0.331	0	-0.068	0		0	0	0	0
W	-0.687	0	0	0.1		-0.354	0	0	0.035
T	-0.988	-0.63	0.028	0.118		-0.489	-0.537	-0.006	0.04
G'	-1.618	-1.652	-0.04	0.159		-0.553	-1.174	-0.007	0.007
D	-2.488	0	0	0.169		-1.449	0	0	0.087
L	-3.143	-1.02	-0.693	0.158		-2.862	-1.105	0.047	0.21
G	-5.457	-2.622	-2.157	0.201		-4.992	-4.195	0.1	0.155

Design	Set-Up	
Winding	Pattern	
Slot 1-1	13T	AST25
Slot 2-2	13T	
Slot 3-3	10T	(5 deg. cut)
Slot 3-4	7T	COM1
Slot 3-5	7T	mag (1.9)
Slot 4-5	7T	cast.
Slot 4-6		
Slot 5-9		
Slot 6-10	1T	

DELTA
SOFTWARE
TO
HARDWARE

BRX	BRY	XCOMA	YCOMA
-0.032	0	0.019	0
-0.331	0	0.068	0
0.333	0	0	-0.065
0.499	0.093	-0.034	-0.078
1.065	0.478	0.033	-0.152
1.039	0	0	-0.082
0.281	-0.085	0.74	0.052
0.465	-1.573	2.257	-0.046

CASE 2		HARD	WARE	SOFT	WARE	DELTA		MAGNETS	
			modified	yokering					
	HARD	WARE	DELTA			SOFT	WARE	DELTA	
	BRX	BRY	XCOMA	YCOMA		BRX	BRY	XCOMA	YCOMA
R	0.428	0	0.051	0		0.587	0	-0.04	0
C	1.827	0	0.135	0		1.562	0	0.016	0
W	-1.282	0	0	-0.105		-0.525	0	0	0.06
T	-1.312	-1.216	0.047	0.402		0.549	-0.816	-0.092	-0.024
G'	-1.516	2.12	-0.098	0.453		2.542	0.036	0.01	-0.144
D	-4.457	0	0	-0.629		-3.348	0	0	0.361
L	-3.872	-1.916	-0.366	0.504		0.395	-4.059	-0.327	-0.144
G	6.016	-1.947	-1.097	-0.67		8.702	-0.439	-0.354	-0.681

Design	Set-Up	
Winding	Pattern	
Slot 1-1	13T	AST25
Slot 2-2	13T	RAS4
Slot 3-3	10T	(5 deg. cut)
Slot 3-4	7T	COM1
Slot 3-5	7T	
Slot 4-5	7T	cast.
Slot 4-6		
Slot 5-9		
Slot 6-10	1T	

DELTA
SOFTWARE
TO
HARDWARE

BRX	BRY	XCOMA	YCOMA
0.159	0	-0.091	0
-0.265	0	-0.119	0
0.757	0	0	0.165
1.861	0.4	-0.139	-0.426
4.058	-2.084	0.108	-0.597
1.109	0	0	0.99
4.267	-2.143	0.039	-0.648
2.686	1.508	0.743	-0.011

CASE 2		HARD	WARE	SOFT	WARE	DELTA		COMA	PLATES
			modified	yokering					
	HARD	WARE	DELTA			SOFT	WARE	DELTA	
	BRX	BRY	XCOMA	YCOMA		BRX	BRY	XCOMA	YCOMA
R	0.061	0	0.066	0		0	0	0	0
C	0.463	0	0.082	0		0	0	0	0
W	-1.242	0	0	2.092		-0.657	0	0	1.601
T	-0.989	-1.746	0.205	1.873		-0.722	-0.82	0.017	1.383
G'	-1.62	-2.724	0.168	1.282		-0.721	-1.01	0.115	0.895
D	-3.3	0	0	4.352		-2.017	0	0	3.971
L	-3.334	-3.333	0.524	-2.123		-2.115	-2.529	-0.135	3.144
G	-4.793	-4.731	0.349	2.441		-2.239	-3.608	0.062	1.779

Design	Set-Up	
Winding	Pattern	
Slot 1-1	13T	AST25
Slot 2-2	13T	RAS4
Slot 3-3	10T	(5 deg. cut)
Slot 3-4	7T	
Slot 3-5	7T	mag (1.9)
Slot 4-5	7T	cast.
Slot 4-6		
Slot 5-9		
Slot 6-10	1T	

DELTA
SOFTWARE
TO
HARDWARE

BRX	BRY	XCOMA	YCOMA
-0.061	0	-0.066	0
-0.463	0	-0.082	0
0.585	0	0	-0.491
0.267	0.926	-0.188	-0.49
0.899	1.714	-0.053	-0.387
1.283	0	0	-0.381
1.219	0.804	-0.659	5.267
2.554	1.123	-0.287	-0.662

CASE 2		HARD	WARE	SOFT	WARE	DELTA		ASTIG.	PLATES
			modified	yokering					
	HARD	WARE	DELTA			SOFT	WARE	DELTA	
	BRX	BRY	XCOMA	YCOMA		BRX	BRY	XCOMA	YCOMA
R	0.03	0	0.004	0		0	0	0	0
C	0.218	0	0.068	0		0	0	0	0
W	1.115	0	0	-0.319		2.702	0	0	-0.962
T	1.548	0.975	0.027	-0.348		3.675	2.538	-0.035	-1
G'	2.721	1.731	0.158	-0.382		6.759	4.538	-0.021	-1.104
D	3.182	0	0	-0.721		8.649	0	0	-2.098
L	4.69	1.798	-0.129	-0.93		12.493	4.136	-0.321	-2.26
G	7.227	3.242	-0.179	-1.207		28.074	7.391	-1.568	-2.931

Design	Set-Up	
Winding	Pattern	
Slot 1-1	13T	
Slot 2-2	13T	RAS4
Slot 3-3	10T	(5 deg. cut)
Slot 3-4	7T	COM1
Slot 3-5	7T	mag (1.9)
Slot 4-5	7T	cast.
Slot 4-6		
Slot 5-9		
Slot 6-10	1T	

DELTA
SOFTWARE
TO
HARDWARE

BRX	BRY	XCOMA	YCOMA
-0.03	0	-0.004	0
-0.218	0	-0.068	0
1.587	0	0	-0.643
2.127	1.563	-0.062	-0.652
4.038	2.807	-0.179	-0.722
5.467	0	0	-1.377
7.803	2.338	-0.192	-1.33
20.847	4.149	-1.389	-1.724

REFERENCE LISTING:

[1] 'Progress in the Theory of Electron Beam Deflection'
E.F. Ritz, Jnr.
Electron Optical Systems, Scanning Electron Microscopy, Pg.97-108, 1984

[2] 'An Analytical Method for Calculating the Magnetic Field due to a Deflection Yoke'
Basab B. Dasgupta
RCA Review Vol. 44, No. 3, Pg 404-23, Sept. 1983

[3] 'The Deflection Coil of the 30AX Colour Picture System'
W.A. L. Heijemans, J.A.M. Nieuwendijk and N.G. Vink
Philips Technical Review, Vol. 39, no 6/7, Pg. 154-171, 1980

[4] 'Analysis of Magnetic Plates attached to a Deflection Yoke with a Hybrid Method'
T. Nakagawa, S. Okuda, et al
Conference Record of the 1988 International Display Research Conference
IEE Cat No. 88-CH-2678-1, Pg. 23-26, 1988, IEEE, New York

[5] 'An Analytical Study of the Winding Harmonics of a Saddle Deflection Coil'
Basab B. Dasgupta
RCA Review Vol. 45, No. 3., Pg. 461-471, Sept. 1984

[6] 'Computation of Deflection defocusing in CRT Electron Beams with three Dimensional Non-linear Analysis of Magnetic Fields'
M. Watanabe, S. Shirai, M. Fukushima
Conference Record of the 1988 International Display Research Conference
IEEE Cat No. 88-CH-2678-1, Pg. 125-128, 1988, IEEE, New York

[7] 'Three Dimensional Magnetic Field Analysis of a Deflection Yoke with a Slot Core(CRT)'
Takafumi Nakagawa and Soichiro Okuda et al
Proceedings of the SID, Vol. 31/3, No. 3., Pg. 193-196, 1990

[8] 'Computer Design of Colour CRT Deflection Coils Using Additional Small Windings'
Makoto Watanabe, Yukio Nakamua, et al
1991 SID international Symposium Digest of Technical Papers, Pg.879-881, 1991

[9] N.V. Philips Gloeilampenfabrieken, Eindhoven
Date of Publication 31/08/88, Bulletin 88/35
Patent Number 87201036.8; EP 0249 280 A1

[10] '107 cm screen Diagonal 16:9 Colour CRT for HDTV Displays'
Mitsuda K., Sugawara K. et al.
Matsushita Electron Corporation, Osaka, Japan
Conf. Record of 1991 International Display Research Conference 1991, IEE
Cat No. 91-CH-3071-8, Pg. 35-38, 1991, IEEE, New York

[11] Murata, Patent Reference Number : 0 581 586, 28/7/92

[12] ' Designing Self-Converging CRT Deflection Yokes'
Basab B. Dasgupta
Information Displays, Vol.8, No. 1, Pg. 15-19, Jan 1992

[13] 'The Calculation of the Deflection Magnetic field and the Electron Beam Trajectory for Colour Television'
Yutaka Yokota, Sanyo Electric Company, IEEE Transactions on Consumer Electronics
Vol. CE-25, Pg. 91-99, Nov. 1979

[14] 'The Design of Deflection Units for Monochrome Data-graphic Displays'
A.A. S. Sluyterman, N.V. Philips Gloeilampenfabrieken
Electronic Displays 1982 and Information Display Systems, Pg. 11, Network Exhibition Buckingham, U.K., Session 2

[15] 'Harmonic Analysis of a Planar Wound Toroidal Deflection Coil'
Basab B. Dasgupta, RCA Consumer Electronics
IEEE Transactions on Consumer Electronics, Vol. CE-29, No 4., Pg. 508-515, November 1983.

[16] 'Progress in the Theory of Electron Beam Deflection'
E.F. Ritz, Jnr, Tektronix, Inc.
Scanning electron Microscopy, Pg. 97-108, 1984

[17] 'Magnetic Deflection in Television Picture Tubes'
R. Vonk
Philips Technical Review, Vol. 32, 1971, no 3/4

[18] 'Effect of Finite Coil Thickness in a Magnetic Deflection System'
Basab B. Dasgupta
Journal of Applied Physics., Vol. 54, No. 3, Pg. 1626-1627, March 1983

[19] 'Computer Simulation of Double Mussel Deflection Coil Winding'
Hans Penninga
Journal of the Society for Information Display, Vol. 1, No. 1, Pg. 11-14, Jan. 1993

[20] 'Lectures on Electromagnetic Theory'
L. Solymar
Oxford University Press, 1884

[21] 'Transmission and Propagation of Electromagnetic Waves'
K.F. Sander and G.A.L Reed
Cambridge University Press, 1987

[22] 'Control Systems Engineering'
Stephen P. Banks
Prentice Hall International, 1986

[23] 'DUCAD User Manual - User's Reference Manual, DUCAD 1.2.1.'
Leo Beckers
PPD - R & C/AD - TVR -55-96-PB-D118
RAF4, June 10 1996